UNIVERSITY OF COPENHAGEN
FACULTY OF SCIENCE

PhD Thesis

Martin Olesen

High resolution climate simulation

Methods for improving and customising climate information with focus on outreach and uncertainty assessment

Supervisors:

Jens Hesselbjerg Christensen, Professor
Climate Physics, Niels Bohr Institute, University of Copenhagen

Eigil Kaas, Professor
Climate Physics, Niels Bohr Institute, University of Copenhagen

Peter Lang Langen, Climate Scientist
Research and Development, Danish Meteorological Institute

This thesis has been submitted to the PhD School of The Faculty of Science, University of Copenhagen on January 18, 2019

Preface

Ph.D. Thesis

Faculty of Science, University of Copenhagen

Author: Martin Olesen

E-mail: mol@dmi.dk

Institutions: Research and development, Danish Meteorological Institute

Centre for Ice and Climate, Niels Bohr Institute, University of Copenhagen

Supervisors: Jens Hesselbjerg Christensen, Climate Physics, Niels Bohr Institute, University of Copenhagen

Eigil Kaas, Climate Physics, Niels Bohr Institute, University of Copenhagen

Peter Lang Langen, Research and Development, Danish Meteorological Institute

This PhD research is part of the ERC funded ice2ice project mentioned in Acknowledgements. The overall aim of ice2ice is to investigate what happens, if the Arctic sea ice abruptly disappears. The hypothesis is that the Arctic sea ice cover exerts important controls on past and future temperature in Greenland and ice sheet variations. Testing this hypothesis involves the following research goals: *a) Describe nature, timing and extent of abrupt events across climate archives, b) Resolve mechanisms behind sudden demise of Arctic sea ice cover, c) Determine the impact of Arctic sea ice on climate and the Greenland ice sheet & e) Identify risk that rapid diminution of Arctic sea ice could give future abrupt changes*.

From these research goals and the overall aim, the ice2ice project task 2.1 is formulated: *"Investigate the surface mass balance and dynamical response of the Greenland Ice Sheet to past and present Arctic sea ice changes"*. This PhD research is directly related to project task 2.1. Read more about ice2ice on: https://ice2ice.w.uib.no/.

Acknowledgements

First of all I owe many thanks to my supervisor, Jens Hesselbjerg Christensen for being helpful and supporting and for our interesting discussions both on and off topic, but also for being an inspiring mentor. I am thankful to my principal supervisor Eigil Kaas for good discussions and for raising relevant questions during the research period. Many colleagues at Danish Meteorological Institute (DMI) have helped me with this project. I would like to thank my colleague Peter Thejll for statistical support, Christian Rodehacke for programming support and Fredrik Boberg for general support and beneficial team work with developing climate indices for Greenland, Ruth Mottram for providing data.

I would like to acknowledge Ice2ice for making this project possible and for providing a number of relevant workshops, meetings and courses highly relevant for this research and for keeping up my motivation all the way through the PhD period. I would like to thank ice2ice colleagues at UniResearch Climate and Geophysical Institute in Bergen for welcoming me during my 3 month change of scientific environment in Norway. I would like to acknowledge the Greenland Self-Government in Nuuk for supporting the development of the scientific reports and for hosting the workshop where relevant sectors were represented in developing ideas for specific climate indices.

I acknowledge the World Climate Research Programme's Working Group on Regional Climate, and the Working Group on Coupled Modelling, former coordinating body of CORDEX and responsible panel for CMIP5. We also thank the climate modelling groups (listed in Table 5-1) for producing and making available their model output. The research leading to these results has received funding from the European Research Council under the European Union's Seventh Framework Programme (FP7/2007-2013) / ERC Grant Agreement n.610055 as part of the ice2ice project and from the Danish Cooperation for Environment in the Arctic (DANCEA) under the Danish Energy Agency.

Abstract

Application of a single high-resolution regional climate model (RCM) simulation for Greenland implies detailed information on the model performance compared to in situ observations and other RCMs. Projections of future climate change based on an ensemble of climate models are more robust than estimates based on a single model. In this thesis a statistical method to better frame results based on the RCM HIRHAM5 is utilized to assess uncertainties of projected climate change results. Expected future climate changes and associated uncertainties in Greenland are estimated for the periods 2031-2050 and 2081-2100. This analysis is based on HIRHAM5 at a horizontal resolution of approximately 5.5 km, emission scenarios used by IPCC and on European regional climate studies (EURO-CORDEX). Using HIRHAM5 simulations over Greenland in combination with an ensemble of coarser RCM simulations from a different geographical setting; EURO-CORDEX, we investigate to what extent the uncertainty of projected high-resolution climate change can be evaluated from corresponding temperature spread in a wider set of global climate models (GCMs), CMIP5. Furthermore, HIRHAM5 is compared with in situ observation records through spatially linked correlated patterns for temperature and precipitation. Improved climate information is achieved by combining long weather records from the Greenlandic coastal stations and proxy measurements of temperature and solid accumulation from deep ice cores and HIRHAM5 simulations. HIRHAM5 provides physically consistent information of temperature, precipitation, snow fall, melt, evaporation and surface mass balance (SMB) for the period1980-2014. Our proposed uncertainty assessment method establishes a foundation on which high-resolution and relative costly regional climate projections in general can be assessed. Also when using only a single RCM without the presence of analogous downscaling experiments with other RCMs and GCMs, the uncertainty assessment is relying on already existing information from CMIP5. Thus, the uncertainty of a wide range of climate indices that scale with temperature can be evaluated and quantified through the inter-model temperature spread within CMIP5. Changes in growing season, number of frost days and consecutive dry days are presented as index examples. This investigation shows with high confidence that HIRHAM5 is representative of the ensemble of RCMs within EURO-CORDEX. By relating large scale correlations of various climate variables deduced from HIRHAM5, observed temperature and precipitation in situ records are prolonged 500 years back in time based on proxy data from deep ice cores. SMB for selected drainage basins on the Greenland ice sheet and for the Renland ice cap are reconstructed and show decreasing trend lines towards present. The SMB for the drainage basin nearest Tasiilaq, decreases from + 0.5 mm weq/yr for 1898-2014 to -5.4 mm weq/yr in 1980-2014. Correspondingly, the SMB for the drainage basin nearest Danmarkshavn decreases from -0.3 mm weq/yr for 1950-2014 to -1.1 mm weq/yr in 1980-2014, and the SMB of the Renland ice cap decreases from +2.4 mm weq/yr for 1950-2007 to -4.7 mm weq/yr in 1980-2007. Finally, the correlation patterns of temperature and precipitation illustrate the coverage of correlated weather stations and ice core drill site locations across Greenland. In situ observation records reflect with high confidence the spatial correlation patterns calculated from HIRHAM5 for both temperature and precipitation.

Resumé

Anvendelse af en enkelt regional klimamodel (RCM) for Grønland forudsætter detaljeret viden om, hvordan modellen klarer sig både i forhold til in situ observationer og i forhold til andre RCM'er. Fremskrivninger af fremtidige klimaændringer baseret på et ensemble af klimamodeller er generelt mere robuste end skøn baseret på en enkelt modelsimulering. I denne afhandling introduceres, testes og anvendes statistisk metoder til bedre at vurdere resultater, som er baseret på en enkelt RCM i forhold til usikkerheden af estimerede igangværende- og fremtidige klimaændringer i Grønland. Analysen er baseret på den regionale klimamodel HIRHAM5 med en horisontal opløsning på ca. 5,5 km, på udledningsscenarier anvendt af IPCC samt på europæiske regionale klimastudier (EURO-CORDEX). Med udgangspunkt i HIRHAM5 simuleringer over Grønland i kombination med et ensemble af grovere opløste RCM-simuleringer fra en anden geografisk placering, EURO-CORDEX, undersøges i hvilket omfang usikkerheden af forventede klimaændringer med høj opløsning kan vurderes ud fra temperaturspredningen i et bredere udsnit af globale klimamodeller; CMIP5. Forventede klimaændringer og tilhørende usikkerheder i Grønland er fremskrevet for perioderne 2031-2050 og 2081-2100 i forhold til referenceperioden 1991-2010. Endvidere sammenlignes HIRHAM5 med observationer fra grønlandske målestationer ved hjælp af geografisk korrelerede områder af temperatur og nedbør. Forbedret klimainformation opnås ved at kombinere lange vejroptegnelser fra de grønlandske kyststationer og proxymålinger af temperatur og akkumulation af sne fra dybe iskerner med HIRHAM5 simuleringer. HIRHAM5 giver fysisk konsistent beskrivelse af parametre som temperatur, nedbør, snefald, afsmeltning, fordampning og overflademassebalance (SMB) for perioden 1980-2014. Metoden til vurdering og kvantificering af usikkerhed præsenteret i denne afhandling etablerer et fundament, hvorpå højopløselige og relativt dyre regionale klimaprognoser kan vurderes generelt. Ved anvendelse af kun en enkelt RCM uden tilsvarende simuleringer med andre RCM'er afhænger usikkerhedsvurderingen af allerede eksisterende information fra CMIP5. Således kan usikkerheden af en bred vifte af klimaindeks, der skalerer med temperatur, evalueres og kvantificeres gennem spredningen af CMIP5-estimerede temperaturer. Ændringer i vækstsæson, antal frostdage og på længden af tørkeperioder præsenteres som eksempler. Undersøgelsen viser, at HIRHAM5 er repræsentativ for ensemblet af RCM'er i EURO-CORDEX. Med udgangspunkt i geografiske storskala-korrelationer af temperatur og nedbør udledt fra HIRHAM5 forlænges observerede temperatur- og nedbørtidsserier med op til 500 år tilbage i tiden på basis af proxy data fra dybe iskerner. SMB for udvalgte dræningsbassiner på Grønlands indlandsis og for Renlands iskappe rekonstrueres og viser en aftagende tendens frem mod 2014. SMB i dræningsbassinet nærmest Tasiilaq falder fra + 0,5 mm væ/år for 1898-2014 til -5,4 i 1980-2014. Tilsvarende falder SMB for dræningsbassinet nærmest Danmarkshavn fra -0,3 mm væ/år for 1950-2014 til -1,1 i 1980-2014, og SMB af Renlands iskappe falder fra + 2,4 mm væ/år for 1950-2007 til -4,7 mm i 1980-2007. Endvidere illustrerer korrelationskort for temperatur og nedbør dækningen af korrelerede vejrstationer og iskerneboringer på tværs af Grønland. Indbyrdes korrelationer mellem observerede tidsserier afspejler med få undtagelser de korrelerede temperatur- og nedbørtidsserier beregnet ud fra HIRHAM5.

Table of content

1 Outline

This PhD thesis is based on four journal papers, a series of scientific reports and an educational book chapter. The four journal papers and the book chapter are attached in continuation of this thesis, and links to the reports are available in this Outline.

Paper I Olesen, M., Christensen, J.H., Kaas, E., Boberg, F., 2018a. Robustness of high-resolution regional climate projections for Greenland: a method for uncertainty distillation. Clim. Res. 76, 253–268. [Published Nov 2018]

Paper II Olesen, M., Kaas, E., Christensen, J.H., Holme, C., 2019c Time evolution of Greenland surface mass balance by combining high-resolution climate modelling, in situ observations and ice cores. The Cryosphere [in review, 2019]

Paper III Boberg, F., Langen, P.L., Mottram, R.H., Christensen, J.H., Olesen, M., 2018. 21st-century climate change around Kangerlussuaq, west Greenland: From the ice sheet to the shores of Davis Strait. Arct. Antarct. Alp. Res. 50, S100006. [Published Apr 2018]

Paper IV Holme, C., Gkinis, V., Lanzky, M., Morris, V., Olesen, M., Thayer, A., Vaughn, B.H., Vinther, B.M., 2018. Varying regional δ18O–temperature relationship in high resolution stable water isotopes from East Greenland. Clim. Past Discuss. 1–26. [in review, 2019]

Report I Christensen, J.H., Olesen, M., Boberg, F., Stendel, M., Koldtoft, I., 2015a. Fremtidige klimaforandringer I Grønland: Kujalleq Kommune (Scientific report 15-04 (1/6)). Danish Meteorological Institute.

Report II Christensen, J.H., Olesen, M., Boberg, F., Stendel, M., Koldtoft, I., 2015b. Fremtidige klimaforandringer I Grønland: Sermersooq Kommune (west) (Scientific report 15-04 (2/6)). Danish Meteorological Institute.

Report III Christensen, J.H., Olesen, M., Boberg, F., Stendel, M., Koldtoft, I., 2015c. Fremtidige klimaforandringer I Grønland: Sermersooq Kommune (East) (Scientific report 15-04 (3/6)). Danish Meteorological Institute.

Report IV Christensen, J.H., Olesen, M., Boberg, F., Stendel, M., Koldtoft, I., 2015f. Fremtidige klimaforandringer I Grønland: Qeqqata Kommune (Scientific report 15-04 (4/6)). Danish Meteorological Institute.

Report V Christensen, J.H., Olesen, M., Boberg, F., Stendel, M., Koldtoft, I., 2015d. Fremtidige klimaforandringer I Grønland: Qaasiutsup Kommune (Scientific report 15-04 (5/6)). Danish Meteorological Institute.

Report VI Christensen, J.H., Olesen, M., Boberg, F., Stendel, M., Koldtoft, I., 2015e. Fremtidige klimaforandringer I Grønland: Nationalparken (Scientific report 15-04 (6/6)). Danish Meteorological Institute

Report VII Christensen, J.H., Olesen, M., Boberg, F., Stendel, M., Koldtoft, I., 2015g. Climate indices for vulnerability assessments - Greenland (Scientific report 15-04 (index catalogue)). Danish Meteorological Institute.

Book Chapter Olesen, M., Arnbjerg-Nielsen, K., Hansen, A.S., 2015. "What is a climate model?", chapter 3 in "Climate adaptation - why and how?", Miljøbiblioteket. Aarhus University Press.

For Paper I and II the author has participated in all phases from idea to publication and is responsible for the data analysis, visualization and final paper writing. Paper III is a continuation of the reports I-VII and climate data delivery for the Greenland Self-Government. The author has contributed to Paper III in full. For Paper IV the author is responsible for the sections involving regional climate modelling and spatial correlation analysis.

The scientific reports on climate change in Greenland include observations, climate projections simulated with regional climate model (RCM), HIRHAM5 and a selection of derived climate indices. The 7 reports are available here: http://www.dmi.dk/laer-om/temaer/klima/groenlands-klima/. The author has contributed to all phases from index development, data analysis visualization and report writing. In addition to that, the author was responsible for the climate data preparation for the web-solution with interactive climate index maps hosted at Asiaq, the Greenlandic survey, available at: https://kort.nunagis.gl/klimadata/#about. Additional educational and outreach material is published in Greenlandic: (http://www.dmi.dk/fileadmin/user_upload/Groenland/Klimaforandringer_i_Groenland_pixi.pdf).

The reports are prepared on the assumption that uncertainties are assessable from an ensemble of global climate model (GCM) projections and therefore rely on the validity of the uncertainty assessment method tested in Paper I. Finally the author is fully responsible for the educational book chapter. The chapter is targeted students as well as local, regional and national climate adaptation purposes and hence published (not open access and in Danish) https://unipress.dk/udgivelser/k/klimatilpasning/

The journal Papers I-IV and the scientific reports I-VII focus on the past, present and future climate in Greenland, whereas the book chapter is an introduction to climate modelling and climate change in Denmark in a climate adaptation context. The research presented in Paper I and II and in the scientific reports I-VII are the focal point of this PhD thesis. Paper I is presented in Chapter 5 and Paper II is presented in Chapter 6, where also some results from Paper IV is presented. Parts of Paper III are shown in Section 4.4 in Chapter 4, where also the scientific reports are presented.

2 Objectives

This PhD research focuses on Greenland, seen from a high-resolution RCM, HIRHAM5 and involves methods developed for validation and time series reconstruction in an ice2ice perspective. The overall aim of the ice2ice project is to investigate the consequences of abruptly disappearing of the Arctic sea ice. The hypothesis is that the Arctic sea ice cover exerts important controls on past and future temperature in Greenland and ice sheet variations. Testing this hypothesis involves the following research goals:

- *Describe nature, timing and extent of abrupt events across climate archives*
- *Resolve mechanisms behind sudden demise of Arctic sea ice cover*
- *Determine the impact of Arctic sea ice on climate and the Greenland ice sheet*
- *Identify risk that rapid diminution of Arctic sea ice could give future abrupt changes*

To investigate these research goals and to understand and quantify past and future surface mass balance (SMB) and dynamical response to Arctic sea ice changes, a validated high-resolution regional climate model (RCM) covering the Artic and Greenland is essential. Therefore, a subtask in the ice2ice project is to validate the RCM, HIRHAM5 used in this project for both past and future simulations. The validation involves new methods for uncertainty assessment and for reconstruction of SMB, temperature and precipitation time series back in time, based on HIRHAM5. Altogether, this leads to the following PhD plan formulations:

"High-resolution regional climate modelling in the Arctic

The focus will be on performance of the regional climate model HIRHAM5 over Greenland and with a special emphasis of representing the local climate at the east cost of Greenland, in particular the complex Scoresbysund setting. Focus is on local surface mass balance over the ice sheet and the Renland glacier in particular. The work will contribute to the development of a dynamic high-resolution system model of the Greenland ice sheet, the coastal regions and interactions with the surrounding ocean,

and to study changes to the ice sheet as a consequence of changes in Arctic climate and sea ice."

"The state-of-the-art model, HIRHAM5 will be validated for present day conditions emphasizing East Greenland and the Renland glacier in particular. This will be done by gathering additional observations to existing data sets for the region. Some of these data will utilize the ice2ice consortium (NBI and Uni Bergen) to access both in situ as well as proxy data that can represent climate parameters for this part of Greenland. Work will go into analysing detailed surface characteristics that has not been scrutinized sufficiently to secure the necessary accuracy. E.g. it is known that data sets used to characterize the glaciated and unglaciated have certain inconsistencies."

"The overall objective of these efforts is to investigate if the regional climate signal over East Greenland/Renland is consistent with an overall working hypothesis in ice2ice, namely that sudden reductions in sea ice was a key player in explaining the abrupt temperature changes in the past (Dansgaard-Öschger events). For such consistency analysis the model results will be compared with climate reconstructions from the ice2ice activities both on Renland and on the continental shelf, which is at the core of ice2ice activities at NBI and in Bergen, respectively."

Validation of the HRIHAM5 is done by combining information already available from the regional and global climate model communities and information from in situ weather records and ice core proxy data, by introducing new statistically founded methods. This comprises development and quantification of relevant climate indices including associated uncertainties. It also involves identifying spatially linked weather patterns across Greenland as well as prolonging and repairing weather records and climate model simulations. Paper I focuses on multi model inter-comparison of HIRHAM5, whereas Paper II focus on validation of HIRHAM5 against observations.

Paper I: In addition to high-resolution climate simulations, climate adaptation in Greenland is highly dependent on the associated uncertainty estimates. A single high-resolution RCM is generally insufficient to quantify the uncertainty of a given scenario projection. For Greenland this is a challenge due to lack of costly high-resolution experiments for this region. Therefore, a new method to assess climate projection uncertainties is introduced and validated in Paper I.

The hypothesis is that the uncertainties of climate indices deduced from a high-resolution RCM can be quantified via an ensemble of GCMs knowing the relationship between the

RCM indices and the driving GCM temperature. Besides a model inter-comparison task with focus on HIRHAM5, this leads to the following more specific research questions:

Q1. To what extend is climate change information and associated uncertainties quantifiable from a single high-resolution climate model simulation?

Q2. Is the relationship between RCM derived indices and GCM temperature a general condition or specific for the HIRHAM5-EC-Earth model setup?

Q3. Is the relationship between HIRHAM5 indices and temperature from its driving GCM transferrable from one region to another?

Q4. Is the variance of the RCM ensemble used in this study embraced by the variance of corresponding ensemble of GCMs?

Q5. Model Intercomparison: Is HIRHAM5 a representative RCM among other of RCMs?

Paper II: In an ice2ice perspective, it is highly relevant to reconstruct the dynamically consistent HIRHAM5 simulated SMB back in time, using ice cores for every drainage basins to cover the entire Greenland ice sheet. A reconstructed SMB time series covering the entire Greenland ice sheet will enable investigating the ice2ice main hypothesis, of abrupt changes of the Greenland ice sheet and dynamical processes linked to changes in the Arctic sea ice. Spatial correlation maps are prepared for temperature and precipitation fields from a HIRHAM5 simulation based on atmospheric re-analysis data. The correlation patterns are validated against in situ observations and applied for extending observation records as well as surface mass balance simulations for the Greenland ice sheet back in time. The following research questions are addressed in Paper II:

Q6. Validation of HIRHAM5 with observations: Do weather observations agree with the simulated correlation patterns for temperature and precipitation?

Q7. Can changes in surface mass balance trends be identified from reconstructed climate model simulations?

Paper III: The HIRHAM5 historical simulation (1991-2010) is validated against observations of temperature and surface mass balance and a reanalysis simulation with focus on the area around Kangerlussuaq in west Greenland. Changes in precipitation and

temperature and surface mass balance of the ice sheet are quantified for two different scenarios mid-century and end-century, and the following hypothesis is addressed:

Q8. A high-resolution climate simulation (5.5km) will add value to the representation of weather and climate information both on and off the Greenland ice sheet. And in addition to a re-analysis downscaling experiment based on observations, a historical run based on a GCM is necessary to quantify unbiased projected climate changes.

Paper IV: The contribution to Paper IV serves as an example of applying spatial correlation patterns of temperature for validating ice core proxy signals for δ18O and for localizing significantly correlated observation records in an ice2ice relevant context. This paper also prepares the ground for SMB time series reconstruction several thousand years back in time based on an RCM simulation and ice cores, instead of an RCM and in situ observations as in Paper II. This will be discussed in Chapter 7.

3 General introduction

This chapter will give a short introduction to the scientific background for the research presented in this thesis with focus on observations and future projections of the global climate and the climate in Greenland in particular. The level of detailed climate information in Greenland will be a central point in the following chapters.

3.1 Observed global temperature

Global mean temperature has been observed for many decades (IPCC, 2013), and it has increased on the order of 1 ˚C over the last 100 years, see Figure 3.1 which shows the global mean temperature provided by The Hadley Centre/CUR (Jones et al., 1999), NASA/GISS (Hansen et al., 2010), NOAA/Global temperature (Zhang et al., 2015) and ERA-Interim (Dee et al., 2011). An important thing to notice here, is that the differences between the four datasets are minor compared to the overall global warming. The warming rate is varying due to natural variability and a slowdown in the temperature increase, often referred to as the hiatus was observed from the beginning of the 21st century and about 10 years ahead. Contributors to the slowdown are proposed to be volcanic eruptions (Haywood et al., 2013; Santer et al., 2014), enhanced heat uptake in the deep ocean (Chen and Tung, 2014; Meehl et al., 2011; Watanabe et al., 2013), Pacific surface cooling (Kosaka and Xie, 2013) and changes in wind driven circulations (England et al., 2014). Huber and Knutti (2014) concludes that there is "little evidence for a systematic overestimation of the temperature response to increasing atmospheric CO_2 concentrations in the Coupled Model Intercomparison Project (CMIP5) (Taylor et al. 2011), from the beginning of this century. Nevertheless, the slowdown has come to an end in recent years (again see Figure 3.1), and stronger warming trends together with reconsolidating climate models makes it more confident than previously that human activities have strong impacts on the long-term global warming (Medhaug et al., 2017; Rahmstorf et al., 2017).

The differences between the global mean temperature anomalies datasets in Figure 3.1 are mainly due to how the four institutes calculating the time series, treat the data. NOAA

for instance is relatively conservative and fills fewer gaps. NASA on the other hand assumes that temperature anomalies stay coherent at distances of up to 1200km from a weather station. CRU discards all grid cells with no observations during a month. This result in different spatial observation coverage and hence different global mean temperature estimates. However, since 1990 the estimated temperature anomalies from the four institutes tend agree more than previous decades.

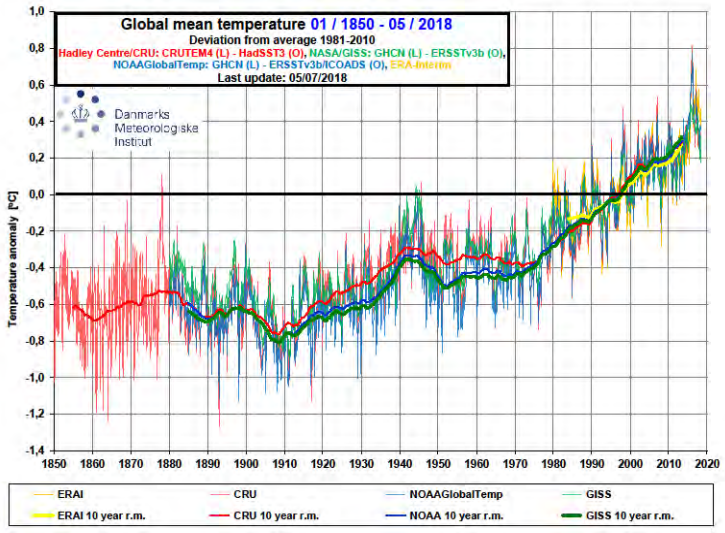

Figure 3.1: Global mean temperature relative to the 1981-2010 observed since 1850 from 4 institutes (NCDC (blue), GISS (green), CRU (red) and ERA-Interim (yellow)). Thin lines are monthly mean temperatures and thick lines are 10 year running mean values. From (Stendel and Olesen, 2018).

The spatial distribution of the temperature increase from NOAA's Merged Land–Ocean Surface Temperature (IPCC, 2013; Vose et al., 2012) is shown in Figure 3.2 as linear trends from 1901-2012, although most warming occurred from 1900 to around 1940 and again from the beginning of the 1970's, which stands out distinctly in Figure 3.1. The spatial warming distribution highlights the regional temperature-sensitivity to climate change. A notable feature clearly emerging in Figure 3.2 is the relatively large area in the North Atlantic Ocean with a negative temperature trend, the so-called "cold blob". This feature is placed just south of deep convection zone, indicating that it involves an adjustment of this circulation and is linked with the weakening of the Atlantic meridional overturning circulation (AMOC) (Drijfhout et al., 2012). The cold area is possibly a result of cold surface water building up in the North Atlantic instead of sinking, caused

by additional cold fresh water from the rapid melting of the Greenland ice sheet and glaciers. This disturbs the Atlantic overturning circulation and will also have an effect on future climate projections (Rahmstorf et al., 2015).

Another important detail is the sparse observation coverage in the Arctic region, which may have caused an underestimated trend during 1998-2012 (Cowtan and Way, 2013; Rahmstorf et al., 2017). The sparsely coverage of in situ observations is also seen for both temperature and precipitation in Greenland in Figure 3.4, (Cappelen, 2018).

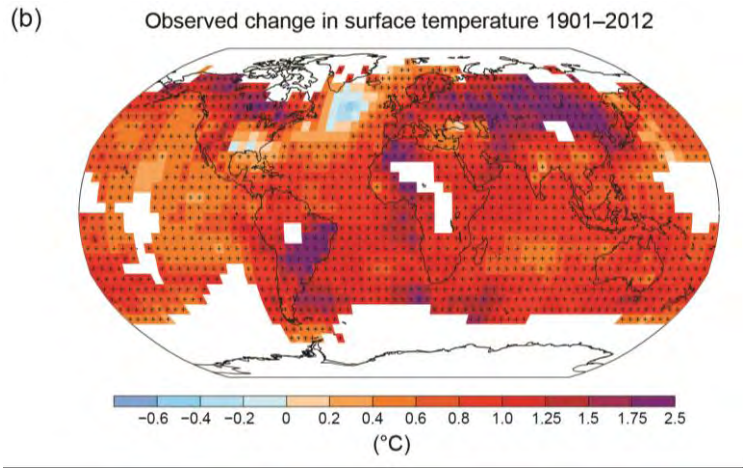

Figure 3.2: Observed changes in surface temperature from 1901 – 2012 calculated as linear trends. The plot is based on NOAA's land-ocean temperature (Vose et al., 2012). Black plus signs indicate statistically significant trends at a 90% confidence level. White areas indicate insufficient observation coverage. The light blue in the North Atlantic show a cooling in the sub-polar North Atlantic ("the cold blob"). From (IPCC, 2013).

3.2 Observations in Greenland

Temperature and precipitation have been observed in Greenland for more than 100 years. Ilulissat and Qaqortoq reach back to 1808 and Nuuk back to 1785 (see Figure 3.3). For the first decades of the records, however, the data quality is poor. Different types of errors have been characterized: "Peak values" (values that are clearly inconsistent with the general the time series trend), "offset values" (consecutive values that suddenly changes to a different value level, typically caused by instrument calibration), "frozen

values" (stalled values over a period of time), "scattered values" (values including missing time steps) and simply missing values (Boas and Wang, 2016) and thus the datasets are comprehensively quality controlled and errors have been removed. This means that missing data do occur regularly due to the challenging weather conditions and remote locations, where calibration and maintenance is done infrequently (Today, less than annually. In the past many stations were manually surveyed on a daily basis).

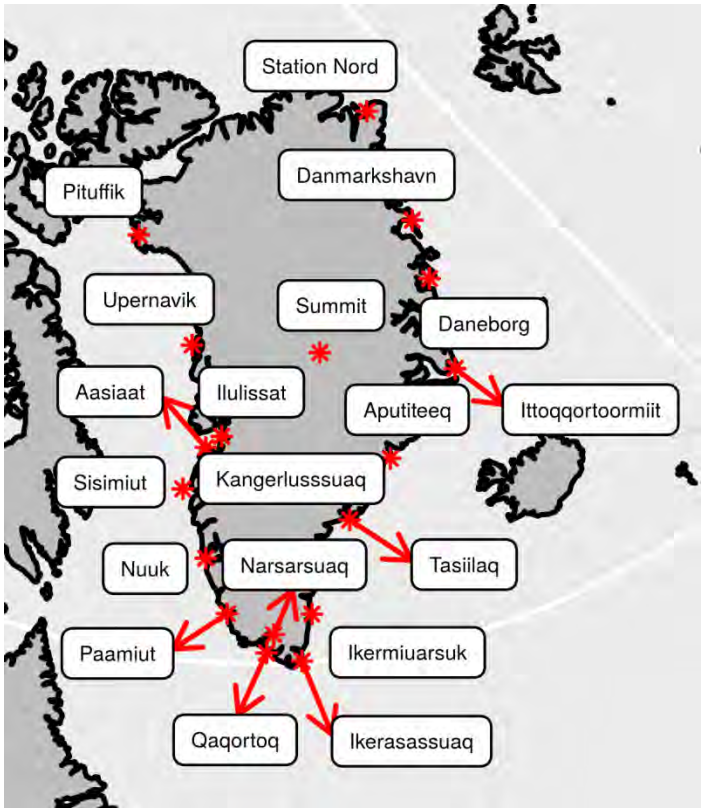

Figure 3.3: Location of the 19 weather stations used in this research.

A selection of the highest quality time series for temperature (measured 2 m above the ground) and precipitation (measured 3 m above the ground) are presented as annual mean and accumulated values respectively in Figure 3.4 and Figure 3.5. For temperature the values are relative to the mean of the observation period. A common reference period is problematic as a result of missing data and different lengths of the observation records.

Temperature observations in Greenland show a very strong warming the recent 20 to 30 years most pronounced at the west coast. Dividing the annual temperature records into

seasons the recent warming is strongest during the winter season (Hanna et al., 2012, 2008). Before the 1990 the records does not show any significant increase for annual mean temperature.

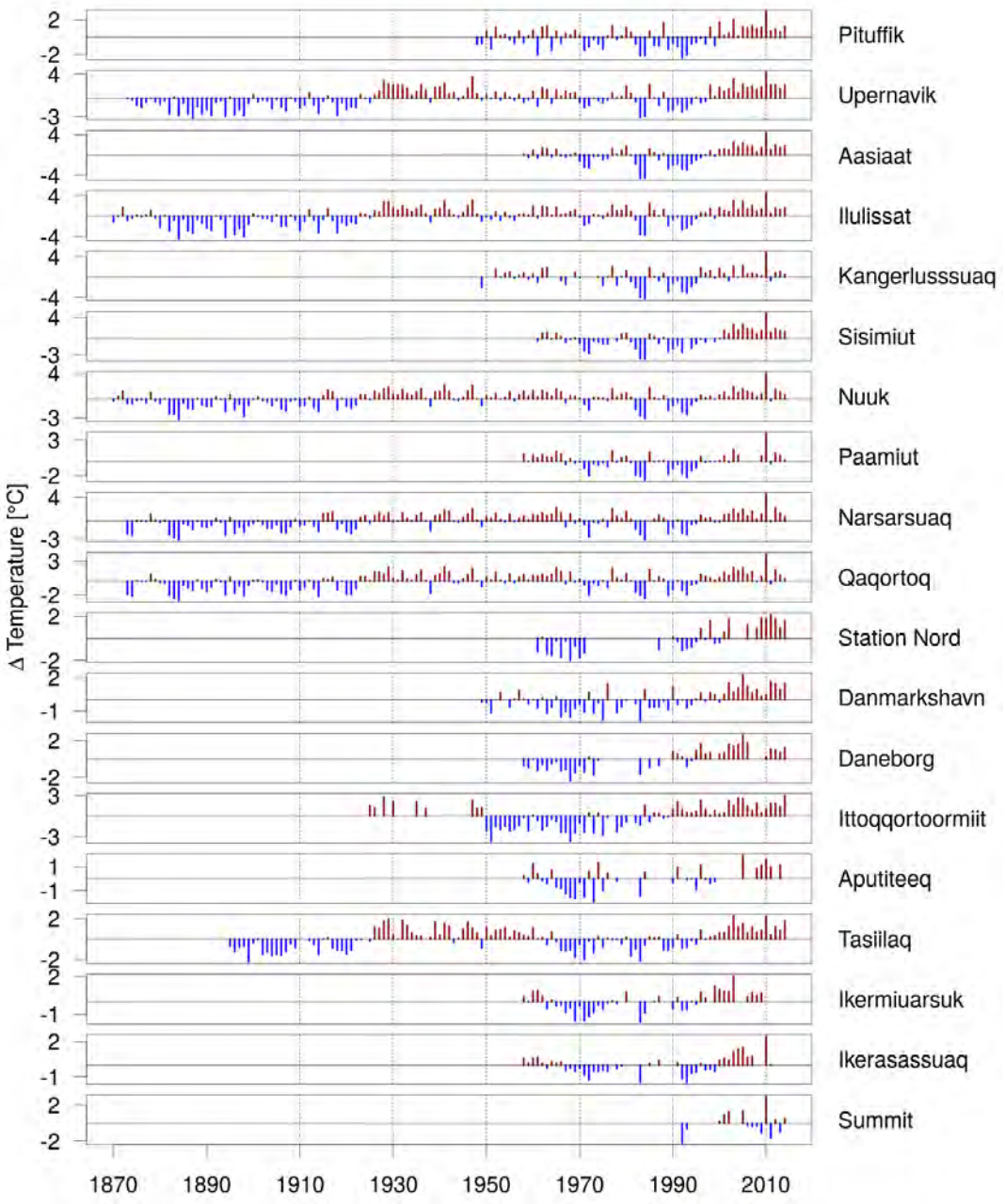

Figure 3.4: Annual mean temperature observed from DMI-weather stations along the coast in Greenland. Temperatures are normalized to the mean of the time series, where blue and red bars are smaller and larger than the mean. Only annual values with full monthly coverage are represented.

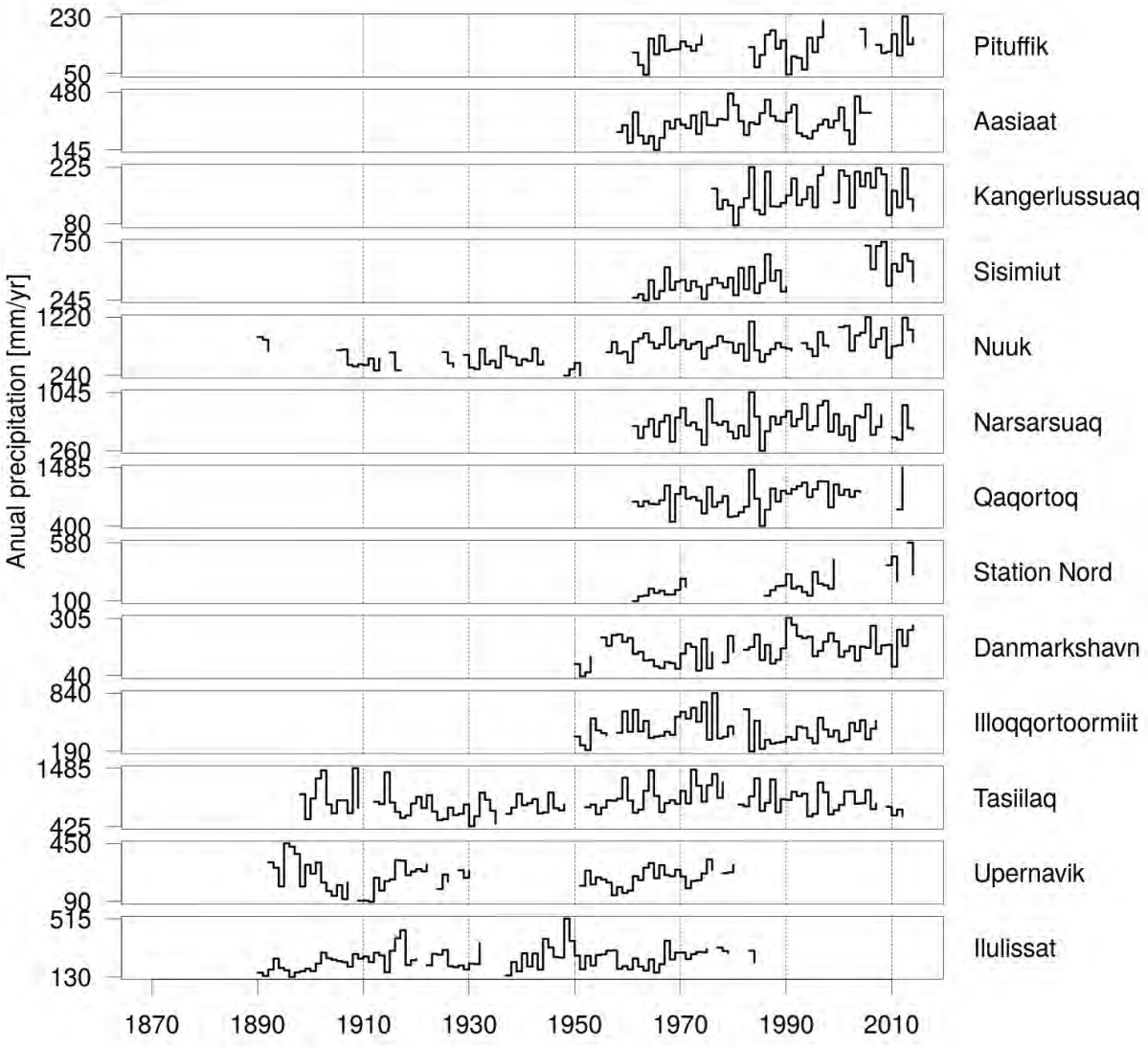

Figure 3.5: Annual precipitation observations from DMI-weather stations along the coast in Greenland. Only annual values with full monthly coverage are represented.

By comparison to temperature, potential changes in precipitation during the measurement period are relatively unclear. Figure 3.5 indicates that the quality of precipitation observations is poor in general and underlines the need for methods of reconstructing the time series and of closing the gaps. In addition to this, errors in precipitation measurements associated with snowfall and drifting snow are difficult to correct for. Less than 50% of the actual precipitation falling as snow will be caught in a unshielded

precipitation gauges, when the wind speed exceeds 5 m/s. (Kochendorfer et al., 2017). Functions to correct for that kind of errors are developed, but typically require wind speed as input, which is problematic for the long weather records in Greenland, where wind has not been continuously measured.

3.3 Projected global climate change

The ongoing and future climate change depends above all on the concentration of greenhouse gases in the atmosphere (IPCC, 2013). Global circulation models (GCMs), also referred to as general climate models or earth system models (ESMs) are used to simulate projections of the future global climate on the basis of the greenhouse gas concentration in the atmosphere now and throughout the 21st century. A group of various climate modellers and emission experts have within the framework of IPCC developed four scenarios of Representative Concentration Pathways (RCPs) that describes different trajectories of greenhouse gas emissions. The four scenarios are RCP2.6, RCP4.5, RCP6.0 and RCP8.5, where the numbers indicate the radiative forcing in W/m^2 in year 2100. In this project only RCP4.5 and RCP8.5 are applied. RCP8.5 determines an increasing radiative forcing pathway leading to 8.5 W/m^2 in 2100 and continuing beyond 2100. RCP4.5 is an a stabilization scenario, where the radiative forcing increases and stabilizes at 4.5 W/m^2 in 2100 (Vuuren et al., 2011).

The climate system includes a variety of physical processes, such as cloud processes and radiative processes, which interact on both temporal and spatial scales. Due to the limited resolution of the models, many of these processes are not resolved adequately by the models and must therefore be parametrized. Different parametrizations are an important reason why climate model results differ (Lock, 2001).

GCM results are compared in the Coupled Model Intercomparison Projects CMIP, established by the Working Group on Coupled Modelling (WGCM) in 1996 supported by the Earth System Grid Federation (ESGF), which is a decentralized database for handling climate science data. CMIP is currently preparing its phase 6, whereas the GCMs used in this research are 39 GCMs from phase 5 (CMIP5), as listed in Appendix A,
Table A-1. CMIP5 promoted a standard set of model simulations in order to evaluate how realistic the model simulations are in representing the recent past and the future climate change, and to understand some of the factors responsible for differences in model projections. This includes quantifying some key feedbacks such as those involving clouds and the carbon cycle (Taylor et al., 2011).

According to (IPCC, 2013) there is very high confidence that models reproduce the general features of the global-scale annual mean surface temperature increase over the historical period, including the more rapid warming in the second half of the 20th century, and the cooling immediately following large volcanic eruptions.

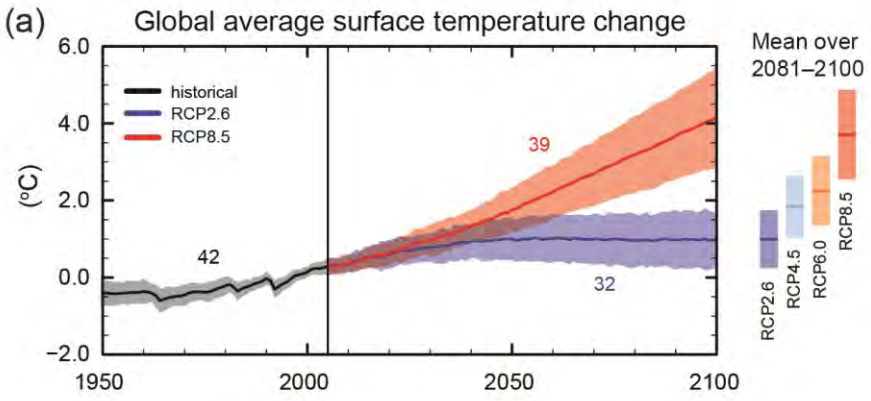

Figure 3.6: Global mean temperature change relative to 1986-2005 simulated by CMIP5. The control run 1950-2005 has been simulated with 42 GCMs (black line), future projections for scenario RCP8.5 is simulated with 39 GCMs from 2005 to 2100 (red line) and 32 GCMs have simulated the temperature change for the RCP4.5 scenario (blue line). The shaded areas correspond to the 66% likely range of the model ensemble.

GCMs simulate the global climate at relatively course resolution (100-200 km). On this scale Greenland is often represented as one big block of ice with no ice free land surrounding it. Furthermore, they are not accounting for physical processes at the surface of the ice sheet (Cullather et al., 2014). Therefore downscaling is highly required to extract climate information on very local scales, as shown by e.g. Boberg et al. (2018) and Lucas-Picher et al. (2012). Downscaling is a method for obtaining high-resolution climate information from global climate models (GCMs) with a relatively coarse resolution (100 to 300 km). A dynamical downscaling is done with an RCM with a relatively high resolution (10-50 km) for a limited sub-domain driven by boundary conditions from a GCM.

3.4 Projected Arctic climate change

The Arctic plays an important role in the global climate system and has notable influence on the global energy budget. The region has for instance contributed to the continental global warming during the recent decades (Huang et al., 2017). For the arctic region the CMIP5 ensemble exhibits additional warming referred to as the polar amplification (Bracegirdle and Stephenson, 2012). The influence also occurs from opposite directions. For instance, changes in the Greenland blocking index (the 500 m geopotential height for the area averaged over 60-80˚N and 280-340˚E, as defined by Fang (2004)) is related to changes in temperature and precipitation beyond Greenland and the Arctic (Hanna et al., 2016).

A subset of GCMs from CMIP5 is downscaled with different RMCs for the Arctic and is available within the COordinated Regional climate Downscaling EXperiment (Arctic-CORDEX. The GCMs are dynamically downscaled to a pan-Arctic domain at a 50 km horizontal resolution (Koenigk et al., 2015). Data available for this region is mainly targeted analysis on larger scales like Arctic conditions linked to the Atlantic Oscillation (AO), North Atlantic Oscillation (NAO) and Greenland blocking index (GBI), like e.g. Akperov et al. (2018).

For climate analysis in Greenland with focus on villages, a spatial resolution finer than 50 km is required, as the topography is complex and exhibits large variations within one 50 km grid cell. So, for this purpose high-resolution downscaling experiments are necessary.

This also leads in the direction of the scope of this PhD project, which is to improve the knowledge we already have available, by introducing new statistically founded methods. This involves development and quantification of relevant climate indices as well as associated uncertainties. Furthermore, it also involves information about spatially linked weather patterns across Greenland to be prolonged and expanded temporally and spatially. The outcome will be a longer time span coverage with reliable weather information for the Greenland domain on a very high spatial resolution.

Chapter 4 presents results from a 5.5 km dynamical downscaling with the RCM, HIRHAM5. Chapter 5 introduces a statistical method to evaluate the uncertainty of the results presented in chapter 4, and in chapter 6 the HIRHAM5 simulation is compared to in situ observations.

4 Data applied for climate adaptation in Greenland

This chapter presents parts of the scientific reports on climate change in Greenland (Christensen et al., 2015a-g), which include climate projections simulated with HIRHAM5 as well as a selection of climate indices derived from HIRHAM5. This chapter is based on the meteorological parts of the reports, including background information about the data. Here passages from the project assignment and selected paragraphs from the reports are translated and adjusted. Furthermore, this chapter gives an overall introduction to HIRHAM5, from which the focal model experiments throughout this PhD research are done. Finally, results from Paper III (Boberg et al., 2018) validating HIRHAM5 are presented.

4.1 The demand for improved climate data in Greenland

The future climate change in the Arctic regions is expected to be strong. Consequently, the living conditions for humans, animals and plants will change, and the Arctic society is facing a great challenge in order to adapt to the future climate. Greenlandic farmers experience that the natural agricultural production conditions have changed over recent years. This is assumed to be a consequence of global climate change (Lehmann et al., 2017). Recent evidence suggests that shrubs are currently expanding locally across the entire Arctic, although at regionally varying rates (Elmendorf et al., 2012).

New woody species are likely to enter Greenland during the 21st century. Normand et al., (2013) found that a majority of the non-native species are suitable for the climate conditions in certain parts of Greenland today, even in areas with no native trees. Observed tree planting approaches and analyses of analogous climate conditions elsewhere point towards the potential for invasions of woody species.

Even though conditions appropriate for certain wood and shrub species are present locally, specific information about where the conditions occur is essential. Therefore, assessment of climate change and its implications for the growing season and other climate indices requires high resolution historical data and projections in order to assess

temperature variations far from in situ temperature observations (Westergaard-Nielsen et al., 2018).

4.2 The initiative for the scientific reports I-VI

The Greenland Self-Government continually publishes climate change reports specified for key sectors in the society. In 2012, the consultancy COWI published data and reports regarding the impacts of climate change in Greenland; this data has until recently formed the basis of the climate adaptation reports in Greenland. The assessment of future climate change in Greenland was based on the relatively general assessment reports from the Intergovernmental Panel on Climate Change, IPCC, from 2007 (IPCC, 2007). Hence, focused future climate adaptation assessments on sector level, would require improved and updated climate information on regional scale.

The HIRHAM5 simulations establish an improved database and provide knowledge for climate change adaptation in Greenland, including both meteorological and oceanographic conditions. Based on an RCM, the aim is to determine likely regional climate change for Greenland, as well as to develop an easily accessible internet-based database for climate impact studies. The result will among other things contribute to assessments of the available data as guidelines for future data collection and monitoring. Furthermore, improved knowledge on climate change in Greenland contributes to the Greenland Self-Government's climate adaptation efforts and feeds directly into the sectoral climate adaptation reports and the Greenland Self-Government's cooperation on climate adaptation with the municipalities and other national stakeholders (e.g. within the framework of the Arctic Council, https://arctic-council.org/index.php/en/).

HIRHAM5 is developed further within activities at Greenland Climate Research Centre at Greenland Institute of Natural Resources, and enables analysis of climatic conditions in Greenland at a 5.5 km spatial resolution. Hereby, many of the climatic conditions related to Greenland's complex topography of fjords and mountains can be described in detail for the first time. To meet the Greenlandic Self Government's demand for climate information, a catalogue covering the entire Greenland is provided. The catalogue comprises 66 different indices based on data from HIRHAM5. Together with the scientific Greenland climate reports, the catalogue supplies short and long term projections as maps for the twenty-year time slices 2031-2050 and 2081-2100.

All future projections are based on the RCP scenarios (Vuuren et al., 2011). By use of statistical methods, results from HIRHAM5 are related to projections based on the more general global simulations which the latest IPCC assessment report is based on. This

method provides the possibility to estimate the accuracy of the indices provided in the catalogue (Christensen et al., 2015g).

4.3 User involvement

Development of relevant climate indices is done through dialogue with the end-users from relevant sectors in Greenland. The involvement of stakeholders and end-users in general was done through a user workshop in Nuuk in November 2015

The workshop was targeted at end-users like Greenlandic citizens and stakeholders from different relevant sectors. The workshop consisted of presentations of the new climate data available for climate change adaptation in Greenland, including the preliminary developed climate index, and was followed up by group discussions where challenges and opportunities related to climate change were discussed.

The workshop highlighted the following challenges:

- A warmer climate will lead to new species, including invasive species, varieties and diseases.
- Cold weather operations will be challenged, including cultivation of potatoes.
- The future precipitation will not necessarily fall when the need is there. The rain events will be more extreme and occurrence less often during the summer.
- Extreme precipitation will result in soil depletion (lime and fertilizer). Thus, restoration will be more time consuming.
- More time and resources on preventive work is required.

And the following possibilities:

- Less cold summers will result in faster growth rates.
- Production of new species.
- Agricultural areas can be made wider and expanded with e.g. cattle.
- Increased production of roughage and hay will mean less import.
- Greater self-sufficiency in the country.
- Be sustainable economically.
- Longer season for tourism.
- Use of wild animals that do not need feeding.

The challenges are primarily dominated by increasing temperatures and changes in precipitation patterns on local scale, whereas possibilities mainly are temperature dependent. The outcome from the workshop is in line with Arctic Council report (AMAP,

2017a). The Arctic Council concludes that a climate adaptation strategy should reflect a broad context involving socio-economic and ecosystem factors as well as local knowledge from residents in relevant areas. Furthermore, the Arctic council underlines the importance of leadership at national, regional and local level combined with the need of useable scientific background.

Solutions to meet the challenges were discussed, leading to the following conclusions. There is a wish to establishing a task force and online platform that will contain data and input from researchers, stakeholders and other end-users, to ensure gathering of knowledge and a continuous dialogue about climate adaptation. The task force should provide an overview of potential synergies concerning climate challenges and cross-sectoral opportunities as well as broad scientific climate information. In this way, transparency among sector plans can be maintained.

Now, more than two years later a common online platform is up and running. Here, a selection of projected climate indices is available in NunaGis, a web based map tool (Asiaq, 2018, https://kort.nunagis.gl/klimadata/#about). Various kinds of material have been prepared and distributed to different target groups, e.g. climate relevant teaching material based on the climate simulations from HIRHAM5 for high schools and easy-to-reach material consisting of selected climate index examples for the municipalities.

4.4 HIRHAM5 – a regional climate model

The development of HIRHAM was first documented in 1992 by Christensen and Van Meijgaard (1992). HIRHAM combines physical parameterization from the General Circulation or Climate Model (GCM) ECHAM used at the Max Planck Institute for Meteorology in Hamburg, and dynamics from the Nordic - Dutch - Irish HIgh Resolution Limited Area Model (HIRLAM). Since then the model has been subject to general updates (Christensen et al., 2006) to newer versions of HIRLAM and ECHAM, resolution optimization, and improvements consisting of additional schemes for e.g. ice dynamics (Langen et al., 2015; Lucas-Picher et al., 2012; Mottram et al., 2017b). HIRHAM5 is in its latest version a combination of dynamics from the numerical weather prediction model HIRLAM7 (Eerola, K, 2006) and physics from the GCM ECHAM5 (Roeckner et al., 2003). The subsurface scheme in HIRHAM5 has been extended to deal with liquid water flow and retention on the Greenland ice sheet (Langen et al., 2017)

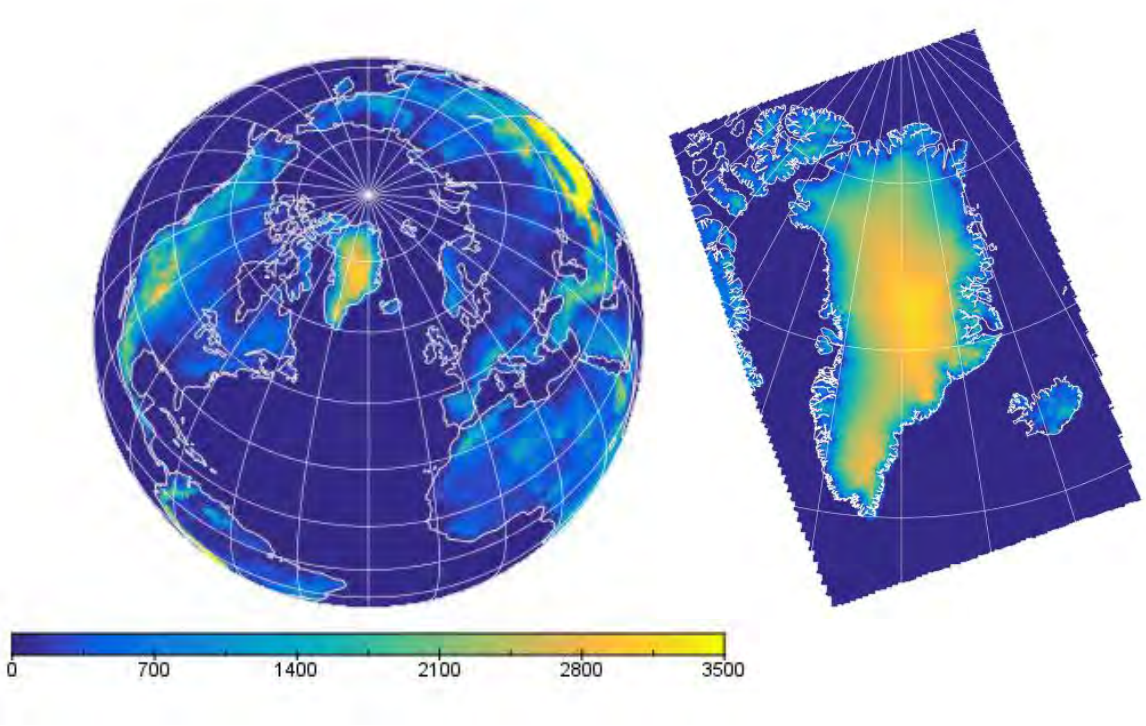

Figure 4.1: Global topography as described in the GCM, EC-Earth (left) and topography from the climatology in the RCM, HIRHAM5 (right) shown for the downscaling domain over Greenland and Iceland. The domain grid is a rotated lat-lon grid with North Pole at latitude = 37˚N and longitude = -153˚E.

HIRHAM5 requires three types of input files: Boundary files, climatology files and sea surface temperature files. For the evaluation experiment used in this research, HIRHAM5 is forced with the European re-analysis dataset, ERA-Interim from ECMWF (Dee et al., 2011), on the lateral boundaries. For the scenario and control simulations, HIRHAM5 is nested in the GCM EC-Earth and forced with six-hourly lateral boundaries, and receives sea surface temperatures and sea ice coverage on a daily basis. EC-Earth is developed by the EC-Earth consortium (Hazeleger et al. 2012) and the version used in this study is configured at a 125 x 125 km resolution (T159) and uses 62 vertical layers. The simulation is calculated on a rotated longitude latitude grid, where the North Pole is rotated to 37˚N degrees and -153˚W.

For the Greenland simulations, HIRHAM5 is downscaled to a 0.05 × 0.05 degrees horizontal resolution (approximately 5.5 km). For downscaling to this relatively high resolution for Greenland it turns out that the parametrization is unproblematic. One reason may be that mass fluxes in Greenland are mainly dominated by large scale dynamics rather than convection on local scales (Chen et al., 1997), and hence less

resolution sensitive. A double nesting approach could be relevant for this dramatic resolution refinement from the ERA-interim resolution at 80 km to the HIRHAM5 resolution at 5.5 km, but as the downscaled domain is relatively large an intermediate resolution nesting is redundant and only results in minor differences (Larsen et al., 2013; Matte et al., 2016).

The evaluation experiment covers 35 years (1980-2014). Five different 20-year time slices are downscaled for the three periods 1991-2010 (a historical control run), 2031-2050 (for RCP4.5 and RCP8.5) and 2081-2100 (for RCP4.5 and RCP8.5). Notice that the reference period for this run differs from the standard reference period (1986-2005).

The importance of a present-day control run for future scenario runs was demonstrated in Boberg et al. (2018). Snowmelt and runoff are significantly smaller in the control run with EC-Earth on the boundaries than in the evaluation experiment with ERA-Interim on the lateral boundaries. Comparing EC-Earth driven scenarios with a corresponding EC-Earth driven control run assumes that the magnitude of the climate signal depends linearly of the reference state (Boberg and Christensen, 2012), which is not always a valid assumption for e.g. estimated surface mass balance of the Greenland ice sheet (Fettweis et al., 2012).

Results from the HIRHAM5 5.5 km-resolution downscaling for the Greenland domain is accessible in the reports (Christensen et al., 2015a-f) mentioned above. A small subset of climate indices derived from HIRHAM5 is presented in section 4.4.1.2.

4.4.1 Results from HIRHAM5 5.5 km downscaling

The scientific reports (Christensen et al., 2015a-f) present estimated and expected climate change in Greenland based on the latest RCP scenario calculations focusing on climate change within this century. The assessment of future climate change is based on RCP4.5 and RCP8.5 emission scenarios and climate changes are expected to increase towards year 2100. Projections of future climate change based on an ensemble of climate models are more robust, than estimates based on a single model (Christensen et al., 2007a; Madsen et al., 2012; Murphy et al., 2004; Parker, 2013). In this study robustness is used in line with the IPCC guidance, where “evidence is most robust when there are multiple, consistent independent lines of high-quality evidence” (Mastrandrea et al., 2011). Here a statistical method to better frame results based on the DMI high-resolution regional model is utilized to assess uncertainties of projected climate change results. Validation of this method is presented in chapter 5. Climate variability and change are from the

HIRHAM5 simulations expected to increase towards 2100 in terms of higher temperatures, more winter precipitation, more frequent and more extreme weather events and a continuing loss of sea ice.

For presenting the HIRHAM5 results Greenland is divided into 6 parts, the National park and the four municipalities: Kummune Kujalleq, Kommuneqarfik Sermersooq, Qeqqata Kommunia and Qaasuitsuq Kommunia, where Sermersooq is divided into a western and an eastern part, see Figure 4.2 and Figure 4.3. Meanwhile, Qaasuirsuq Kommunia has been split into two smaller municipalities, Kommune Qeqertalik and Anannaata Kommunia.

4.4.1.1 Temperature and precipitation

2-meter temperature and daily precipitation is standard output from the HIRHAM5 downscaling. From the projections in Figure 4.2, the temperature is expected to increase everywhere on the ice free land points in Greenland for the RCP8.5 scenario, 1-2 degrees already in 2031-2050 and up to 8 degrees in 2081-2100. In the late century plot in Figure 4.2 the polar amplification appears as northward heating gradient, with most warming in the northern part. For observed temperatures in the North Atlantic Ocean, there has been a cooling over the region south-east of Greenland, “the cold blob” (see Figure 3.2). For future climate projections this feature appears as an area with less warming in the North Atlantic Ocean and is linked to the weakening of the Atlantic meridional overturning circulation (AMOC) (Drijfhout et al., 2012).

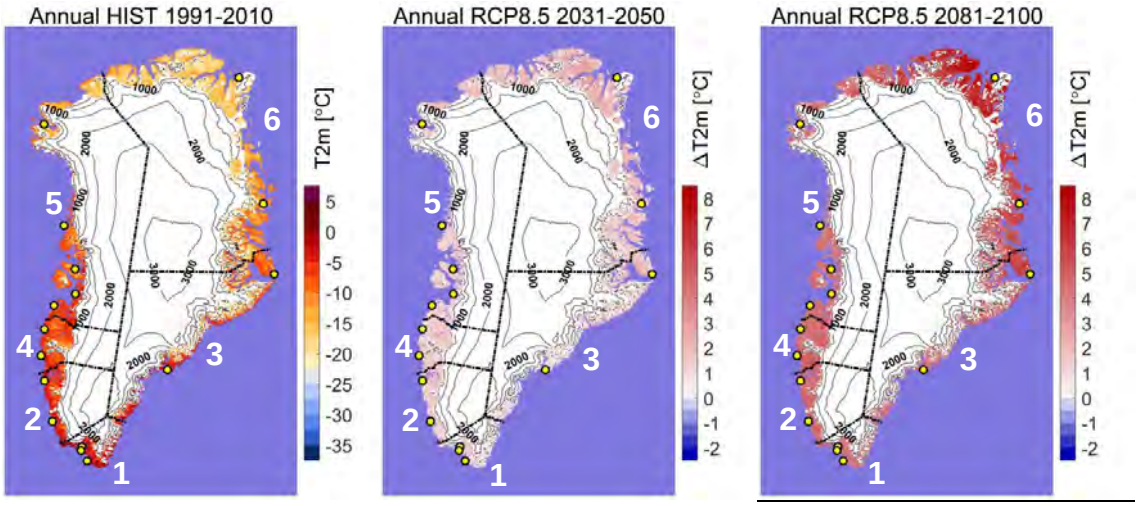

Figure 4.2: Annual mean temperature for a reference period (1991-2010), change 2031-2050 relative to 1991-2010 and change in 2081-2100 relative to 1991-2010 (from left to right) Greenland is divided into 6 parts (numbered on the right map): Kummune Kujalleq (1), Kommuneqarfik Sermersooq west (2), Kommuneqarfik Sermersooq east (3), Qeqqata Kommunia (4), Qaasuitsuq Kommunia (5) and the National park (6). From Christensen et al. (2015g).

For precipitation the projections are less robust than for temperature, some simulations predict more precipitation in Greenland and some predict less. The HIRHAM5 downscaling show a precipitation increase in some parts of Greenland e.g. the northeast coast and a reduction in other parts e.g. the southeast coast in 2031-2050, whereas more precipitation is expected for the whole domain by the end of the 21st century for the RCP8.5 scenario.

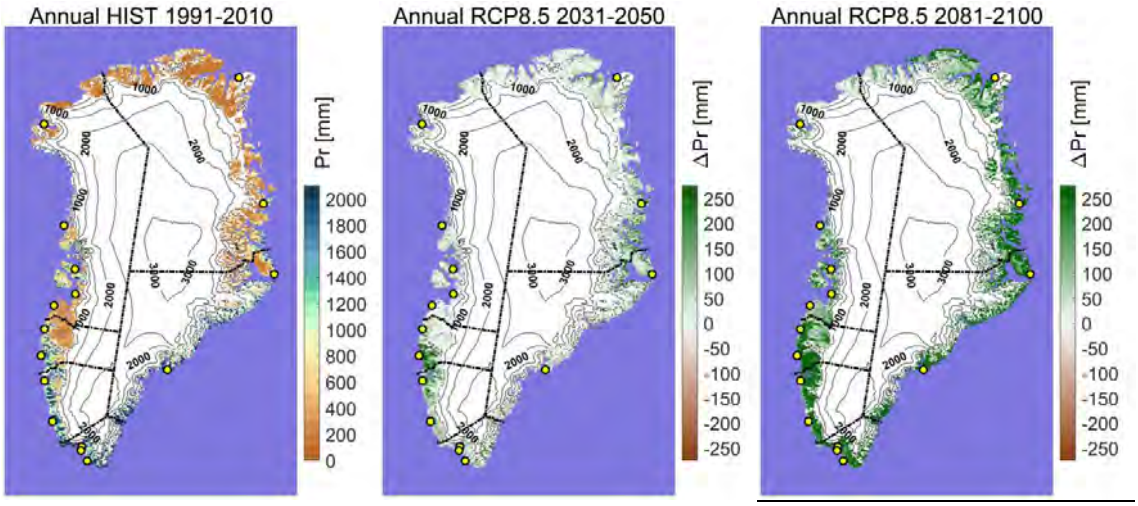

Figure 4.3: As Figure 4.2 but for annual precipitation.

4.4.1.2 Examples of climate indices for Kujalleq Kommune

On the basis of temperature, precipitation, wind and humidity from HIRHAM5 a list of 66 climate indices are calculated, see Appendix A, Table A-2. Here 3 examples of climate index developments calculated from HIRHAM5 are shown: Growing season onset, growing season length and permafrost index. The two first will be evaluated in the following sections.

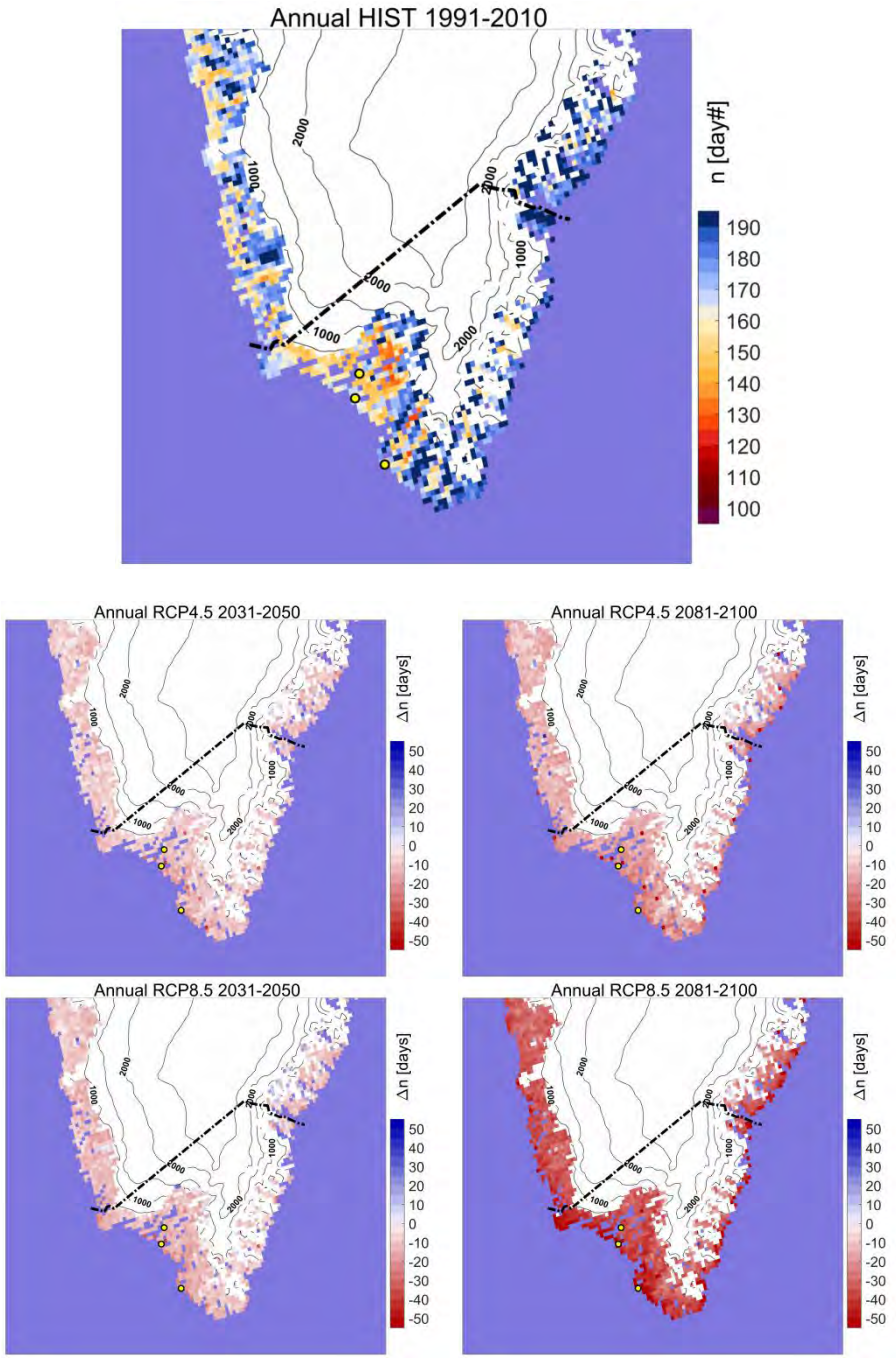

Figure 4.4: Growing season onset (day number) downscaled to 5.5 km for a control run 1991-2010 (a), for the RCP4.5 scenario (b) and (c) and for the RCP8.5 scenario (d) and (e). The scenario runs are changes in day number with respect to the control run and displayed as mean changes for periods 2031-2050 (b) and (d) and 2081-2100 (c) and (e). The white area is regarded as fixed ice sheet in the simulation and the black line is the Kommune Kujalleq municipality border. From Christensen et al. (2015a)

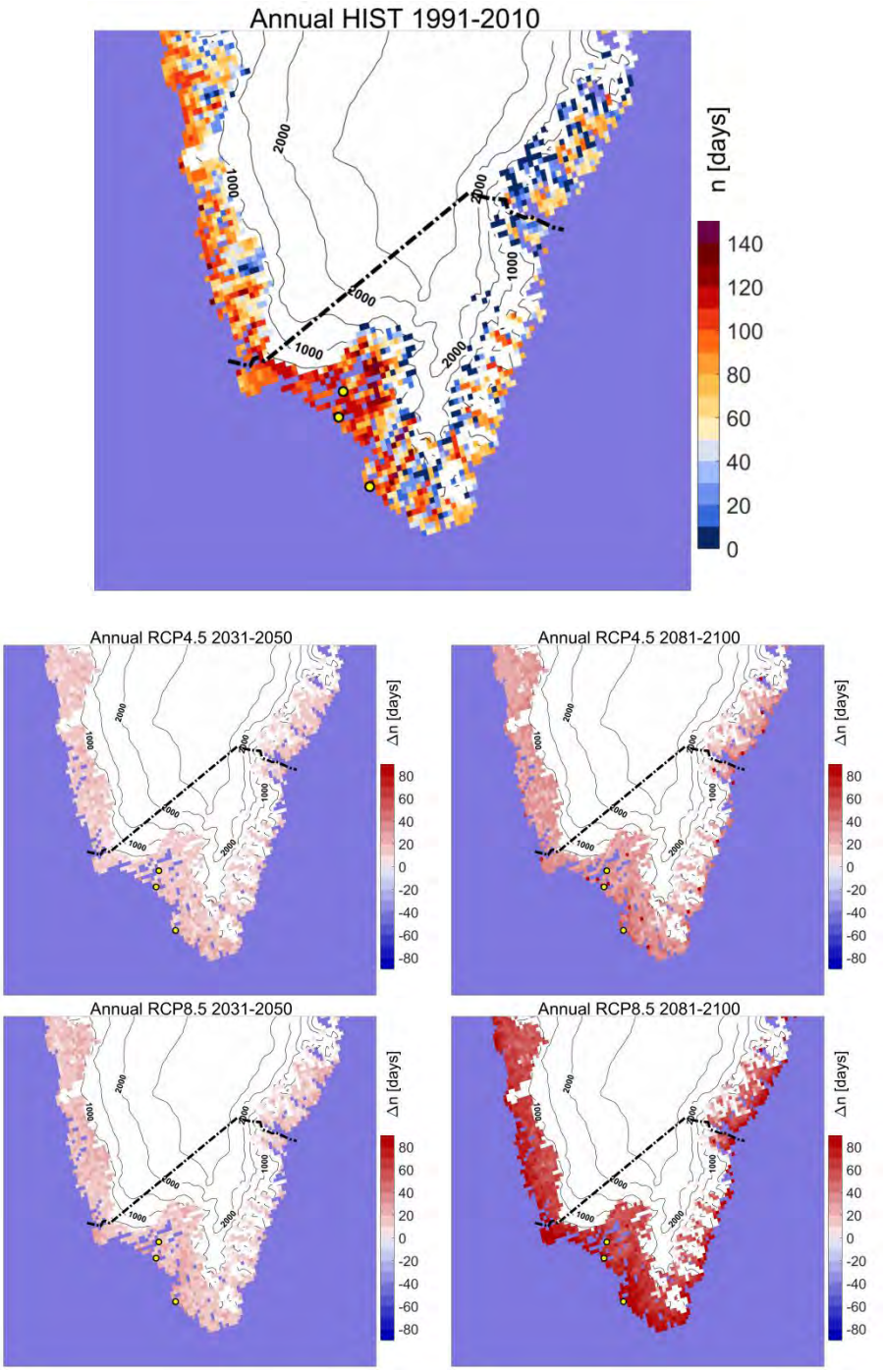

Figure 4.5: Growing season length (days) downscaled to 5.5 km for a control run 1991-2010 (a), for the RCP4.5 scenario (b) and (c) and for the RCP8.5 scenario (d) and (e). The scenario runs are changes in number of day with respect to the control run and displayed as mean changes for periods 2031-2050 (b) and (d) and 2081-2100 (c) and (e). The white area is regarded as fixed ice sheet in the simulation and the black line is the Kommune Kujalleq municipality border. From Christensen et al. (2015a)

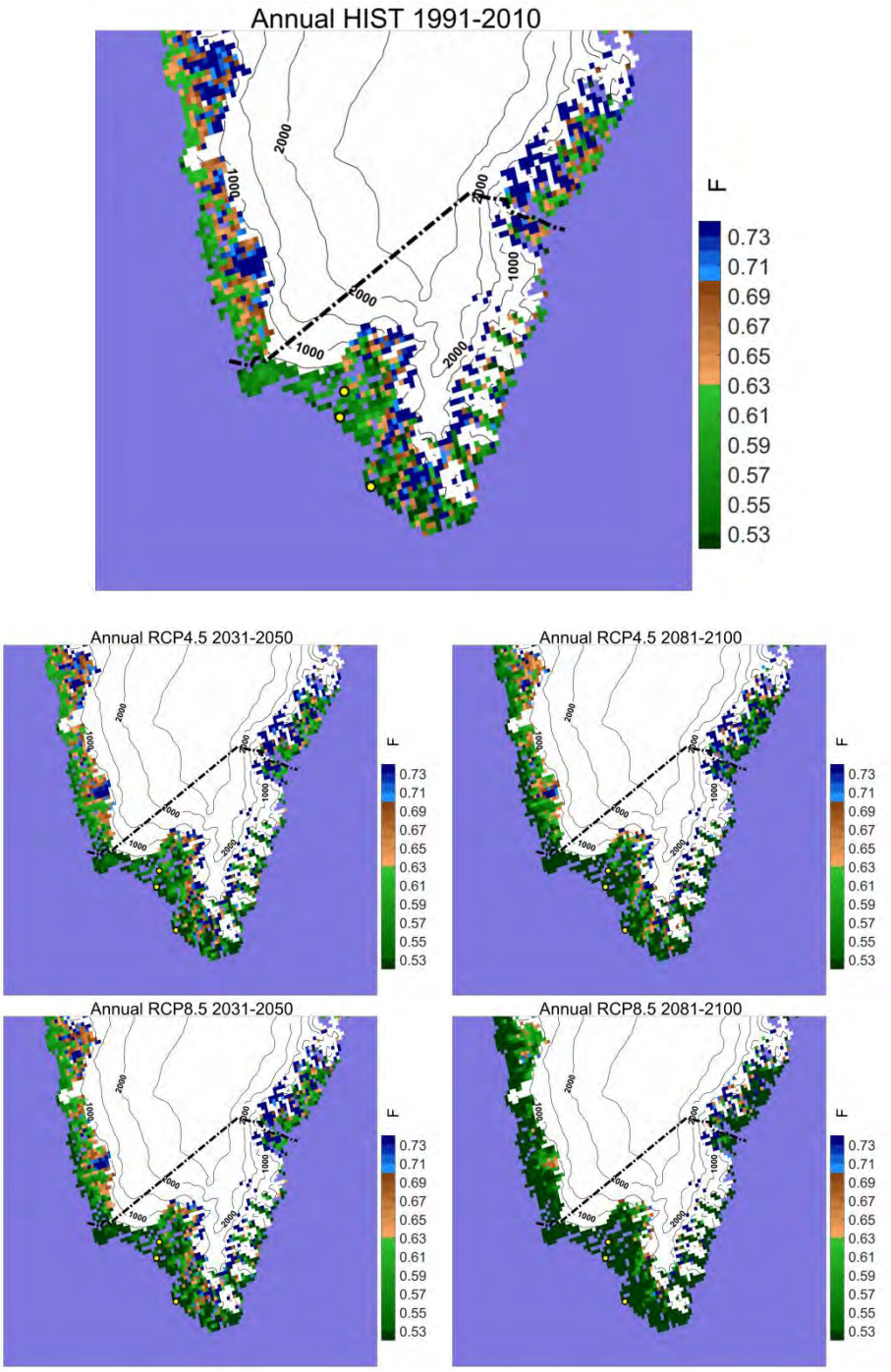

Figure 4.6: Permafrost index calculated from the 5.5 km HIRHAM5 simulation for a control run 1991-2010 (a), for the RCP4.5 scenario (b and c) and for the RCP8.5 scenario (d and e). The scenario runs are displayed as mean index values for periods 2031-2050 (b and d) and 2081-2100 (c and e). The white area is regarded as fixed ice sheet in the simulation and the black line is the Kommune Kujalleq municipality border. From Christensen et al. (2015a)

4.4.2 Climate change in Qeqqata in west Greenland

Boberg et al. (2018) focus on climate change on and off the ice sheet with the 5.5 km resolution model setup for the Qeqqata municipality. Here an increase in temperature and precipitation for the end of the 21st century are found to be between 2.5 and 3 °C for the RCP4.5 scenario and between 4.8 and 6.0 °C for the RCP8.5 scenario for ice free areas. For precipitation the increase is estimated to 20-30 % for the RCP4.5 scenario and 30-80 % for the RCP8.5 scenario. Temperature increase and increased runoff rates from the glaciers have a clear finger print on the SMB, where the ablation area (the area on the ice sheet with negative SMB) expands to higher elevations, and causes the ice sheet to retreat.

A HIRHAM5-ERA-Interim and a HIRHAM5-EC-Earth driven historical run is validated against in situ observations for temperature in the area around Kangerlussuaq. Comparing the GCM-driven simulation with observations shows an offset of 4°C for both Sisimiut and Kangerlussuaq for temperatures below -10°C. Above -10°C both the ERA-Interim and EC-Earth driven simulation match very well observations as shown in Figure 4.7.

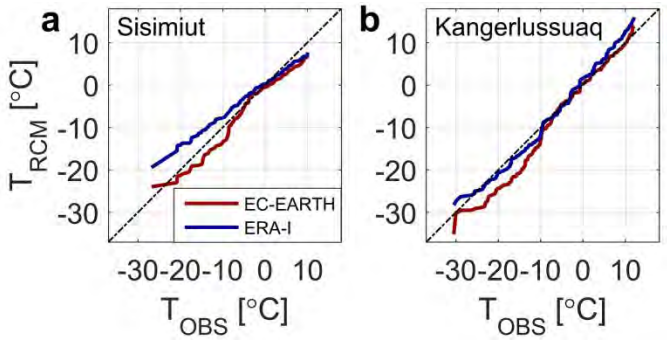

Figure 4.7: Q-Q plots of monthly mean temperatures (model vs. observations). The EC-Earth and ERA-Interim driven simulation are shown in red and blue. From Boberg et al., 2018.

The HIRHAM5 simulations are compared with six models with a 50 km horizontal resolution, demonstrating the need for high resolution model simulations over Greenland for the ice sheet grid points, especially for precipitation in areas with complex and steep topography. Further validation of HIRHAM5 against observations is shown in Paper II (Olesen et al., 2019) in Chapter 6, whereas a comparison with other RCMs is presented in paper I (Olesen et al., 2018a) in Chapter 5.

4.5 Robustness assessed with CMIP5

The global climate models in CMIP5, which form the basis of IPCC's assessment reports, also form the basis for the robustness of the data base we have developed with the HIRHAM5 model for the six scientific reports (Christensen et al., 2015a-f). In the reports we have chosen to provide a graphical evaluation of the projection based on the HIRHAM5 simulations, which establishes a link between the climate indices and the CMIP5 simulations.

Each index is correlated with annual mean temperature. The idea is that relatively simple relationships are expected between many of the derived climate indices and the corresponding temperature conditions. This is also confirmed by visual inspection of the plot in Figure 4.8. For each index, the best fitted regression line is specified and facilitates a simple scaling of the HIRHAM5-simulated data on the basis of the entire CMIP5 ensemble.

As an example, the index growing season length based on 5 ° C in Figure 4.8 shows the relationship between index and average temperatures for each of the years in all HIRHAM simulations as one dot - current climate (1991-2010); RCP4.5 and RCP8.5 (2031-2050); RCP4.5 and RCP8.5 (2081-2100). The colour indicates which simulation, the data is derived from. The brown regression line is the best fit for data points.

The vertical green line in Figure 4.8 shows the mean temperature for the CMIP5 models for the RCP8.5 scenario, in the period 2031-2050 and for South Greenland. The point where the green line intersects the brown curve corresponds to the growing season index value for the CMIP5 models. A measure of uncertainty is then derived by using the spread corresponding to 1 standard deviation of temperature projected by the CMIP5 models for the area.

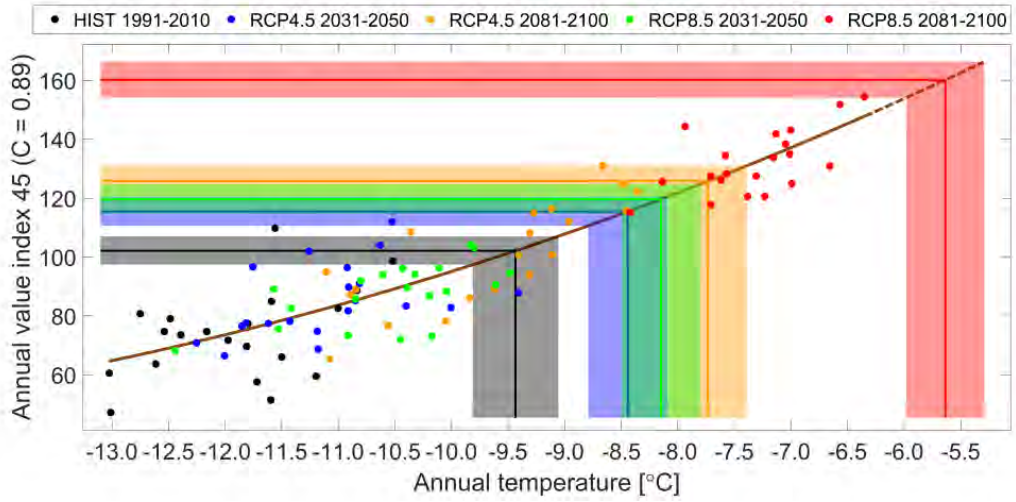

Figure 4.8: Correlated values of growing season length and annual mean temperature for South Greenland based on HIRHAM5 (dots). The brown curve is a best fitted regression line. The green vertical line indicates the 20-year mean temperature (2031-2050) for the CMIP5 models for the RCP8.5 scenario. Its intersection with the regression line gives the corresponding value for the index for the CMIP5 models. The shaded area indicates a standard deviation of the CMIP5 mean. From Christensen et al. (2015a-f).

Even though there are good indications that the uncertainty assessment method is valid, when the data was published, it had not yet been validated. The data provided for climate change adaptation, and the associated uncertainty quantification in particular, depend on the reliability of this assessment method. The method is tested, adjusted and validated by Olesen et al. (2018a), which is presented in chapter 5.

5 Climate indices

This chapter is based on the Paper I: " robustness of high-resolution regional climate projections for Greenland: A method for uncertainty distillation" (Olesen et al., 2018a) and contains full text sections from the paper. Section 5.7 discusses the index uncertainty assessment a bit further, and put the findings into perspective of the work presented in the scientific climate reports (Christensen et al., 2015a-f). This chapter accomplishes the aim of comparing the HIRHAM5 simulation with an ensemble of equivalent RCM simulations.

5.1 Introduction

The climate in the Arctic is in rapid transition. The global mean temperature is increasing, and due to various feedback mechanisms, the Arctic region including Greenland will likely experience even faster and higher temperature increases than most other parts of the world – often referred to as Artic amplification, described and quantified by e.g. (Pithan & Mauritsen 2014).

These temperature increases will have strong impacts in Greenland, both in populated regions along the coasts and on the ice sheet (AMAP, 2017b). These changes will, and already do require customized adaptation strategies. Infrastructure, agriculture, fishery, tourism and other sectors in Greenland are already being affected by climate change and these impacts will increase further with increasing temperatures (Christensen et al. 2015, Rosen 2016, Lehmann et al. 2017). Related barriers and opportunities have broad political attention, also in Greenland, and detailed knowledge on climate change is greatly demanded by the Greenlandic Self-Government (Landbrugspolitiske Redegørelse 2007).

5.1.1 Climate indices

Customised climate indices from high-resolution climate simulations are practical and valuable for local sector adaptation strategies in Greenland. Length and onset of growing

season and number of frost days are examples of highly useful climate indices designed for climate adaptation of agriculture in Southern Greenland (Christensen et al. 2015, Lehmann et al. 2017). Definitions of climate indices in this study are from Persson et al. (2007), who involved the Swedish Commission of Climate and Vulnerability and other stakeholders in selecting and defining relevant climate indices with a focus on northern Europe.

Climate indices can be used to infer complex weather dependent relations in a simpler manner than by using observed meteorological conditions or direct model output data from climate models. More than 60 different climate index projections with focus on Greenland were published by Christensen et al. (2015) targeting climate adaptation needs in Greenland. Focus was on the relatively small part of Greenland with a settled population and the work resulted in 6 district reports targeting the administrative level of Greenlandic municipalities. In these reports the idea of assessing the projected index uncertainty for one single high-resolution regional climate simulation with the use of CMIP5 was introduced but never formally validated.

5.1.2 High-resolution information from regional climate models

Optimizing adaptation to the future climate in Greenland requires high-resolution climate simulations to capture climate impacts in the inhabitable coastal areas with a highly complex topography with steep mountains and complex meandering coast lines, multiple glaciers and fjord systems.

Dynamical downscaling of a GCM will in general, and for Greenland in particular, add value to the already existing climate information for historical simulations as well as for future climate projections (Lucas-Picher et al. 2012, Rummukainen 2016). Figure 5.1 illustrates the geographical resolution when downscaling the GCM, EC-Earth (Hazeleger et al. 2012) to 5.5km with the RCM, HIRHAM5 (Christensen et al., 2006). 5.5 km is just enough to e.g. get the fjords surrounding Narsaq in southern Greenland resolved and hence distinguish and identify the fjord and mountain weather characteristics, also depicted in Figure 5.1. In the case when the climate indices are based on high temporal resolution (daily values) and conducted on the basis of fine scale features, the added value by using very high resolution RCMs has been demonstrated and summarized in several studies (Christensen et al., 2007b; Christensen and Christensen, 2003; Feser et al., 2011; Giorgi et al., 2016; Luca et al., 2015; Lucas-Picher et al., 2012; Mayer et al., 2015; Rockel, 2015).

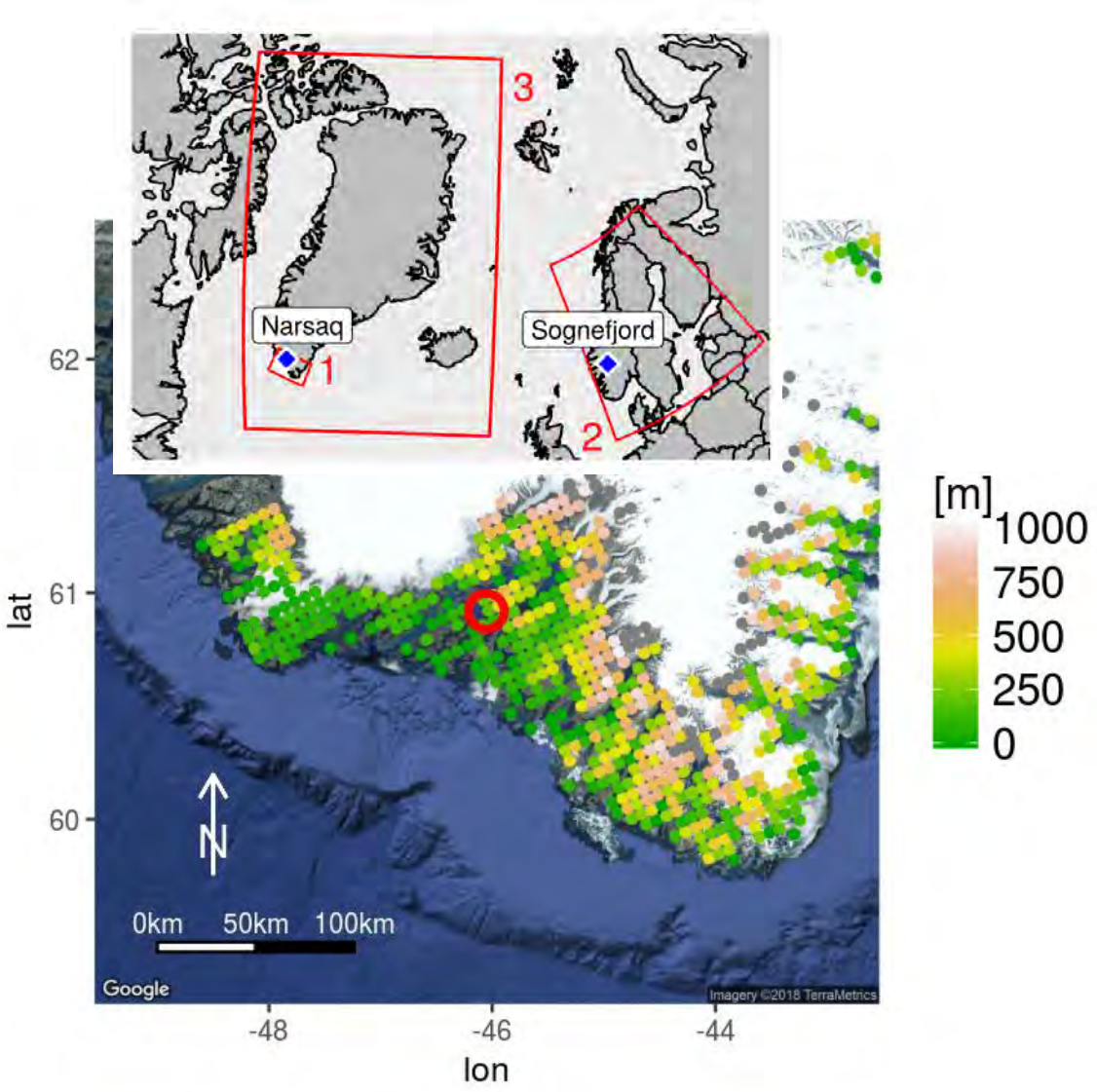

Figure 5.1: Model topography in South Greenland represented as ice free HIRHAM5 grid points on land around the village Narsaq (marked with a red circle). The color map corresponding to domain 1 in the key map has a horizontal resolution of 5.5km. Scandinavia (domain 2) and the head of Sognefjord will be subject to further analysis in this study.

5.1.3 Uncertainty assessment

The uncertainties associated with projected climate index changes for a given climate scenario have to be evaluated and quantified in order to ensure a robust scientific base for climate adaptation planning. The present work provides supporting documentation for the uncertainty assessments of simulated climate index changes for Greenland adopted by Christensen et al. (2015).

So far, uncertainties associated with downscaling of climate projections have primarily been based on using results from an ensemble of RCMs nested in different GCMs (Pan et al. 2001, Déqué 2007, Jacob et al. 2014, Vautard et al. 2014). However, due to limited computer resources, multiple high-resolution simulations (such as those presented in this study) are so far not available for large, remote and sparsely populated regions like Greenland. Since one single regional climate simulation is insufficient for any proper uncertainty analysis (IPCC, 2013; Madsen et al., 2012; McSweeney et al., 2015), an alternative method to evaluate the uncertainties related to a single climate simulation is required. Here such a method is proposed and evaluated.

5.1.4 Pattern scaling

The method builds on the theoretical scalability assumption, where there is a linear relation between annual mean temperature change (here from the GCM) and the response of a temperature dependent variable (here the climate index) (Mitchell et al. 1999, Tebaldi & Arblaster 2014). The technique is an attempt to estimate the anomaly in a climate variable for a particular location or grid point for a given period that would have been obtained from additional regional climate simulations for a specific scenario.

In this study we are not confining ourselves to simple linear relations between the climate index and annual mean temperature. On the other hand we are not extrapolating beyond existing high-end scenario temperature ranges either. The analysis will in the following be performed within a temperature range, where the relationship between the climate index and the annual mean temperature is identified.

5.2 Uncertainty assessment method

5.2.1 Models

The model configuration we want to test in this study, is the RCM, HIRHAM5 described in section 4.4. In order to verify the propounded uncertainty assessment method, the focus is shifted to Europe where multiple high-resolution downscaling experiments are available within the COordinated Regional climate Downscaling EXperiment for Europe (EURO-CORDEX) (Jacob et al. 2014). The EURO-CORDEX-11 (here referred to as CORDEX) ensemble as of July 2017 contains 5 GCMs and 6 RCMs combined as 15 downscaling experiments for the RCP4.5 and RCP8.5 scenarios for Europe at 0.11 degrees (approximately 12 km) resolution. The GCM-RCM matrix is shown in Table 5-1.

	GCMs				
RCMs	*CNRM-CERFACS-CNRM-CM5*	*ICHEC-EC-EARTH*	*IPSL-CM5A-MR*	*MOHC-HadGEM2-ES*	*MPI-M-MPI-ESM-LR*
DMI-HIRHAM5		EXP 7			
SMHI-RCA4	EXP 2	EXP 5	EXP 8	EXP 11	EXP 14
KNMI-RACMO22E		EXP 4 EXP 6		EXP 10	
CLMcom	EXP 1	EXP 3		EXP 9	EXP 12
MPI-REMO					EXP 13 EXP 15

Table 5-1: GCM-RCM matrix with available EURO-CORDEX experiments for Europe for the RCP4.5 and 8.5 scenarios at 0.11 degrees spatial resolution from 2006-2100. EXP numbers refer to downscaling experiments in Figure 5.7 and Figure 5.8.

For climate index calculation, both temperature and land area fraction fields are required. The RCMs used in this study are: CCLM (Rockel et al. 2008), HIRHAM5 (Christensen et al., 2006, 1998), ALARO-0 (Giot et al. 2016), RACMO2 (Van Meijgaard et al. 2012), RCA4 (Kupiainen et al. 2011, Samuelsson et al. 2011) and REMO (Jacob et al. 2012). Furthermore 18 EURO-CORDEX EURO-44 combinations are applied for larger area studies.

We also use 39 GCM simulations from the Coupled Model Intercomparison Project Phase 5 (CMIP5) (Taylor et al. 2011) with spatial resolutions ranging from 0.5 to 4

degrees. Here we use the entire set for projected temperature changes in RCP85 by the end of the 21st century. From CMIP5 a subset of five GCMs are used for the EURO-CORDEX downscaling experiments: CNRM (Voldoire et al., 2013), IPSL (Dufresne et al., 2013), MOHC HadGEM2 (Collins et al., 2011) and MPI-M-MPI-ESM-LR (Giorgetta et al., 2013).

5.2.2 Technique for uncertainty assessment

Our hypothesis is that uncertainty related to a single high-resolution downscaled regional climate projection can be assessed by converting statistical information deduced from CMIP5 to the single high-resolution downscaled projection. The over-all idea is to convert the spread of annual mean temperature from CMIP5 simulations for a given RCP scenario into uncertainty of an RCM-derived climate index, e.g. growing season onset or growing season length for the same scenario. Conversion of CMIP5 temperature spread is done through a correlation setup between an RCM derived climate index and GCM-temperatures as explained through the following steps. The concept is illustrated in Figure 5.2 and already mentioned in section 4.5, but some modifications have, after the reports I-VI were published, improved the technique.

Temperature dependent climate indices are calculated from the high-resolution RCM simulation (in this study HIRHAM5). Here we test the indices growing season length and onset, both of particular relevance for southern Greenland. The growing season length is defined as the number of days between the first occurrence of at least 4 consecutive days with daily mean temperatures above 5 °C and the first occurrence of 4 consecutive days with a temperature below 5 °C.

RCM derived climate indices are shown against corresponding annual mean temperature at the nearest grid point from the forcing GCM in which the RCM is nested (in this study EC-Earth). This is done for index and temperature changes for each model year with respect to the mean climatology for a base line period. Here chosen as 1986-2005 following IPCC (2013).

A linear or second order regression line as well as confidence and prediction (tolerance) intervals are then fitted to the RCM derived climate indices and corresponding GCM annual mean temperatures. Following the IPCC definition of “likely” (66-100% probability) on the likelihood scale (Mastrandrea et al. 2011), confidence and prediction levels are accordingly set to 66%. The confidence interval relates to the best fitted regression line, whereas the prediction interval represents the year-to-year variability in the climate index. The prediction interval embraces 66% of the simulated growing season

lengths for a given temperature interval, shown as the blue lines enclosing 66% of the points in Figure 5.2.

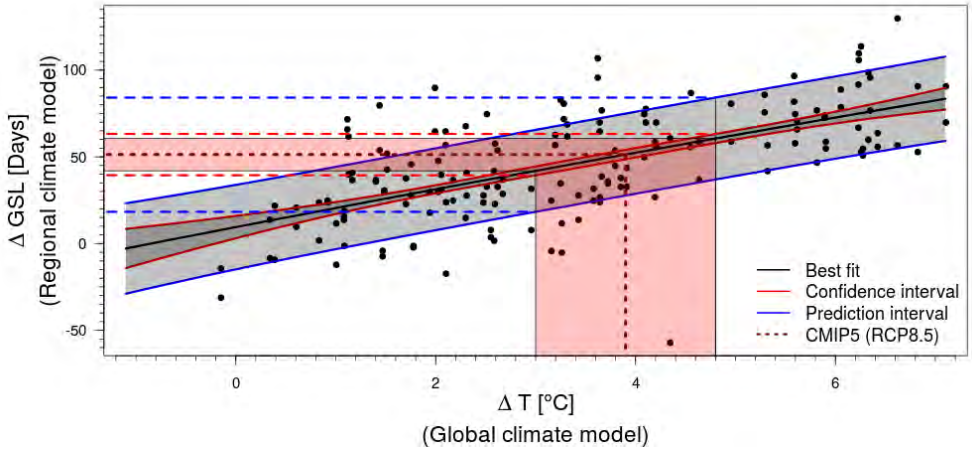

Figure 5.2: Change in growing season length (GSL) for Narsaq (mean value of the four nearest grid points) for 2081-2100 relative to 1991-2010. Each dot represents change in GSL for one year from HIRHAM5 as a function of annual mean temperature change from EC-Earth for a historical run (1951-2005, black dots) and an RCP8.5 scenario run (2006-2100). The black is the best fitted regression line and its confidence interval (95% confidence level) is indicated with red lines. The blue lines are the prediction intervals indicating the year-to-year variability of the growing season length for a given temperature change. CMIP5 temperature change in the period 2081-2100 for the RCP8.5 scenario is shown as vertical dashed red line and the red shaded area indicates "likely" spread of the 39 CMIP5 models. Horizontal dashed lines point to the level of projected change in GSL for CMIP5 mean temperature change and corresponding "likely" spread (in dark and light red), and that combined with the "likely" range of year-to-year GSL variability (in blue).

The prediction interval is the confidence interval for the response variable (here, the predicted change for a given climate index) to the predictor (here, the GCM annual mean temperature) (von Storch and Zwiwes, 1998). The prediction bounds follow the general expression:

sample estimate ± (t-multiplier × standard error).

The formula notation is:

$$\hat{y}_h \pm t_{\left(\frac{\alpha}{2}, n-2\right)} \times \sqrt{MSE \times \left(1 + \frac{1}{n} + \frac{(x_h - \overline{x})^2}{\sum(x_i - \overline{x})^2}\right)}$$

$\hat{y}_h$, is the predicted value, where the predictor is x_h

$t_{\left(\frac{\alpha}{2},n-2\right)}$, is the t-multiplier with n-2 degrees of freedom

$\sqrt{MSE \times \left(1+\frac{1}{n}+\frac{(x_h-\overline{x})^2}{\sum(x_i-\overline{x})^2}\right)}$, is the standard error of the prediction.

In Figure e.g. Figure 5.2, Figure 5.3 and Figure 5.4 and the prediction as well as the confidence intervals appear as shallow hyperbolas. The confidence intervals for the regression line is

$$\hat{y}_h \pm t_{\left(\frac{\alpha}{2},n-2\right)} \times \sqrt{MSE \times \left(\frac{1}{n}+\frac{(x_h-\overline{x})^2}{\sum(x_i-\overline{x})^2}\right)}$$

The equation for prediction intervals differs from the corresponding equation for the confidence intervals associated with the regression line by having an extra MSE term, which is caused by the unknown variance of the prediction estimate.

The "likely" range of 20-year mean temperature projections from CMIP5 can be converted to a measure of index uncertainty through the intersection with the best fitted regression line as illustrated with colour-shaded vertical and horizontal bars in Figure 5.2.

The estimated index uncertainty depends on the correlation strength and the slope of the regression line. A low correlation coefficient will expand the uncertainty range and vice versa a high coefficient will narrow the index uncertainty range towards the corresponding "likely" range of GCM annual mean temperature projections. The slope of the regression line is a measure of the index's sensitivity to temperature and hence climate change. The uncertainty range can be deduced from where the CMIP5 shaded areas intersect with the regression lines for confidence and prediction intervals shown in Figure 2.

The current uncertainty assessment method is based on the so called delta change bias correction approach which according to Maraun (2016) is not a real bias correction but rather a way to employ the climate change response from the RCM to adjust the observations. But it also provides a simple measure of model agreement on the climate change signal (Giorgi & Mearns 2003), which is what we are interested in here. Furthermore it facilitates interpretation and direct use of estimated climate index changes and associated uncertainties in a climate adaptation context. With this technique, changes in climate indices can in this sense be directly added to current observations.

Through a statistically significant correlation between an RCM derived climate index and the corresponding driving GCM annual mean temperature, the "likely" spread of the GCM ensemble for that region can be translated into a projected climate index

uncertainty. This method allows for quantifying uncertainty of climate index changes on very local scale, *in casu* simulated with a single high-resolution RCM.

Whereas the application of the method is motivated from the need of high-resolution climate simulations for Greenland, the method needs an ensemble of RCM and GCMs to be tested. Available simulations from Arctic CORDEX (Akperov et al., 2018; Giorgi et al., 2009) are insufficient and only available at coarse resolution (50 km). Therefore, the uncertainty assessment method is evaluated for northern Europe, where the amount of downscaling experiments is much larger and performed at more comparable resolution. We focus on Scandinavia, which for some areas has somewhat comparable climate characteristics as the populated areas in southern Greenland. Finally, the tested uncertainty assessment method is applied for the high-resolution HIRHAM5 simulations over first a Norwegian site, Sognefjord and for Greenland with focus on Narsaq, see Figure 5.1.

5.2.3 Assumptions

The index uncertainty assessment method requires the following four assumptions to be fulfilled:

5.2.3.1 HIRHAM5 index and EC-Earth temperature correlation (assumption I)

A statistically significant correlation between a HIRHAM5 derived climate index and EC-Earth simulated annual mean temperature is necessary to ensure a meaningful uncertainty conversion. A strong correlation leads to relatively low uncertainties for projected climate indices, whereas a weak correlation coefficient indicates relatively large uncertainties.

Temperature dependent climate indices are calculated from the HIRHAM5 - EC-Earth downscaling (also part of EURO CORDEX) for Sognefjord. A linear regression model including confidence and prediction intervals is fitted to the HIRHAM5 derived climate indices and corresponding annual mean temperature from the driving model, EC-Earth as in Figure 2. This is done for a number of climate indices (here only growing season length and onset are shown as our first choice, but we also briefly discuss number of frost days and consecutive dry days) and tested on specific locations as well as for the Scandinavian region as a whole.

5.2.3.2 General RCM-index and GCM-temperature correlation (assumption II)

The method requires that the correlation between a HIRHAM5-derived climate index and the corresponding EC-Earth-simulated annual mean temperature represents a general

index-temperature dependency. In addition to that the projected temperature from HIRHAM5 should be drawn from the same distribution as the CORDEX ensemble. Some climate indices involve thresholds and may therefore be sensitive to biases.

The consistency of index-temperature correlations among the individual CORDEX downscaling experiments (HIRHAM5-EC-Earth included) is therefore tested to ensure that HIRHAM is representative for the CORDEX ensemble. Furthermore, HIRHAM5 and seven other RCM downscaling experiments forced with the European re-analysis dataset ERA-Interim from ECMWF (Dee et al. 2011) are also compared to show individual performances with identical boundary conditions as also shown by Christensen et al. (2008).

5.2.3.3 Transferability of index relation (Assumption III)

The derived relationship between HIRHAM5 indices and EC-Earth-temperature has to be transferable from one region to another. If the relationship between HIRHAM5 and EC-Earth for Scandinavia holds for Greenland, we assume that the general RCM-index GCM-temperature dependency (assumption II) sustains.

To test the transferability assumption, climate index correlation-analysis for Europe at a grid point near Sognefjord is compared to a corresponding analysis for Greenland at a grid point near Narsaq. See locations in Figure 5.1. Narsaq is relevant because of its agriculture activities. The Sognefjord grid point is relevant because it is comparable to Narsaq with its location in a west-faced fjord system at the same latitude and affected by similar topography influenced weather systems.

5.2.3.4 CMIP5 and CORDEX Variance (Assumption IV)

The "likely" range of projected temperature from CMIP5 has to embrace the "likely" temperature range on smaller scale from the CORDEX projections. If the "likely" RCM temperature range exceeds the "likely" GCM temperature range, we will not necessarily capture a full 66% "likely" range from CMIP5.

To check this the 17th and 83rd percentiles of CMIP5 and CORDEX temperature projections are compared to make sure, that the boundaries of the "likely" ranges are overlapping both at the high and low end of the projected temperature distribution.

5.3 Results

5.3.1 HIRHAM5 index and EC-Earth temperature correlation (assumption I)

In Figure 5.3 the change in growing season length (w.r.t. 1986-2005) calculated from (EURO CORDEX based) HIRHAM5 on a 12 km spatial resolution is shown as function of corresponding annual mean temperature from the forcing GCM, EC-Earth. The correlation coefficient of the linear regression is $r = 0.78$. Growing season onset is shown in Figure 5.4 and is less correlated ($r = 0.59$).

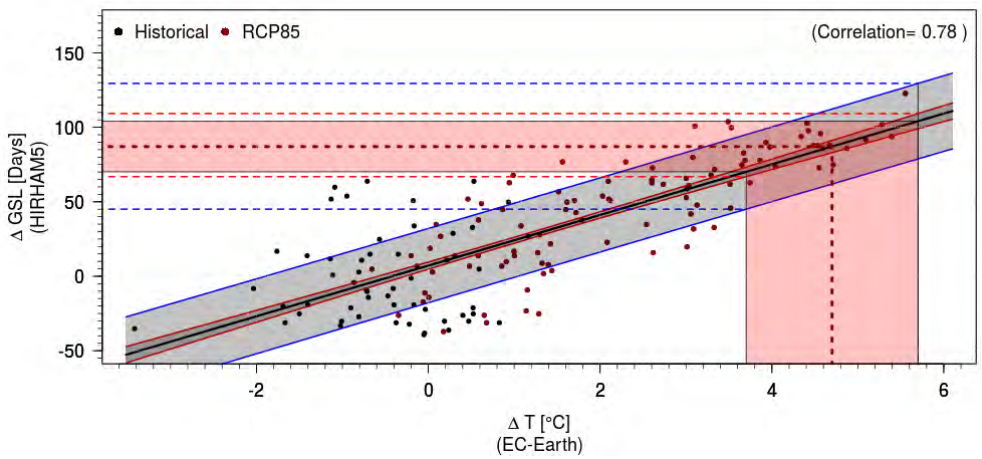

Figure 5.3: Changes in growing season length (GSL) for the Sognefjord grid point w.r.t. 1986-2005. Each dot represents change in GSL for one year from HIRHAM5 as function of annual mean temperature change from EC-Earth for a historical run (1951-2005, black dots) and an RCP8.5 scenario run (2006-2100, red dots). The black is the best fitted regression line and its confidence interval (95% confidence level) is indicated with red lines. The blue lines are the prediction intervals indicating the year-to-year variability of the growing season length for a given temperature change. CMIP5 temperature change in the period 2081-2100 for the RCP8.5 scenario is shown as vertical dashed red line and the red shaded area indicates "likely" spread of the 39 CMIP5 models. Horizontal dashed lines point to the level of projected change in GSL for CMIP5 mean temperature change and corresponding "likely" spread (in dark and light red), and that combined with the "likely" range of year-to-year GSL variability (in blue).

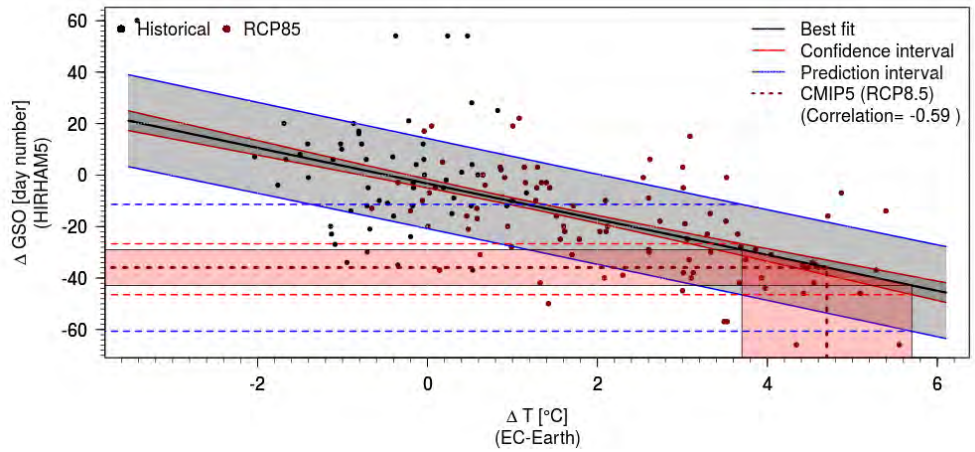

Figure 5.4: Changes in growing season onset (GSO) for Sognefjord grid point w.r.t. 1986-2005. Each dot represents change in GSO given as annual values from HIRHAM5 as a function of annual mean temperature change from EC-Earth for a historical run (1951-2005, black dots) and an RCP8.5 scenario run (2006-2100, red dots). The black is the best fitted regression line and its confidence interval (95% confidence level) is indicated with red lines. The blue lines are the prediction intervals indicating the year-to-year variability of the growing season length for a given temperature change. CMIP5 temperature change in the period 2081-2100 for the RCP8.5 scenario is shown as vertical dashed red line and the red shaded area indicates "likely" spread of the 39 CMIP5 models. Horizontal dashed lines point to the level of projected change in GSO for CMIP5 mean temperature change and corresponding "likely" spread (in dark and light red), and that combined with the "likely" range of year-to-year GSO variability (in blue).

Moving from one grid point to the entire Scandinavian domain (Domain 2 in Figure 5.1) the correlation coefficients for each grid point are shown for the growing season length and onset in Figure 5.5 and 6. The correlation between the climate index and the annual mean temperature differ across Scandinavia, but remains in the range 0.6 to 0.9 for growing season length and -0.8 to -0.4 for growing season onset, as highlighted in the density plots (top left) in Figure 5.5 and Figure 5.6.

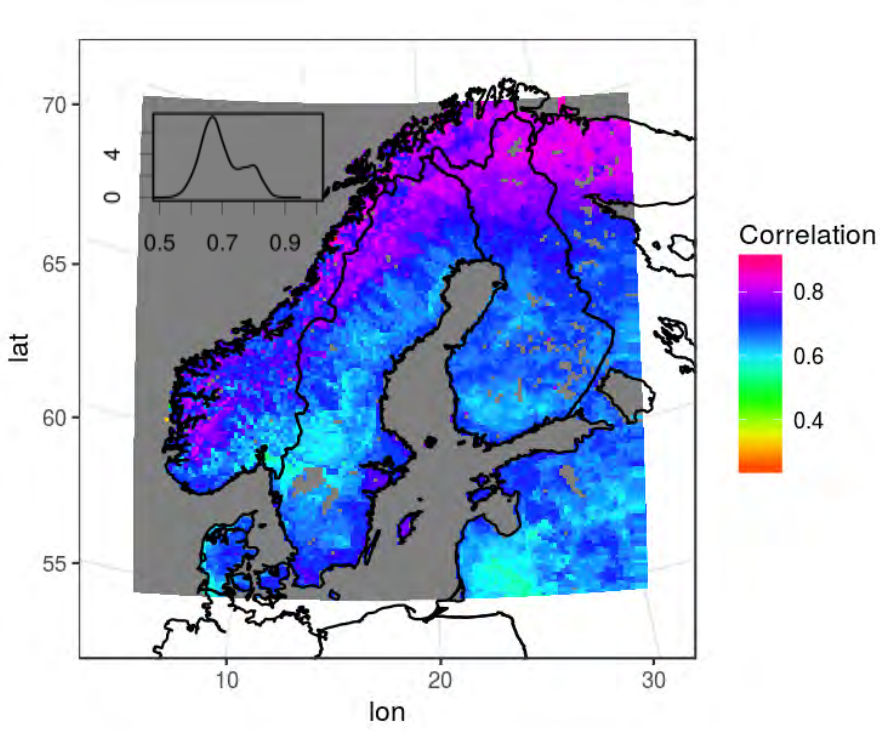

Figure 5.5: Correlation coefficients (Pearson's r) between growing season length from HIRHAM5 and annual mean temperature from EC-Earth for Scandinavia for the RCP8.5 scenario from 2006 to 2100. The density of correlation coefficients is shown in the top left corner.

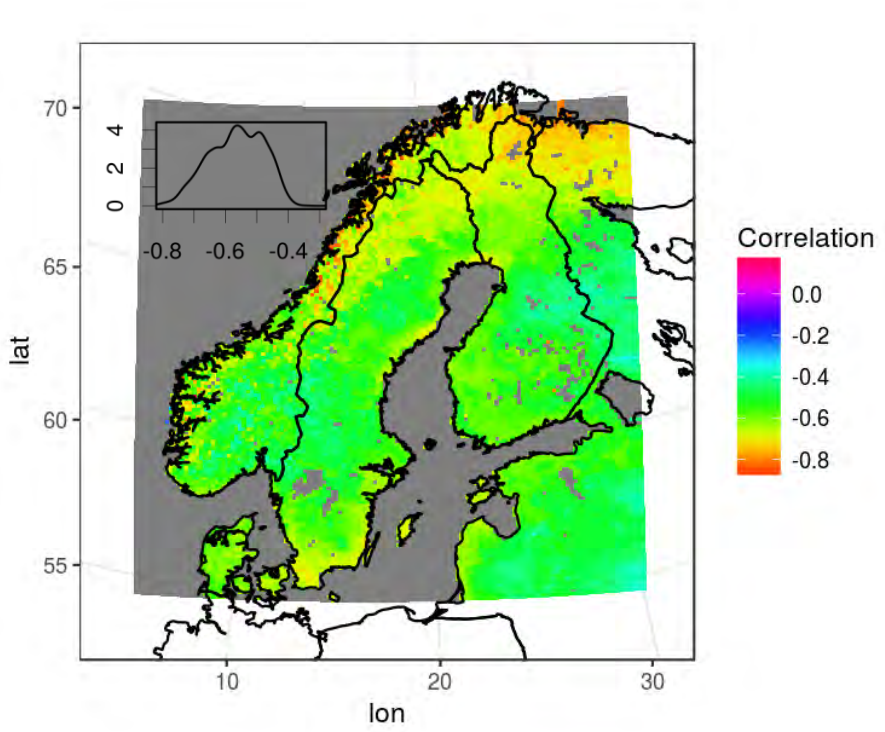

Figure 5.6: Correlation coefficients (Pearson's r) between growing season onset from HIRHAM5 and annual mean temperature from EC-Earth for Scandinavia for the RCP8.5 scenario from 2006 to 2100. The density of correlation coefficients is shown in the top left corner.

5.3.2 General RCM-index GCM-temperature correlation (assumption II)

The correlation between climate indices (growing season length and onset) and annual mean temperatures among the individual regional and global models within EURO CORDEX is compared and shown in Figure 5.7 and Figure 5.8 for Scandinavia and the Sognefjord grid point.

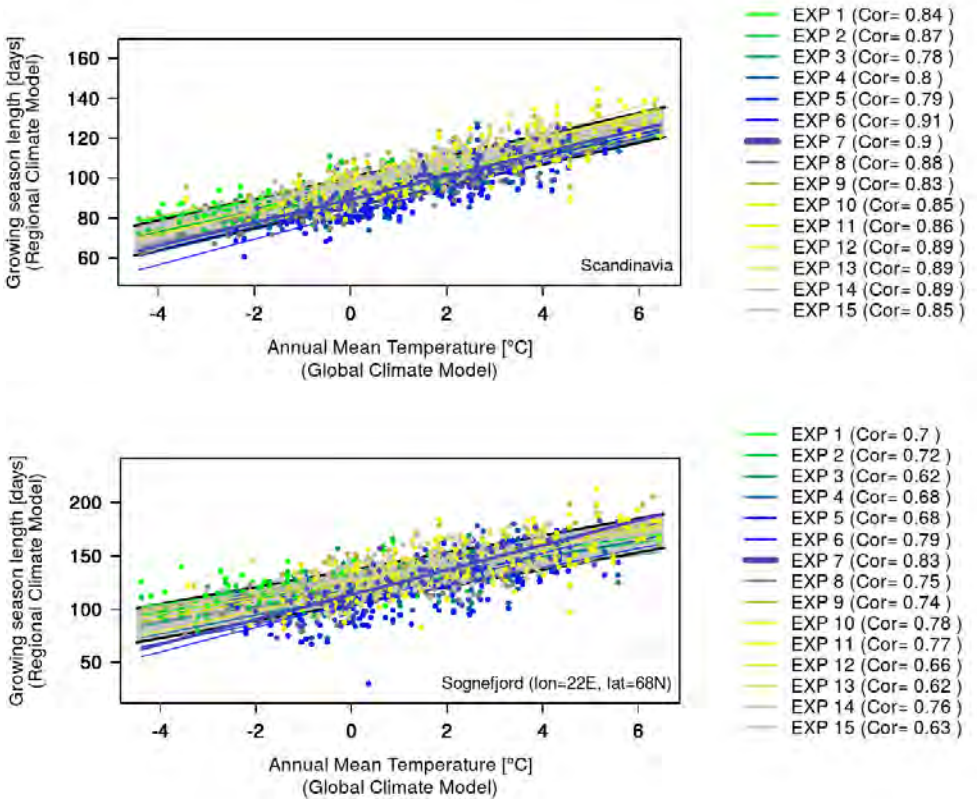

Figure 5.7: Growing season length calculated from 15 EURO-CORDEX simulations for Scandinavia (top) and for Sognefjord (bottom) correlated with annual mean temperature from the respective forcing GCMs for the RCP8.5 scenario experiments from 2006 to 2100. The grey shaded area represents the "likely" prediction interval of the entire index-temperature population. EXP numbers (right column) refer to downscaling experiments listed in Table 5-1.

Annual mean temperatures for Scandinavia from the 15 EURO-CORDEX members are close to being normally distributed and a Student's t-test is used to test the null Hypothesis: *HIRHAM5 simulation are indistinguishable from the CORDEX ensemble of annual mean temperatures.* The resulting test confirms that HIRHAM5 is indistinguishable from the merged EURO-CORDEX evaluation experiments and cannot be rejected at the 95% confidence level. The box and whiskers plots in Figure 5.9 support this finding.

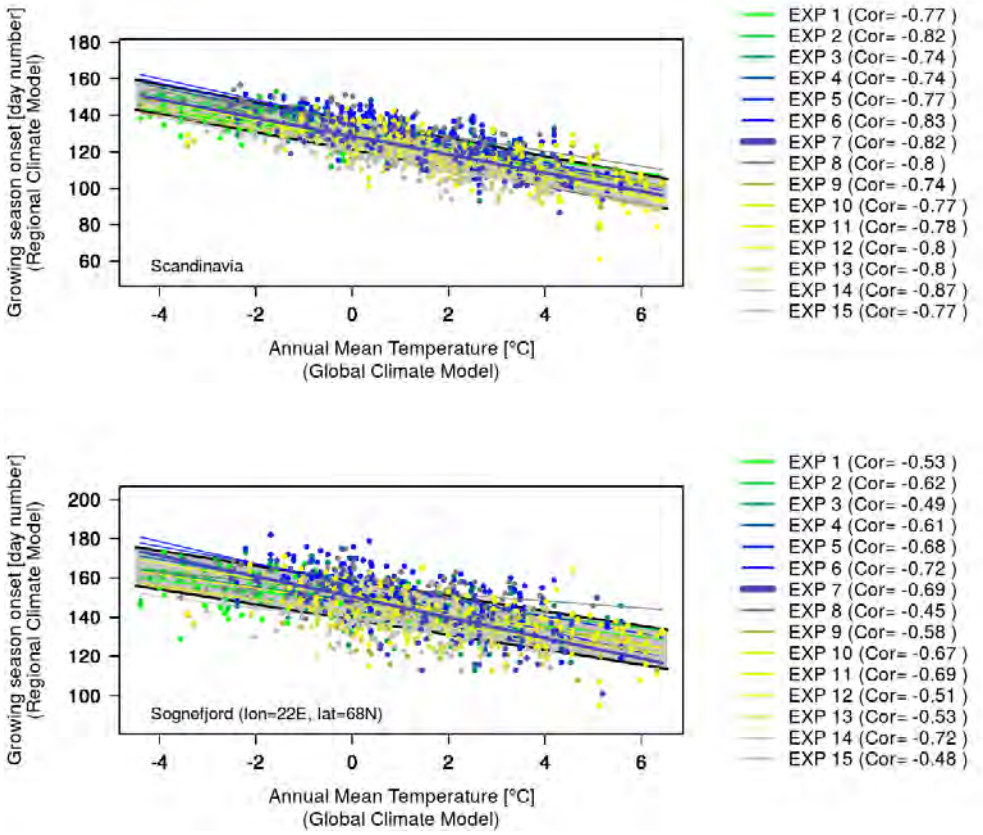

Figure 5.8: As Figure 5.7 but for growing season onset.

The boxes and whiskers in Figure 5.9 show the upper and lower quantiles and upper and lower fences of RCM-projected annual mean temperatures divided between five different GCMs for Scandinavia and Sognefjord. The GCMs introduce the first levels of uncertainty propagation from large to small scale temperature projections.

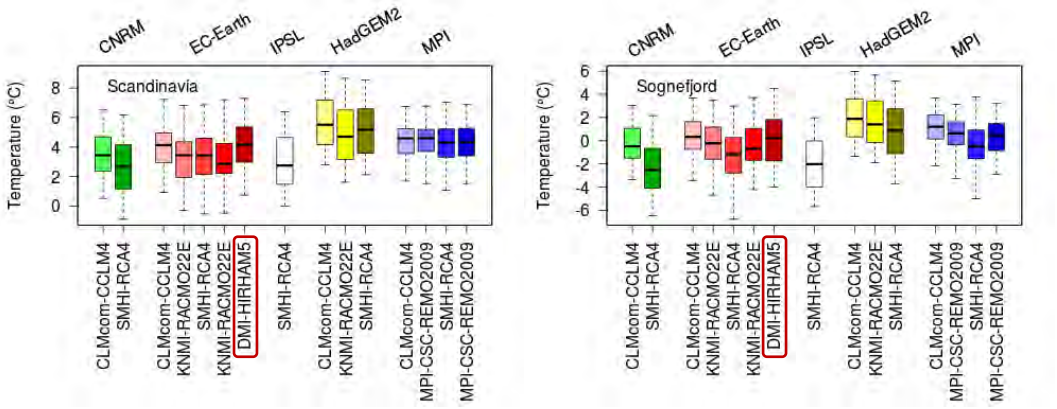

Figure 5.9: Annual mean temperature for 2006-2100 for the RCP8.5 scenario simulated with the RCMs in CORDEX cf. Table 5-1. The driving models are grouped colour wise (green: CNRM-CERFACS-CNRM-CM5, red: ICHEC-EC-EARTH, white: IPSL-ENERIS, yellow: MOHC-HadGEM2-ES and blue: MPI-M- MPI-ESM-LR). HIRHAM5 is highlighted in red. Scandinavia to the left and Sognefjord to the right.

5.3.3 Transferability of index relation (Assumption III)

The relationship between climate indices from HIRHAM5 and annual mean temperature from EC-Earth holds for both Sognefjord and Narsaq. Figure 5.10 shows a statistically significant correlation between climate index changes and changes in annual mean temperature for both the Sognefjord grid point and the Narsaq grid point ($r = 0.78$) and ($r = 0.75$) respectively. The slopes of the two regression lines are different though, 17 days/˚C for Sognefjord and 11 days/˚C for Narsaq.

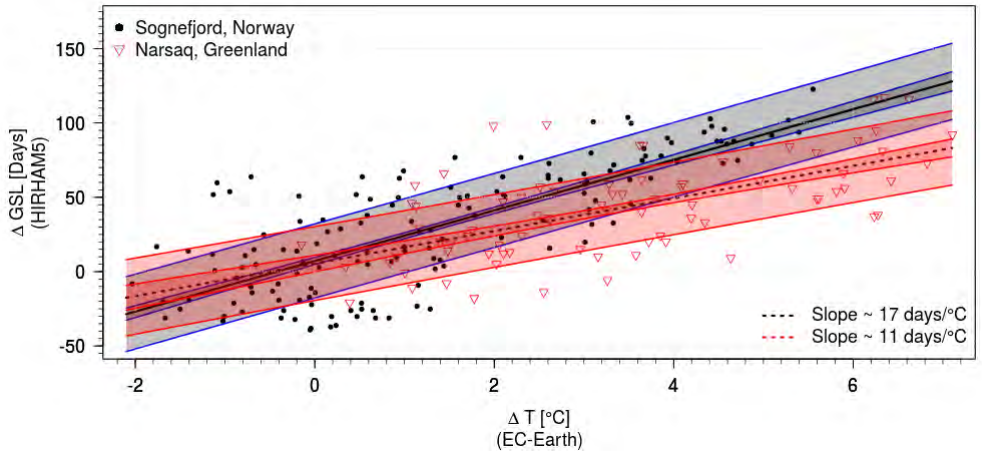

Figure 5.10: Growing season length from HIRHAM5 as a function of annual mean temperature from EC-Earth for Sognefjord (black) also shown in Figure 5.3 and Narsaq (red) also shown in Figure 5.13. The black lines represent the best fit regression lines for each data set. Light and dark shaded areas are the "likely" prediction and confidence intervals.

5.3.4 CMIP5 and CORDEX Variance (Assumption IV)

The 17th and 83rd percentiles (representing the "likely" range) of CORDEX and CMIP5 projected annual mean temperature are compared by subtracting the respective percentiles based on CORDEX from those based on CMIP5 and displayed in Figure 5.11. For blue (red) areas the CMIP5 percentiles are lower (larger) than corresponding CORDEX percentiles. The GCMs are remapped to the CORDEX grid with nearest neighbour weights.

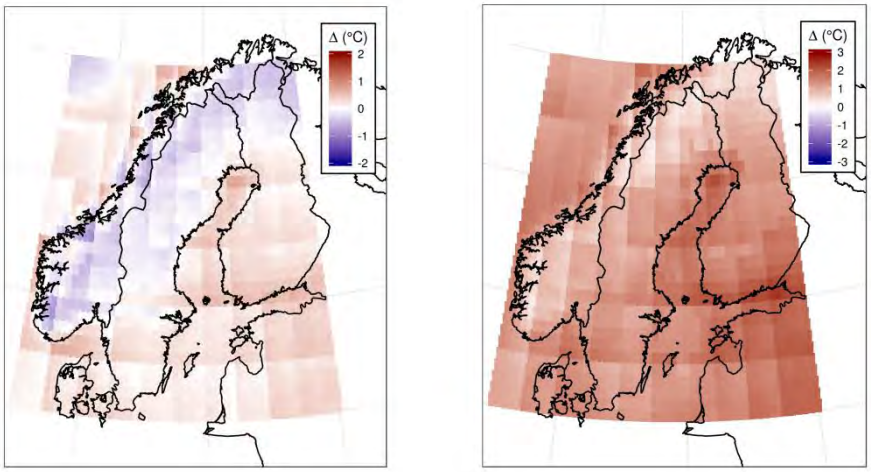

Figure 5.11: Differences in low-end projections (17th percentiles, left) and high-end projections (83rd percentiles, right) between CMIP5 and CORDEX (CMIP5 minus CORDEX) projected annual mean temperature changes for the RCP8.5 scenario from 1986-2005 to 2081-2100.

5.4 Discussion

5.4.1 Assumption I

In Figure 5.3 (growing season length) we find a correlation coefficient ($r = 0.78$) on local scale enabling uncertainty to be quantified at this high resolution. For Sognefjord we meet the high correlation requirement anticipated in assumption I. For growing season onset in Figure 5.4 the correlation with annual mean temperature is lower, but still provides valid and useful information for assessing the uncertainties associated with projected climate index. For the two indices shown here the uncertainty is assessable using the established relationship and the converted CMIP5 temperature changes indicated as vertical shaded areas in Figure 5.3 and Figure 5.4

Not all indices show the same convincingly high temperature dependence as for growing season length and onset, but lower correlation merely results in wider confidence range and prediction intervals on the index-temperature correlation graph. This means that the uncertainty for a given index depends on the correlation coefficient, where a strong correlation narrows down the index uncertainty and a weak correlation blows it up. We suggest interpreting this as a realistic feature describing the actual index uncertainty for a future climate projection.

This should be distinguished from the climate index sensitivity of annual mean temperature change, which is indicated by the slope of the regression lines in e.g. Figure 5.3 and Figure 5.4. Strong dependency (steep slope) increases the "likely" index uncertainty range, whereas weak temperature dependency (shallow slope) decreases the index uncertainty for a constant correlation coefficient.

From Figure 5.2 it is clear that EC-Earth shows a significantly larger temperature increase than other CMIP5 members. Almost all annual mean temperatures from EC-Earth 2081-2100 (based on RCP4.5 and RCP8.5, in total 40 points on in the plot) exceed the general CMIP5 spread. An important factor here is that EC-Earth simulates the 21st century about 2 ˚C colder in the Arctic related to an excessive Arctic sea ice cover and therefore also a larger temperature increase in the Arctic area, when sea ice starts to disappear (Koenigk et al. 2013).

However, this will not affect the correlation and shape of the regression line because the index is derived from HIRHAM5 in matching warmer conditions. On the other hand this method actually avoids overestimating the expected change in length of growing season. So this adds to the benefits of using the proposed uncertainty quantification method.

5.4.2 Assumption II

RCM conducted climate indices exhibit statistically significant and good correlation with its forcing GCM for the entire CORDEX ensemble. The correlation for each CORDEX member is evidently larger when considering the entire Scandinavia than for a selected location.

In Figure 5.7 and Figure 5.8 all regression models show the same tendency. By merging all data points for the 15 RCMs, the majority of the individual regression lines fall within the 66% prediction range (the grey shaded areas in Figure 5.7 and Figure 5.8) for Scandinavia in general but also for the specific Sognefjord grid point. However, some of the regressions escape the prediction interval for low and high-end GCM temperatures, especially for temperatures outside the projected range for the given GCM.

The analysis and quantification of climate index uncertainties should be done for limited areas or even at grid point level to benefit optimally from the high-resolution climate change simulation. By considering too large areas the added information value from the GCM downscaling will vanish (Rockel 2015).

HIRHAM5 is indistinguishable from the CORDEX ensemble, where according to Jacob et al. (2014) projected temperature changes within CORDEX are significant with a t-test

or Mann-Whitney-Wilcoxon test and robust with more than 66% of the models agreeing on direction of projected temperature changes.

5.4.3 Assumption III

Figure 5.10 together with Figure 5.5 and Figure 5.6 illustrate that the climate index temperature relation calculated from HIRHAM5 and EC-Earth is statistically significant for Nasaq in Greenland and Sognefjord in Norway and the entire Scandinavian domain. Figure 5.7 and Figure 5.8 show that the latter holds for the entire CORDEX ensemble and this gives us confidence in assuming the same relationship holds for Greenland.

Figure 5.10 shows that the correlation is kept for the two locations, however the different slopes indicates different temperature sensitivities for Narsaq and Sognefjord. This emphasises the importance of analysing every grid point of interest separately to ensure reliable estimates of climate index changes and associated uncertainty estimates.

5.4.4 Assumption IV

The "likely range of CORDEX temperature changes is to a large extent captured by CMIP5 projected temperature changes. In Figure 5.11 and Figure 5.12 the 83rd percentile temperature projections from CMIP5 is clearly larger than from CORDEX, which is required to ensure that CMIP5 embraces the high-end of the CORDEX "likely" range. Likewise the difference between the CMIP5 and CORDEX low-end projections should be negative or close to zero to ensure that CMIP5 also captures the low-end from CORDEX as well. This is only true for approximately half the land points in Scandinavia, however positive areas in Figure 5.11 do not exceed 0.5 ˚C and are confined to areas with little topography (Greenland in general has a complex topography similar to the Norwegian west coast). The relatively small difference is also illustrated in the density plots in Figure 5.12. The fact that CMIP5 consists of 39 GCMs whereas only 5 GCMs are downscaled within CORDEX is probably the main reason why CMIP5 to a large extent embraces the variance of CORDEX. By selecting 5 out of 39 GCMs, the 83rd percentile will probably decrease and the 17th percentile increase due to the model selection itself. Applying CMIP5 ensemble mean and "likely" range for projected temperature changes as an estimate of expected temperature changes will almost cover the expected "likely" range of CORDEX temperature changes. The role of boundary conditions from the GCM is generally greater than the role of the RCM, in particular for temperature (Déqué et al., 2007).

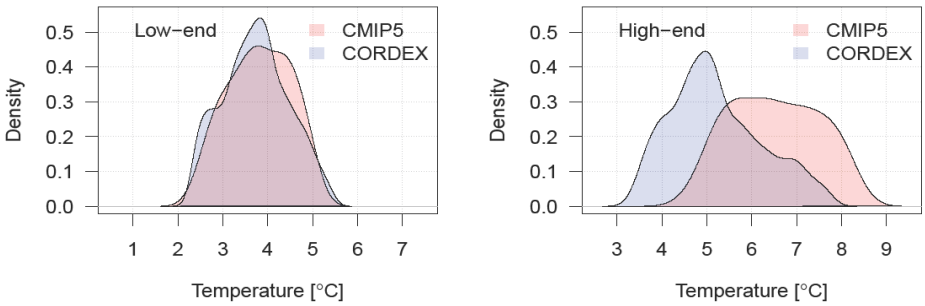

Figure 5.12: Density plot of CMIP5 and CORDEX temperature changes from 1986-2005 to 2081-2100 for all Scandinavian grid points. Left shows low-end of "likely" range (17th percentile) and right shows high-end of "likely" range (83rd percentile).

This argument is supported by the box and whisker plots in Figure 5.9 where the individual GCMs show different characteristics in terms of median values and 50% likely ranges. The differences or uncertainties are mainly caused by the GCM global energy budget and the climate sensitivity, which again is influenced by atmospheric stability and cloud feedback mechanisms etc. (Kjellström et al., 2013; Lenderink et al., 2007). The next level of uncertainty is introduced by the RCMs in terms of small-scale physical processes like small-scale convection and fine scale-interactions involving orography and land-sea transitions. The RCMs in Figure 5.9 also tend to show only limited divergence from its driving GCM, indicating that the GCMs to a large extent control the temperature changes. This was in fact a main motivation for the design of the method proposed in the present paper.

5.4.5 The uncertainty assessment technique in general

In addition to temperature dependent climate indices, we have also looked into precipitation derived climate indices (not shown). Correlations were tested against GCM temperature and GCM precipitation. This proved to demonstrate some limitations of this approach to an uncertainty quantification method. The precipitation derived indices do not show statistically significant correlation with temperature projections. However, some precipitation dependent indices do correlate with annual mean precipitation, but the inter-model "likely" range of CMIP5 precipitation projections is relatively large. Hence, in practice converting that into an index uncertainty appears as unusable or at best serves to underline the relatively large uncertainty that always appears to be associated with regional precipitation projections. On regional and very local scale we do not necessarily expect the precipitation to scale with increasing global annual mean temperature predicted by the GCMs. The precipitation sensitivity to global warming can even be

found to be smaller in an emission scenario with larger greenhouse gas concentrations and aerosol emissions (Shiogama et al. 2009). Hence the amount of precipitation is dependent on other parameters than temperature.

That being said when changes in a given climate index is not correlated with the general temperature changes, the changes may not be significant at all and mostly be an artefact of natural variability. So, one might argue that with our method, all changes in relevant climate indices are assessable, but the resulting change may be seen as not being statistically significant and exhibiting a large year to year variation. The change in consecutive dry days shown in Figure 5.14 is an example of that.

The reports mentioned in the introduction (Christensen et al. 2015) present changes in more than 60 different indices for 2031-2050 and 2081-2100 for RCP4.5 and RCP8.5 relative to the historical period 1991-2010 based on dynamical downscaling with HIRHAM5 to 5.5 km. Corresponding uncertainties have been quantified applying a variant of the method presented here. However the indices are derived from daily temperature, precipitation, humidity and wind projections and do not all correlate well (if at all) with annual mean temperature changes in the driving GCM. Practically all climate indices, which are not derived from temperature do not show the statistically significant correlation to annual mean temperature required to take advantage from this uncertainty assessment method.

In the attempt to develop and optimise the uncertainty assessment method we had to choose one out of three possible index-temperature correlations. Correlation between HIRHAM5 derived climate indices and: 1) HIRHAM5 simulated annual mean temperature changes. 2) CMIP5 annual mean temperatures changes. 3) The forcing GCM, EC-Earth simulated annual mean temperature.

The first solution clearly results in highest correlation coefficients but the link to CMIP5 mean values and uncertainty information disappears. For the indices shown in Figure 5.13 it would be unknown if the relatively high increase in annual mean temperature compared to CMIP5 originated from the GCM or from the RCM.

The second suggestion results in too low correlation coefficients caused by the altered year-to-year variability as well as differences in topography and land sea masks due to the jump in resolution between the driving model and the regional model. The third option offering the highest possible correlation coefficient keeping the link to CMIP5 through the forcing GCM was therefore preferred. GCM-RCM comparison analysis (not shown) show significant differences between HIRHAM5 and EC-Earth for Scandinavia both for absolute and for delta change values. Therefore the link to the global models is required to ensure the full “likely” range for projected climate index changes.

Another way to improve the uncertainty assessment technique could be by e.g. correlating growing season onset from HIRHAM5 with mean spring temperature from the driving model EC-Earth and use the available spring temperature variances from CMIP5. This will through higher correlation coefficients provide less uncertain projections. Likewise growing season length could be correlated with relevant months from the GCM. But this is beyond the scope of the present work. However the main reason for scaling with global annual mean temperature is that it scales better with global annual mean temperature than does seasonal mean, which also allows for better scale results between models. See e.g. (Lynch et al., 2017; Osborn et al., 2018).

5.5 Application to Greenland

The uncertainty assessment method is here applied for agriculture relevant climate indices in southern Greenland around Narsaq, see key map in Figure 5.1. Here we present projected changes in the climate indices growing season length and onset, frost days and consecutive dry days and quantify the corresponding uncertainties using the propounded technique.

If we follow the RCP8.5 scenario, an extension of growing season in Nasaq of 48 days towards the end of this century compared to 1991-2010 is expected. The corresponding uncertainty displayed in Figure 5.13 is assessed to be ± 15 days, see table 2. The uncertainty estimate takes into account the "likely" range of projected CMIP5 simulations (horizontal red dashed lines). The year-to-year variability from HIRHAM5 combined with CMIP5 "likely" range is shown with the horizontal blue dashed lines. The "likely" range of projected change in growing season length in Nasaq including the year-to-year variability is with this method projected to be 48 ± 36 days. This implies that even for a year with a short growing season by the end of this century, it will be longer the average length of today.

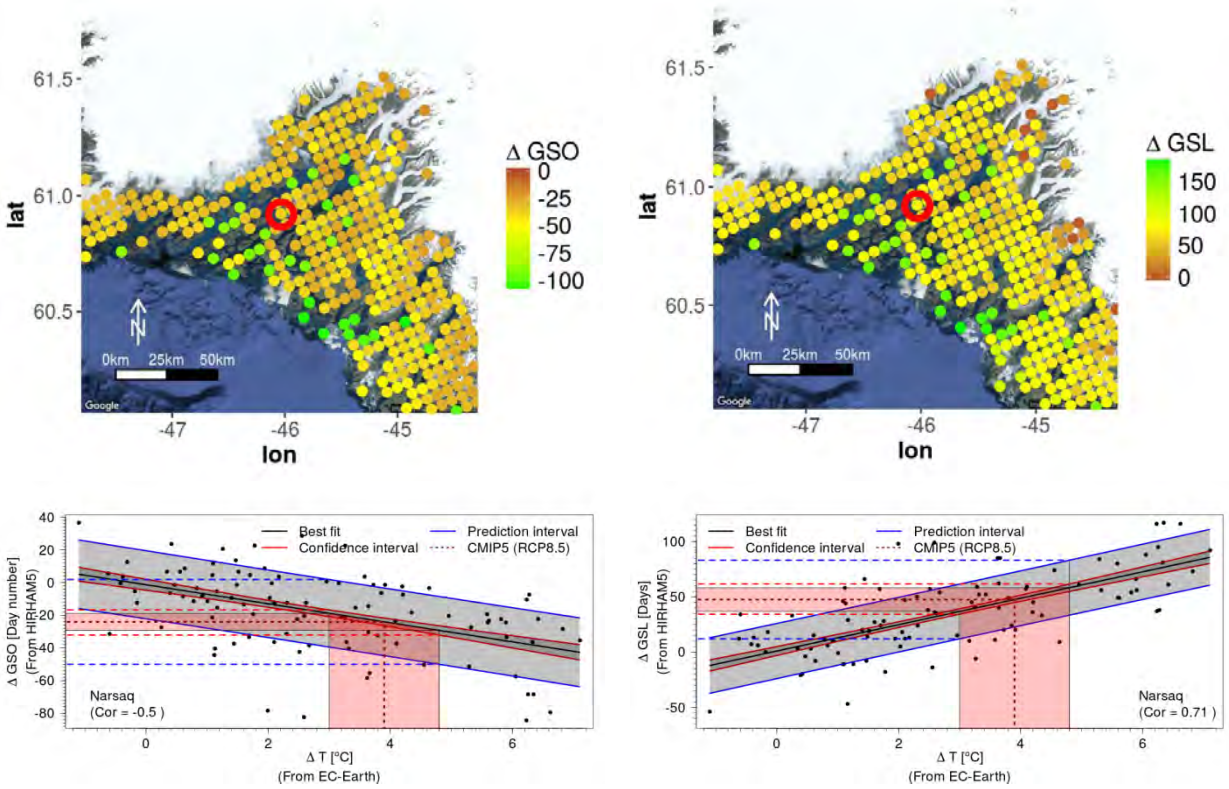

Figure 5.13: Projected changes in growing season onset (left) and length (right). The maps show changes for 2081-2100 relative to 1991-2010 for RCP8.5 for the area around Narsaq (red circle on the maps) in south Greenland. The graphs show changes in annual indices from HIRHAM5 as a function of annual mean temperature changes from EC-Earth. Each point represents one year 2031-2050 and 2081-2100 relative to 1991-2010 for RCP4.5 and RCP8.5. CMIP5 ensemble mean (and "likely" ranges) temperature changes from 1991-2010 to 2081-2100 are displayed as vertical red dashed lines and red shaded areas. The black, red and blue lines are the best fitted linear regression model, its confidence interval and its prediction interval respectively. The blue dashed lines represent projected prediction intervals.

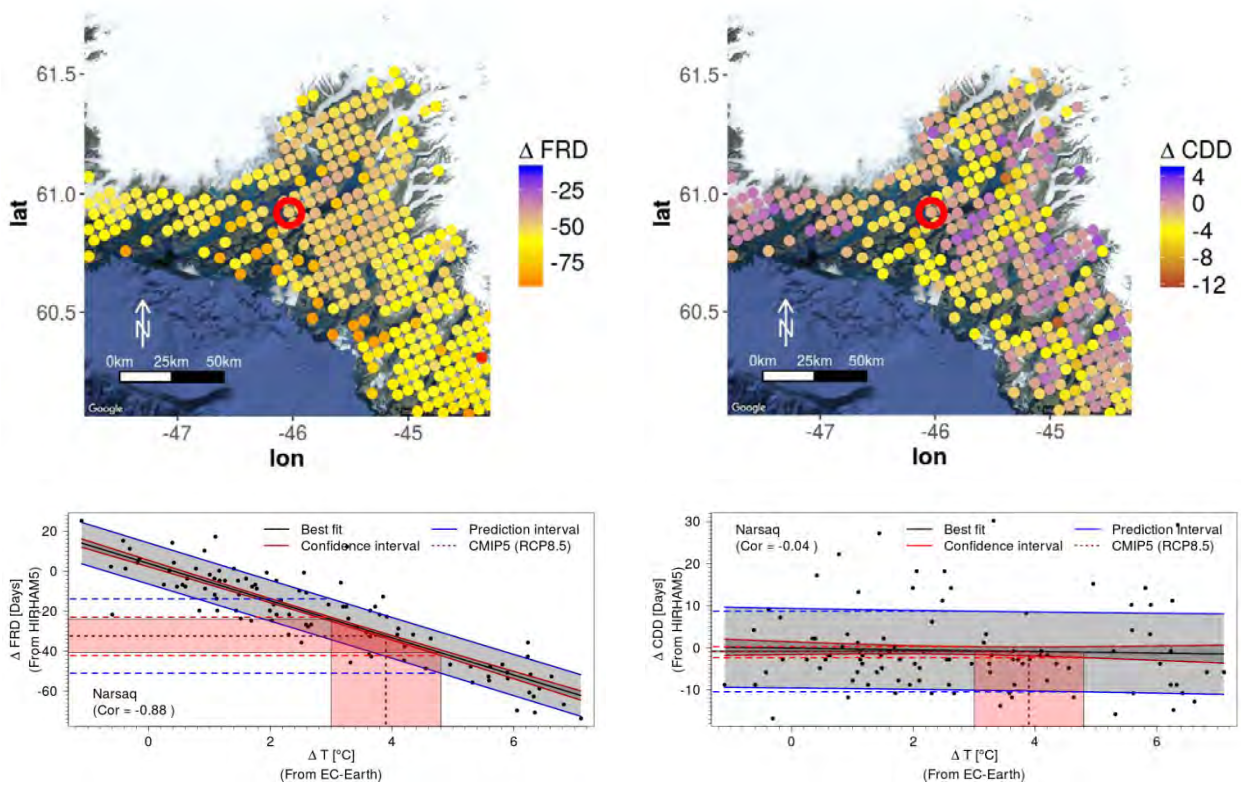

Figure 5.14: Projected changes in number of annual frost days (left) and longest period with consecutive dry days (right) for 2081-2100 relative to 1991-2010 for the RCP8.5 scenario in Narsaq (red circle on the maps) and the surroundings. The graphs (bottom) show the relationship between the climate index from HIRHAM5 and annual mean temperature from EC-Earth for the ice free land point nearest Nasaq. Each point represents one year for the time slices 1991-2010, 2031-2050 and 2081-210 for the scenarios RCP45 and RCP85. The CMIP5 projected temperature change for the RCP85 scenario in 2081-2100 including its "likely" spread is indicated with vertical dashed red line and red shaded area. Black, red and blue lines represent best fitted regression line, its confidence interval and prediction interval. The horizontal dashed lines show the corresponding "likely" ranges of projected climate indices. The "likely" spread of CMIP5 mean temperature converted into "likely" spread of projected index values (red dashed lines) and to "likely" spread of year-to-year variability (horizontal blue dashed lines).

The growing season is with HIRHAM5 expected to start almost one month earlier by the end of the 21st century than 1990-2010 (-25 ± 7 days) including the "likely" spread of CMIP5 and -25 ± 15 days also including the year-to-year variability, see Figure 5.13. Equivalently the amount of frost days displayed in Figure 5.14 is expected to decrease by 32 ± 9 days including the "likely" CMIP5 spread and 32 ± 19 days also including year-

to-year variability. For consecutive dry days, the HIRHAM5 simulation identifies no statistically significant changes towards year 2100 (-1 ± 2 days / ± 10 days) compared to 1991-2010, see Figure 5.14. This index does not correlate with annual mean temperature (r = -0.04), therefore the uncertainty of ± 10 days exclusively represents the year-to-year variability, which is not expected to change during this century.

As described above the method prepares the ground for different index uncertainty interpretations. One useful application here is the estimated change in the length of the growing including the "likely" range based on the CMIP5 estimates of the projected index. The year-to-year variability can be compared to present day local conditions to evaluate if the result is consistent with observations. Projected changes for the four mentioned indices are listed in Table 5-2.

The projected index change and uncertainty can also be assessed for a given temperature increase. A two-degree warming for the area around Narsaq will expand the growing season with approximately 26 ± 24 days (read off directly from Figure 5.13 bottom right) including the "likely" prediction range. In the same way changes in onset of growing season and number of frost nights are projected and evaluated.

Projected changes in growing season length and frost days towards the end of the 21st century in southern Greenland will make it possible to grow new crops with short growing season, such as barley. The climate change also provides longer growing season for growing potatoes and vegetables, however the dominant crop in Greenland will probably still be pasture by the end of this century (Lehmann et al., 2017).

Index (days)	*Index change*	*CMIP5 related uncertainty*	*Total uncertainty (incl. CMIP5 & year-to-year)*
Length of growing season	48	15	36
Onset of growing season	-25	7	15
Frost days	-32	9	19
Consecutive dry days	-1	2	10

Table 5-2: Projected changes in climate indices relevant for agriculture in Narsaq and the surrounding area.

5.6 Conclusions

We have analysed a series of global and regional climate models and shown that temperature dependent climate indices correlate well with temperature. In particular, correlations between HIRHAM5-based climate indices and EC-Earth annual mean temperatures can be seen as representative of the full information deducible from the EURO CORDEX ensemble. We also find that the "likely" range of projected CMIP5 temperatures is larger than of projected CORDEX temperatures for the upper end of the "likely" range and comparable to CORDEX temperatures for the low-end. The spread of projected temperature changes from the CMIP5 ensemble will therefore most likely cover the individual RCM projections for a given location.

Precipitation related indices like consecutive dry days are in general not significantly correlated with annual mean temperatures at regional level, but do correlate with annual mean precipitation. Accordingly, the "likely" range of CMIP5 projected annual mean precipitation is very large compared to projected annual mean temperature. Hence, the uncertainty range will exceed the climate change signal. But, this may well depict state-of-the-art, as model variability in precipitation projection is often very large at the grid point level (IPCC, 2013). For the index; consecutive dry days, which does not correlate with annual mean temperature, only the "likely" year-to-year variability can be quantified by use of this uncertainty assessment method.

On the other hand, we find that the spread of CMIP5 annual mean temperature change to a large degree is convertible to HIRHAM5-projected climate index uncertainty for changes in growing season length and onset and for frost days. The uncertainty assessment method thus utilizes uncertainty quantification of projected changes in climate indices from a single RCM for a geographical domain like Greenland, where only one or a few RCMs are available.

5.7 Limitations and perspectives

Building on the findings disused in Section 5.4, this section presents some extra results concerning the limitations of the uncertainty assessment method and some reconsiderations according to the scientific reports (Christensen et al., 2015a-f). Here we take a closer look at the precipitation dependent climate indices, where the uncertainty method results in wide uncertainty ranges.

5.7.1 Temperature independent climate indices

The index "longest dry period" i.e. longest period of consecutive dry days is not significantly correlated with annual mean temperature. However, the index do correlate with annual precipitation as shown in Figure 5.15, which is also the case for the extreme precipitation index in Figure 5.16. Extreme precipitation is defined as the number of days per year with more than 20 mm precipitation.

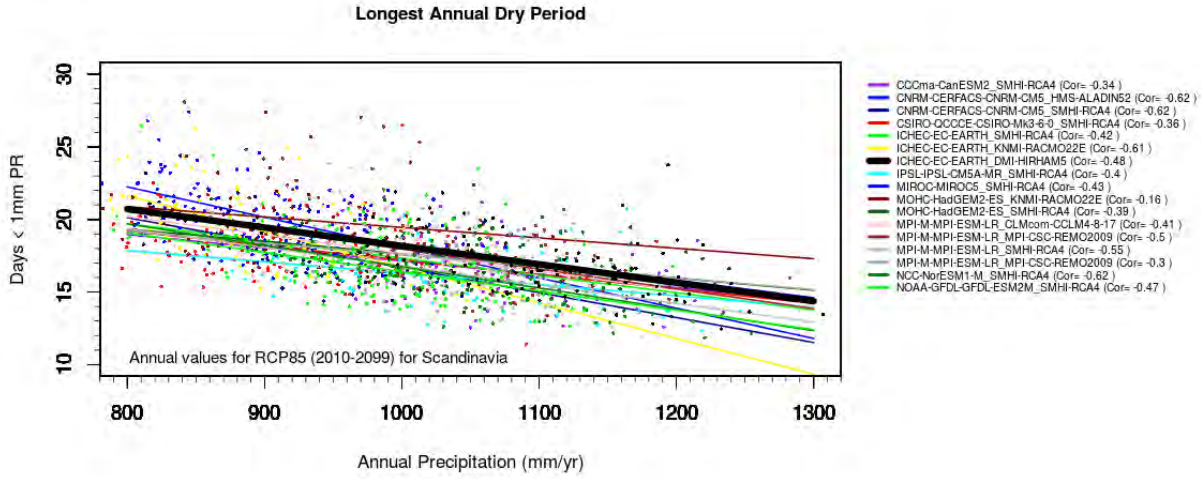

Figure 5.15: Longest dry period calculated for the EURO-CORDEX models and correlated with their individual forcing GCMs. Regression line colours correspond to colour dots and the downscaling experiment listed in the legend. The regression line for HIRHAM5 is highlighted as the thick black line.

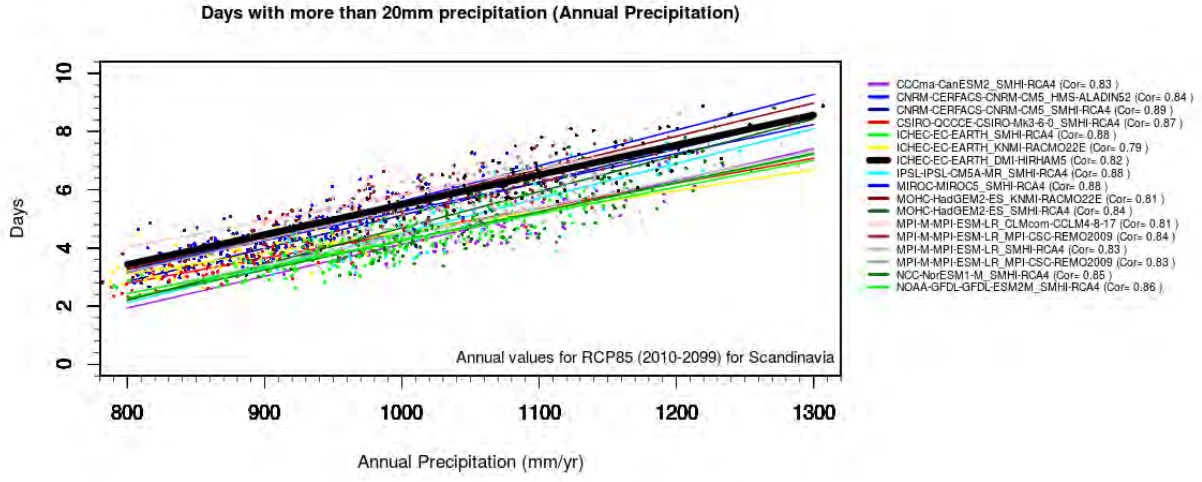

Figure 5.16: As Figure 5.15, but for heavy precipitation (days with precipitation > 20 mm).

Annual precipitation is not significantly correlated with annual mean temperature at grid point level for HIRHAM5 and EC-Earth. Focusing on larger spatial or temporal scales (monthly to seasonally) may change this relationship. Koenigk et al. (2015) showed that precipitation is linearly related with temperature for the wintertime averaged over the region 70-90˚N for a RCA – EC-Earth simulation.

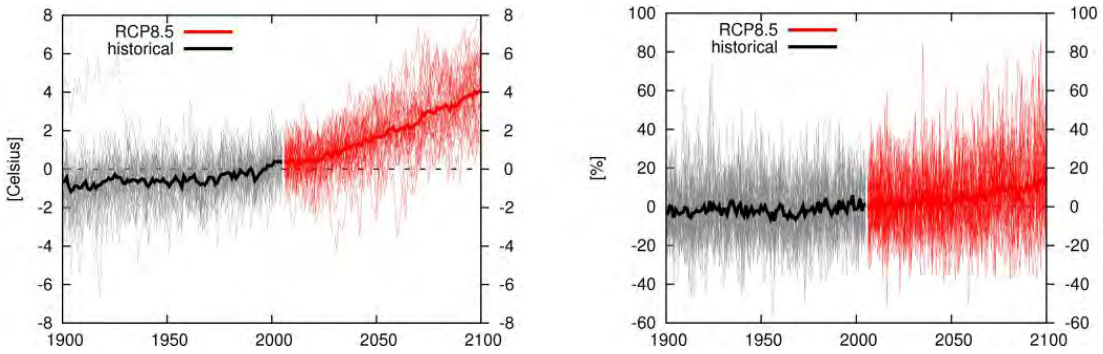

Figure 5.17: Annual mean temperature change (left plot) and relative precipitation change (right plot) for CMIP5 relative to 2086-2005 for the land point nearest Narsaq. Figures are generated from climate explorer (Trouet and Van Oldenborgh, 2013).

The CMIP5 ensemble is not designed for uncertainty assessment, as the ensemble members are neither random nor systematically selected, and therefore inter-dependencies may occur among the models (Knutti and Sedláček, 2013). Nevertheless, it specifies a likely range of model projected future temperatures (IPCC, 2013). However, when CMIP5 projections for precipitation are not robust for the given region (see Figure 5.17) the method cannot be used for uncertainty assessment with precipitation as the relating parameter.

5.7.2 Perspective of the climate reports

From the findings by Olesen et al. (2018a) the following recommendations of improvement of the scientific reports on climate change in Greenland (Christensen et al., 2015a-f) are suggested.

1. The uncertainty should be evaluated on grid point level or for limited areas to take full advantage of the added value by downscaling the GCM EC-Earth to 5.5 km resolution.
2. The year-to-year variability should be considered and quantified, as it clarifies whether a given climate index is projected to change significantly compared to the signal from the year-to-year variability.
3. The climate index from HIRHAM5 should be related to annual mean temperature from its forcing GCM, EC-Earth to ensure the link to the ensemble of GCMs, CMIP5 and to keep a link between the climate index and annual mean temperature simultaneously.

6 Correlation patterns and surface mass balance time series reconstruction

This chapter is based on Paper II "Time evolution of Greenland surface mass balance by combining high-resolution climate modelling, in situ observations and ice cores" (Olesen et al., 2019) and contains full text sections from the paper. In addition to that, more details are added. This chapter accomplishes the aim of validating the HIRHAM5 simulation against observations through spatial correlation patterns and correlation matrices.

6.1 Introduction

Weather and climate information across in situ climate stations, ice cores and a high-resolution RCM simulation make it possible to close gaps in observational time series and to extend RCM simulations beyond the simulation period (Langen et al., 2015; Vinther et al., 2006). Greenland temperature records, and precipitation records in particular, suffer under gaps and various error types (Boas and Wang, 2016) in otherwise valuable observation records. SMB simulated with the RCM, HIRHAM5, based on the re-analysis, ERA-Interim, reaches back to year 1980, where ERA-Interim begins. For outlined areas on the Greenland ice sheet, the HIRHAM5-simulated SMB are extendable, in cases of sufficient knowledge about correlated temperature and precipitation records (Langen et al., 2015). Spatial correlation patterns of temperature and precipitation for Greenland will in this context link the outlined area to relevant weather records. In this study extension and gap filling are implemented with a technique using temperature and precipitation correlation patterns across Greenland. Spatial correlation maps are prepared from a high-resolution HIRHAM5 simulation (Langen et al., 2017) based on observations through the re-analysis ERA-Interim (Dee et al., 2011).

6.1.1 Temperature and precipitation observations in Greenland

Long continuous temperature and precipitation time series are of utmost importance for identifying and understanding past climate variability, and for detecting more recent changes linked to global warming. Information on past and present climate in Greenland is essential for understanding and adapting to present and projected future climate changes in Greenland. But this information is also valuable for aligning ice core proxy times series and comparisons at longer time-scales (Jones and Mann, 2004; Masson-Delmotte et al., 2015; Vinther et al., 2010).

Weather and climate in Greenland have been systematically observed and recorded for more than a century from in situ stations near the towns of Nuuk, Tasiilaq, Upernavik and Ilulissat (Cappelen, 2018). These weather records are displayed together with a selection of the highest quality time series for temperature and precipitation in Figure 3.4 and Figure 3.5. On longer time scales, proxy records of temperature and solid accumulation are reconstructed from deep ice cores from the Greenland ice sheet. The proxy data has a temporally resolution at annual to seasonal centuries and millennia back in time (Andersen et al., 2006; Vinther et al., 2010). In addition to observations and proxy records, the weather and climate in Greenland from 1980-2014 is simulated with the RCM, HIRHAM5 (Christensen et al., 2006) based on a re-analysis product of gridded weather records as an evaluation simulation (Lucas-Picher et al., 2012).

Unfortunately gaps and errors do occur in observed temperature and precipitation time series. This is due to the remote and poorly accessible location of the stations that are exposed to tough weather conditions. Attempts to extend and repair observation time series have among others been made by Vinther et al. (2010a). They used the neighbouring observation stations to close time series gaps to reconstruct intact observation records. In the current research, observation time series are reconstructed from correlation patterns together with observation time series and ice core proxy data, by identifying linked areas with highly correlated characteristics.

Surface mass balance of the Greenland ice sheet

Over the last decades many contributions to understanding and quantifying the SMB of the Greenland ice sheet have been published (Calanca et al., 2000; Box et al., 2012; Box, 2013; Mottram et al., 2017a; Hanna et al., 2005; Cogley, 2009). Most of them with focus on state of the art maps of SMB, melt and solid accumulation distributions on the ice sheet. Correlation and alignment of individual pointwise ice core proxy time series have been published by e.g. (Vinther et al., 2010).

In this study a further step is taken to calculate spatial correlation maps for melt, summer temperature and solid accumulation for the entire Greenland ice sheet, based on the HIRHAM5 evaluation experiment mentioned above. The maps disclose connected characteristics all across Greenland. Thus, when weather records are available within the area of linked characteristics, it allows for extending simulated SMB time series back in time, if the weather records and simulated SMB are correlated in a statistically significant manner (referred to as "significantly correlated" throughout this paper).

The reconstruction procedures assume that temperature and melt time series, as well as precipitation and solid accumulation time series, are significantly correlated, which is invariant over time.

Spatial correlation

Correlation maps determine valuable weather patterns across Greenland and guides in selecting linked time series at different locations, both for information comparison and data exchange. Correlated time series for selected grid points have already been calculated for a number of weather and climate parameters to link the Greenland ice sheet to large scale weather conditions like e.g. NAO or Greenland blocking index (Ballinger et al., 2017; Box et al., 2012; Hutterli et al., 2005; Ortega et al., 2014).

In addition to repairing and extending time series, spatial correlation patterns can provide an overview of the current climate information coverage of already existing weather stations and ice core drill site locations. If the correlation patterns reflect real in situ observations, they may provide a valuable basis for identifying sparsely covered areas when preparing new drill sites and new weather stations.

The correlation patterns over Greenland are deduced from the dynamical downscaling model, HIRHAM5, and are therefore physically consistent throughout the domain. Correlation patterns give an idea of the dominating scale of weather systems for a given location. In section 6.3.2 we prepare and validate high-resolution correlation maps for summer temperature and solid accumulation, and in section6.3.4 and 6.3.5 we fill the gaps in observation time series and extend HIRHAM5-simulated SMB time series. Uncertainties associated with time series reconstruction will be assessed by incorporating results from (Olesen et al., 2018a). While previous work (Boberg et al., 2018; Langen et al., 2015) has focused on model performance on the western part of Greenland, our main foci are locations on the east coast: Renland, Danmarkshavn and Tasiilaq, where Renland is a focus catchment in the ice2ice project, and hence of special interest in this work.

6.2 Method

6.2.1 Model and data description

The RCM setup used in this study is HIRHAM5 driven by ERA-Interim for (1980-2014) as described in section 4.4. Weather observations used in this study consist of monthly temperature and precipitation observation records collected and quality checked by the Danish Meteorological Institute (DMI) (Cappelen, 2018). Only years with full 12-month coverage are included in the correlation calculations.

Ice core proxy data for temperature ($\delta^{18}O$) and accumulation rates are deduced from GRIP, NGRIP, DYE-3, NEEM, Camp Century and Renland documented by Andersen et al. (2006) and Vinther et al. (2010b). The ice core drill site locations are displayed in Figure 6.1. The temporal resolution of $\delta^{18}O$ provides two annual seasons, identified as winter from November to April and summer from May to October, whereas accumulation rates are on an annual scale.

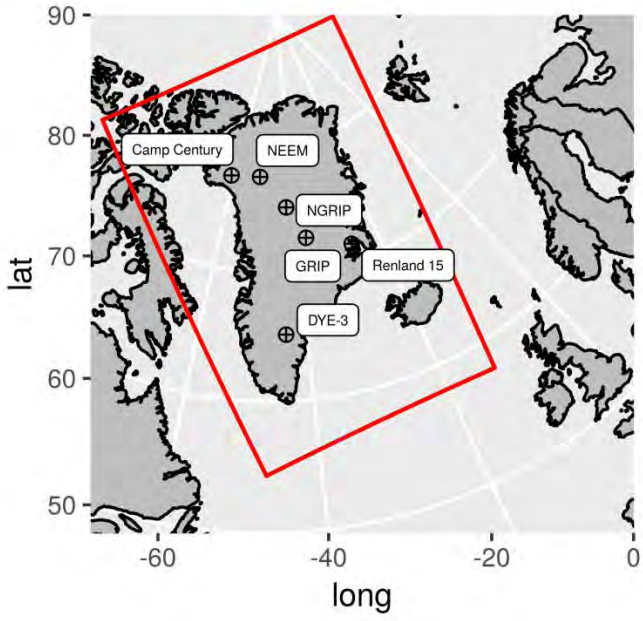

Figure 6.1: Location of the six deep ice cores used in this research. The red square encloses the HIRHAM5 domain on a rotated grid of 5.5 km resolution.

6.2.2 Preparation and validation of spatial correlation patterns

Spatial correlation patterns for are prepared by calculating Pearson's correlation coefficient, *r,* between time series for one selected grid point, *X,* and all land grid points, $Y_{i,j}$, in the domain of 402 × 602 grid points (corresponding to 0.05 × 0.05 degrees).

$$r(X, Y_{i,j}) = \frac{n\sum_{t=1}^{n} x_t y_{i,j,t} - \sum_{t=1}^{n} x_t \sum_{t=1}^{n} x_t y_{i,j,t}}{\sqrt{n\sum_{t=1}^{n} x_t^2 - \left(\sum_{t=1}^{n} x_{,t}\right)^2}\sqrt{n\sum_{t=1}^{n} y_{i,j,t}^2 - \left(\sum_{t=1}^{n} y_{i,j,t}\right)^2}} \qquad (5.1)$$

Where n is the number of years, x_t is the time series on the selected location and $y_{i,j,t}$ refers to the time series at the grid point *(i, j).*

For all correlation maps presented in this study, the distribution of significant correlation coefficients within a 95 % confidence level is colour-indicated from yellow to black on the maps. The critical 95% confidence value is calculated by bootstrapping the 35 time steps (the HIHRAM5 simulation period) with replacement.

HIRHAM5 based correlation patterns presented in this study are:

- Summer temperatures (mean values of June, July and August) for all DMI-stations and ice core drill site locations
- Solid accumulation for ice core drill site locations
- Annual precipitation for all DMI-stations.

Validation of the correlation patterns is primarily based on observations from coastal weather stations, where correlation patterns predicted from the correlation maps (from HIRHAM5 data) are tested between available observed temperature and precipitation time series. In this context, matrices with correlation coefficients for all weather station combinations give a good indication of the HIRHAM5-observation consistency. In addition to that, a corresponding matrix containing degrees of freedom (*df*) associated with each correlation test is presented to help explaining differences between HIRHAM5 and observations. For Pearson's correlation test *df* equals the number of overlapping time steps minus 2. $df = n_{overlap} - 2$ (von Storch and Zwiwes, 1998). Studies on ice core proxy data alignments are also used in this evaluation process (Andersen et al., 2006; Holme et al., 2019; Vinther et al., 2010). Finally, the correlation maps are evaluated by comparing

correlation patterns with dominating weather patterns and topography dependent weather events. For this evaluation the topography field within HIRHAM5 (used as part of the stationary climate input files) is compared with the correlation patterns based on individual weather stations.

6.2.3 SMB reconstruction

Reconstruction of HIRHAM5-simulated SMB time series is based on the general relation between SMB, precipitation (PR), evaporation (E), and runoff (R):

$$SMB = PR - E - R \qquad (5.2)$$

Precipitation equals the sum of solid accumulation (snowfall) and rain, and runoff is equal to liquid water from melt (M) on the ice sheet plus rain minus refreezing (RF). (Langen et al., 2015). Therefore,

$$SMB = Solid\ acc - E - M + RF \qquad (5.3)$$

High correlation between refreezing and melt plus rain justifies regression of simulated SMB from solid accumulation minus evaporation and melt. Simulated SMB time series can then be reconstructed from a fitted partial regression function of observed annual precipitation and summer temperature. This assumes that annual solid accumulation is closely linked to annual precipitation over the ice sheet, and that annual melt is linked to summer (JJA) temperature.

$$SMB_{recon} = \alpha PR_{OBS} - \left(\beta_1 T_{OBS} + \beta_2 T_{OBS}^2 + \beta_0\right) \qquad (5.4)$$

This idea was introduced by Langen et al. (2015) with focus on Nuuk and Nuuk fjord. The assumed link between melt and summer temperatures as well as solid accumulation and annual precipitation will be shown for time series for the drill site locations for solid accumulation-evaporation and annual precipitation and for drainage basins defined by Zwally et al. (2012) for simulated melt and JJA-temperature.

In this study, three reconstruction examples are presented. Here the relationships between melt and temperature, and solid accumulation and precipitation will be calculated as field averaged melt and solid accumulation values. The areas will be the most representative drainage basins defined by Zwally et al. (2012). See Figure 6.2.

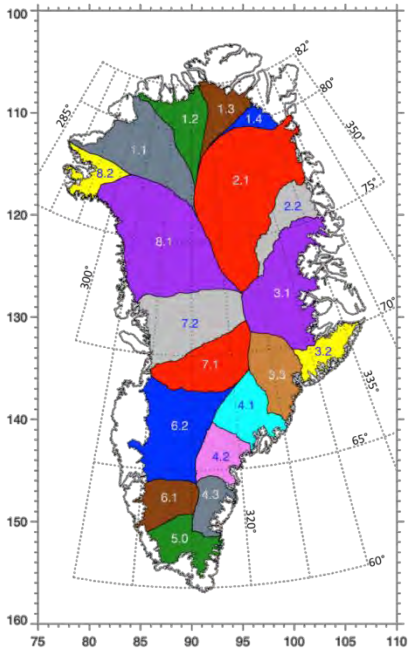

Figure 6.2: Drainage basins for the Greenland ice sheet divided into 19 basins that reach the coast. From (Zwally et al., 2012).

6.2.4 OBS reconstruction

Reconstruction of observed temperature and precipitation time series through correlation patterns and correlated time series are carried out directly from the best correlated observation time series and best correlated ice core (if any significantly correlated ice core proxies are available). All time series are standardized to zero mean and standard deviation of one before reconstruction.

Ice cores consist of stable water isotopes (δ18O) stratified in well preserved annual layers. This feature offers two valuable properties. First, the isotopic composition correlates with the temperature in the cloud at the time of condensation (Dansgaard, 1964, 1954). Thus, ice core δ18O measurements can be used to reconstruct past temperature at the drill site. Second, the temperature correlated δ18O oscillations provide a measure of past annual accumulation rate if a depth-age chronology is available.

This study utilizes ice core measurements from Renland (past 214 years) and DYE-3 (past 500 years) to extend the weather records from the DMI-station in Tasiilaq. Previously, (Vinther et al., 2010) demonstrated that δ18O from DYE-3 correlated with the regional temperature back in time. For Renland, we use a stack of three local ice cores (presented in Holme et al. (2019)). If available, it is beneficial to use a δ18O stack as it amplifies the signal part of the data and thus its correlation with the local atmospheric conditions. While Holme et al. (2019) found that this δ18O stack is not significantly correlated with Icelandic temperature in the period 1830-1910, we here assume that it still reflects the Greenlandic climate conditions back in time (acknowledging that it still remains uncertain to what extent the linear relationship between Renland δ18O and regional temperatures have varied back in time).

Precipitation can be reconstructed through an ice core's depth-age relationship. As each annual layer has a specific thickness depending on the amount of precipitation, past accumulation rate can be estimated if an annual layer's age is known together with the amount of thinning the layer has experienced.

6.2.5 Uncertainties

Uncertainties associated with the reconstructed time series are calculated by fitting a regression function to periods with an overlap between the simulated and reconstructed time series. From the regression function both prediction and confidence intervals are calculated. The confidence interval is used as a measure for the reconstructed regression line uncertainty, while the prediction interval is applied as a measure of the mean difference between the two time series for a given value. The prediction interval is calculated to contain 95% of the difference, and corresponds to the confidence interval for the response variable to the predictor (von Storch and Zwiwes, 1998). The prediction bounds follow the general expression: *sample estimate ± (t-multiplier × standard error).*

The formula notation is:

$$\hat{y}_h \pm t_{\left(\frac{\alpha}{2},n-2\right)} \times \sqrt{MSE \times \left(1 + \frac{1}{n} + \frac{(x_h - \overline{x})^2}{\sum(x_i - \overline{x})^2}\right)} \qquad (5.5)$$

$\hat{y}_h$, is the predicted value, where the predictor is x_h.

$t_{\left(\frac{\alpha}{2},n-2\right)}$, is the t-multiplier with n-2 degrees of freedom, where α is the confidence level.

$\sqrt{MSE \times \left(1 + \frac{1}{n} + \frac{(x_h - \overline{x})^2}{\sum(x_i - \overline{x})^2}\right)}$, is the standard error of the prediction, where MSE, is mean square error.

In Figure 6.3 the predictions and confidence intervals appear as shallow hyperbolas. The confidence intervals for the regression line is

$$\hat{y}_h \pm t_{\left(\frac{\alpha}{2}, n-2\right)} \times \sqrt{MSE \times \left(\frac{1}{n} + \frac{(x_h - \overline{x})^2}{\sum(x_i - \overline{x})^2}\right)} \quad (5.6)$$

The equation for prediction intervals differs from the corresponding equation for the confidence intervals associated with the regression line by having an extra MSE term, which is caused by the unknown variance of the prediction. An example is shown in Figure 6.3. By using this approach, each reconstructed value is given a specific uncertainty interval. Relatively small and high precipitation values are associated with large uncertainties. This idea was also presented in Olesen et al. (2018a). Uncertainties are calculated for both simulated SMB-reconstructions and for reconstructions of observation time series.

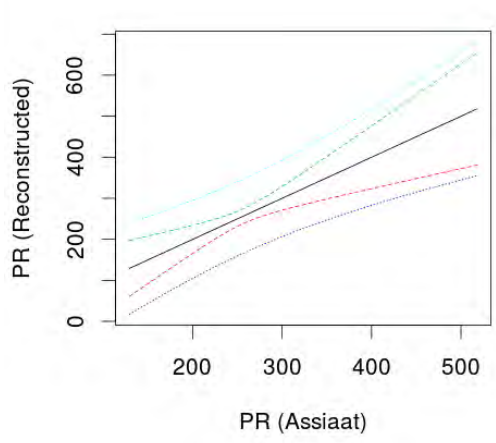

Figure 6.3: Linear regression between observed and reconstructed precipitation (black line). Turquoise and blue lines are the upper and lower 66% prediction intervals containing 66 % of observed and reconstructed values. A green and red line refers to the regression line and denotes the 66% confidence interval of the regression line.

Reconstructed SMB time series including uncertainty intervals are compared with solid accumulation from upstream ice core measurements at locations that, according to the

correlation patterns, are expected to be significantly correlated with the relevant drainage basin.

6.2.6 Spatial observation coverage across Greenland

Temperature and precipitation nearby an observation station or ice core drill site are generally strongly correlated with the observation point, but areas over longer distances may also be strongly correlated. In this context, spatial correlation patterns provide a useful tool to evaluate the extent to which a given parameter is spatially covered by observation stations and ice core drill sites across Greenland. Some areas are covered by more than one weather station or ice core drill site location for a given parameter, whereas other areas are not covered at all.

The coverage of observation locations all across Greenland is investigated by combining all the correlation maps for a given parameter. This analysis is done by generating maps where each land grid point represents the highest correlation coefficient extracted from all the correlation maps based on individual observation and ice core locations.

6.3 Results

6.3.1 Weather records

Precipitation and temperature records from DMI-weather stations in Greenland used in this study consist of 13 weather stations for precipitation and 19 stations for temperature. Annual precipitation and annual mean temperature records are shown in Figure 3.4 and Figure 3.5. Years with one or more missing monthly values are discarded. The time period starts from the first full 12-month observation year and ends with the last year of the HIRHAM5 simulation (2014).

6.3.2 Spatial correlation patterns

Correlation patterns presented here are calculated from equation 5.1 for annual precipitation and summer temperature for the DMI-weather stations, and solid accumulation minus evaporation and summer temperatures for 6 deep ice core drill site locations on the Greenland ice sheet. In the following three examples are presented. Maps for other areas are presented in appendix B.

Correlation patterns for annual precipitation (1980-2014) correlated with the HIRHAM5 simulated time series for the land grid points closest to Nuuk, Tasiilaq and Danmarkshavn are shown in Figure 6.4. Similar maps are presented in Figure 6.5 for summer temperature (JJA). The critical correlation coefficient for statistically significant correlation within a 95% confidence level is r = 0.33. The critical value is fixed to yellow on the correlation maps. While dark colours represent a high correlation, everything towards red colours is not significantly correlated with the selected grid point.

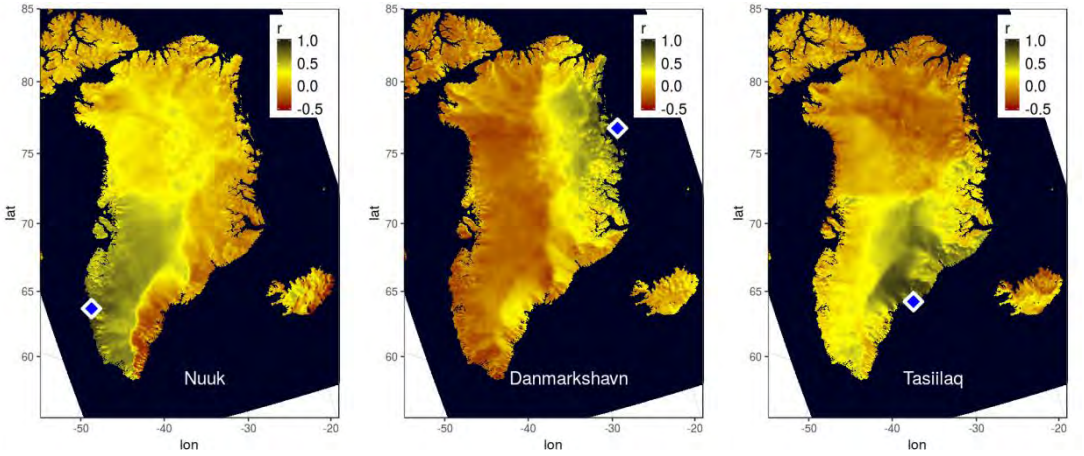

Figure 6.4: Correlation patterns for HIRHAM5 simulated annual precipitation time series 1980-2014. The maps represent correlation coefficients between each land grid point and the grid point closest to the weather stations in Nuuk, Danmarkshavn and Tasiilaq (from left to right). Critical correlation coefficient for statistical significance at a 95% confidence level is r = 0.33 (yellow).

The correlation patterns in Figure 6.4 are dominated by well-defined areas, where precipitation is significantly correlated to the weather station of interest. For the weather station in Nuuk the precipitation is strongly correlated in the area west of the ice sheet ridge in south Greenland, while some areas east of the ridge (the darkest red areas) are close to or just significantly anti-correlated to precipitation observed in Nuuk. The ice ridge represents an almost instantaneous shift from positive to negative correlation coefficients. Corresponding correlation patterns emerges on the correlation maps for Danmarkshavn and Tasiilaq.

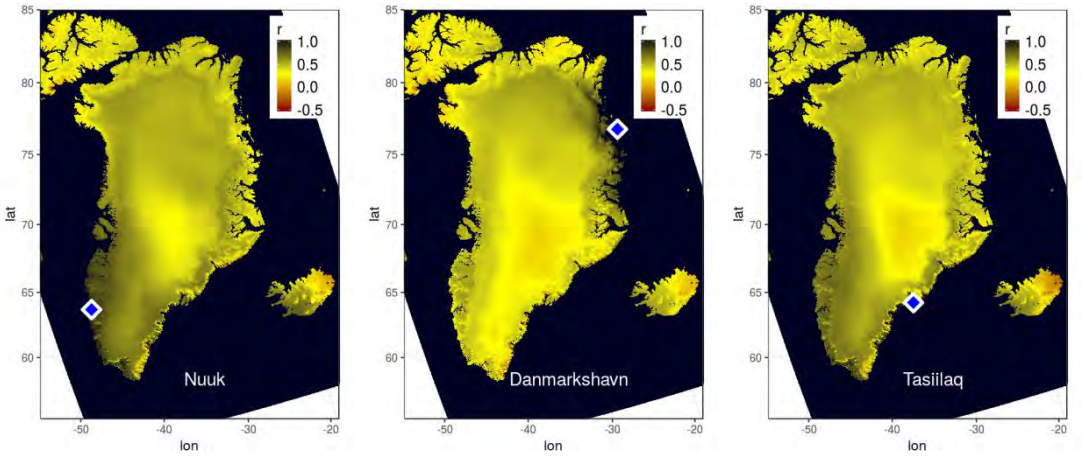

Figure 6.5: Correlation patterns for HIRHAM5 simulated summer (JJA) mean temperature time series 1980-2014. The maps represent correlation coefficients between each land grid point and the grid point closest to the weather stations in Nuuk, Danmarkshavn and Tasiilaq (from left to right). Critical correlation coefficient for statistical significance at a 95% confidence level is r = 0.33 (yellow).

Spatial correlation patterns for temperature in Figure 6.5 show more smooth correlation patterns compared to the precipitation correlation patterns. There are no areas, where temperature is close to anti-correlated with the temperature time series at the weather station grid point. The correlation pattern appears to be altitude dependent, and in a band along the ice sheet edge, temperatures are slightly stronger correlated with the temperature at the grid point nearest the weather station. This tendency appears most distinct for correlation coefficients w.r.t. Nuuk. The correlation for precipitation seems to depend on the topography slope direction rather than on altitude, in contrast to the temperature correlation patterns.

6.3.3 Validation of correlation patterns

Correlation patterns prepared from the HIRHAM5 simulation are compared with observations to verify if the patterns appearing on the maps in Figure 6.4 and Figure 6.5 also appear in an analogous combination of observation records.

6.3.3.1 Correlation matrices for precipitation

For each possible combination of weather stations the correlation coefficients are calculated and presented as correlation matrices for observed precipitation records in Figure 6.6 (top right). The corresponding relationships for HIRHAM5 time series in land grid points closest to the weather station locations are displayed after the same procedure (top left). Yellow is constrained at r = 0.33, which for HIRHAM5 corresponds to the critical value of statistically significant correlation within a 95% confidence level. For the observations the critical value for significant correlation is varying among the possible combinations of weather station records because of unequal record overlaps. As the critical value depends on the length of the overlapping records, the colour key for observation combinations only represents the correlation coefficient and not whether or not a combination is significantly correlated. Therefore the p-values, considering varying degrees of freedom, are displayed separately in the two bottom plots.

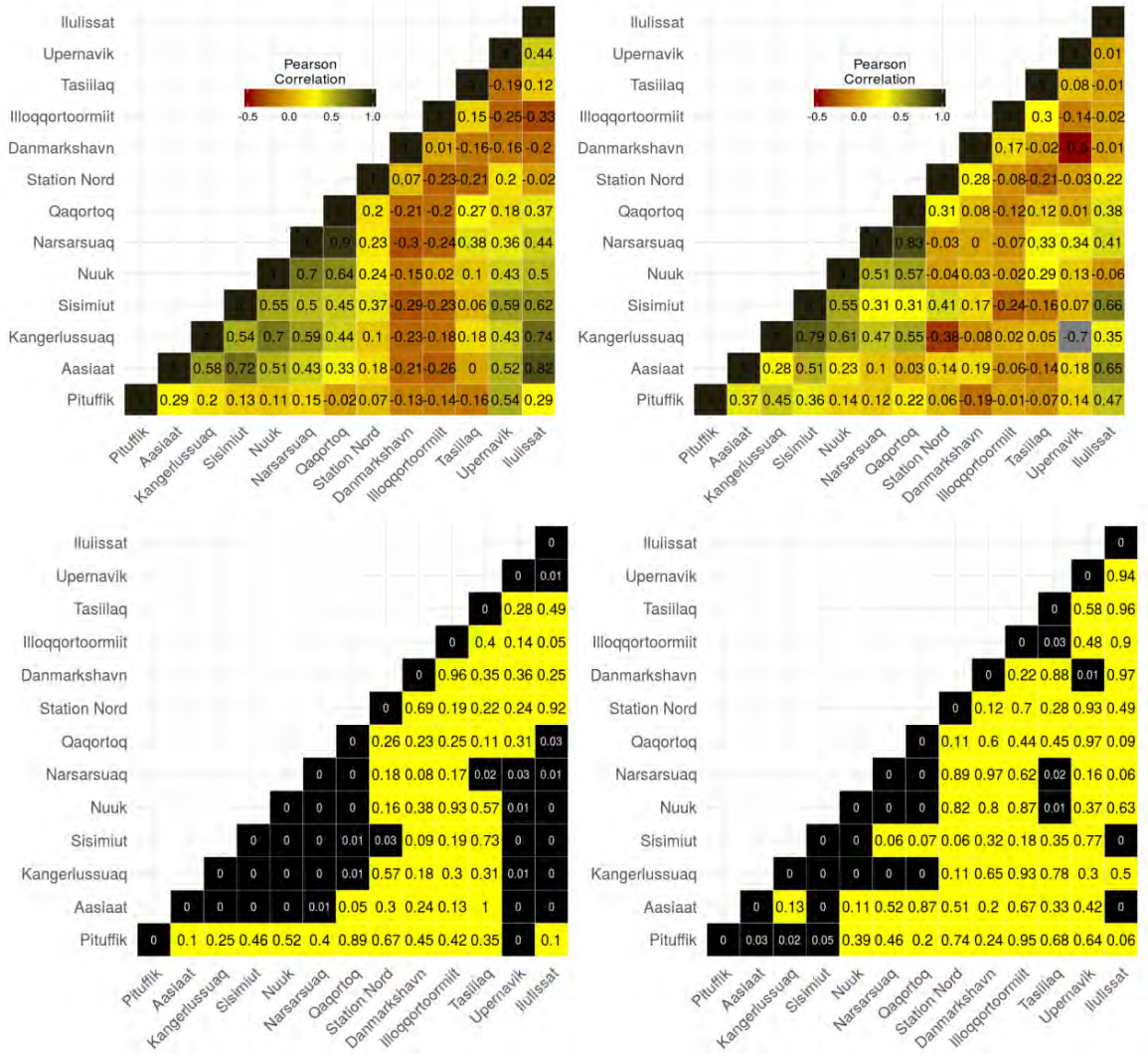

Figure 6.6: Correlation matrices for simulated (top left) and observed (top right) precipitation at 13 weather stations. Statistically significant (at a 95% confidence level) correlated weather station combinations are marked with black for simulations and observations (bottom left and right). P-values are shown for the not significantly correlated station combinations (yellow squares).

Pearson's correlation coefficients for the HIRHAM5 simulation are calculated for 35 year time series (with degrees of freedom, $df = 33$) whereas for observations, the number of overlapping years is varying from 4 to 107 years. The degrees of freedom corresponding to the correlation test for observations in Figure 6.6 (top right matrix) is presented in Figure 6.7. Red colours indicates $df_{obs} > df_{HIR}$ and conversely blue colours indicate $df_{obs} < df_{HIR}$.

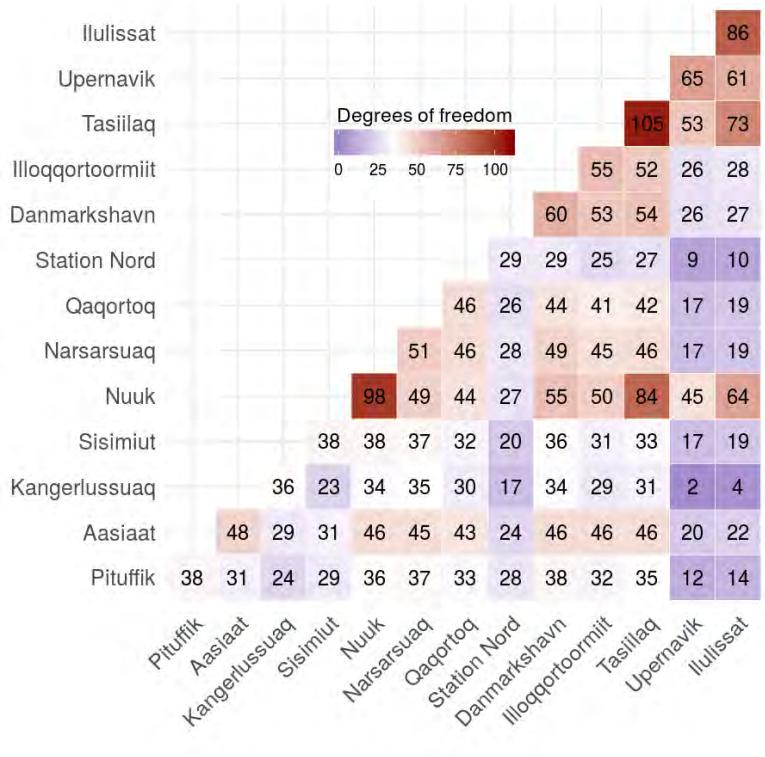

Figure 6.7: Degrees of freedom for observed precipitation for combinations of DMI-weather stations in Greenland. Red colours indicate higher degrees of freedom than in the HIRHAM5 35-year simulation (df > 33) and blue lower degrees of freedom.

6.3.3.2 Correlation matrices for temperature

As for precipitation, correlation matrices are calculated for summer temperature. HIRHAM5 simulated time series and observation records are combined for 19 weather station locations and compared in Figure 6.8. The corresponding degrees of freedom matrix for observation records is shown in Figure 6.9. In contrast to precipitation, the number of statistically significant correlated combinations for temperature is remarkably higher for observation records than for HIRHAM5 simulated time series.

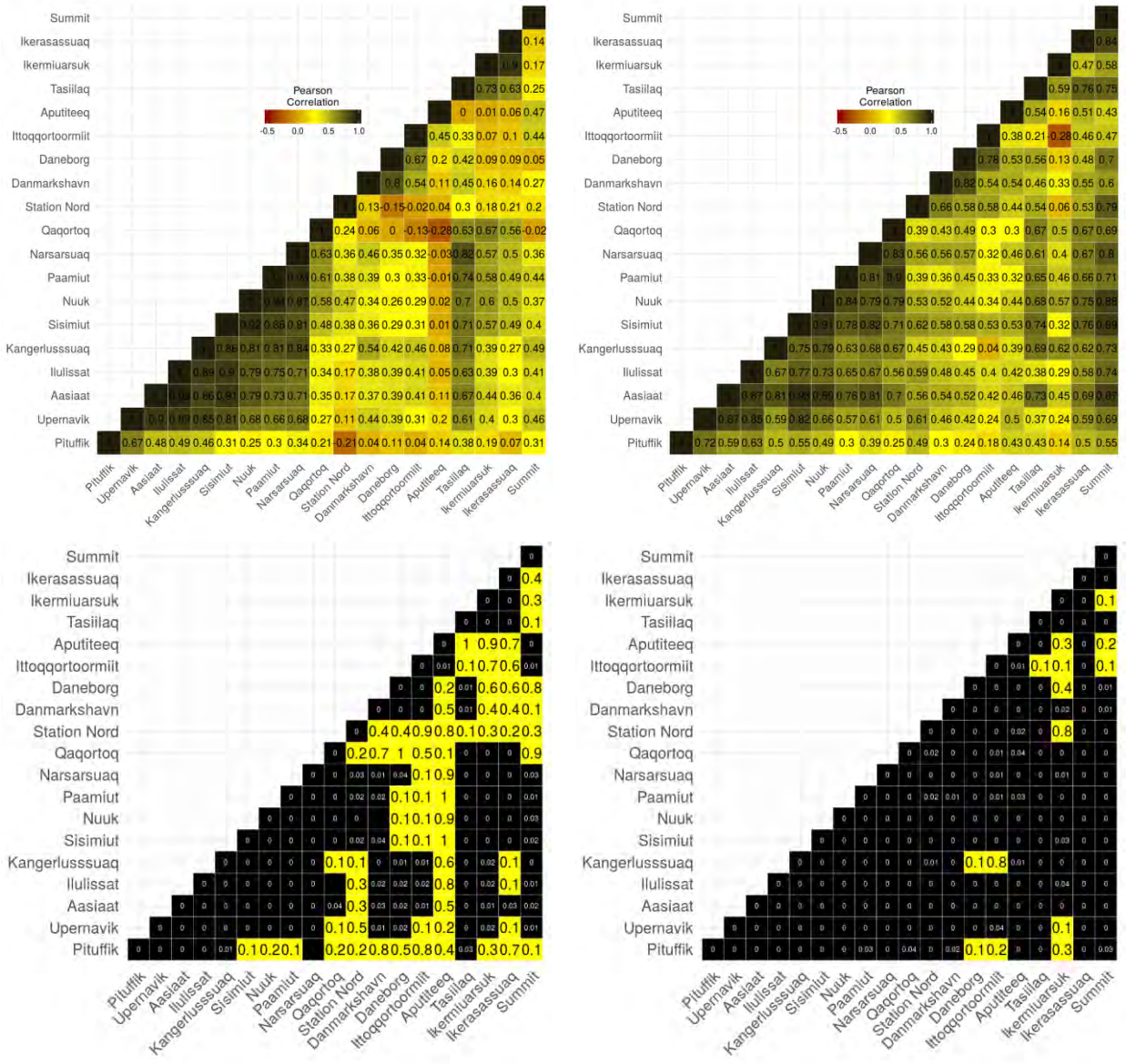

Figure 6.8: Correlation matrices for simulated (top left) and observed (top right) summer temperature at 19 weather stations. Statistically significant (at a 95% confidence level) correlated weather station combinations are marked with black for simulations and observations (bottom left and right). P-values are shown for not significantly correlated station combinations (yellow squares).

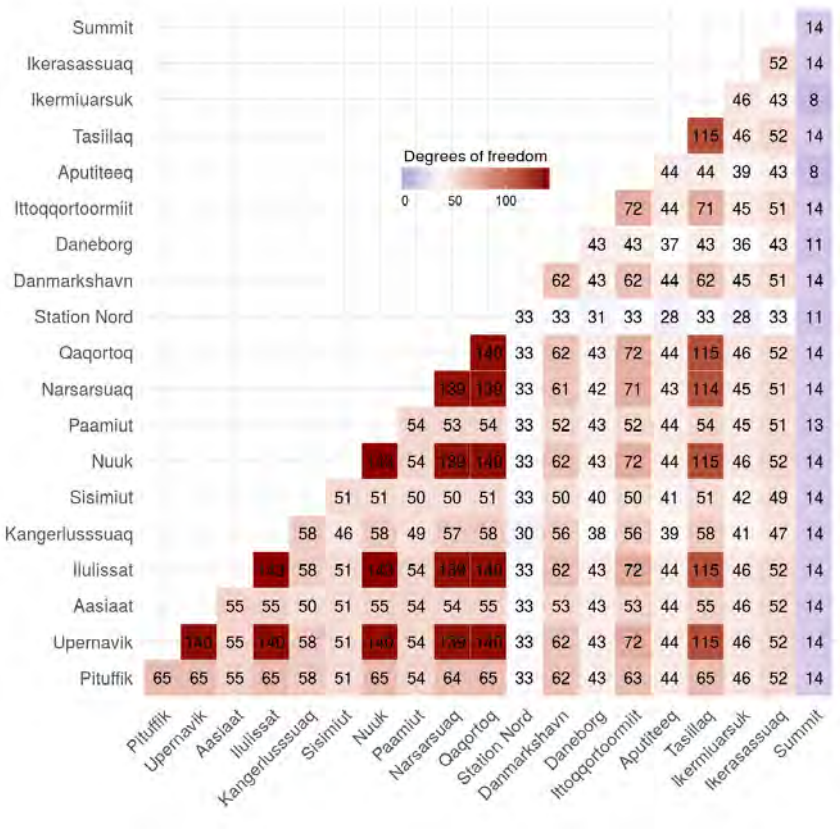

Figure 6.9: Degrees of freedom for observed summer temperature (JJA) for combinations of DMI-weather stations in Greenland. Red colours indicate higher degrees of freedom than in the HIRHAM5 35-year simulation (df > 33) and blue lower degrees of freedom.

6.3.3.3 Slope direction of the Greenland topography

HIRHAM5 is simulated on the basis of a number of fixed climatology input files among which the topography is described via the geopotential height. Figure 6.10 shows the slope direction of the topography. The gradient of each point is calculated from its four neighbour points, but only the direction (not the steepness) is displayed in the figure. Accordingly, ridges that appear sharp and well-defined may be relatively flat and smooth surfaces.

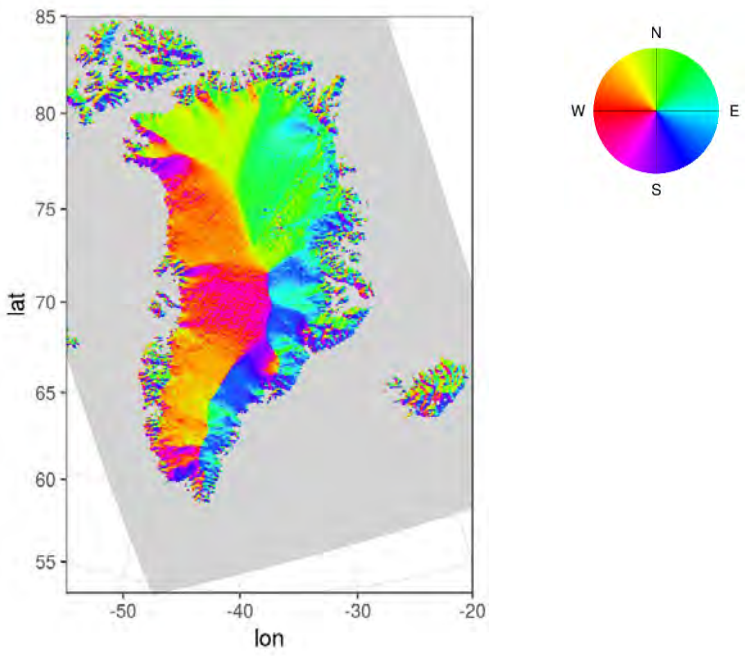

Figure 6.10: Slope direction of the Greenland topography from the HIRHAM5 climatology files. The grey area is the sea-points within the HIRHAM5 simulation domain.

6.3.4 Reconstruction of precipitation and temperature records

6.3.4.1 Reconstruction from correlated observation stations

Precipitation is with a few gaps observed in Ilulissat from 1890 to 1984 (Cappelen, 2018) and will here be an example of an observation record reconstruction. Observed precipitation in Aasiaat and Sisimiut are significantly correlated with precipitation in Ilulissat with correlation coefficients $r = 0.65$ and $r = 0.66$ respectively, see correlation matrices in Figure 6.6. Extension and gap filling is calculated by fitting a linear regression function for the time series overlap between Ilulissat and the two correlated stations. The coefficients, a and b, are then used to reconstruct the precipitation time series in Ilulissat:

$$PR_{Ilul} = a_{ilul,aasi} PR_{aasi} + b_{ilul,aasi} \text{ and}$$

$$PR_{Ilul} = a_{ilul,sisi} PR_{sisi} + b_{ilul,sisi}.$$

A combination of reconstructed precipitation values and originally observed time series from Ilulissat is illustrated in Figure 6.11. Uncertainties associated with the

reconstruction in terms of confidence and prediction intervals are shown as grey and dark grey shaded areas calculated as 66% and 95% prediction intervals from the linear regression functions (equation 5.5).

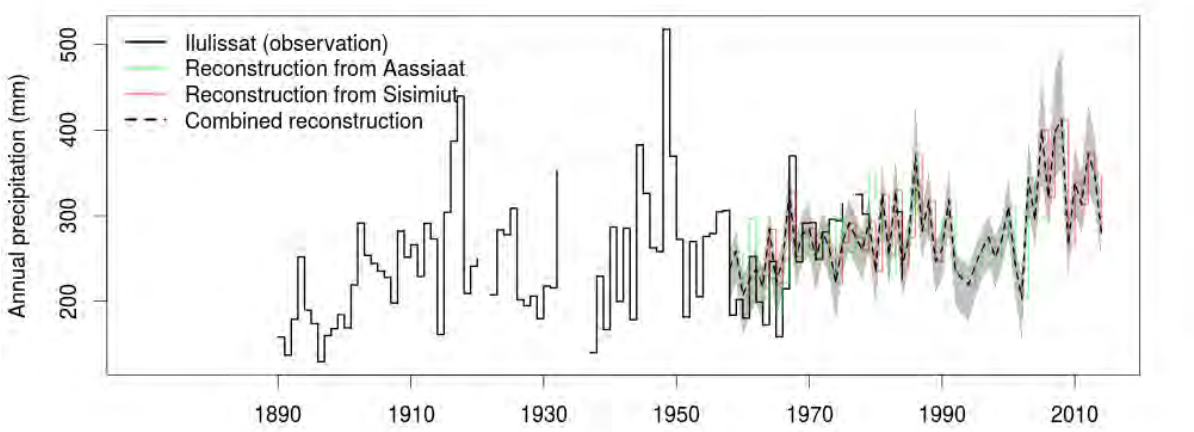

Figure 6.11: Reconstruction of observed precipitation from Ilulissat with observations from Aasiaat (green) and Sisimiut (red). The prediction interval for each reconstructed value is indicated with vertical error bars (66% dark grey and 95% light grey).

6.3.4.2 Reconstruction of temperature records using ice core data

The DMI-weather station in Tasiilaq is here the case proving the benefit of extending weather records from ice core data. According to the correlation patterns in Figure 6.5 temperature is significantly correlated with the Tasiilaq both at DYE-3 and at Renland, whereas only DYE-3 is correlated with Tasiilaq for precipitation. Ice core locations are shown in Figure 6.1.

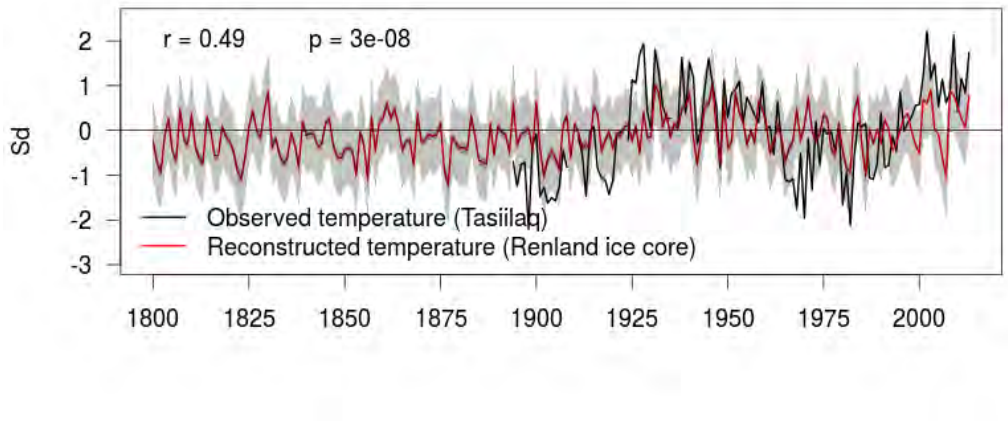

Figure 6.12: Reconstructed annual mean temperature (1800-2014) observation from Tasiilaq based on δ18O records from the Renland ice core (top plot) and a zoom of the overlapping period 1800-2014 (bottom plot). The reconstructed time series (red) is significantly correlated with the observed time series (black) with r = 0.49 and p-value < 0.05. Grey shaded areas correspond to the 66% prediction interval for each reconstructed value and the dark shaded area close to the reconstructed curve is the confidence interval of the regression line.

Annual mean temperature observed at Tasiilaq is significantly correlated with the temperature proxy record from the Renland ice core with a correlation coefficient, r = 0.45. In Figure 6.12 the observed time series is via a regression function between the two time series reconstructed to cover a 215 year period. The reconstructed temperature is damped due to the regression function, but 66% of the damped signal is restored as the prediction interval (equation 5.5), indicated as light grey shaded area.

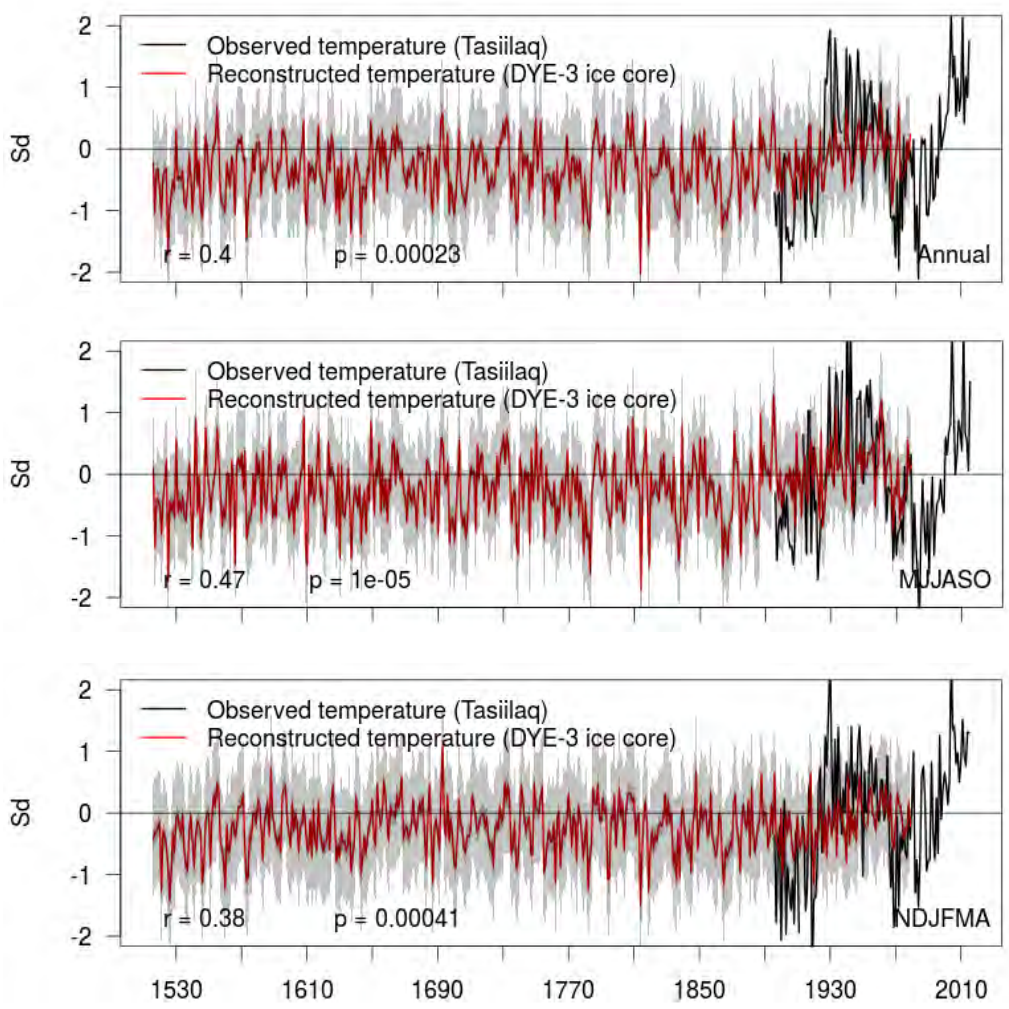

Figure 6.13: 500-year reconstructed temperature from Tasiilaq based on δ18O records from the DYE-3 ice core for annual mean (top), summer (middle) and winter (bottom plot). The reconstructed time series (red) is significantly correlated with the observed time series (black) with r = 0.38 and p-value < 0.05. Grey shaded area corresponds to the 66% prediction interval for each reconstructed value.

Annual mean temperature observed at Tasiilaq is significantly correlated with the temperature proxy record from the DYE-3 ice core with a correlation coefficient, r = 0.40, r = 4.7 and r = 0.38 for annual, summer and winter time series respectively. As for Renland the observed time series is via a regression function between the two time series reconstructed in Figure 6.13 to cover a 500 year period, but here for annual, summer and

winter (top, mid and bottom plot). Again 66% of the damped signal is restored by adding the prediction interval, indicated as light grey shaded area.

6.3.4.3 Reconstruction of precipitation records using ice core data

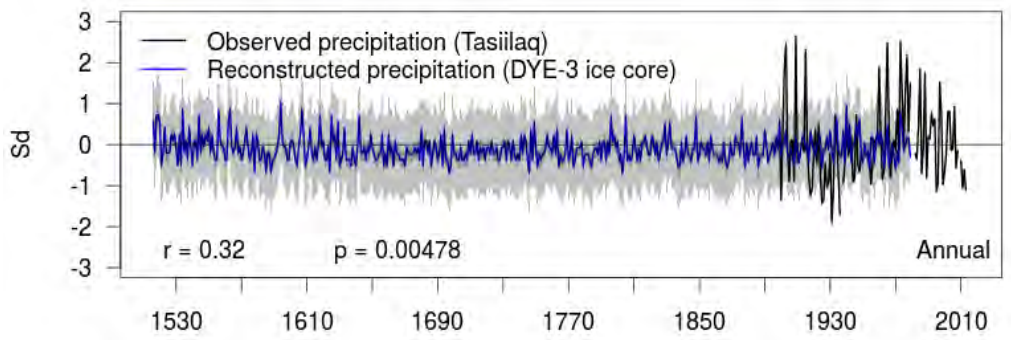

Figure 6.14: Reconstructed annual accumulated precipitation time series from Tasiilaq based on δ18O data from DYE-3 ice core for 1514-2014. The reconstructed time series (blue) is significantly correlated with the observed time series (black) with r = 0.32 and p-value < 0.05. Grey shaded areas correspond to the 66% prediction interval for each reconstructed value.

As for annual mean temperature observed at Tasiilaq, the precipitation is significantly correlated with the accumulation rate from the DYE-3 ice core with a correlation coefficient, r = 0.32 and a p-value, p = 0.0048. As for temperature, precipitation observed in Tasiilaq is reconstructed (see Figure 6.14).

6.3.5 Reconstruction of simulated SMB

Reconstruction of simulated SMB is calculated from observed precipitation and temperature (equation 5.4), and relies on the assumption that these parameters correspond to solid accumulation minus evaporation and melt respectively (see equation 5.2 and 5.3). The first step is to test the relationship between precipitation and solid accumulation as well as summer temperature and melt.

Annual solid accumulation is linearly related with annual precipitation as shown in Figure 6.15 where the solid accumulation fraction of precipitation is reduced for areas with more precipitation like DYE-3, which is also the southernmost ice core drill site

location. In comparison, NGRIP is far from the coast at high altitude, and precipitation falls only as snow.

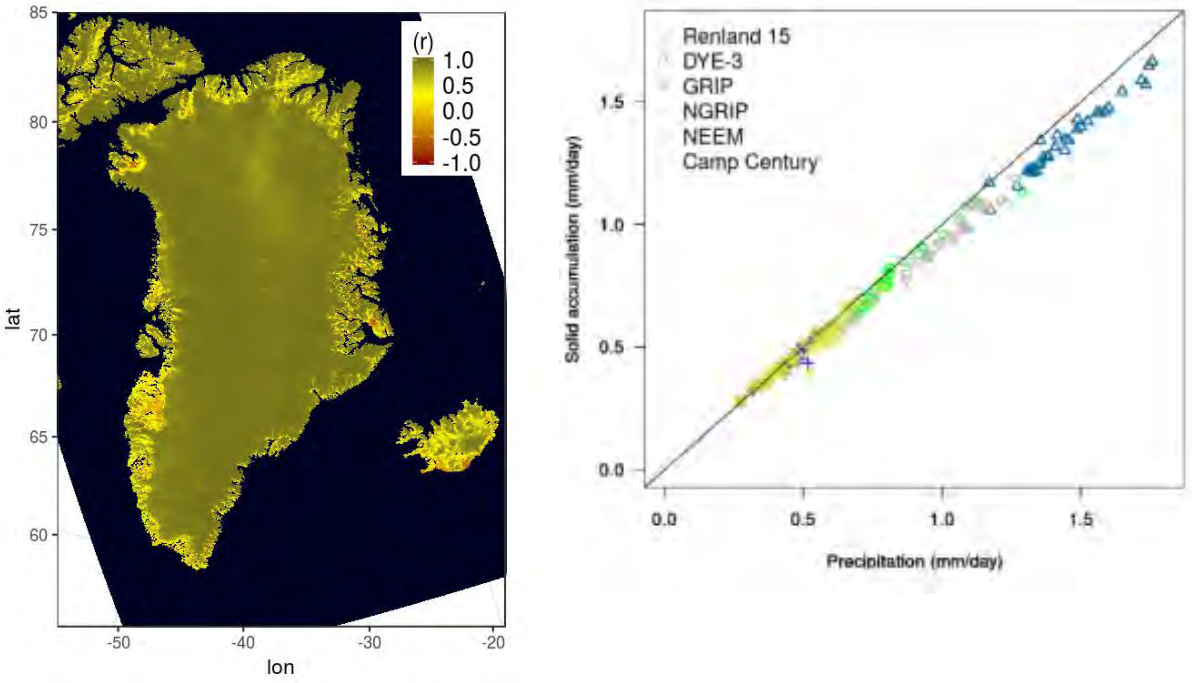

Figure 6.15: Relationship between HIRHAM5 modelled solid accumulation minus evaporation and annual precipitation for the 35-year time period (1980-2014) for each grid point in the domain (left) and for the nearest grid point to the six deep ice core drill site locations on the unity plot (right).

Melt is related to summer temperature through a second order regression function. In Figure 6.16 the best fitted regression lines are plotted for each drainage basin (see Figure 6.2). This is tested similarly for an exponential regression function and a simple linear function for comparison. Pearson's correlation coefficient is calculated as a measure of regression accuracy and is shown for all Zwally drainage basins in Figure 6.16 (bottom right) for each of the three test functions. Areas where no melt take place appear as black areas in the middle of the ice sheet.

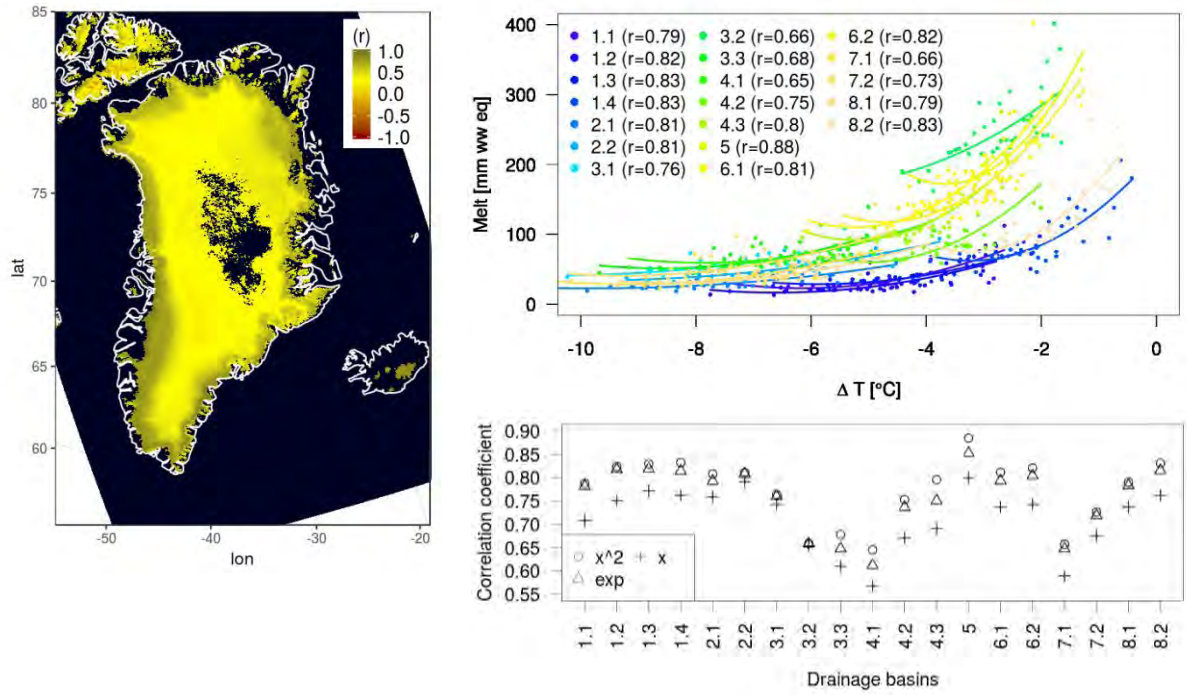

Figure 6.16: Relationship between HIRHAM5 modelled melt and summer mean temperature (JJA) for 1980-2014 for each ice covered grid point in the HIRHAM5 domain on the map (left). Black areas on the ice sheet represent areas with no melt. Relationships between melt and summer temperature for each drainage basin are shown separately with second order regression functions (top right). Correlation coefficients for the second order, linear and exponential regression functions are compared for each drainage basin (bottom right).

6.3.5.1 SMB reconstruction for Tasiilaq

HIRHAM5-simulated SMB is extended back in time with a reconstruction based on observed summer temperatures and annual precipitation measured in Tasiilaq from 1980-2014, using the regression function (equation 5.4).

Melt and solid accumulation as well as modelled SMB are spatially averaged over the drainage basin 4.2 shown in Figure 6.2. Basin 4.2 reaches from the north-south orientated ice sheet ridge to the west coast, and is chosen from the correlation maps with reference point at Tasiilaq in Figure 6.1. Simulated SMB in this drainage basin increases from close to zero near the ice sheet ridge to almost 6 m liquid water equivalents per year for a few grid points on step slops near the coast, see Figure 6.17.

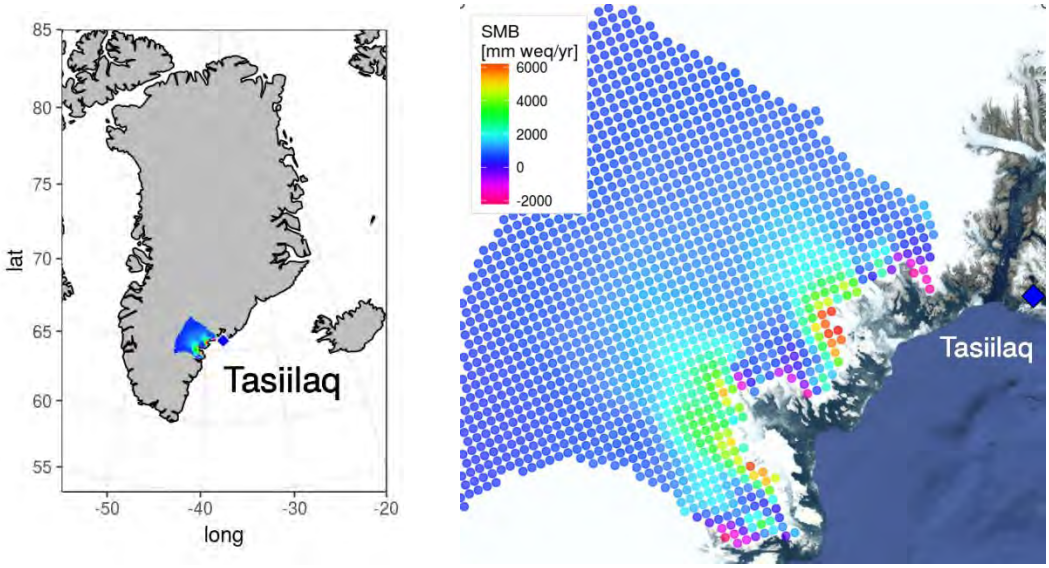

Figure 6.17: Drainage basin 4.2 (Zwally et al., 2012) showing annual mean SMB (1980-2014) simulated with HIRHAM5. The Tasiilaq weather station is indicated with a blue diamond.

In Figure 6.18, we show how observed summer temperature and annual precipitation are significantly correlated with modelled melt and solid accumulation within a 95% confidence level with $r = 0.41$ and $r = 0,64$. This is consistent with the correlation patterns in Figure 6.4 and Figure 6.5. From 1980 to 2014 all time-series are standardized to zero mean and a standard-deviation of one.

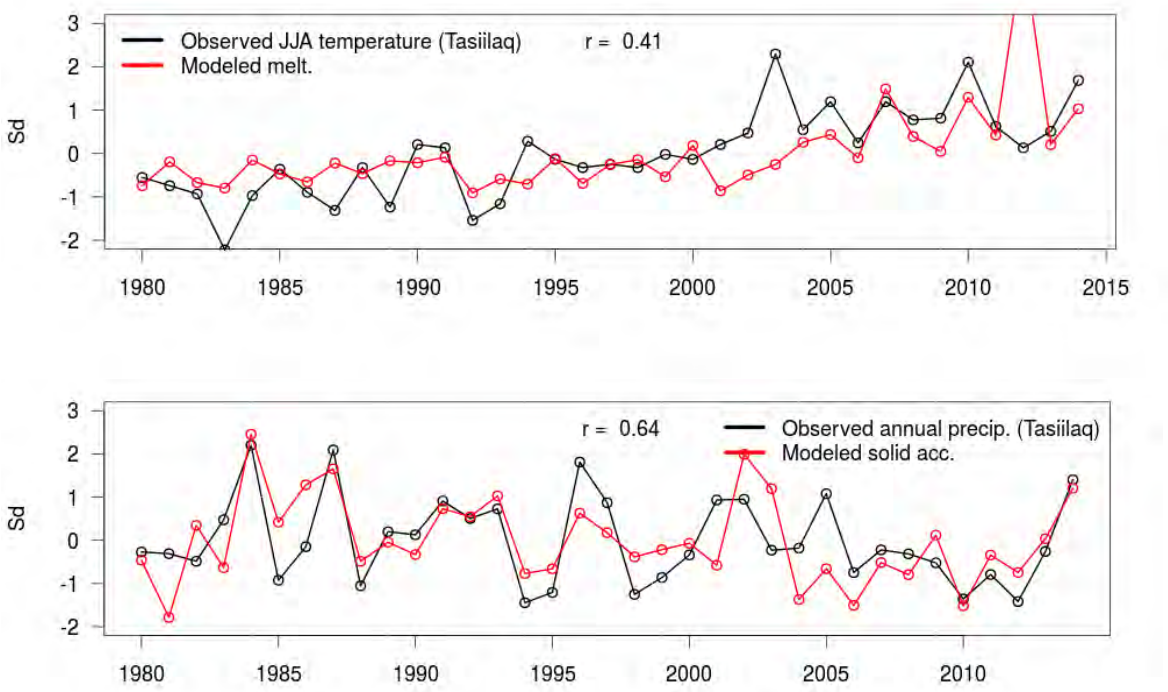

Figure 6.18: Observed summer temperature (JJA) and modelled melt (top plot) and observed precipitation and modelled solid accumulation (bottom plot) for Tasiilaq. All values are standardized to zero mean and one standard deviation.

Precipitation represents the main contribution to the SMB for this area as standardised precipitation shows a steeper slope of the regression line with SMB than standardised temperature does, see Figure 6.19.

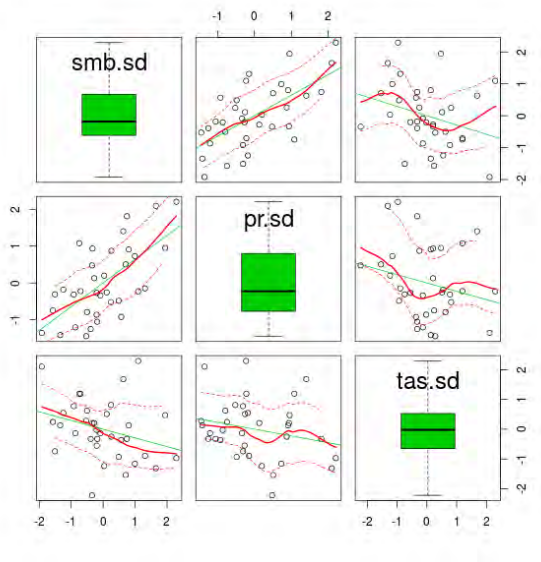

Figure 6.19: Partial regression lines for Tasiilaq. The reconstructed SMB is optimised to fit precipitation and temperature observations to HIRHAM5 simulated SMB for 1980-2014. Smb.sd, pr.sd and tas.sd are standardised SMB, precipitation and temperature.

From the best fitted regression line, uncertainties in terms of confidence interval (equation 5.6) associated with the regression line and the prediction interval (equation 5.5) are illustrated in Figure 6.20. In Figure 6.20 the standardised value of reconstructed SMB equal to one standard deviation for simulated SMB (illustrated with the green dashed line) furthermore illustrates the damping effect of the regression procedure. The intervals are added to the reconstructed SMB values in Figure 6.21.

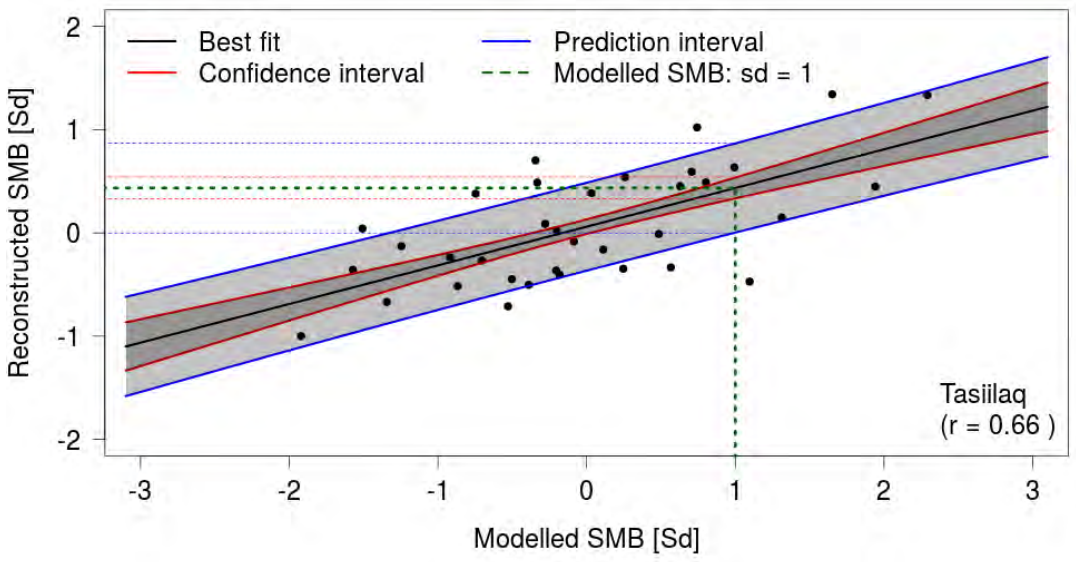

Figure 6.20: Uncertainty estimates of reconstructed SMB. The black line is the best fitted regression line to the reconstructed and modelled SMB. The dark grey shaded area between red lines is the confidence interval for the regression line, and the prediction interval is the light shaded area between the blue lines. Green dashed lines indicate the translation of modelled SMB to reconstructed SMB, including confidence and prediction intervals (red and blue dashed lines).

Surface mass balance is reconstructed from observed temperature, T and precipitation, PR for drainage basin 4.2 from: $SMB_{RECON} = 0.49PR_{OBS} - (0.12T_{OBS} + 0.05T_{OBS}^2)$. The correlation coefficient between modelled SMB and reconstructed SMB for 1980-2014 is r = 0.66, which is stronger than the correlation of simulated melt and observed summer temperature and correlation of simulated solid accumulation and observed precipitation, and hence significantly correlated within a 95% confidence interval.

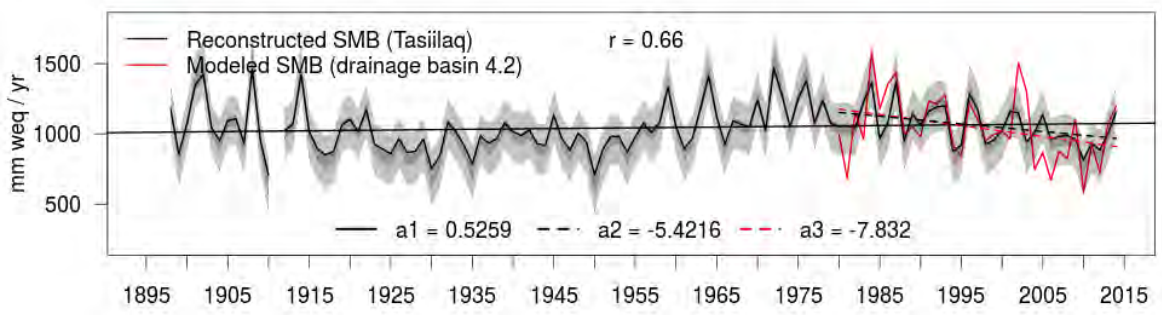

Figure 6.21: Reconstructed SMB for Tasiilaq (basin 4.2) for 1898-2014 (black line), HIRHAM5-simulated SMB for the drainage basin 4.2 from 1980-2014 (red). Confidence interval (dark grey) and prediction interval (light grey) are added the reconstructed SMB curve. The values a1, a2 and a3 are slopes of the regression lines.

Three trend lines are added to the SMB reconstruction in Figure 6.21. The black solid line is considering the full reconstructed period from 1898 to 2014 with an slightly increasing slope, *a1 = 0.5 mm weq/yr per year*, whereas the dashed lines cover the 35-years up to 2014 for reconstructed (black) and HIRHAM5-simulated SMB (red) with decreasing slopes, *a2 = -5.4 mm weq/yr per year* and *a3 = -7.8 mm weq/yr per year* respectively. The trend lines clearly indicate that a reduction in SMB occurs towards 2014. The gap in the beginning of the 20th century is due to missing values in the precipitation records. The 35 year trend line limit is chosen to enable direct comparison of time series.

6.3.5.2 SMB Reconstruction for Danmarkshavn

Reconstruction of SMB follows the same procedure as for Tasiilaq. The drainage basin 2.1 is the most temperature- and precipitation representative area, upstream from Danmarkshavn (see Figure 6.2). Reconstruction of SMB for the drainage basin leading to Danmarkshavn differs from the Tasiilaq, because the dominating contributor here is temperature and not precipitation (see Figure 6.23). The correlation coefficient between observed summer temperatures and modelled melt is *r = 0.73*. Between observed annual precipitation and modelled solid accumulation the correlation coefficient is *r = 0.51*. The reconstructed SMB time series upstream from Danmarkshavn is highly correlated with

modelled SMB with a correlation coefficient, $r = 0.67$ (see Figure 6.24), and hence significantly correlated within a 95% confidence interval.

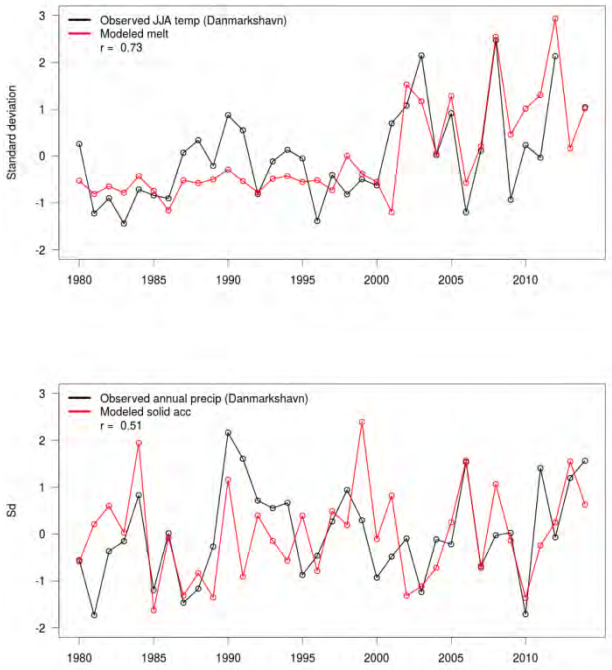

Figure 6.22: Observed summer temperature (JJA) and modelled melt (top) and observed precipitation and modelled solid accumulation (bottom) for Danmarkshavn. All values are standardized with one standard deviation.

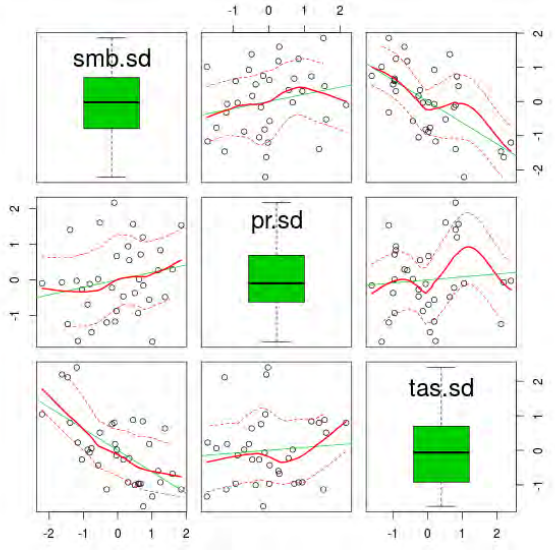

Figure 6.23: Partial regression lines for Danmarkshavn and the drainage basin 2.1. The reconstructed SMB is optimised to fit precipitation and temperature observations to HIRHAM5 simulated SMB for 1980-2014. Smb.sd, pr.sd and tas.sd are standardised SMB, precipitation and temperature.

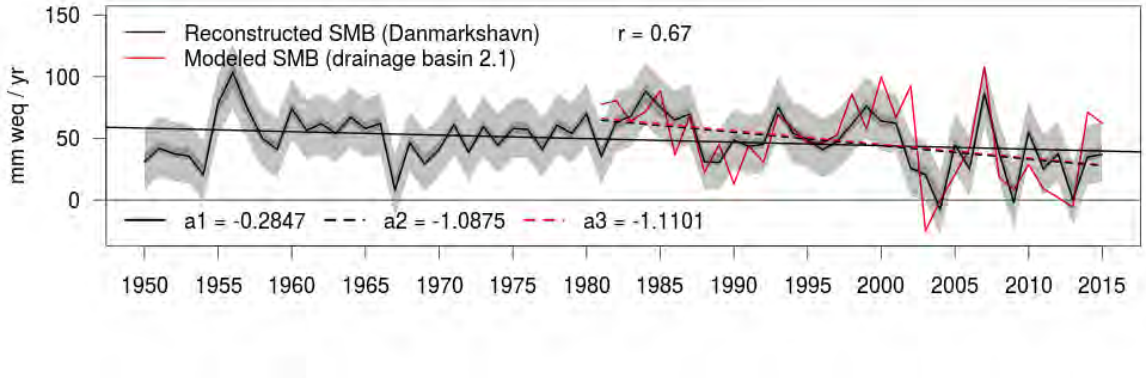

Figure 6.24: Reconstruction of simulated SMB for Danmarkshavn (drainage basin 2.1). The confidence interval for the regression line is shown as dark shaded area, and the prediction interval is light shaded area. The correlation coefficient between the reconstructed time series (black curve) and the simulated time series (red curve) is r = 0.67 for the overlapping period 1980-2014. The values a1, a2 and a3 are slopes of the regression lines.

Three trend lines are added in Figure 6.24. The black solid line is considering the full reconstructed period from 1998 to 2014 with a negative slope, *a1 = -0.2 mm weq/yr per*

year, whereas the dashed lines cover the 35 years up to 2014 for the reconstructed and HIRHAM5-simulated SMB with slopes, *a2 = -1.1 mm weq/yr per year* and *a3 = -1.1 mm weq/yr per year* respectively. Also for Danmarkshavn, the trend lines clearly indicate that the decrease in SMB occurs or speeds up towards 2014.

SMB Reconstruction for Renland

Renland is as mentioned of special interest in this work. The nearest (and highest correlated) weather station to Renland is Ittoqqortoormiit (see Figure 3.3).

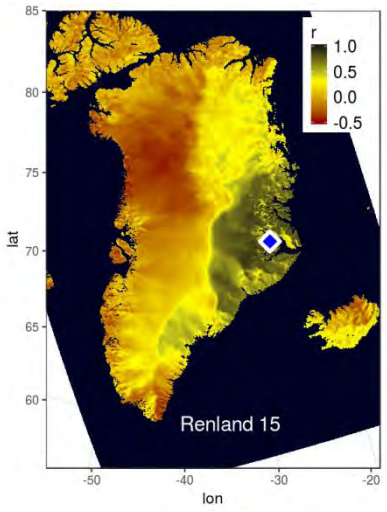

Figure 6.25: Correlation pattern for HIRHAM5 simulated annual precipitation time series 1980-2014. The map represents correlation coefficients between each land grid point and the grid point closest to the drill site at Renland. Critical correlation coefficient for significance at a 95% confidence level is r = 0.33 (yellow).

Observed JJA-temperature and annual mean precipitation measured at Ittoqqortoormiit weather station correlated with modelled annual melt and annual solid accumulation from HIRHAM5 is shown in Figure 6.26. Melt and solid accumulation time series are averaged over all grid points on the Renland ice sheet area displayed in Figure 6.27, which shows the annual mean SMB from 1980-2014. Each dot in the map corresponds to a grid point in the HIRHAM5 high-resolution climate model.

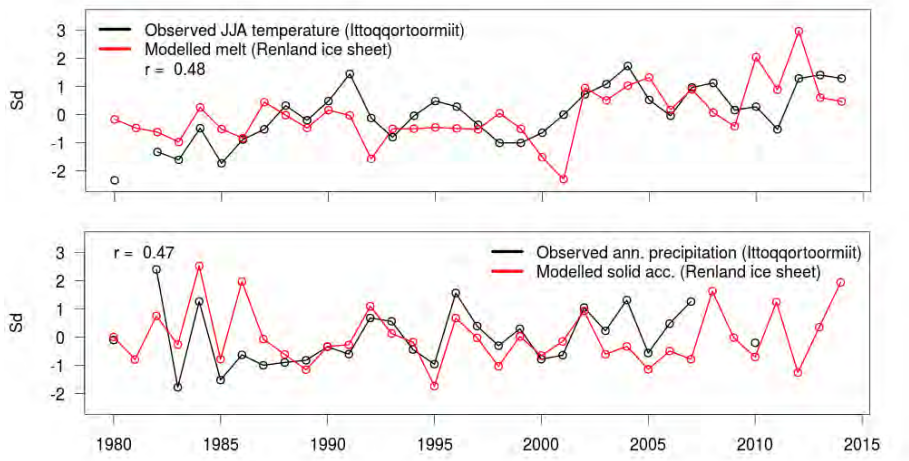

Figure 6.26: Observed summer temperature (JJA) and modelled melt (top) and observed precipitation and modelled solid accumulation (bottom). Observation records come from Ittoqqortoormiit, and model data is from Renland. All values are standardized with one standard deviation.

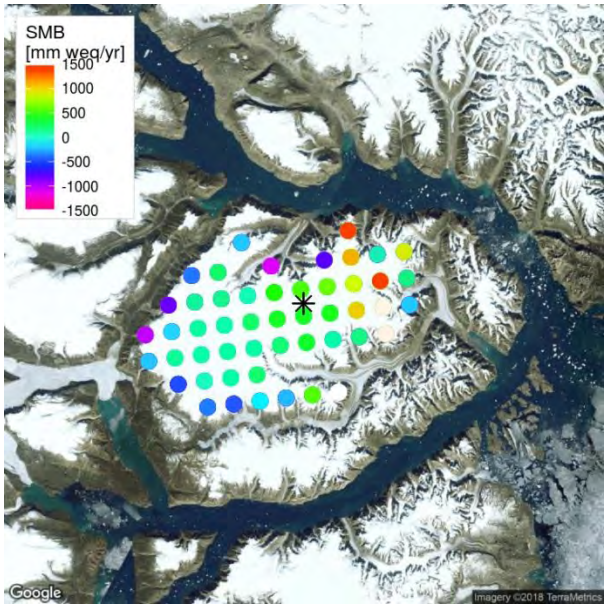

Figure 6.27: Annual mean SMB (1980-2014) simulated with HIRHAM5 on the Renland ice sheet in mm weq/yr. The black star indicates the ice core drill site location.

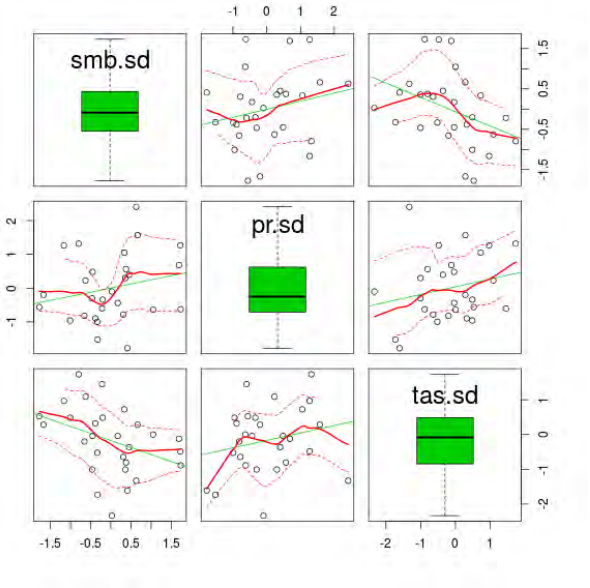

Figure 6.28: Partial regression lines for Renland ice cap and Ittoqqortoormiit. The reconstructed SMB is optimised to fit precipitation and temperature observations to HIRHAM5-simulated SMB for 1980-2014. Smb.sd, pr.sd and tas.sd are standardised SMB, precipitation and temperature.

SMB reconstructed for Renland is based on observations from Ittoqqortoormiit and correlates with the simulated SMB with a correlation coefficient, $r = 0.54$. The degree of freedom is 24 due to observation gaps, but the correlation is still significant within a 95% confidence level. The gaps the reconstructed SMB time series remain open, as neither of the surrounding in situ records are significantly correlated with the precipitation record for Ittoqqortoormiit.

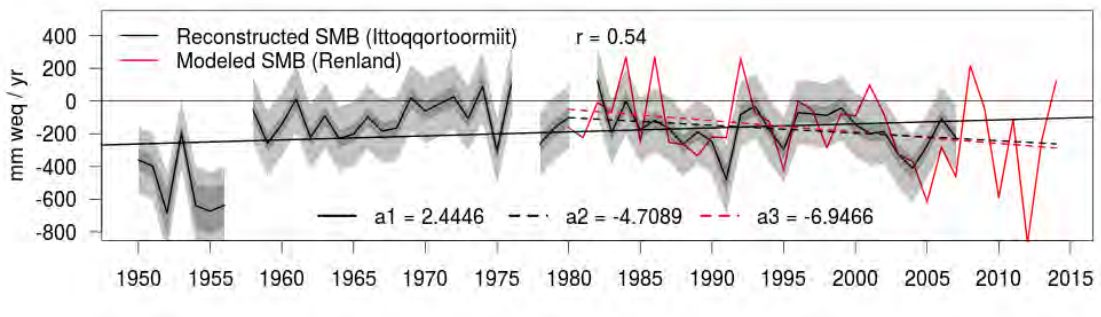

Figure 6.29: Reconstruction of SMB for the Renland ice cap for 1950-2007 (black line), modelled SMB from 1980-2014 (red). Confidence interval (dark grey) and prediction interval (light grey) are added to the SMB reconstruction. The values a1, a2 and a3 are slopes of the regression lines.

Three trend lines are added in Figure 6.29. The black solid line is considering the full reconstructed period from 1950 to 2014 with a slope, *a1 = 2.4 mm weq/yr per year*, whereas the dashed lines cover 35 years up to 2014 for reconstructed (black) and HIRHAM5-simulated SMB (red) with slopes, *a2 = -4.7 mm weq/yr per year* and *a3 = -6.9 mm weq/yr per year* respectively. As for Tasiilaq and Danmarkshavn, the trend lines for Renland SMB development clearly indicate that the decrease is most pronounced towards 2014.

Results from the three SMB reconstructions: Tasiilaq, Danmarkshavn and Renland are shown in Table 6-1.

	Pearson's r	Slope a1	Slope a2	Slope a3
Tasiilaq	0.66	0.53	-5.42	-7.83
Danmarkshavn	0.67	-0.28	-1.09	-1-11
Renland	0.54	2.44	-4.71	-6.95

Table 6-1: Correlation coefficients between reconstructed and HIRHAM5-simulated SMB and regression line slopes for the full reconstructed SMB period (a1) and for 1980-2014 for the reconstructed SMB (a2) and simulated SMB (a3).

6.3.6 Merged spatial correlation coverage

Correlation maps for 6 and 12 ice core locations are merged by selecting the highest coefficients among the correlation coefficients calculated for each ice core locations separately. The left map in Figure 6.30 show the spatial coverage of six deep ice cores (Vinther et al., 2010b) together, whereas the right map also includes six shallow transverse cores (not yet documented).

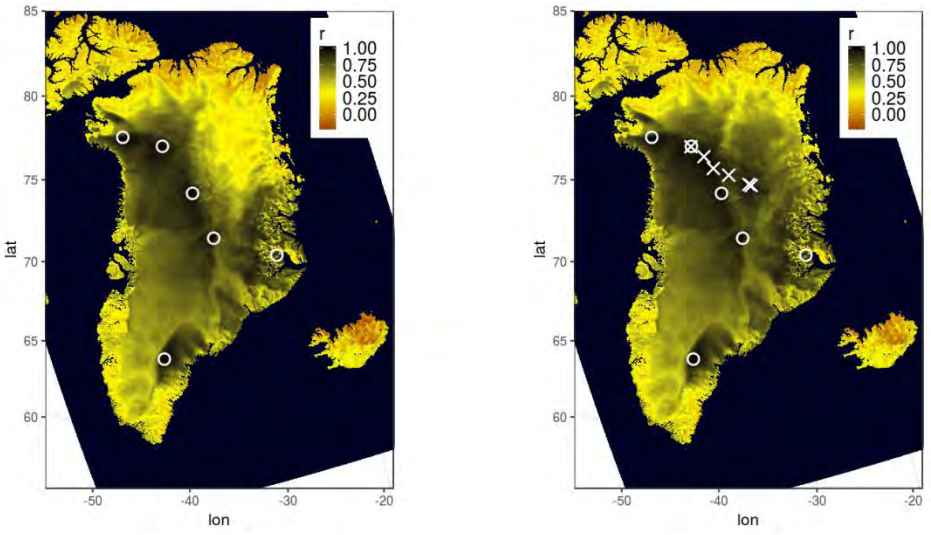

Figure 6.30: Merged solid accumulation correlation maps for the six deep ice core locations (red circles, left) combined with the transverse shallow cores (crosses, right).

6.4 Discussion

6.4.1 Validation of correlation patterns

6.4.1.1 Precipitation

The correlation matrices based on HIRHAM5 simulated and observed precipitation are used to evaluate the correlation patterns and appear to have similar structures (see the two top plots in Figure 6.6). From the two bottom plots it is clear that HIRHAM5 predicts more significantly correlated location combinations than observed. The difference is mainly due to gaps in observation records that reduce the amount of overlapping time steps and hence reduces the degrees of freedom, which again increases the critical value for significant correlation. When only 15 years of the observed precipitation is overlapping with the HIRHAM5 simulation period, the degrees of freedom is $df = 13$, and the critical value for significant correlation within a 95% confidence interval increases to $r_{crit} = 0.51$. Therefore, higher correlation coefficients are required to meet the criteria for statistically significant correlation.

More than half of the significant correlation combinations that appear in the HIRHAM5 simulated precipitation and not found in observed precipitation are involving the weather stations in Upernavik and Ilulissat, where observation of precipitation stopped in the

80's. Correlation combinations with short overlapping time periods are thus subject to low degrees of freedom, as shown in Figure 6.7. One exception here is the absent correlation between observed precipitation in Ilulissat and Nuuk and the difference here cannot be explained with an increased critical value for significant correlation.

HIRHAM5 and observation records show consistently that Ittoqqortoormiit and Danmarkshavn do not correlate with any other observation station. Also, Pituffik appears relatively isolated from other stations, except for a weak but statistically significant correlation with Aasiaat ($r = 0.37$) and Kangerlussuaq ($r = 0.45$), which is only depicted from observations.

Five significantly correlated combinations in the observation records should not correlate according to HIRHAM5. Two out of the five can be explained by relatively high degrees of freedom for the long observed time series in Tasiilaq, Nuuk and Ittoqqortoormiit. In total, that confines it to 3 out of 78 combinations that are found within the observation records but not captured by HIRHAM5. These, together with the opposite mismatch mentioned above for Nuuk and Ilulissat, may be caused by imprecise topography descriptions within HIRHAM5. In summary, an overall agreement in the location specific cross correlations of observed and simulated precipitation is identified with only a few exceptions.

6.4.1.2 Temperature

In Figure 6.8 we see that the number of significant correlated combinations is notable larger for observed than for simulated temperature. The observed temperature records are relatively long and with fewer missing values compared to the precipitation records, and therefore the critical value for statistical significance is correspondingly low. Nevertheless, some unexpected differences do occur: Temperature observed at Station Nord does correlate significantly with five other station records, which is not found for Station Nord in the simulation, even though the degrees of freedom are comparable. Similarly, temperature observed at Summit is significantly correlated with six other weather stations, which is not depicted by HIRHAM5, even though the degrees of freedom of time series for Summit does not exceed $df = 12$.

The disagreement between observed and simulated significantly correlated station combinations can in the majority of cases be explained with low degrees of freedom caused by gaps and not overlapping precipitation records, and the opposite for the longer temperature records. The gaps and time series overlaps are shown in Figure 3.4 and Figure 3.5, where the 19 observed temperature records and 13 precipitation records are plotted. The number of significantly correlated combinations is from Figure 6.7 and Figure 6.9 clearly expected to be smaller for observed precipitation compared to simulated precipitation and vice versa for temperature.

6.4.1.3 Slope direction and weather systems

The patterns emerging on the correlation maps for precipitation can to large extent be explained by large scale weather systems and topography. Precipitation is in general regulated by water vapour content, atmospheric stability and circulation, and topography, whereas the major precipitation contribution over Greenland is produced by frontal cyclone weather systems (Chen et al., 1997). The geographical distribution of precipitation on climatological scale is mainly caused by the interaction between topography and geostrophic wind patterns. The Greenland ice sheet topography is characterised by possessing influencing physical barriers described by Ohmura and Reeh (1991) as roughly one north-south orientated ridge with three east-west ridges on the western side and two on the eastern site.

Rogers et al. (2004) showed the importance of distinguishing lee cyclones from Icelandic cyclones, as they produce opposite precipitation effects across the ice sheet, which is consistent with the general relationship between precipitation in Greenland, cyclone activity and large scale circulation. This is also consistent with the fact that large scale circulation is the dominating driver of accumulation variations in the central and southern part of Greenland, whereas cyclone activity is higher correlated with accumulation in north eastern Greenland (Hutterli et al., 2005). In a warmer world precipitation will in general increase in Greenland, where the drivers of accumulation changes are the large-scale circulation combined with the local topography (Merz et al., 2013).

By matching precipitation correlation patterns for e.g. Nuuk and Tasiilaq with slope directions in Figure 6.10, the north south oriented ice sheet ridge clearly separates eastern and western correlation regimes caused by westerly and easterly winds and front systems. Smaller ice ridges appearing on the slope direction map are also pronounced in the correlation patterns of the solid accumulation correlated with Renland in Figure 6.25. To summarise, the correlation patterns evaluated in the light of dominating precipitation events in Greenland together with the slope direction map, supports the idea that the HIRHAM5 deduced correlation patterns do represent a real world pattern.

6.4.2 Reconstruction of observations

Temperature and precipitation time series can be reconstructed from correlated weather records for gap filling, and from ice core time series for extending the observation records back in time. Correlation patterns and correlation matrices in particular are practical tools to select the best correlated observation records. In the reconstruction procedure the variance of the reconstructed time series is reduced compared for the

observed records. Reconstruction is calculated through a linear regression function, which at first does not include the variance of the original observation record. To solve this problem, the 66% prediction interval of the response variable is added as a prediction interval. Extension of observed temperature time series back in time show that the warming primarily has occurred within the last three decades. The trends in temperature is increasing gradually towards present consistent with significant temperature increases shown by (Abermann et al., 2017) to be between 0.05 and .015 ˚C $year^{-1}$ for 1996-2014.

6.4.3 Reconstruction of SMB

HIRHAM5-simulated precipitation and temperature is strongly correlated with simulated solid accumulation minus evaporation and melt, as shown in section 6.3.5, which is also evident for observed precipitation and temperature. Based on the convincing linear relationship to solid accumulation, shown in Figure 6.15, precipitation is demonstrated to be a usable estimate for changes in solid accumulation in the reconstruction of simulated SMB. Summer temperature is likewise a good estimate for melt from the drainage basin, close to the location where the temperature is observed. A simulated SMB reconstruction from a partial regression function based on observed precipitation and temperature is therefore expected to produce realistic SMB estimates.

SMB-reconstructions for the three areas based on observations are all significantly correlated with the simulated SMB. Weather stations at Tasiilaq and Danmarkshavn are closer linked to simulated SMB at their respective drainage basins, than Ittoqqortoormiit is to the Renland ice cap. The distance between Renland and Ittoqqortoormiit is about 200 km, but the correlation is higher in the observations, than predicted from the correlation map.

As for observation reconstructions the procedure for SMB reconstruction introduces a damping effect through the regression approximation, resulting in reduced variance compared to original simulated time series. Again, the uncertainties in the form of a prediction interval restores 66% of the damped variance signal, as this prediction interval captures 66% of the simulated SMB variability relative to the regression line. By increasing the prediction interval to 95% confidence level, almost all damping will be restored, but this has the disadvantage of blowing up the uncertainty. Here the IPCC definition of likely range is followed (Mastrandrea et al., 2011).

The reconstruction of SMB in Danmarkshavn in Figure 6.24 shows a convincing correlation with simulated SMB with a correlation coefficient r = 0.67. Contrary to basin 4.2, the SMB in drainage basin 2.1 is predominantly temperature controlled, where

reconstruction from Tasiilaq is dominated by precipitation. The reconstructed SMB time series for basin 2.1 show a less negative trend towards 2014 compared SMB in basin 4.2.

The Renland SMB reconstruction is challenging, because even though the significantly correlated area to Renland is relatively large for precipitation, the three nearest good quality weather records are located in areas at the limit of significant correlation as displayed in Figure 6.25. Tasiilaq is just south of the high correlated area and Danmarkshavn just the north of it and relatively low-lying (11m above sea level) compared to Renland. Considering both precipitation and temperature, Ittoqqortoormiit proves to match the Renland ice core data best, with correlation coefficients, $r = 47$ and 48 for temperature and precipitation, see Figure 6.26. In Figure 6.28 it appears that SMB at Renland is more temperature than precipitation dependent and the SMB reconstruction turns out to be strongly correlated with simulated SMB, with $r = 0.54$. This is stronger than correlations between observed temperature and precipitation and simulated melt and solid accumulation individually. Gaps in the reconstructed SMB time series will occur in all cases, where errors cannot be replaced with other significantly correlated observation records, which can be read directly from Figure 6.6 and Figure 6.8.

The reconstructed and simulated SMB have comparable regression lines for the last 35 years for Tasiilaq, Danmarkshavn and Renland, which to some extent verifies accuracy of the reconstructed time series. Difference in slopes for the reconstructed and simulated time series, a2 and a3 for Renland can be ascribed to the missing values from 2007 and onwards for observations. The accelerating SMB decrease towards present for both Tasiilaq, Danmarkshavn and Renland is consistent with (Box, 2013; Fettweis et al., 2017; Hanna et al., 2011).

6.4.4 Spatial Correlation coverage

The maps in Figure 6.30 indicate to what degree selected ice cores represent surface dynamics on the entire ice sheet represented by HIRHAM5. In this example maps are prepared for solid accumulation. The statistically significant correlation with six deep ice cores, shown in Figure 6.30 (left) covers most of the ice sheet except for the north east part of Greenland National park. The remaining part is embraced by adding six transverse shallow cores Figure 6.30 (right). The area with the lowest correlation coefficients is then the south-eastern part of the ice sheet. The six ice cores do cover most of the ice sheet for significantly correlated grid cells. However, by defining a higher critical value necessary for varies types of investigations, the coverage logically reduces and the deserted areas become more distinct, which may be useful information for future ice core planning.

6.5 Conclusions and perspectives

The spatial correlation patterns simulated with HIRHAM5 are consistent with observations with relatively few exceptions. Correlation patterns for precipitation appearing on the correlation maps do to large extent correspond to the effect of Greenland large scale weather systems and topography across the country. Only one combination of precipitation records showed unexpected absence of correlation in observations despite a relatively long observation records. For temperature only one weather station does correlate significantly with six other stations in observations, and not for HIRHAM5.

Reconstruction of SMB from observation records are significantly correlated with HIRHAM5-simulated SMB for both the Tasiilaq and Danmarkshavn drainage basins and for the Renland ice cap. All three cases show decreasing trend lines for the period 1980 to 2014. Furthermore the trend line slopes are remarkably lower for the last 35 years compared to the full reconstruction periods, which indicates a decreasing or maybe decelerating SMB for these areas. Additionally, the reconstructed SMB time series are confirmed by comparing its trend line slopes with the corresponding slopes of the simulated SMB trend lines in Table 6-1.

The distribution of ice cores does to large extent cover the solid accumulation characteristics across the Greenland ice sheet, meaning that nearly all locations on the ice sheet are correlated with at least one ice core location. The six deep ice cores cover most of the ice, and by adding the six shallow cores, the Greenland ice sheet is close to full covered by ice cores in terms of solid accumulation correlations deduced from HIRHAM5. Another example of applying the HIRHAM5 simulated correlation patterns is presented in Paper IV, where the stable water isotope signal δ18O of ice cores drilled on the Renland ice cap is examined and correlated with HIRHAM5 temperatures.

The aim of Paper IV is to examine how much of the δ18O variability (1801-2014) from an ice cores drilled on the Renland ice cap can be attributed to temperature variations. In the analysis, seasonally averaged δ18O time series are compared with temperature observations on the Greenland east coast (1895-2014) and Iceland (1821-2014) and the HIRHAM5 simulated temperature (1980-2014). The results show that the δ18O variability correlates significantly with regional temperatures on both seasonal and annual scale for 1910-2014, while δ18O is not significantly correlated with Iceland temperatures for longer period 1830-1909.

Comparison of the winter signals of the spatially distributed HIRHAM5 simulated temperature and the Renland δ18O show significant correlations. The correlation is above r=0.5 in almost the entire Greenland, irrespectively of the ice divide (see Figure 6 in Paper IV). This indicates that the winter temperature variability over Greenland is imprinted in the Renland δ18O signal.

Results show that there is no significant correlation between δ18O and temperature east of Renland in sea areas regularly covered by sea ice. For summer and annually mean signals, the correlations are reduced to coefficients between r = 0.4 and r = 0.5 and they only cover the east coast region. These results support the correlations between the δ18O signal and the three observed temperature records that showed high correlations between δ18O and temperature in the 1910-2014 period.

7 Conclusions and perspectives

The first part of this thesis (Chapter 4) presents the demand and delivery of customised climate information and has demonstrated the necessity and added value of high-resolution regional downscaling for Greenland. This involves development and quantification of relevant climate indices as well as associated uncertainties (Chapter 5), but also information of spatially linked weather and SMB patterns across Greenland (Chapter 6).

In Paper I, a new evaluation method used for assessing the uncertainty of RCM projected climate indices, applied in the scientific reports I-VI was tested, adjusted and validated, also with high confidence. The following research questions (Q1-Q5) were explored and conclude in the following answers:

Q1. It was found that the uncertainty assessment method utilizes uncertainty quantification of projected changes in climate indices from one single RCM simulation for a geographical domain like Greenland. The spread of CMIP5 annual mean temperature change is convertible to HIRHAM5 projected climate index uncertainty, when the indices are significantly correlated with the driving GCM temperature. These index-temperature relationships emerge from the uncertainty plots in the scientific report VII for each climate index. However, the RCM indices are here correlated with the corresponding RCM temperature and may achieve higher correlation coefficients, and so narrower uncertainty ranges.

Q2. For the RCM derived indices considered in Paper I, the relationship to the driving GCM temperature reflects a general condition rather than a specific characteristic for the HIRHAM5 - EC-Earth model setup.

Q3. When the relationship between RCM indices and GCM temperature is transferrable from Scandinavia to Greenland, we assume that the relationship is general. The correlation coefficient is to large degree maintained, but the trend line slope is location dependent.

Q4. The variance of the RCM ensemble is embraced by the variance of the GCM selection downscaled within CORDEX, both for the upper and lower boundaries.

Q5. An overall conclusion is that HIRHAM5 is representative of the ensemble of RCM downscaling experiments within CORDEX, both for projected climate changes and for the RCM derived indices related to corresponding GCM temperatures.

From the findings in Paper 1, one RCM simulation elevates to better represent an ensemble of RCMs instead of just being one example from an ensemble of downscaling experiments.

In Paper II, HIRHAM5 is validated against observations through spatial correlation patterns with high confidence. The validation supports a general validation of HIRHAM5 from other studies (Lucas-Picher et al., 2012) as simulating a realistic climate over Greenland at high resolution. The research questions (Q6-Q7) were explored and conclude in the following:

Q6. In situ weather records reflect with high confidence the spatial correlation patterns for both precipitation and temperature deduced from HIRHAM5.

Q7. Changes in SMB are identified from all three SMB reconstructions. SMB during the last 100 years are relatively stable compared to the recent 30 years, where the SMB has been decreasing notably.

In Paper III, future changes in temperature, precipitation and SMB are estimated for 2031-2050 and 2081-2100 relative to 1991-2010 for the scenarios RCP4.5 and RCP8.5 with focus on the area around Kangerlussuaq. This study also verified the hypothesis (Q8), concluding in:

Q8. A high-resolution regional downscaling of 5.5 km does add extra information of e.g. precipitation in a mountainous area compared to a coarser downscaling at 50 km. This has an effect on both ice covered and ice free areas around Kangerlussuaq. A sufficiently high resolution is essential for estimating the SMB and retreat of smaller ice caps. A historical (a present day) simulation based on the driving GCM is necessary to assess and quantify biases for projected climate changes.

Besides resolving Q1-Q8 and the findings presented in Paper I-IV and in the scientific reports I-VII, the high-resolution regional climate model, HIRHAM5 has now been validated against observations and compared with equivalent RCM experiments, both with high confidence.

Reconstructing SMB time series back in time, based on in situ temperature and precipitation observations for Greenland is obviously a challenge, when only few long high quality observation records exist. For precipitation only four records reaches beyond 1950. In Paper II we discarded all years, where one or more monthly values were missing. A next step would be to repeat the exercise on a higher temporal resolution for observations (monthly or daily) and reconstruct the SMB from higher quality observation records. Furthermore this approach can be expanded to the entire Greenland ice sheet divided into its drainage basins, resulting in SMB time evolution reconstructions for different time periods, depending on the observations record lengths. This will altogether provide an improved estimate of the time evolution of the total Greenland SMB, based on high-resolution modelling and in situ observations.

Another perspective in this direction, is to repeat the SMB reconstruction procedure, but for ice cores significantly correlated with HIRHAM5. In this way a reconstructed SMB time evolution will reach thousands of years back based on RCM dynamics and ice core proxy data, and thus reflect the past abrupt changes (Dansgaard-Öschger events) found in the ice cores. The first steps are taken in Paper IV, where the stable isotope signal $\delta^{18}O$ in an ice core is compared with the HIRHAM5 re-analysis simulation. However, in Paper IV it is shown that the amount of $\delta^{18}O$ on Renland reflecting the regional temperature on seasonal to annual scale varies over time. This time dependency needs to be considered for SMB reconstructions further back than 100 years based on ice core proxy data. Nevertheless, a reconstruction of SMB thousands of years back will be highly related to the overall aim of the ice2ice project, investigating the consequences of abruptly disappearing of Arctic sea ice.

List of figures

List of tables

8 References

Abermann, J., Hansen, B., Lund, M., Wacker, S., Karami, M., Cappelen, J., 2017. Hotspots and key periods of Greenland climate change during the past six decades. Ambio 46, 3–11. https://doi.org/10.1007/s13280-016-0861-y

Akperov, M., Rinke, A., Mokhov, I.I., Matthes, H., Semenov, V.A., Adakudlu, M., Cassano, J., Christensen, J.H., Dembitskaya, M.A., Dethloff, K., Fettweis, X., Glisan, J., Gutjahr, O., Heinemann, G., Koenigk, T., Koldunov, N.V., Laprise, R., Mottram, R., Nikiéma, O., Scinocca, J.F., Sein, D., Sobolowski, S., Winger, K., Zhang, W., 2018. Cyclone Activity in the Arctic From an Ensemble of Regional Climate Models (Arctic CORDEX). Journal of Geophysical Research: Atmospheres 123, 2537–2554. https://doi.org/10.1002/2017JD027703

AMAP, 2017a. Adaptation Actions for a Changing Arctic (AACA) - Baffin Bay / Davis Strait Region Overview report. Arctic Monitoring and Assessment Programme (AMAP). Oslo, Norway.

AMAP, 2017b. Snow, Water, Ice and Permafrost in the Arctic (SWIPA). Oslo, Norway.

Andersen, K.K., Ditlevsen, P.D., Rasmussen, S.O., Clausen, H.B., Vinther, B.M., Johnsen, S.J., Steffensen, J.P., 2006. Retrieving a common accumulation record from Greenland ice cores for the past 1800 years. Journal of Geophysical Research: Atmospheres 111. https://doi.org/10.1029/2005JD006765

Asiaq, 2018. Greenland climate index portal - Silap pissusaanut nalunaarsuutit [WWW Document]. URL https://kort.nunagis.gl/klimadata/#about (accessed 8.6.18).

Ballinger, T.J., Hanna, E., Hall, R.J., Miller, J., Ribergaard, M.H., Høyer, J.L., 2017. Greenland coastal air temperatures linked to Baffin Bay and Greenland Sea ice conditions during autumn through regional blocking patterns. Clim Dyn 1–18. https://doi.org/10.1007/s00382-017-3583-3

Boas, L., Wang, P.., 2016. Quality con ntrol of Gre eenlandic weather and climate data a series 1958-2010 (No. 11-16), DMI Report. Danish Meteorological Institute.

Boberg, F., Christensen, J.H., 2012. Overestimation of Mediterranean summer temperature projections due to model deficiencies. Nature Climate Change 2, 433–436. https://doi.org/10.1038/nclimate1454

Boberg, F., Langen, P.L., Mottram, R.H., Christensen, J.H., Olesen, M., 2018. 21st-century climate change around Kangerlussuaq, west Greenland: From the ice sheet to the shores of Davis Strait. Arctic, Antarctic, and Alpine Research 50, S100006. https://doi.org/10.1080/15230430.2017.1420862

Box, J.E., 2013. Greenland Ice Sheet Mass Balance Reconstruction. Part II: Surface Mass Balance (1840–2010). J. Climate 26, 6974–6989. https://doi.org/10.1175/JCLI-D-12-00518.1

Box, J.E., Cressie, N., Bromwich, D.H., Jung, J.-H., van den Broeke, M., van Angelen, J.H., Forster, R.R., Miège, C., Mosley-Thompson, E., Vinther, B.M., McConnell, J.R., 2012. Greenland Ice Sheet Mass Balance Reconstruction. Part I: Net Snow Accumulation (1600–2009). J. Climate 26, 3919–3934. https://doi.org/10.1175/JCLI-D-12-00373.1

Bracegirdle, T.J., Stephenson, D.B., 2012. Higher precision estimates of regional polar warming by ensemble regression of climate model projections. Clim Dyn 39, 2805–2821. https://doi.org/10.1007/s00382-012-1330-3

Calanca, P., Gilgen, H., Ekholm, S., Ohmura, A., 2000. Gridded temperature and accumulation distributions for Greenland for use in cryospheric models. Annals of Glaciology 31, 118–120. https://doi.org/10.3189/172756400781820345

Cappelen, J., 2018. Greenland - DMI Historical Climate Data Collection 1784-2017 (No. 18-04), DMI Report. Danish Meteorological Institute.

Chen, Q., Bromwich, D.H., Bai, L., 1997. Precipitation over Greenland Retrieved by a Dynamic Method and Its Relation to Cyclonic Activity. J. Climate 10, 839–870. https://doi.org/10.1175/1520-0442(1997)010<0839:POGRBA>2.0.CO;2

Chen, X., Tung, K.-K., 2014. Varying planetary heat sink led to global-warming slowdown and acceleration. Science 345, 897–903. https://doi.org/10.1126/science.1254937

Christensen, J.H., Boberg, F., Christensen, O.B., Lucas-Picher, P., 2008. On the need for bias correction of regional climate change projections of temperature and precipitation. Geophys. Res. Lett. 35, L20709. https://doi.org/10.1029/2008GL035694

Christensen, J.H., Christensen, O.B., 2003. Severe Summertime Flooding in Europe. Nature 805–806.

Christensen, J.H., Christensen, O.B., Lenderink, G., Rummukainen, M., Jacob, D., 2007a. ENSEMBLES Regional Climate Modeling: A Multi-model Approach Towards Climate Change Predictions for Europe and Elsewhere. AGU Fall Meeting Abstracts 23, 01.

Christensen, J.H., Hewitson, B., Busuioc, A., Chen, A., Gao, X., Held, I., Jones, R., Kolli, R.K., Kwon, W.-T., Laprise, R., Magana Rueda, V., Mearns, L., Menéndez, C.G., Räisänen, A., Rinke, A., Sarr, A., Whetton, P., 2007b. Regional Climate Projections, Chapter 11 in: Climate Change 2007: The Physical Science Basis. Contribution of Working Group I to the Fourth Assessment Report of the Intergovernmental Panel on Climate Change. Cambridge University Press, Cambridge, United Kingdom and New York, NY, USA.

Christensen, J.H., Olesen, M., Boberg, F., Stendel, M., Koldtoft, I., 2015a. Fremtidige klimaforandringer I Grønland: Kujalleq Kommune (Scientific report 15-04 (1/6)). Danish Meteorological Institute.

Christensen, J.H., Olesen, M., Boberg, F., Stendel, M., Koldtoft, I., 2015b. Fremtidige klimaforandringer I Grønland: Sermersooq Kommune (west) (Scientific report 15-04 (2/6)). Danish Meteorological Institute.

Christensen, J.H., Olesen, M., Boberg, F., Stendel, M., Koldtoft, I., 2015c. Fremtidige klimaforandringer I Grønland: Sermersooq Kommune (East) (Scientific report 15-04 (3/6)). Danish Meteorological Institute.

Christensen, J.H., Olesen, M., Boberg, F., Stendel, M., Koldtoft, I., 2015d. Fremtidige klimaforandringer I Grønland: Qeqqata Kommune (Scientific report 15-04 (4/6)). Danish Meteorological Institute.

Christensen, J.H., Olesen, M., Boberg, F., Stendel, M., Koldtoft, I., 2015e. Fremtidige klimaforandringer I Grønland: Qaasiutsup Kommune (Scientific report 15-04 (5/6)). Danish Meteorological Institute.

Christensen, J.H., Olesen, M., Boberg, F., Stendel, M., Koldtoft, I., 2015f. Fremtidige klimaforandringer I Grønland: Nationalparken (Scientific report 15-04 (6/6)). Danish Meteorological Institute.

Christensen, J.H., Olesen, M., Boberg, F., Stendel, M., Koldtoft, I., 2015g. Climate indices for vulnerability assessments - Greenland (Scientific report 15-04 (index catalogue)). Danish Meteorological Institute.

Christensen, J.H., Olesen, M., Boberg, F., Stendel, M., Koldtoft, I., 2015h. Climate indices for vulnerability assessments - Greenland (Scientific report 15-04 (index catalogue)). Danish Meteorological Institute.

Christensen, J.H., Van Meijgaard, E., 1992. On the construction of a regional atmospheric climate model. Technical Reports - Royal Netherlands Meteorological Institute.

Christensen, O.B., Christensen, J.H., Machenhauer, B., Botzet, M., 1998. Very High-Resolution Regional Climate Simulations over Scandinavia—Present Climate. J. Climate 11, 3204–3229. https://doi.org/10.1175/1520-0442(1998)011<3204:VHRRCS>2.0.CO;2

Christensen, O.B., Drews, M., Christensen, J.H., Dethloff, K., Ketelsen, K., Hebestadt, I., Rinke, A., 2006. The HIRHAM regional climate model version 5. (DMI Technical Report No. 06-17). DMI, Copenhagen, Denmark.

Cogley, J.G., 2009. Geodetic and direct mass-balance measurements: comparison and joint analysis. Annals of Glaciology 50, 96–100. https://doi.org/10.3189/172756409787769744

Collins, W.J., Bellouin, N., Doutriaux-Boucher, M., Gedney, N., Halloran, P., Hinton, T., Hughes, J., Jones, C.D., Joshi, M., Liddicoat, S., Martin, G., O'Connor, F., Rae, J., Senior, C., Sitch, S., Totterdell, I., Wiltshire, A., Woodward, S., 2011. Development and evaluation of an Earth-System model – HadGEM2. Geosci. Model Dev. 4, 1051–1075. https://doi.org/10.5194/gmd-4-1051-2011

Cowtan, K., Way, R.G., 2013. Coverage bias in the HadCRUT4 temperature series and its impact on recent temperature trends. Quarterly Journal of the Royal Meteorological Society 140, 1935–1944. https://doi.org/10.1002/qj.2297

Cullather, R.I., Nowicki, S.M.J., Zhao, B., Suarez, M.J., 2014. Evaluation of the Surface Representation of the Greenland Ice Sheet in a General Circulation Model. J. Climate 27, 4835–4856. https://doi.org/10.1175/JCLI-D-13-00635.1

Dansgaard, W., 1964. Stable isotopes in precipitation. Tellus 16, 436–468. https://doi.org/10.1111/j.2153-3490.1964.tb00181.x

Dansgaard, W., 1954. The O18-abundance in fresh water. Geochimica et Cosmochimica Acta 6, 241–260. https://doi.org/10.1016/0016-7037(54)90003-4

Dee, D.P., Uppala, S.M., Simmons, A.J., Berrisford, P., Poli, P., Kobayashi, S., Andrae, U., Balmaseda, M.A., Balsamo, G., Bauer, P., Bechtold, P., Beljaars, A.C.M., van

de Berg, L., Bidlot, J., Bormann, N., Delsol, C., Dragani, R., Fuentes, M., Geer, A.J., Haimberger, L., Healy, S.B., Hersbach, H., Hólm, E.V., Isaksen, L., Kållberg, P., Köhler, M., Matricardi, M., McNally, A.P., Monge-Sanz, B.M., Morcrette, J.-J., Park, B.-K., Peubey, C., de Rosnay, P., Tavolato, C., Thépaut, J.-N., Vitart, F., 2011. The ERA-Interim reanalysis: configuration and performance of the data assimilation system. Q.J.R. Meteorol. Soc. 137, 553–597. https://doi.org/10.1002/qj.828

Déqué, M., 2007. Frequency of precipitation and temperature extremes over France in an anthropogenic scenario: Model results and statistical correction according to observed values. Global and Planetary Change, Extreme Climatic Events 57, 16–26. https://doi.org/10.1016/j.gloplacha.2006.11.030

Déqué, M., Rowell, D.P., Lüthi, D., Giorgi, F., Christensen, J.H., Rockel, B., Jacob, D., Kjellström, E., Castro, M. de, Hurk, B. van den, 2007. An intercomparison of regional climate simulations for Europe: assessing uncertainties in model projections. Climatic Change 81, 53–70. https://doi.org/10.1007/s10584-006-9228-x

Drijfhout, S., van Oldenborgh, G.J., Cimatoribus, A., 2012. Is a Decline of AMOC Causing the Warming Hole above the North Atlantic in Observed and Modeled Warming Patterns? J. Climate 25, 8373–8379. https://doi.org/10.1175/JCLI-D-12-00490.1

Dufresne, J.-L., Foujols, M.-A., Denvil, S., Caubel, A., Marti, O., Aumont, O., Balkanski, Y., Bekki, S., Bellenger, H., Benshila, R., Bony, S., Bopp, L., Braconnot, P., Brockmann, P., Cadule, P., Cheruy, F., Codron, F., Cozic, A., Cugnet, D., Noblet, N. de, Duvel, J.-P., Ethé, C., Fairhead, L., Fichefet, T., Flavoni, S., Friedlingstein, P., Grandpeix, J.-Y., Guez, L., Guilyardi, E., Hauglustaine, D., Hourdin, F., Idelkadi, A., Ghattas, J., Joussaume, S., Kageyama, M., Krinner, G., Labetoulle, S., Lahellec, A., Lefebvre, M.-P., Lefevre, F., Levy, C., Li, Z.X., Lloyd, J., Lott, F., Madec, G., Mancip, M., Marchand, M., Masson, S., Meurdesoif, Y., Mignot, J., Musat, I., Parouty, S., Polcher, J., Rio, C., Schulz, M., Swingedouw, D., Szopa, S., Talandier, C., Terray, P., Viovy, N., Vuichard, N., 2013. Climate change projections using the IPSL-CM5 Earth System Model: from CMIP3 to CMIP5. Clim Dyn 40, 2123–2165. https://doi.org/10.1007/s00382-012-1636-1

Eerola, K, 2006. About the performance of HIRLAM version 7.0. HIRLAM Newsletter 51, 93–102.

Elmendorf, S.C., Henry, G.H.R., Hollister, R.D., Björk, R.G., Boulanger-Lapointe, N., Cooper, E.J., Cornelissen, J.H.C., Day, T.A., Dorrepaal, E., Elumeeva, T.G., Gill, M., Gould, W.A., Harte, J., Hik, D.S., Hofgaard, A., Johnson, D.R., Johnstone, J.F., Jónsdóttir, I.S., Jorgenson, J.C., Klanderud, K., Klein, J.A., Koh, S., Kudo, G., Lara, M., Lévesque, E., Magnússon, B., May, J.L., Mercado-Dı´az, J.A., Michelsen, A., Molau, U., Myers-Smith, I.H., Oberbauer, S.F., Onipchenko, V.G., Rixen, C., Schmidt, N.M., Shaver, G.R., Spasojevic, M.J., Þórhallsdóttir, Þ.E., Tolvanen, A., Troxler, T., Tweedie, C.E., Villareal, S., Wahren, C.-H., Walker, X., Webber, P.J., Welker, J.M., Wipf, S., 2012. Plot-scale evidence of tundra vegetation change and links to recent summer warming. Nature Climate Change 2, 453–457. https://doi.org/10.1038/nclimate1465

England, M.H., McGregor, S., Spence, P., Meehl, G.A., Timmermann, A., Cai, W., Gupta, A.S., McPhaden, M.J., Purich, A., Santoso, A., 2014. Recent intensification of wind-driven circulation in the Pacific and the ongoing warming hiatus. Nature Climate Change 4, 222–227. https://doi.org/10.1038/nclimate2106

Fang, Z.-F., 2004. Statistical relationship between the northern hemisphere sea ice and atmospheric circulation during wintertime, in: Observation, Theory and Modeling of Atmospheric Variability, World Scientific Series on Asia-Pacific Weather and Climate. WORLD SCIENTIFIC, pp. 131–141.

Feser, F., Rockel, B., von Storch, H., Winterfeldt, J., Zahn, M., 2011. Regional Climate Models Add Value to Global Model Data: A Review and Selected Examples. Bull. Amer. Meteor. Soc. 92, 1181–1192. https://doi.org/10.1175/2011BAMS3061.1

Fettweis, X., Box, J.E., Agosta, C., Amory, C., Kittel, C., Lang, C., van As, D., Machguth, H., Gallée, H., 2017. Reconstructions of the 1900–2015 Greenland ice sheet surface mass balance using the regional climate MAR model. The Cryosphere 11, 1015–1033. https://doi.org/10.5194/tc-11-1015-2017

Fettweis, X., Franco, B., Tedesco, M., van Angelen, J.H., Lenaerts, J.T.M., van den Broeke, M.R., Gallee, H., 2012. Estimating Greenland ice sheet surface mass balance contribution to future sea level rise using the regional atmospheric climate model MAR [WWW Document]. Cryosphere discussions. URL http://dspace.library.uu.nl/handle/1874/272819 (accessed 7.9.18).

Giorgetta, M.A., Jungclaus, J., Reick, C.H., Legutke, S., Bader, J., Böttinger, M., Brovkin, V., Crueger, T., Esch, M., Fieg, K., Glushak, K., Gayler, V., Haak, H., Hollweg, H.-D., Ilyina, T., Kinne, S., Kornblueh, L., Matei, D., Mauritsen, T., Mikolajewicz, U., Mueller, W., Notz, D., Pithan, F., Raddatz, T., Rast, S., Redler, R., Roeckner, E., Schmidt, H., Schnur, R., Segschneider, J., Six, K.D., Stockhause, M., Timmreck, C., Wegner, J., Widmann, H., Wieners, K.-H., Claussen, M., Marotzke, J., Stevens, B., 2013. Climate and carbon cycle changes from 1850 to 2100 in MPI-ESM simulations for the Coupled Model Intercomparison Project phase 5. Journal of Advances in Modeling Earth Systems 5, 572–597. https://doi.org/10.1002/jame.20038

Giorgi, F., Jones, C., Asrar, G.R., 2009. Addressing climate information needs at the regional level: the CORDEX framework. World Meteorological Organization (WMO) Bulletin 58, 175.

Giorgi, F., Mearns, L.O., 2003. Probability of regional climate change based on the Reliability Ensemble Averaging (REA) method. Geophys. Res. Lett. 30, 1629. https://doi.org/10.1029/2003GL017130

Giorgi, F., Torma, C., Coppola, E., Ban, N., Schär, C., Somot, S., 2016. Enhanced summer convective rainfall at Alpine high elevations in response to climate warming. Nature Geoscience 9, 584–589. https://doi.org/10.1038/ngeo2761

Giot, O., Termonia, P., Degrauwe, D., De Troch, R., Caluwaerts, S., Smet, G., Berckmans, J., Deckmyn, A., De Cruz, L., De Meutter, P., Duerinckx, A., Gerard, L., Hamdi, R., Van den Bergh, J., Van Ginderachter, M., Van Schaeybroeck, B., 2016. Validation of the ALARO-0 model within the EURO-CORDEX

framework. Geosci. Model Dev. 9, 1143–1152. https://doi.org/10.5194/gmd-9-1143-2016

Hanna, E., Cropper, T.E., Hall, R.J., Cappelen, J., 2016. Greenland Blocking Index 1851–2015: a regional climate change signal. International Journal of Climatology 36, 4847–4861. https://doi.org/10.1002/joc.4673

Hanna, E., Huybrechts, P., Cappelen, J., Steffen, K., Bales, R.C., Burgess, E., McConnell, J.R., Steffensen, J.P., Van Den Broeke, M., Wake, L., Bigg, G., Griffiths, M., Savas, D., 2011. Greenland Ice Sheet surface mass balance 1870 to 2010 based on Twentieth Century Reanalysis, and links with global climate forcing. Journal of Geophysical Research: Atmospheres 116.

Hanna, E., Huybrechts, P., Janssens, I., Cappelen, J., Steffen, K., Stephens, A., 2005. Runoff and mass balance of the Greenland ice sheet: 1958-2003. Journal of Geophysical Research-Atmospheres 110, D13108. https://doi.org/10.1029/2004JD005641

Hanna, E., Huybrechts, P., Steffen, K., Cappelen, J., Huff, R., Shuman, C., Irvine-Fynn, T., Wise, S., Griffiths, M., 2008. Increased Runoff from Melt from the Greenland Ice Sheet: A Response to Global Warming. J. Climate 21, 331–341. https://doi.org/10.1175/2007JCLI1964.1

Hanna, E., Mernild, S.H., Cappelen, J., Steffen, K., 2012. Recent warming in Greenland in a long-term instrumental (1881–2012) climatic context: I. Evaluation of surface air temperature records. Environ. Res. Lett. 7, 045404. https://doi.org/10.1088/1748-9326/7/4/045404

Hansen, J., Ruedy, R., Sato, M., Lo, K., 2010. GLOBAL SURFACE TEMPERATURE CHANGE. Reviews of Geophysics 48. https://doi.org/10.1029/2010RG000345

Haywood, J.M., Jones, A., Jones, G.S., 2013. The impact of volcanic eruptions in the period 2000–2013 on global mean temperature trends evaluated in the HadGEM2-ES climate model. Atmospheric Science Letters 15, 92–96. https://doi.org/10.1002/asl2.471

Hazeleger, W., Wang, X., Severijns, C., Ştefănescu, S., Bintanja, R., Sterl, A., Wyser, K., Semmler, T., Yang, S., Hurk, B. van den, Noije, T. van, Linden, E. van der, Wiel, K. van der, 2012. EC-Earth V2.2: description and validation of a new seamless earth system prediction model. Clim Dyn 39, 2611–2629. https://doi.org/10.1007/s00382-011-1228-5

Holme, C., Gkinis, V., Lanzky, M., Morris, V., Olesen, M., Thayer, A., Vaughn, B.H., Vinther, B.M., 2019. Varying regional δ^{18}O–temperature relationship in high resolution stable water isotopes from East Greenland. Climate of the Past Discussions 1–26. https://doi.org/https://doi.org/10.5194/cp-2018-169

Huang, J., Zhang, X., Zhang, Q., Lin, Y., Hao, M., Luo, Y., Zhao, Z., Yao, Y., Chen, X., Wang, L., Nie, S., Yin, Y., Xu, Y., Zhang, J., 2017. Recently amplified arctic warming has contributed to a continual global warming trend. Nature Climate Change 7, 875–879. https://doi.org/10.1038/s41558-017-0009-5

Huber, M., Knutti, R., 2014. Natural variability, radiative forcing and climate response in the recent hiatus reconciled. Nature Geoscience 7, 651–656. https://doi.org/10.1038/ngeo2228

Hutterli, M.A., Raible, C.C., Stocker, T.F., 2005. Reconstructing climate variability from Greenland ice sheet accumulation: An ERA40 study. Geophysical Research Letters 32. https://doi.org/10.1029/2005GL024745

IPCC (Ed.), 2013. Climate Change 2013 - The Physical Science Basis: Working Group I Contribution to the Fifth Assessment Report of the Intergovernmental Panel on Climate Change. Cambridge University Press, Cambridge.

IPCC, 2007. Climate change 2007 - Contribution of Working Group I to the Fourth Assessment Report of the Intergovernmental Panel on Climate Change. Cambridge University Press, Cambridge.

Jacob, D., Elizalde, A., Haensler, A., Hagemann, S., Kumar, P., Podzun, R., Rechid, D., Remedio, A.R., Saeed, F., Sieck, K., Teichmann, C., Wilhelm, C., 2012. Assessing the Transferability of the Regional Climate Model REMO to Different COordinated Regional Climate Downscaling EXperiment (CORDEX) Regions. Atmosphere 3, 181–199. https://doi.org/10.3390/atmos3010181

Jacob, D., Petersen, J., Eggert, B., Alias, A., Christensen, O.B., Bouwer, L.M., Braun, A., Colette, A., Déqué, M., Georgievski, G., Georgopoulou, E., Gobiet, A., Menut, L., Nikulin, G., Haensler, A., Hempelmann, N., Jones, C., Keuler, K., Kovats, S., Kröner, N., Kotlarski, S., Kriegsmann, A., Martin, E., Meijgaard, E. van, Moseley, C., Pfeifer, S., Preuschmann, S., Radermacher, C., Radtke, K., Rechid, D., Rounsevell, M., Samuelsson, P., Somot, S., Soussana, J.-F., Teichmann, C., Valentini, R., Vautard, R., Weber, B., Yiou, P., 2014. EURO-CORDEX: new high-resolution climate change projections for European impact research. Reg Environ Change 14, 563–578. https://doi.org/10.1007/s10113-013-0499-2

Jones, P.D., Mann, M.E., 2004. Climate over past millennia. Reviews of Geophysics 42. https://doi.org/10.1029/2003RG000143

Jones, P.D., New, M., Parker, D.E., Martin, S., Rigor, I.G., 1999. Surface air temperature and its changes over the past 150 years. Reviews of Geophysics 37, 173–199. https://doi.org/10.1029/1999RG900002

Kjellström, E., Thejll, P., Rummukainen, M., Christensen, J.H., Boberg, F., Christensen, O.B., Maule, C.F., 2013. Emerging regional climate change signals for Europe under varying large-scale circulation conditions. Climate Research 56, 103–119. https://doi.org/10.3354/cr01146

Knutti, R., Sedláček, J., 2013. Robustness and uncertainties in the new CMIP5 climate model projections | Nature Climate Change. Nature Climate Change, 3 369–373.

Kochendorfer, J., Rasmussen, R., Wolff, M., Baker, B., Hall, M.E., Meyers, T., Landolt, S., Jachcik, A., Isaksen, K., Brækkan, R., Leeper, R., 2017. The quantification and correction of wind-induced precipitation measurement errors. Hydrology and Earth System Sciences 21, 1973–1989. https://doi.org/https://doi.org/10.5194/hess-21-1973-2017

Koenigk, T., Berg, P., Döscher, R., 2015. Arctic climate change in an ensemble of regional CORDEX simulations. Polar Research 34, 24603. https://doi.org/10.3402/polar.v34.24603

Koenigk, T., Brodeau, L., Graversen, R.G., Karlsson, J., Svensson, G., Tjernström, M., Willén, U., Wyser, K., 2013. Arctic climate change in 21st century CMIP5

simulations with EC-Earth. Clim Dyn 40, 2719–2743. https://doi.org/10.1007/s00382-012-1505-y

Kosaka, Y., Xie, S.-P., 2013. Recent global-warming hiatus tied to equatorial Pacific surface cooling. Nature 501, 403–407. https://doi.org/10.1038/nature12534

Kupiainen, M., Samuelsson, P., Jones, C., Jansson, C., Will´En, U., Hansson, U., Ullerstig, A., Wans, S., Döscher, R., 2011. Rossby Centre regional atmospheric model, RCA4.

Landbrugspolitiske redegørelse, 2007. , Visioner for det Grønlandske Landbrug. Departementet for Fiskeri, Fangst og Landbrug.

Langen, P.L., Fausto, R.S., Vandecrux, B., Mottram, R.H., Box, J.E., 2017. Liquid Water Flow and Retention on the Greenland Ice Sheet in the Regional Climate Model HIRHAM5: Local and Large-Scale Impacts. Front. Earth Sci. 4. https://doi.org/10.3389/feart.2016.00110

Langen, P.L., Mottram, R.H., Christensen, J.H., Boberg, F., Rodehacke, C.B., Stendel, M., van As, D., Ahlstrøm, A.P., Mortensen, J., Rysgaard, S., Petersen, D., Svendsen, K.H., Aðalgeirsdóttir, G., Cappelen, J., 2015. Quantifying energy and mass fluxes controlling Godthåbsfjord freshwater input in a 5 km simulation (1991-2012). J. Climate. https://doi.org/10.1175/JCLI-D-14-00271.1

Larsen, M.A.D., Thejll, P., Christensen, J.H., Refsgaard, J.C., Jensen, K.H., 2013. On the role of domain size and resolution in the simulations with the HIRHAM region climate model. Clim Dyn 40, 2903–2918. https://doi.org/10.1007/s00382-012-1513-y

Lehmann, J.O., Sharif, B., Kjeldsen, C., 2017. Mulighed for klimatilpasning i landbrugserhvervet - satus og handlemuligheder.

Lenderink, G., Ulden, A. van, Hurk, B. van den, Keller, F., 2007. A study on combining global and regional climate model results for generating climate scenarios of temperature and precipitation for the Netherlands. Clim Dyn 29, 157–176. https://doi.org/10.1007/s00382-007-0227-z

Lock, A.P., 2001. The Numerical Representation of Entrainment in Parameterizations of Boundary Layer Turbulent Mixing. Mon. Wea. Rev. 129, 1148–1163. https://doi.org/10.1175/1520-0493(2001)129<1148:TNROEI>2.0.CO;2

Luca, A.D., Elía, R. de, Laprise, R., 2015. Challenges in the Quest for Added Value of Regional Climate Dynamical Downscaling. Curr Clim Change Rep 1, 10–21. https://doi.org/10.1007/s40641-015-0003-9

Lucas-Picher, P., Wulff-Nielsen, M., Christensen, J.H., Aðalgeirsdóttir, G., Mottram, R., Simonsen, S.B., 2012. Very high resolution regional climate model simulations over Greenland: Identifying added value. Journal of Geophysical Research: Atmospheres 117, n/a–n/a. https://doi.org/10.1029/2011JD016267

Lynch, C., Hartin, C., Bond-Lamberty, B., Kravitz, B., 2017. An open-access CMIP5 pattern library for temperature and precipitation: description and methodology. Earth System Science Data 9, 281–292. https://doi.org/https://doi.org/10.5194/essd-9-281-2017

Madsen, M.S., Maule, C.F., MacKellar, N., Olesen, J.E., Christensen, J.H., 2012. Selection of climate change scenario data for impact modelling. Food Additives

& Contaminants: Part A 29, 1502–1513. https://doi.org/10.1080/19440049.2012.712059

Maraun, D., 2016. Bias Correcting Climate Change Simulations - a Critical Review. Curr Clim Change Rep 2, 211–220. https://doi.org/10.1007/s40641-016-0050-x

Masson-Delmotte, V., Steen-Larsen, H.C., Ortega, P., Swingedouw, D., Popp, T., Vinther, B.M., Oerter, H., Sveinbjornsdottir, A.E., Gudlaugsdottir, H., Box, J.E., Falourd, S., Fettweis, X., Gallée, H., Garnier, E., Gkinis, V., Jouzel, J., Landais, A., Minster, B., Paradis, N., Orsi, A., Risi, C., Werner, M., White, J.W.C., 2015. Recent changes in north-west Greenland climate documented by NEEM shallow ice core data and simulations, and implications for past-temperature reconstructions. The Cryosphere 9, 1481–1504. https://doi.org/10.5194/tc-9-1481-2015

Mastrandrea, M.D., Mach, K.J., Plattner, G.-K., Edenhofer, O., Stocker, T.F., Field, C.B., Ebi, K.L., Matschoss, P.R., 2011. The IPCC AR5 guidance note on consistent treatment of uncertainties: a common approach across the working groups. Climatic Change 108, 675–691. https://doi.org/10.1007/s10584-011-0178-6

Matte, D., Laprise, R., Thériault, J.M., 2016. Comparison between high-resolution climate simulations using single- and double-nesting approaches within the Big-Brother experimental protocol. Clim Dyn 47, 3613–3626. https://doi.org/10.1007/s00382-016-3031-9

Mayer, S., Maule, C.F., Sobolowski, S., Christensen, O.B., Sørup, H.J.D., Sunyer, M.A., Arnbjerg-Nielsen, K., Barstad, I., 2015. Identifying added value in high-resolution climate simulations over Scandinavia. Tellus A: Dynamic Meteorology and Oceanography 67, 24941. https://doi.org/10.3402/tellusa.v67.24941

McSweeney, C.F., Jones, R.G., Lee, R.W., Rowell, D.P., 2015. Selecting CMIP5 GCMs for downscaling over multiple regions. Clim Dyn 44, 3237–3260. https://doi.org/10.1007/s00382-014-2418-8

Medhaug, I., Stolpe, M.B., Fischer, E.M., Knutti, R., 2017. Reconciling controversies about the "global warming hiatus." Nature 545, 41–47. https://doi.org/10.1038/nature22315

Meehl, G.A., Arblaster, J.M., Fasullo, J.T., Hu, A., Trenberth, K.E., 2011. Model-based evidence of deep-ocean heat uptake during surface-temperature hiatus periods. Nature Climate Change 1, 360–364. https://doi.org/10.1038/nclimate1229

Merz, N., Raible, C.C., Fischer, H., Varma, V., Prange, M., Stocker, T.F., 2013. Greenland accumulation and its connection to the large-scale atmospheric circulation in ERA-Interim and paleoclimate simulations. Clim. Past 9, 2433–2450. https://doi.org/10.5194/cp-9-2433-2013

Mitchell, J.F.B., Johns, T.C., Eagles, M., Ingram, W.J., Davis, R.A., 1999. Towards the Construction of Climate Change Scenarios. Climatic Change 41, 547–581. https://doi.org/10.1023/A:1005466909820

Mottram, R., Boberg, F., Langen, P., Yang, S., Rodehacke, C., Christensen, J.H., Madsen, M.S., 2017a. Surface mass balance of the Greenland ice sheet in the regional climate model HIRHAM5: Present state and future prospects 105–115.

Mottram, R., Boberg, F., Lang Langen, P., Yang, S., Rodehacke, C., Christensen, J., Madsen, M., 2017b. Surface Mass balance of the Greenland ice Sheet in the

Regional Climate Model HIRHAM5: Present State and Future Prospects 75, 105–115. https://doi.org/10.14943/lowtemsci.75.105

Murphy, J.M., Sexton, D.M.H., Barnett, D.N., Jones, G.S., Webb, M.J., Collins, M., Stainforth, D.A., 2004. Quantification of modelling uncertainties in a large ensemble of climate change simulations. Nature 430, 768–772. https://doi.org/10.1038/nature02771

Normand, S., Randin, C., Ohlemüller, R., Bay, C., Høye, T.T., Kjær, E.D., Körner, C., Lischke, H., Maiorano, L., Paulsen, J., Pearman, P.B., Psomas, A., Treier, U.A., Zimmermann, N.E., Svenning, J.-C., 2013. A greener Greenland? Climatic potential and long-term constraints on future expansions of trees and shrubs. Philos Trans R Soc Lond B Biol Sci 368. https://doi.org/10.1098/rstb.2012.0479

Ohmura, A., Reeh, N., 1991. New precipitation and accumulation maps for Greenland. Journal of Glaciology 37, 140–148. https://doi.org/10.3189/S0022143000042891

Olesen, M., Arnbjerg-Nielsen, K., Hansen, A.S., 2015. What is a climate model, chapter 3 in Klimatilpasning, Hvorfor og hvordan?, Miljøbiblioteket. Aarhus University Press.

Olesen, M., Christensen, J.H., Kaas, E., Boberg, F., 2018a. Robustness of high-resolution regional climate projections for Greenland: a method for uncertainty distillation. Climate Research 76, 253–268. https://doi.org/10.3354/cr01536

Olesen, M., Christensen, J.H., Kaas, E., Holme, C., 2019. Time evolution of Greenland surface mass balance by combining high resolution climate modelling, in situ oberservations and ice cores. The Cryosphere [in review].

Ortega, P., Swingedouw, D., Masson-Delmotte, V., Risi, C., Vinther, B.M., Yiou, P., Vautard, R., Yoshimura, K., 2014. Characterizing atmospheric circulation signals in Greenland ice cores: insights from a weather regime approach. Clim Dyn 43, 2585–2605. https://doi.org/10.1007/s00382-014-2074-z

Osborn, T.J., Wallace, C.J., Lowe, J.A., Bernie, D., 2018. Performance of Pattern-Scaled Climate Projections under High-End Warming. Part I: Surface Air Temperature over Land. J. Climate 31, 5667–5680. https://doi.org/10.1175/JCLI-D-17-0780.1

Pan, Z., Christensen, J.H., Arritt, R.W., Gutowski, W.J., Takle, E.S., Otieno, F., 2001. Evaluation of uncertainties in regional climate change simulations. J. Geophys. Res. 106, 17735–17751. https://doi.org/10.1029/2001JD900193

Parker, W.S., 2013. Ensemble modeling, uncertainty and robust predictions. Wiley Interdisciplinary Reviews: Climate Change 4, 213–223. https://doi.org/10.1002/wcc.220

Persson, G., Bärring, L., Kjellström, E., Strandberg, G., Rummukainen, M., 2007. Climate indices for vulnerability assessments (No. 111). Swedish Meteorological and Hydrological Institute.

Pithan, F., Mauritsen, T., 2014. Arctic amplification dominated by temperature feedbacks in contemporary climate models. Nature Geoscience 7, 181–184. https://doi.org/10.1038/ngeo2071

Rahmstorf, S., Box, J.E., Feulner, G., Mann, M.E., Robinson, A., Rutherford, S., Schaffernicht, E.J., 2015. Exceptional twentieth-century slowdown in Atlantic Ocean overturning circulation. Nature Climate Change 5, 475–480. https://doi.org/10.1038/nclimate2554

Rahmstorf, S., Foster, G., Cahill, N., 2017. Global temperature evolution: recent trends and some pitfalls. Environ. Res. Lett. 12, 054001. https://doi.org/10.1088/1748-9326/aa6825

Rockel, B., 2015. The Regional Downscaling Approach: a Brief History and Recent Advances. Curr Clim Change Rep 1, 22–29. https://doi.org/10.1007/s40641-014-0001-3

Rockel, B., Will, A., Hense, A., 2008. The Regional Climate Model COSMO-CLM (CCLM). Meteorologische Zeitschrift 347–348. https://doi.org/10.1127/0941-2948/2008/0309

Roeckner, E., Bäuml, G., Bonaventura, L., Brokopf, R., Esch, M., Giorgetta, M., Hagemann, S., Kirchner, I., Kornblueh, L., Manzini, E., 2003. The atmospheric general circulation model ECHAM 5. PART I: Model description.

Rogers, J.C., Bathke, D.J., Mosley-Thompson, E., Wang, S.-H., 2004. Atmospheric circulation and cyclone frequency variations linked to the primary modes of Greenland snow accumulation. Geophysical Research Letters 31. https://doi.org/10.1029/2004GL021048

Rosen, J., 2016. Arctic Dreams. Nature News 532, 296. https://doi.org/10.1038/532296a

Rummukainen, M., 2016. Added value in regional climate modeling. WIREs Clim Change 7, 145–159. https://doi.org/10.1002/wcc.378

Samuelsson, P., Jones, C.G., Will´En, U., Ullerstig, A., Gollvik, S., Hansson, U., Jansson, E., Kjellstro¨M, C., Nikulin, G., Wyser, K., 2011. The Rossby Centre Regional Climate model RCA3: model description and performance. Tellus A: Dynamic Meteorology and Oceanography 63, 4–23. https://doi.org/10.1111/j.1600-0870.2010.00478.x

Santer, B.D., Bonfils, C., Painter, J.F., Zelinka, M.D., Mears, C., Solomon, S., Schmidt, G.A., Fyfe, J.C., Cole, J.N.S., Nazarenko, L., Taylor, K.E., Wentz, F.J., 2014. Volcanic contribution to decadal changes in tropospheric temperature. Nature Geoscience 7, 185–189. https://doi.org/10.1038/ngeo2098

Shiogama, H., Emori, S., Takahashi, K., Nagashima, T., Ogura, T., Nozawa, T., Takemura, T., 2009. Emission Scenario Dependency of Precipitation on Global Warming in the MIROC3.2 Model. J. Climate 23, 2404–2417. https://doi.org/10.1175/2009JCLI3428.1

Stendel, M., Olesen, M., 2018. Det globale klima frem til i dag [WWW Document]. URL www.dmi.dk/klima/klimaet-frem-til-i-dag/globalt

Taylor, K.E., Stouffer, R.J., Meehl, G.A., 2011. An Overview of CMIP5 and the Experiment Design. Bull. Amer. Meteor. Soc. 93, 485–498. https://doi.org/10.1175/BAMS-D-11-00094.1

Tebaldi, C., Arblaster, J.M., 2014. Pattern scaling: Its strengths and limitations, and an update on the latest model simulations. Climatic Change 122, 459–471. https://doi.org/10.1007/s10584-013-1032-9

Trouet, V., Van Oldenborgh, G.J., 2013. KNMI Climate Explorer: A Web-Based Research Tool for High-Resolution Paleoclimatology. Tree-Ring Research 69, 3–13. https://doi.org/10.3959/1536-1098-69.1.3

Van Meijgaard, E., Van Ulft, L.H., Lenderink, G., De Roode, S.R., Wipfler, E.L., Boers, R., van Timmermans, R.M.A., 2012. Refinement and application of a regional atmospheric model for climate scenario calculations of Western Europe. KVR.

Vautard, R., Gobiet, A., Sobolowski, S., Kjellström, E., Stegehuis, A., Paul Watkiss, Mendlik, T., Landgren, O., Nikulin, G., Teichmann, C., Jacob, D., 2014. The European climate under a 2 °C global warming. Environ. Res. Lett. 9, 034006. https://doi.org/10.1088/1748-9326/9/3/034006

Vinther, B.M., Andersen, K.K., Jones, P.D., Briffa, K.R., Cappelen, J., 2006. Extending Greenland temperature records into the late eighteenth century. Journal of Geophysical Research: Atmospheres 111. https://doi.org/10.1029/2005JD006810

Vinther, B.M., Jones, P.D., Briffa, K.R., Clausen, H.B., Andersen, K.K., Dahl-Jensen, D., Johnsen, S.J., 2010. Climatic signals in multiple highly resolved stable isotope records from Greenland. Quaternary Science Reviews 29, 522–538. https://doi.org/10.1016/j.quascirev.2009.11.002

Voldoire, A., Sanchez-Gomez, E., Mélia, D.S. y, Decharme, B., Cassou, C., Sénési, S., Valcke, S., Beau, I., Alias, A., Chevallier, M., Déqué, M., Deshayes, J., Douville, H., Fernandez, E., Madec, G., Maisonnave, E., Moine, M.-P., Planton, S., Saint-Martin, D., Szopa, S., Tyteca, S., Alkama, R., Belamari, S., Braun, A., Coquart, L., Chauvin, F., 2013. The CNRM-CM5.1 global climate model: description and basic evaluation. Clim Dyn 40, 2091–2121. https://doi.org/10.1007/s00382-011-1259-y

von Storch, H., Zwiwes, F.W., 1998. Statistical analysis climate research | Climatology and climate change. Cambridge University Press.

Vose, R.S., Arndt, D., Banzon, V.F., Easterling, D.R., Gleason, B., Huang, B., Kearns, E., Lawrimore, J.H., Menne, M.J., Peterson, T.C., Reynolds, R.W., Smith, T.M., Williams, C.N., Wuertz, D.L., 2012. NOAA's Merged Land-Ocean Surface Temperature Analysis. Bulletin of the American Meteorological Society. https://doi.org/10.1175/BAMS-D-11-00241.1

Vuuren, D.P. van, Edmonds, J., Kainuma, M., Riahi, K., Thomson, A., Hibbard, K., Hurtt, G.C., Kram, T., Krey, V., Lamarque, J.-F., Masui, T., Meinshausen, M., Nakicenovic, N., Smith, S.J., Rose, S.K., 2011. The representative concentration pathways: an overview. Climatic Change 109, 5. https://doi.org/10.1007/s10584-011-0148-z

Watanabe, M., Kamae, Y., Yoshimori, M., Oka, A., Sato, M., Ishii, M., Mochizuki, T., Kimoto, M., 2013. Strengthening of ocean heat uptake efficiency associated with the recent climate hiatus. Geophysical Research Letters 40, 3175–3179. https://doi.org/10.1002/grl.50541

Westergaard-Nielsen, A., Karami, M., Hansen, B.U., Westermann, S., Elberling, B., 2018. Contrasting temperature trends across the ice-free part of Greenland. Scientific Reports 8, 1586. https://doi.org/10.1038/s41598-018-19992-w

Zhang, H.-M., Huang, B., Lawrimore, J., Menne, M., Smith, T.M., 2015. NOAA Global Surface Temperature Dataset, Version 4.0.

Zwally, H.J., Mario, B.G., Matthew, A.B., Jack, L.S., 2012. Antarctic and Greenland Drainage Systems, GSFC Cryospheric Sciences Laboratory [WWW Document].

URL http://icesat4.gsfc.nasa.gov/cryo_data/ant_grn_drainage_systems.php (accessed 2.6.18).

List of Abbreviations

AMOC	Atlantic Meridional Overturning Circulation
CDD	Consecutive Dry Days
CMIP5	Coupled Model Intercomparison Project, phase 5
CORDEX	COordinated Regional climate Downscaling EXperiment
df	Degrees of freedom
GCM	Global Climate Model
GSL	Growing Season Length
GSO	Growing Season Onset
FRD	FRost Days
HIRHAM5	Regional climate model: A combination of the High Resolution Limited Area Model (HIRLAM) and the ECMWF Hamburg (ECHAM) GCM, version 5
HIRLAM	HIgh Resolution Limited Area Model
IPCC	Intergovernmental Panel on Climate Change
JJA	June, July, August
MJJASO	May, June, July, August, September, October
NAO	North Atlantic Oscillation
NDJFMA	November, December, January, February, March, April
PR	Precipitation
RCM	Regional Climate Model
RCP	Representative Concentration Pathways
sd	Standard deviation
SMB	Surface Mass Balance
TAS	Near-Surface Air Temperature (2 m)
weq	Water EQuivalent

Appendix A

A-1 CMIP5 models and grid resolution

GCM	Atmospheric Grid		Ocean Grid	
	Latitude	Longitude	Latitude	Longitude
ACCESS1.0	1.25	1.87	lat(i,j)	lon(i,j)
ACCESS1.3	1.25	1.87	lat(i,j)	lon(i,j)
BCC-CSM1.1	2.79	2.81	0.33, 1	1
BCC-CSM1.1(m)	2.79	2.81	0.33, 1	1
BNU-ESM	2.79	2.81	0.33, 1	1
CCSM4	0.94	1.25	lat(i,j)	lon(i,j)
CESM1(BGC)	0.94	1.25	lat(i,j)	lon(i,j)
CESM1(CAM5)	0.94	1.25	lat(i,j)	lon(i,j)
CESM1(WACCM)	1.88	2.5	lat(i,j)	lon(i,j)
CMCC-CM	0.74	0.75	lat(i,j)	lon(i,j)
CMCC-CMS	3.71	3.75	lat(i,j)	lon(i,j)
CNRM-CM5	1.40	1.40	lat(i,j)	lon(i,j)
CSIRO-Mk3.6.0	1.86	1.87	0.93, 0.94	1.875
CanESM2	2.79	2.81	0.93, 1.14	1.40625
EC-EARTH	1.12	1.12	lat(i,j)	lon(i,j)
FGOALS-g2	2.79	2.81	0.5, 1	1
GEOS-5	2	2.5	1	1
GFDL-CM3	2	2.5	0.33, 1	1
GFDL-ESM2G	2.02	2	0.37, 0.5	1
GFDL-ESM2M	2.02	2.5	0.33, 1	1
GISS-E2-H	2	2.5	1	1
GISS-E2-H-CC	2	2.5	1	1
GISS-E2-R	2	2.5	1	1.25
GISS-E2-R-CC	2	2.5	1	1.25
HadGEM2-AO	1.25	1.87	0.33, 1	1
HadGEM2-CC	1.25	1.87	0.33, 1	1
HadGEM2-ES	1.25	1.87	0.33, 1	1
INM-CM4	1.5	2	0.5	1
IPSL-CM5A-LR	1.89	3.75	lat(i,j)	lon(i,j)
IPSL-CM5A-MR	1.26	2.5	lat(i,j)	lon(i,j)

GCM	Atmospheric Grid Latitude	Ocean Grid Longitude	lat(i,j) Latitude	lon(i,j) Longitude
MIROC-ESM-CHEM	2.79	2.81	0.55, 1.71	1.40
MIROC5	1.40	1.40	0.5, 0.5	1.40
MPI-ESM-LR	1.86	1.87	lat(i,j)	lon(i,j)
MPI-ESM-MR	1.86	1.87	lat(i,j)	lon(i,j)
MRI-CGCM3	1.12	1.12	0.5, 0.5	1
NorESM1-M	1.89	2.5	lat(i,j)	lon(i,j)
NorESM1-ME	1.89	2.5	lat(i,j)	lon(i,j)

Table A-1: Global climate models (GCMs) used in AR5 and in this project.

A-2 Climate indices

Index	Index description
Mean temperature	Daily mean temperature at 2 m height, mean value
Max temperature	Daily maximum temperature at 2 m height, mean value
Min temperature	Daily minimum temperature at 2 m height, mean value
Frost days	Number of days when daily minimum temperature at 2 m is below 0^{o}C
10˚C days	Number of days when daily maximum temperature at 2 m is above 10^{o}C
-7˚C days	Number of days when daily maximum temperature at 2 m is below -7^{o}C
Longest dry period	Longest continuous period with precipitation below 1 mm
Dry days	Number of days with precipitation below 1 mm
Heavy precipitation	Number of days with precipitation above 10 mm
Extreme precipitation	Number of days with precipitation above 25 mm
Accumulated precipitation	Precipitation, summed up
Highest daily precipitation	Maximum precipitation intensity (yearly maximum)
Accumulated rain	Amount of rainfall, summed up
Annual snowfall	Amount of snowfall, summed up
Rain fraction	Rainfall fraction of total precipitation
Effective precipitation	Precipitation minus evaporation, summed up

Index	Index description
Highest Effective 7-day precipitation	Highest effective precipitation during a continuous 7-day period
Highest Effective 14-day precipitation	Highest effective precipitation during a continuous 14-day period
Highest Effective 30-day precipitation	Highest effective precipitation during a continuous 30-day period
Highest Effective 60-day precipitation	Highest effective precipitation during a continuous 60-day period
Highest 7-day precipitation	Highest precipitation during a continuous 7-day period
Evaporation	Evaporation, summed up
Cold rainy days	Number of days during the year when daily maximum temperature at 2 m is below 1^{o}C and rainfall is above 0.5mm (model adjusted ”days with freezing rain”)
Heat radiation	Mean value of incoming longwave radiation
Humid days > 10˚C	Number of days when the relative humidity (daily mean) is above 60% and daily mean temperature at 2 m is above 10^{o}C
Net runoff	Net runoff, summed up
Net runoff	Net runoff over glacier, summed up
Snow season length > 2 cm	Number of days with snow cover (snow depth above 2 cm)
Snow season length 2-10 cm	Number of days with snow depth between 2 and 10 cm

Index	Index description
Snow season length 10-20 cm	Number of days with snow depth between 10 and 20 cm
Snow season length > 20 cm	Number of days with snow depth above 20 cm
Global radiation	Mean value of incoming short wave radiation
17˚C - days	Number of degree days when daily maximum temperature at 2 m is above 17^{o}C
15˚C -days	Longest continuous period with daily maximum temperature at 2 m above 15^{o}C
End of growing season (5˚C)	Daynumber for the end of the last continuous 4-day period with daily mean temperature at 2 m above 5^{o}C
End of growing season (2˚C)	Daynumber for the end of the last continuous 4-day period with daily mean temperature at 2 m above 2^{o}C
Start of growing season (5˚C)	Daynumber for the end of the first continuous 4-day period with daily mean temperature at 2 m above 5^{o}C
Start of growing season (2˚C)	Daynumber for the end of the first continuous 4-day period with daily mean temperature at 2 m above 2^{o}C (”start of growing season (2^{o}C)”)
10˚C -days	Number of degree days for daily mean temperature at 2 m above 10^{o}C
8˚C -days during growing season	Number of degree days for daily mean temperature at 2 m is above 8^{o}C during the growing season (5^{o}C)
Heating degree days (HDD) < 12˚C	Number of degree days for daily mean temperature at 2 m below 12^{o}C
Last spring frost	Last daynumber (<240) when daily minimum temperature at 2 m is below 0^{o}C

Index	Index description
Warm nights	Number of days when daily minimum temperature at 2 m is above 12^{o}C (model adjusted ”tropical nights”)
Length of growing season (2˚C)	Number of days between the end of the first continuous 4-day period with daily mean temperature at 2 m above 2^{o}C and the end of the last continuous 4-day period with daily mean temperature at 2m above 2^{o}C
Length of growing season (5˚C)	Number of days between the end of the first continuous 4-day period with daily mean temperature at 2 m above 5^{o}C and the end of the last continuous 4-day period with daily mean temperature at 2m above 5^{o}C
Freezing point days	Number of days when daily mean temperature at 2 m has been both above and below 0^{o}C (daily maximum temperature at 2 m above 0^{o}C and daily minimum temperature at 2 m below 0^{o}C)
7˚C -days	Number of days when the daily mean surface temperature is below -7^{o}C
Wind speed	Daily mean wind speed at 10m, mean value
Permafrost index	Permafrost index ($\frac{\sqrt{DDF}}{\sqrt{DDT}+\sqrt{DDF}}$, where DDF(DDT) = degree-days of freezing(thawing))
Thawing degree days (DDT)	Number of degree days when daily mean temperature at 2 m is above 0^{o}C
Fishing days 20 m/s	Number of days when 10m wind speed is below 20m/s
Fishing days 15 m/s	Number of days when 10m wind speed is below 15m/s

Index	Index description
Freezing degree days (DDF)	Number of degree days when daily mean temperature at 2 m is below 0^{o}C
Length of thawing season	from 0^{o}C crossing dates using a 21-day moving average of daily mean temperature at 2 m
Length of freezing season	from 0^{o}C crossing dates using a 21-day moving average of daily mean temperature at 2 m
Winter melt days	Melt events during winter (number of days with daily maximum temperature at 2m above 0^{o}C and 29-day running mean of daily mean temperature at 2m below -5^{o}C)
Snow cover season onset	Daynumber, after day 220, of the first 5 consecutive days with snow cover above 2cm
Snow cover season end	Daynumber of the first 5 consecutive days with snow cover below 2 cm
Snow cover season change in onset	Standard deviation of annual values of index 52
Snow cover season change in end	Standard deviation of annual values of index 53
Mosquito season onset	Daynumber, after 10 continuous days with daily mean temperature at 2 m above 0^{o}C, when daily maximum temperature at 2 m is above 10^{o}C and the relative humidity is above 45%
Mosquito season end	Daynumber, after day 220, of the first 5 consecutive days with daily mean temperature at 2 m below 0^{o}C
Mosquito season length	Difference between Indices 57 and 56

Index	Index description
Dry period during growing season (5˚C)	Longest continuous period with precipitation below 1 mm (”dry period”) during growing season (5^{o}C)
Sun hours	Daily mean sunshine hours, mean value

Table A-2: Climate Indices calculated for Greenland and for the 6 regions , the National park, Kummune Kujalleq, Kommuneqarfik Sermersooq west, Sermersooq East, Qeqqata Kommunia and Qaasuitsuq Kommunia. Based on (Christensen et al., 2015a-f)

Appendix B

Correlation patterns for precipitation

Correlation maps for HIRHAM5 simulated annual precipitation time series 1980-2014. The maps represent correlation coefficients between each land grid point and the grid point closest to the DMI-weather stations. Critical correlation coefficient for statistical significance at a 95% confidence level is r = 0.33 (yellow).

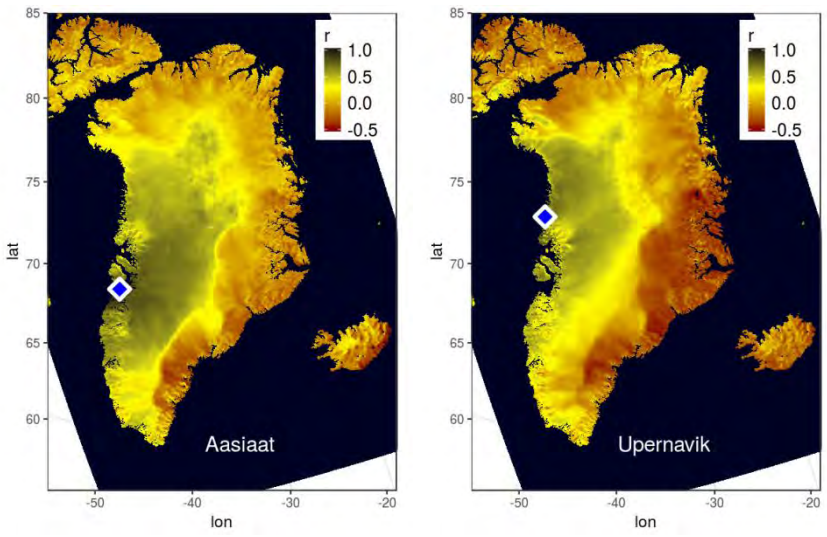

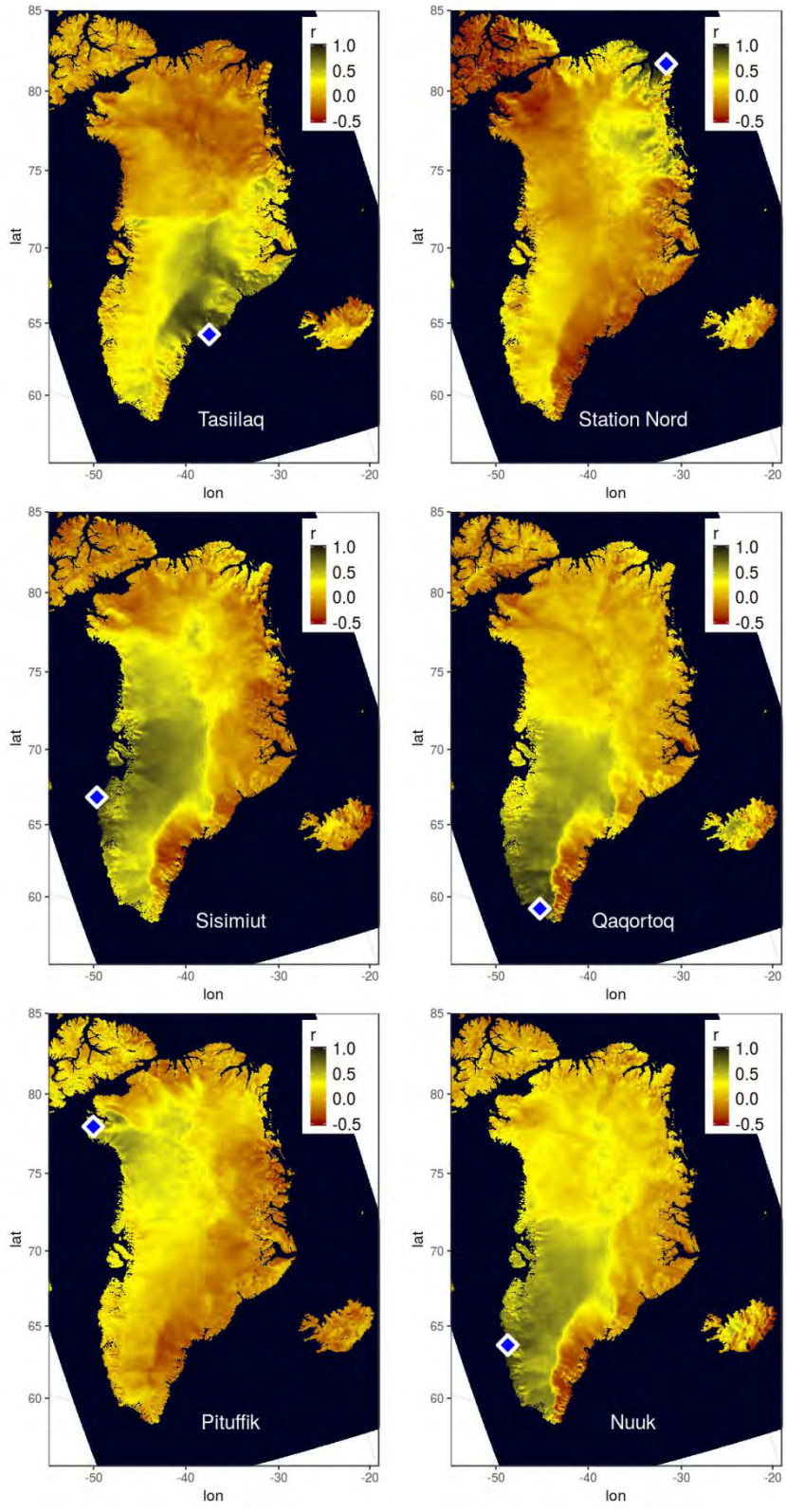
r
1.0
0.5
0.0
-0.5
lat
lon
85
80
75
70
65
60
-50
-40
-30
-20
Tasiilaq
Station Nord
Sisimiut
Qaqortoq
Pituffik
Nuuk

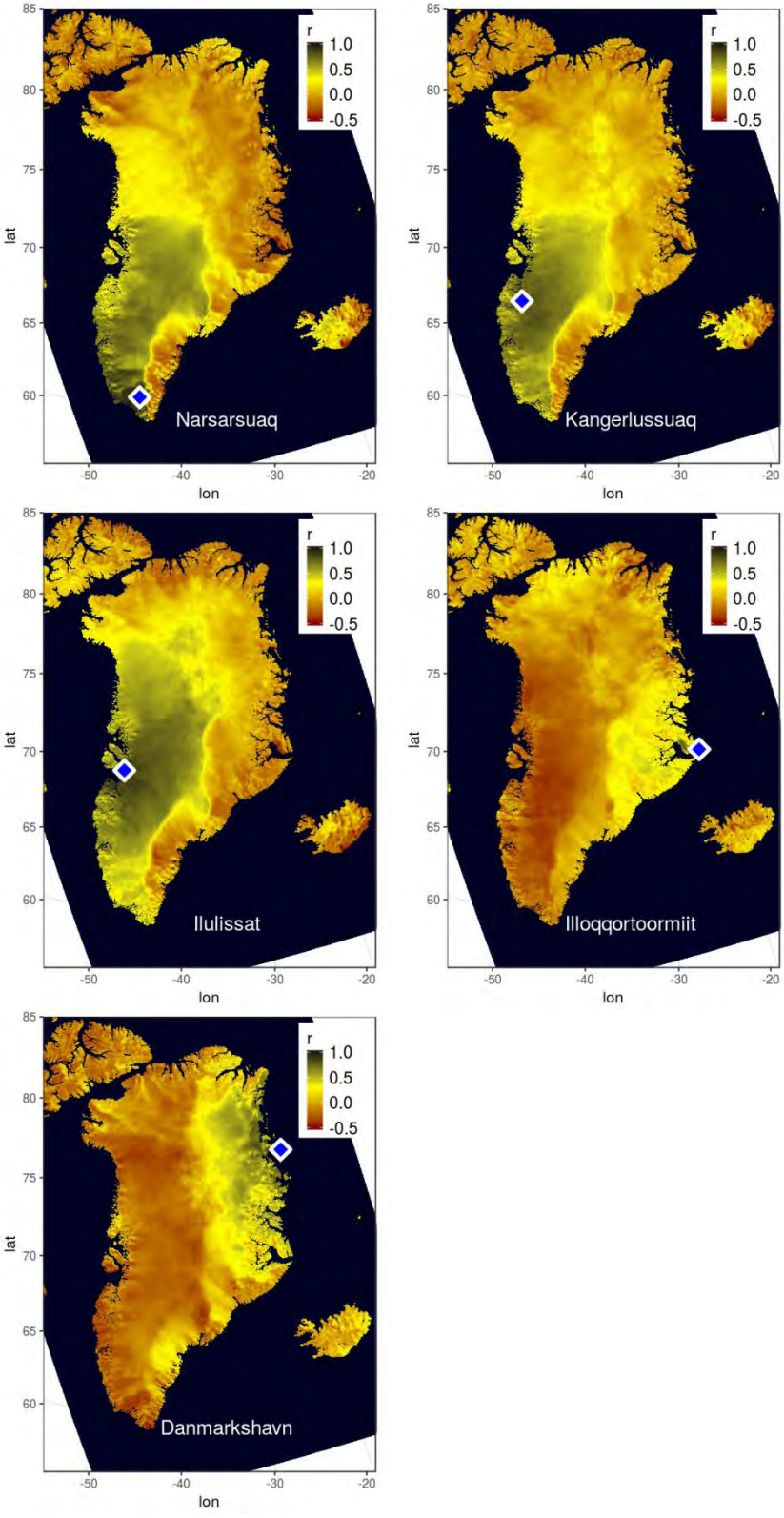
r
1.0
0.5
0.0
-0.5
lat
lon
85
80
75
70
65
60
-50
-40
-30
-20
Narsarsuaq
Kangerlussuaq
Ilulissat
Illoqqortoormiit
Danmarkshavn

Correlation patterns for summer temperature (JJA)

Correlation maps for HIRHAM5 simulated summer (JJA) mean temperature time series 1980-2014. The maps represent correlation coefficients between each land grid point and the grid point closest to the DMI-weather stations. Critical correlation coefficient for statistical significance at a 95% confidence level is r = 0.33 (yellow).

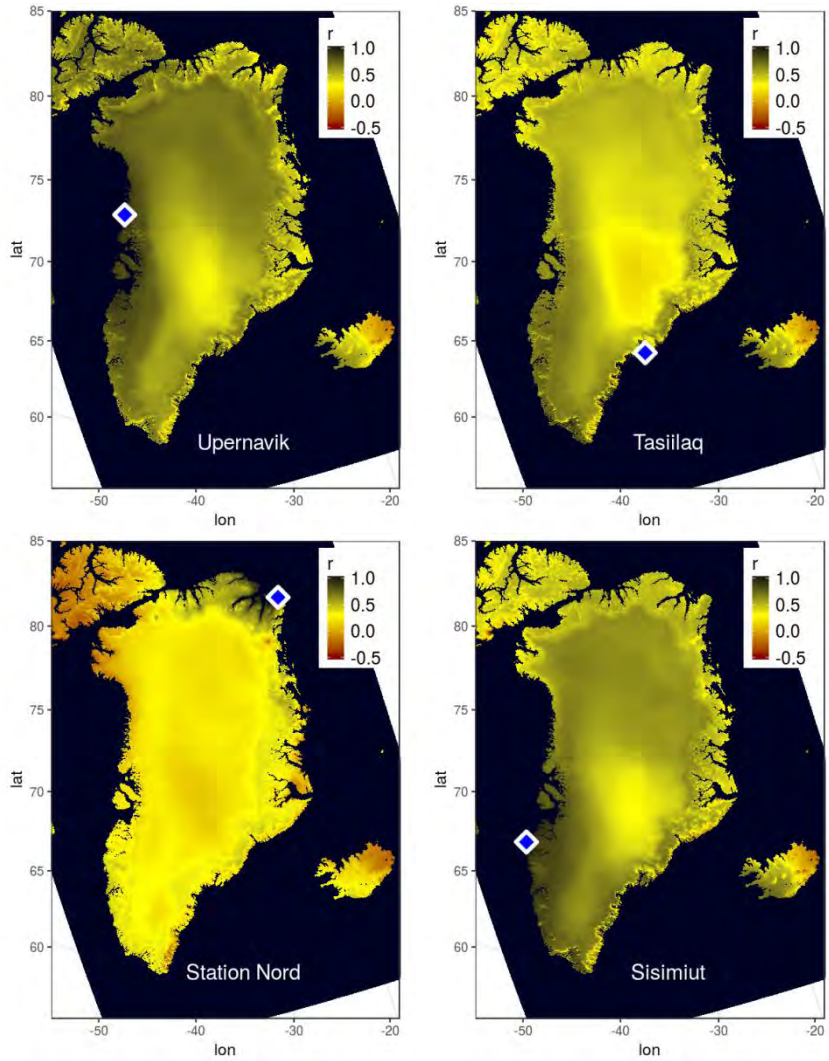

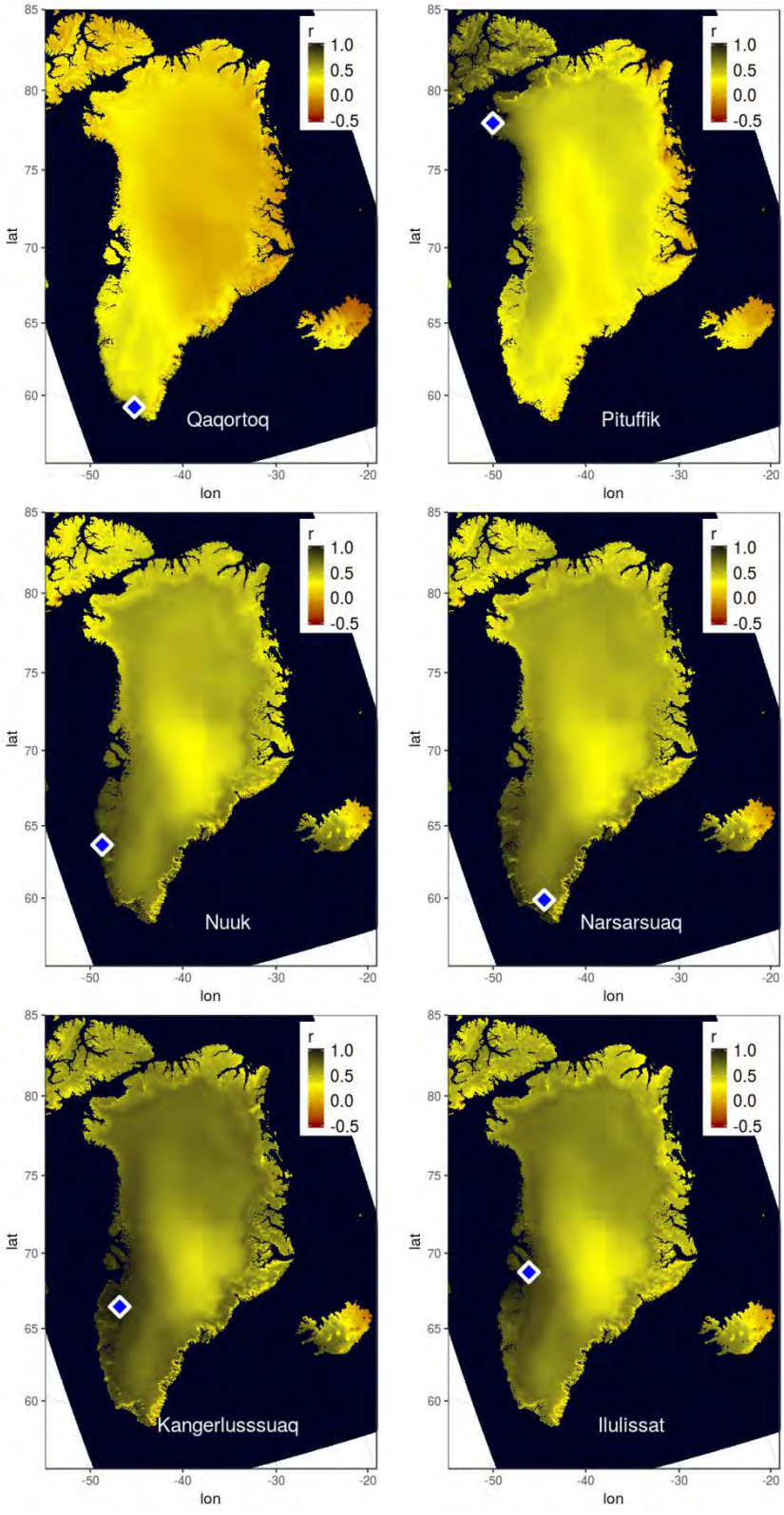
r
1.0
0.5
0.0
-0.5
lat
lon
85
80
75
70
65
60
-50
-40
-30
-20
Qaqortoq
Pituffik
Nuuk
Narsarsuaq
Kangerlusssuaq
Ilulissat

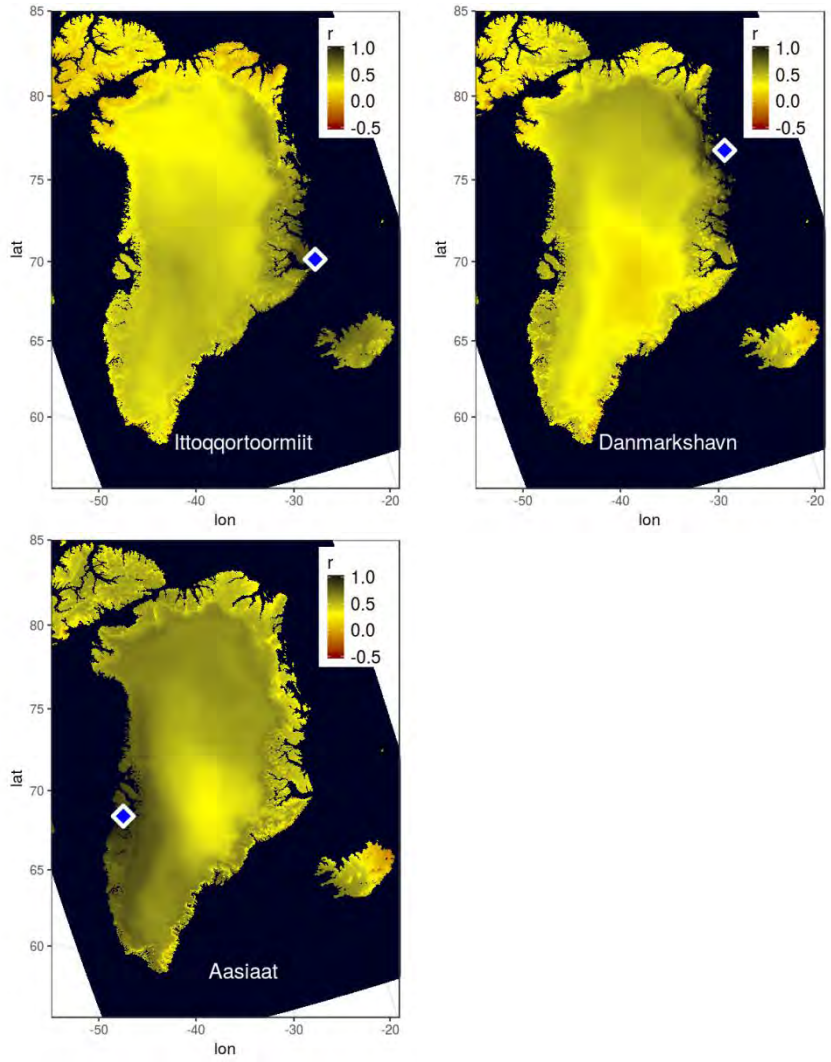
r
1.0
0.5
0.0
-0.5
lat
lon
Ittoqqortoormiit
Danmarkshavn
Aasiaat
85
80
75
70
65
60
-50
-40
-30
-20

Correlation patterns for solid accumulation

Correlation maps for HIRHAM5 simulated solid accumulation time series 1980-2014. The maps represent correlation coefficients between each land grid point and the grid point closest to six deep ice core drill site locations. Critical correlation coefficient for statistical significance at a 95% confidence level is r = 0.33 (yellow).

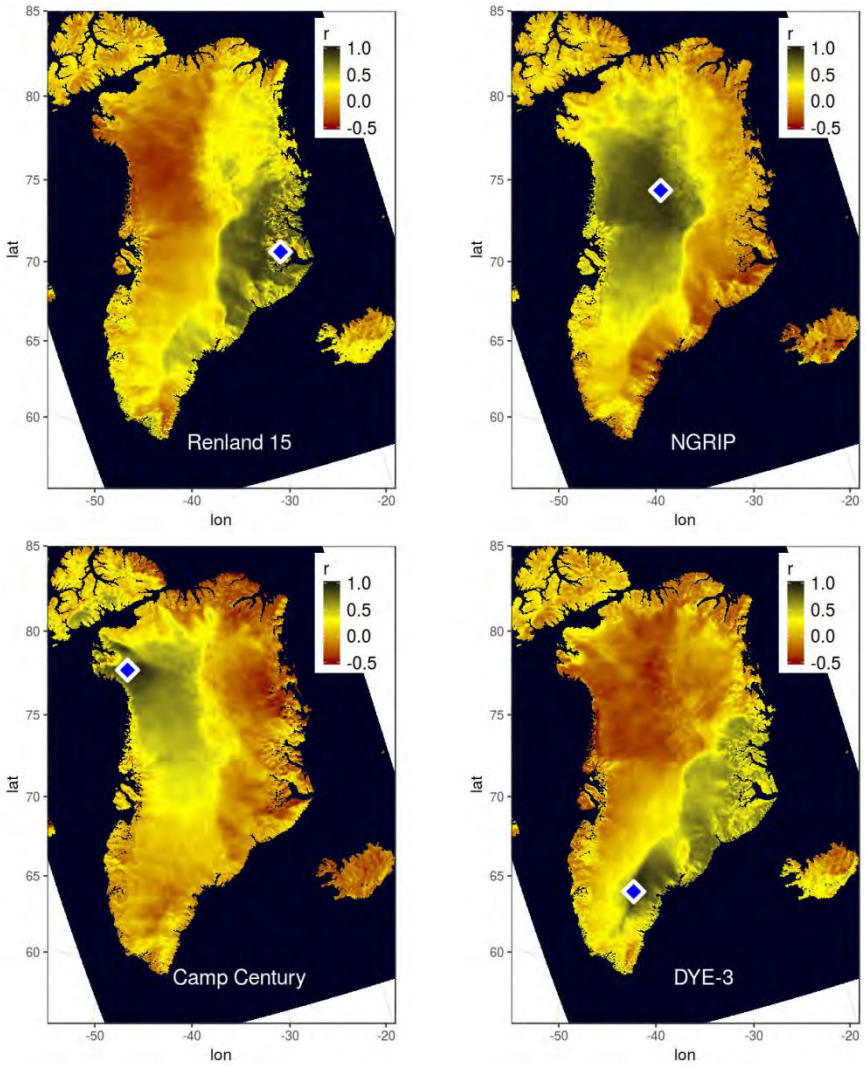

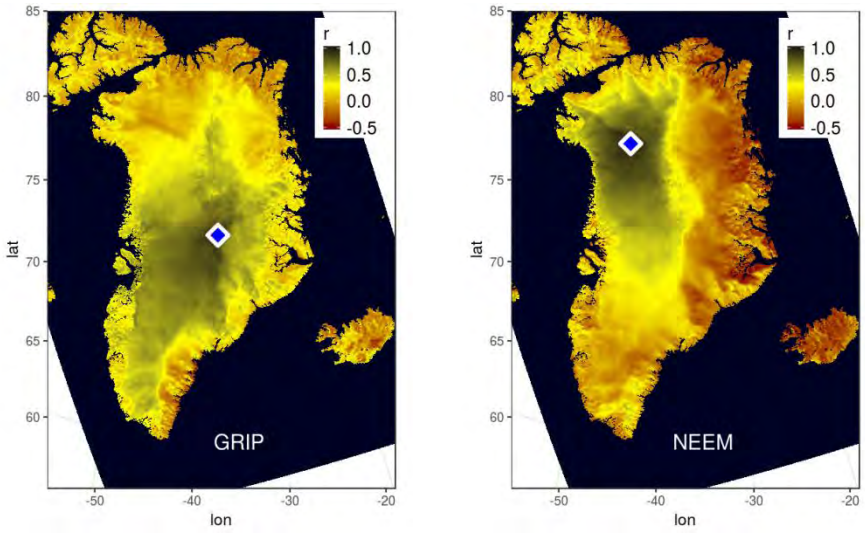
r
1.0
0.5
0.0
-0.5
GRIP
NEEM
lat
lon
85
80
75
70
65
60
-50
-40
-30
-20

Paper I Olesen, M., Christensen, J.H., Kaas, E., Boberg, F., 2018a. Robustness of high-resolution regional climate projections for Greenland: a method for uncertainty distillation. Clim. Res. 76, 253–268. [Published Nov 2018]

Vol. 76: 253–268, 2018
https://doi.org/10.3354/cr01536

CLIMATE RESEARCH
Clim Res

Published online November 14

Robustness of high-resolution regional climate projections for Greenland: a method for uncertainty distillation

Martin Olesen[1,*], Jens Hesselbjerg Christensen[1,2,3], Eigil Kaas[2], Fredrik Boberg[1]

[1]Danish Meteorological Institute, Lyngbyvej 100, 2100 Copenhagen Ø, Denmark
[2]Niels Bohr Institute, Juliane Maries Vej 30, 2100 Copenhagen Ø, Denmark
[3]NORCE Norwegian Research Centre, Bjerknes Centre for Climate Research, Jahnebakken 5, 5007 Bergen, Norway

ABSTRACT: Managing adaptation to climate changes in Greenland will depend, to a large degree, on high-resolution climate simulations and associated uncertainty estimates. A single high-resolution climate simulation is generally insufficient to quantify the uncertainty of a given scenario projection. For Greenland, this becomes a critical issue because of a lack of high-resolution climate experiments for this region. Therefore, we introduce and test a new method to solve this uncertainty assessment problem. Using the regional climate model (RCM) HIRHAM5 over Greenland in combination with an ensemble of RCM simulations from a different geographical setting, (i.e. EURO-CORDEX), we investigate to what extent the uncertainty of projected climate change at high resolution can be evaluated from corresponding temperature spreads in a wider set of global climate models (GCMs), that is, CMIP5. The study is based on a set of time-slice simulations downscaled with HIRHAM5 at 5.5 km resolution for the RCP4.5 and RCP8.5 scenarios for Greenland with boundary information from the GCM EC-Earth. Our proposed uncertainty assessment method establishes a foundation on which high-resolution and relatively costly regional climate projections can be assessed as well as when using only a single RCM without the presence of analogous downscaling experiments with other RCMs and GCMs, and instead relying on existing information from CMIP5. Thus, the uncertainty of a wide range of climate indices that scales with temperature can be evaluated and quantified through the inter-model temperature spread within CMIP5.

KEY WORDS: Greenland · Climate change · Climate indices · Uncertainty quantification · Climate adaptation

1. INTRODUCTION

The climate in the Arctic is in rapid transition. The global mean temperature is increasing, and because of various feedback mechanisms, the Arctic region, which includes Greenland, will likely experience even faster and higher temperature increases than most other parts of the world; this is often referred to as Arctic amplification (e.g. Pithan & Mauritsen 2014).

These temperature increases will have substantial impacts in Greenland, both in populated regions along the coasts and on the ice sheet (AMAP 2017). Temperature changes will, and already do, require customised adaptation strategies. Infrastructure, agriculture, fishery, tourism and other sectors in Greenland are already being affected by climate change, and the impacts will increase further with increasing temperatures (Christensen et al. 2015, Rosen 2016, Lehmann et al. 2017). Related barriers and opportunities have broad political attention in Greenland, and detailed knowledge on climate change is greatly demanded by Greenlandic self-governance bodies (DFFL 2007).

*Corresponding author: mol@dmi.dk

Publisher: Inter-Research · www.int-res.com

1.1. Climate indices

Customised climate indices from high-resolution climate simulations are practical and valuable for local sector adaptation strategies in Greenland. Length and onset of the growing season and number of frost days are examples of highly useful climate indices designed for climate adaptation of agriculture in southern Greenland (Christensen et al. 2015, Lehmann et al. 2017). Definitions of climate indices in this study are from Persson et al. (2007), who involved the Swedish Commission of Climate and Vulnerability and other stakeholders in selecting and defining relevant climate indices with a focus on northern Europe.

Climate indices can be used to infer complex weather-dependent relations in a simpler manner than by using observed meteorological conditions or direct model output data from climate models. More than 60 different climate index projections with a focus on Greenland were published by Christensen et al. (2015), targeting climate adaptation needs in Greenland. The focus was on the relatively small part of Greenland where the population is settled, and the work resulted in 6 district reports targeting the administrative level of Greenlandic municipalities. In these reports, the idea of assessing the projected index uncertainty for a single high-resolution regional climate simulation with the use of CMIP5 was introduced but never formally validated.

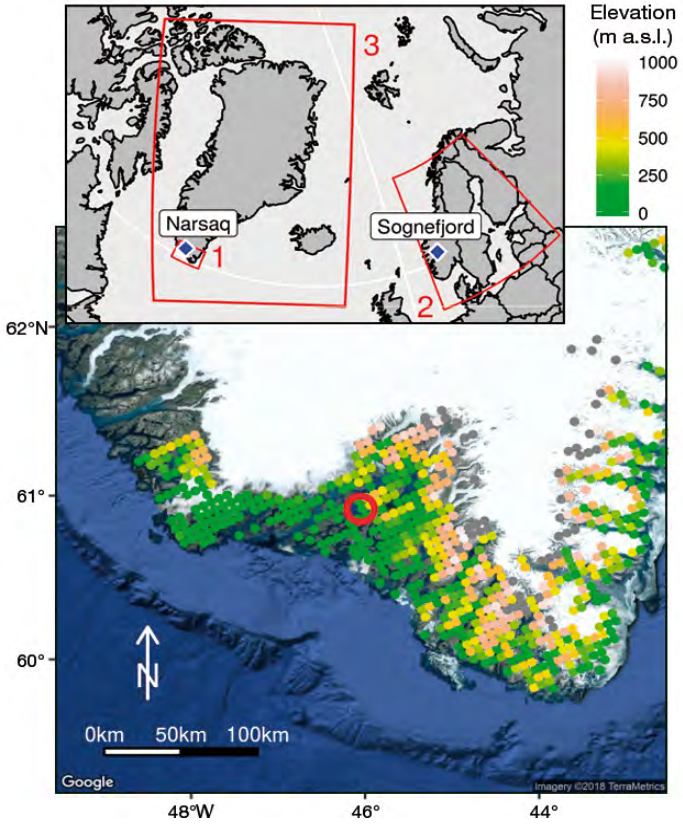

Fig. 1. Model topography in southern Greenland represented as ice-free HIRHAM5 grid points on land around the village of Narsaq (marked with a red circle). The colour map corresponding to Domain 1 in the inset has a horizontal resolution of 5.5 km. Scandinavia (Domain 2) and the head of Sognefjord are subject to further analysis in this study. Domain 3 represents the lateral boundary of this HIRHAM5 simulation. Narsaq and the head of Sognefjord are marked with blue diamonds in the inset

1.2. High-resolution information from regional climate models

Optimising adaptation to the future climate in Greenland requires high-resolution climate simulations to capture climate impacts in the inhabitable coastal areas, where topography is highly complex with steep mountains and complex meandering coastlines, multiple glaciers and fjord systems.

Dynamical downscaling of a global climate model (GCM) will in general and for Greenland in particular add value to the existing climate information for historical simulations as well as for future climate projections (Lucas-Picher et al. 2012, Rummukainen 2016). Fig. 1 illustrates the geographical resolution when downscaling the GCM EC-Earth (Hazeleger et al. 2012) to 5.5 km with the regional climate model (RCM) HIRHAM5 (Christensen et al. 2006). This distance (5.5 km) is just enough to resolve the fjords surrounding Narsaq in southern Greenland and, hence, distinguish and identify fjord and mountain weather characteristics. The spatial resolution is illustrated in Fig. 1, where only ice free land points are represented with coloured dots. Especially when the climate indices are based on high temporal resolution (daily values) and conducted on the basis of fine-scale features, the added value by using very high resolution RCMs has been demonstrated and summarised previously (e.g. Christensen & Christensen 2003, Christensen et al. 2007, Feser et al. 2011, Lucas-Picher et al. 2012, Di Luca et al. 2015, Mayer et al. 2015, Rockel 2015, Giorgi et al. 2016).

1.3. Uncertainty assessment

The uncertainties associated with projected climate index changes under a given climate scenario have to be evaluated and quantified to ensure a robust scientific base for climate adaptation planning. The present work provides supporting documenta-

tion for the uncertainty assessments of simulated climate index changes for Greenland adopted by Christensen et al. (2015).

So far, uncertainties associated with downscaling of climate projections have primarily been based on using results from an ensemble of RCMs nested in different GCMs (e.g. Pan et al. 2001, Déqué 2007, Jacob et al. 2014, Vautard et al. 2014). However, because of limited computer resources, multiple high-resolution simulations (such as those presented in this study) are so far not available for large, remote and sparsely populated regions like Greenland. Since a single regional climate simulation is insufficient for any proper uncertainty analysis (e.g. Sloth Madsen et al. 2012, IPCC 2013, McSweeney et al. 2015), an alternative method to evaluate the uncertainties related to a single climate simulation is required. Here such a method is proposed and evaluated.

1.4. Pattern scaling

The method builds on the theoretical scalability assumption, where there is a linear relation between annual mean temperature change (here from the GCM) and the response of a temperature-dependent variable (here the climate indices) (Mitchell et al. 1999, Tebaldi & Arblaster 2014). The technique is an attempt to estimate the anomaly in a climate variable for a particular location or grid point for a given period that would have been obtained from additional regional climate simulations for a specific scenario.

In this study, we are not confining ourselves to simple linear relations between the climate index and annual mean temperature. On the other hand, we are not extrapolating beyond existing high-end scenario temperature ranges either. The analysis presented here is performed within a temperature range, where the relationship between the climate index and the annual mean temperature is identified.

2. METHODS

2.1. Models

The model configuration we want to test in this study is the RCM HIRHAM5 (Christensen et al. 2006) set up with a 5.5 km spatial resolution for a domain covering Greenland and Iceland (Lucas-Picher et al. 2012, Langen et al. 2015, Boberg et al. 2017), domain 3 in Fig. 1. HIRHAM5 is nested within the GCM EC-Earth, is forced with 6 hourly lateral boundaries and receives sea surface temperatures and sea ice coverage on a daily basis. EC-Earth was developed by the EC-Earth consortium (Hazeleger et al. 2012), and the version used in this study is configured at a 125 × 125 km resolution (T159) and uses 62 vertical layers. With this setup, 5 different 20 yr time slices are downscaled for 3 periods, 1991–2010 (a historical run), 2031–2050 (for RCP4.5 and RCP8.5) and 2081–2100 (for RCP4.5 and RCP8.5). Notice that the reference period for this run differs from the standard reference period (1986–2005).

To verify the propounded uncertainty assessment method, the focus is shifted to Europe, where multiple high-resolution downscaling experiments are available within the COordinated Regional climate Downscaling EXperiment for Europe (EURO-CORDEX) (Jacob et al. 2014). The EURO-CORDEX-11 (hereafter referred to as CORDEX) ensemble as of July 2017 contains 5 GCMs and 6 RCMs combined as 15 downscaling experiments for the RCP4.5 and RCP8.5 scenarios for Europe on 0.11° (approximately 12 km) resolution; the GCM–RCM matrix is shown in Table 1. For climate index calculation, both temperature and land area fraction fields are required. The RCMs used in this study are CCLM (Rockel et al. 2008), HIRHAM5 (Christensen et al. 1998, 2006), ALARO-0 (Giot et al. 2016), RACMO2 (van Meijgaard et al. 2012), RCA4 (Kupiainen

Table 1. GCM–RCM matrix with available EURO-CORDEX experiments for Europe for the RCP4.5 and RCP8.5 scenarios at 0.11° spatial resolution from 2006 to 2100. EXP numbers refer to downscaling experiments in Figs. 7 & 8. GCM: general climate model; RCM: regional climate model

GCM– RCM-	CNRM CERFACS-CNRM-CM5	ICHEC-EC EARTH	IPSL-CM5A-MR	MOHC-HadGEM2-ES	MPI-M MPI-ESM-LR
DMI-HIRHAM5		EXP 7			
SMHI-RCA4	EXP 2	EXP 5	EXP 8	EXP 11	EXP 14
KNMI-RACMO22E		EXP 4			
EXP 6		EXP 10			
CLMcom	EXP 1	EXP 3		EXP 9	EXP 12
MPI-REMO					EXP 13
					EXP 15

et al. 2011, Samuelsson et al. 2011) and REMO (Jacob et al. 2012). Furthermore, 18 EURO-CORDEX EURO-44 combinations are applied for larger area studies.

We use 39 GCMs from CMIP5 (Taylor et al. 2012) with spatial resolutions ranging from 0.5° to 4°. Here we use the entire set for projected temperature changes in RCP8.5 by the end of the 21st century. From CMIP5, a subset of 5 GCMs is used for the EURO-CORDEX downscaling experiments: EC-Earth (Hazeleger et al. 2012), CNRM (Voldoire et al. 2013), IPSL (Dufresne et al. 2013), MOHC HadGEM2 (Collins et al. 2011) and MPI-M-MPI-ESM-LR (Giorgetta et al. 2013).

2.2. Technique for uncertainty assessment

Our hypothesis is that uncertainty related to a single high-resolution downscaled regional climate projection can be assessed by converting statistical information deduced from CMIP5 to the single high-resolution downscaled projection. The overall idea is to convert the spread of annual mean temperature from CMIP5 simulations for a given RCP scenario into the uncertainty of an RCM-derived climate index, e.g. growing season onset or growing season length for the same scenario. Conversion of CMIP5 temperature spread is done through a correlation setup between an RCM-derived climate index and GCM temperatures as explained through the following steps (this subsection). The concept is also illustrated in Fig. 2.

Temperature-dependent climate indices are calculated from the high-resolution RCM simulation (in this study HIRHAM5). Here we test the indices growing season length and onset, both of particular relevance for southern Greenland. Growing season length is defined as the number of days between the first occurrence of at least 4 consecutive days with daily mean temperatures above 5°C and the first occurrence of 4 consecutive days with a temperature below 5°C.

RCM-derived climate indices are shown against corresponding annual mean temperature at the nearest grid point from the forcing GCM in which the RCM is nested (in this study EC-Earth). This is done for index and temperature changes for each model year with respect to the mean climatology for a baseline period (1986–2005), also used by IPCC (2013).

A linear or second-order regression line, as well as confidence and prediction (tolerance) intervals, are then fitted to the RCM-derived climate indices and corresponding GCM annual mean temperatures. Following the IPCC definition of likely (66–100% probability) on the likelihood scale (Mastrandrea et al. 2011), confidence and prediction levels are accordingly set to 66%. The confidence interval relates to the best fitted regression line, whereas the prediction interval represents the year-to-year variability in the climate index. The prediction interval embraces 66% of the simulated growing season lengths for a given temperature interval, shown as the blue lines enclosing 66% of the points in Fig. 2.

Finally, the likely range of 20 yr mean temperature projections from CMIP5 can be converted to a measure of index uncertainty through the intersect with the best fitted regression line, as illustrated with colour-shaded vertical and horizontal bars in Fig. 2.

The estimated index uncertainty depends on the correlation strength and the slope of the regression line. A low correlation coefficient will expand the uncertainty range, and vice versa, a high coefficient will narrow the index uncertainty range towards the corresponding likely range of GCM annual mean temperature projections. The slope of the regression line is a measure of the index's sensitivity to temper-

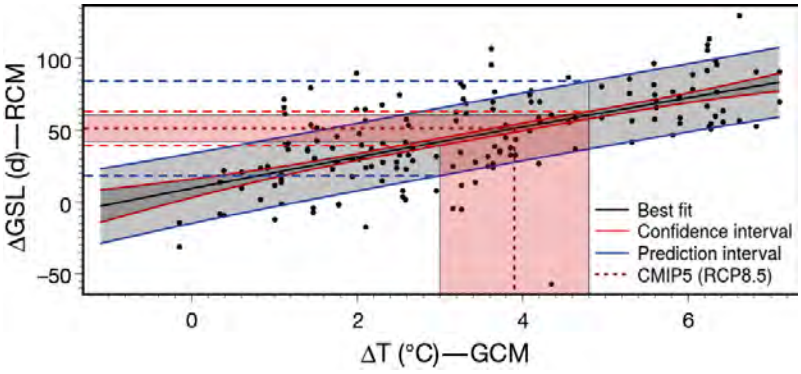

Fig. 2. Changes in growing season length (GSL) for the Sognefjord grid point (1986–2005). Each dot represents change in GSL for 1 yr from HIRHAM5 as a function of annual mean temperature (T) change from EC-Earth for a historical run (1951–2005) and an RCP8.5-scenario run (2006–2100). The black line is the best fitted regression line, and its confidence interval (95% confidence level) is indicated with red lines. The blue lines with grey shading in between are the prediction intervals indicating the year-to-year variability of the GSL for a given temperature change. CMIP5 temperature change in the period 2081–2100 for the RCP8.5 scenario is shown as the vertical dashed red line, and the red shaded area indicates the likely spread of the 39 CMIP5 models. Horizontal dashed lines point to the level of projected change in GSL for CMIP5 mean temperature change and corresponding likely spread (in dark and light red, respectively), and that combined with the likely range of year-to-year GSL variability (blue dashed lines). RCM: regional climate model; GCM: global climate model

ature and hence climate change. The uncertainty range can be deduced from where the CMIP5 shaded areas intersect with the regression lines for confidence and prediction intervals shown in Fig. 2. From this example, the likely increase in number of growing season days for the RCP8.5 scenario by the end of the century can be read to 51 ± 12 d. To this uncertainty estimate we can now add the year-to-year variability range of the index from where the CMIP5-based fit intersects with the blue prediction lines. The change in growing season length will then be 51 d with a total uncertainty of ±33 d.

The current uncertainty assessment method is based on the so-called delta change bias correction approach, which according to (Maraun 2016) is not a real bias correction but rather a way to employ the climate change response from the RCM to adjust the observations. But it also provides a simple measure of model agreement on the climate change signal (Giorgi & Mearns 2003), which is what we are interested in here. Furthermore, it facilitates interpretation and direct use of estimated climate index changes and associated uncertainties in a climate adaptation context. With this technique, changes in climate indices can in this sense be directly added to current observations.

Through a statistically significant correlation between an RCM-derived climate index and the corresponding driving GCM annual mean temperature, the likely spread of the GCM ensemble for that region can be translated into a projected climate index uncertainty. This method allows for quantifying the uncertainty of climate index changes on very local scales, here simulated with a single high-resolution RCM.

Whereas the application of the method is motivated by the need for high-resolution climate simulations for Greenland, the method needs an ensemble of RCMs and GCMs to be tested. Available simulations from Arctic CORDEX (Giorgi et al. 2009, Akperov et al. 2018) are insufficient and only available at coarse resolution (50 km grid). Therefore, the uncertainty assessment method is evaluated for northern Europe, where the number of downscaling experiments is much larger and performed at more comparable resolution. We focus on Scandinavia, which for some areas has somewhat similar climate characteristics to the populated areas in southern Greenland. Finally, the tested uncertainty assessment method is applied to the high-resolution HIRHAM5 simulations first over a Norwegian site, Sognefjord, and then over Greenland, with a focus on Narsaq (see Fig. 1).

2.3. Assumptions

The index uncertainty assessment method requires the following 4 assumptions to be fulfilled:

2.3.1. Assumption I — HIRHAM5 index and EC-Earth temperature correlation

A statistically significant correlation between a HIRHAM5-derived climate index and the EC-Earth simulated annual mean temperature is necessary to ensure a meaningful uncertainty conversion. A strong correlation leads to relatively low uncertainties for projected climate indices, whereas a weak correlation coefficient indicates relatively large uncertainties.

Temperature-dependent climate indices are calculated from the HIRHAM5–EC-Earth downscaling (also part of EURO-CORDEX) for Sognefjord. A linear regression model including confidence and prediction intervals is fitted to the HIRHAM5-derived climate indices and corresponding annual mean temperature from the driving model, EC-Earth, as in Fig. 2. This is done for a number of climate indices (here only growing season length and onset are shown as our first choice, but we also briefly discuss number of frost days and consecutive dry days) and tested on specific locations as well as for the Scandinavian region as a whole.

2.3.2. Assumption II — General RCM index and GCM temperature correlation

The method requires that the correlation between a HIRHAM5-derived climate index and the corresponding EC-Earth simulated annual mean temperature represents a general index–temperature dependency. In addition, the projected temperature from HIRHAM5 should be drawn from the same distribution as the CORDEX ensemble. Some climate indices involve thresholds, and may therefore be sensitive to biases.

The consistency of index–temperature correlations among the individual CORDEX downscaling experiments (HIRHAM5–EC-Earth included) is therefore tested to ensure that HIRHAM is representative for the CORDEX ensemble. Furthermore, HIRHAM5 and 7 other RCM downscaling experiments forced with the European reanalysis dataset ERA-Interim from the European Centre for Medium-Range Weather Forecasts (Dee et al. 2011) are also compared to show individual performances with identical boundary conditions as also shown by Christensen et al. (2008).

2.3.3. Assumption III — Transferability of index relation

The derived relationship between HIRHAM5 indices and EC-Earth temperature has to be transferable from one region to another. If the relationship between HIRHAM5 and EC-Earth for Scandinavia holds for Greenland, we assume that the general RCM index and GCM temperature dependency (Assumption II) sustains.

To test the transferability assumption, a climate index correlation analysis for Europe at a grid point near Sognefjord is compared to a corresponding analysis for Greenland at a grid point near Narsaq (see locations in Fig. 1). Narsaq is relevant because of its agriculture activities. The Sognefjord grid point is relevant because it is comparable to Narsaq, with its location in a west-facing fjord system at the same latitude and its similar orographically influenced weather systems.

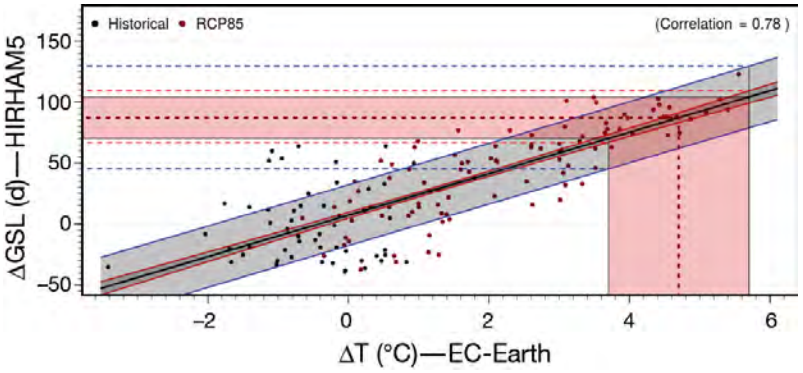

Fig. 3. Changes in growing season length (GSL) for the Sognefjord grid point (1986–2005). Each dot represents change in GSL for 1 yr from HIRHAM5 as a function of annual mean temperature (T) change from EC-Earth for a historical run (1951–2005, black dots) and an RCP8.5-scenario run (2006–2100, red dots). The black line is the best fitted regression line, and its confidence interval (95% confidence level) is indicated with red lines. The blue lines are the prediction intervals indicating the year-to-year variability of the GSL for a given temperature change. CMIP5 temperature change in the period 2081–2100 for the RCP8.5 scenario is shown as the vertical dashed red line, and the red shaded area indicates the likely spread of the 39 CMIP5 models. Horizontal dashed lines point to the level of projected change in GSL for CMIP5 mean temperature change and corresponding likely spread (in dark and light red, respectively), and that combined with the likely range of year-to-year GSL variability (blue dashed lines)

2.3.4. Assumption IV — CMIP5 and CORDEX variance

The likely range of projected temperature from CMIP5 has to embrace the likely temperature range on a smaller scale from the CORDEX projections. If the likely RCM temperature range exceeds the likely GCM temperature range, we will not necessarily capture a full 66% likely range from CMIP5.

To check this, the 17th and 83rd percentiles of CMIP5 and CORDEX temperature projections are compared to make sure that the boundaries of the likely ranges are overlapping at both the high and low ends of the projected temperature distribution.

3. RESULTS

3.1. Assumption I

In Fig. 3, the change in growing season length (1986–2005) calculated from (EURO-CORDEX based) HIRHAM5 on a 12 km spatial resolution is shown as a function of corresponding annual mean temperature from the forcing GCM, EC-Earth. The correlation coefficient of the linear regression is r = 0.78. The growing season onset is shown in Fig. 4 and has a lower correlation (r = 0.59).

Moving from one grid point to the entire Scandinavian domain (Domain 2 in Fig. 1), the correlation coefficients for each grid point are shown for growing season length and onset in Figs. 5 & 6, respectively. As the correlation between the climate index and the annual mean temperature is statistically significant, this assumption is fullfilled. The correlation between the climate index and the annual mean temperature differs across Scandinavia but remains in the range of 0.6 to 0.9 for growing season length and −0.8 to −0.4 for growing season onset, as highlighted in the density plots (top left) in Figs. 5 & 6.

3.2. Assumption II

The correlation between climate indices (growing season length and onset) and annual mean temperatures among the individual regional and global models within EURO-CORDEX is compared and shown in Figs. 7 (length) & 8 (onset) for Scandinavia and the Sognefjord grid point.

Annual mean temperatures for Scandinavia from the 15 EURO-CORDEX members are close to being normally distributed, and a Student's *t*-test is used to test the null hypothesis: HIRHAM5 simulations are indistinguishable from the CORDEX ensemble of an-

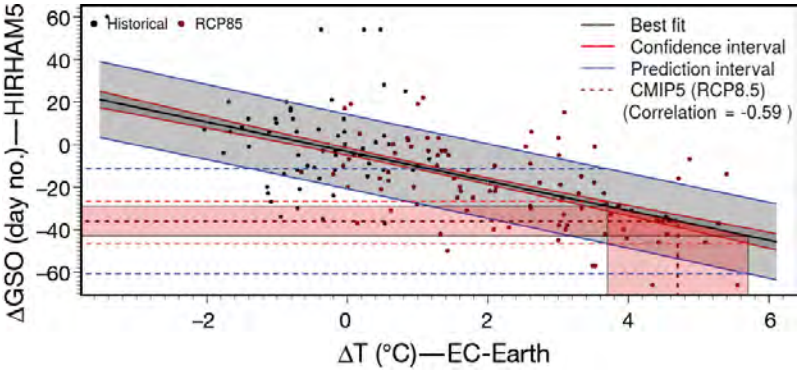

Fig. 4. Changes in growing season onset (GSO) for the Sognefjord grid point (1986–2005). Each dot represents change in GSO given as annual values from HIRHAM5 as a function of annual mean temperature (T) change from EC-Earth for a historical run (1951–2005, black dots) and an RCP8.5-scenario run (2006–2100, red dots). The black line is the best fitted regression line, and its confidence interval (95% confidence level) is indicated with red lines. The blue lines are the prediction intervals indicating the year-to-year variability of the growing season length for a given temperature change. CMIP5 temperature change in the period 2081–2100 for the RCP8.5 scenario is shown as the vertical dashed red line, and the red shaded area indicates likely spread of the 39 CMIP5 models. Horizontal dashed lines point to the level of projected change in GSO for CMIP5 mean temperature change and corresponding likely spread (in dark and light red, respectively), and that combined with the likely range of year-to-year GSO variability (in blue)

3.3. Assumption III

The relationship between climate indices from HIRHAM5 and annual mean temperature from EC-Earth holds for both Sognefjord and Narsaq. Fig. 9 shows a statistically significant correlation between climate index changes and changes in annual mean temperature for both the Sognefjord grid point (r = 0.78) and the Narsaq grid point (r = 0.75). The slopes of the 2 regression lines are different though, 17 d °C^{-1} for Sognefjord and 11 d °C^{-1} for Narsaq.

3.4. Assumption IV

The 17th and 83rd percentiles (representing the likely range) of CORDEX and CMIP5 projected annual mean temperature are compared by subtracting the respective percentiles based on CORDEX from those based on CMIP5 and displayed in Fig. 10. For blue (red) areas, the CMIP5 percentiles are lower (larger) than corresponding CORDEX percentiles. The GCMs are remapped to the CORDEX grid with nearest neighbour weights.

nual mean temperatures. The resulting test confirms that HIRHAM5 is indistinguishable from the merged EURO-CORDEX evaluation experiments and cannot be rejected at the 95% confidence level. The box and whiskers plots (see Fig. 12) support this finding.

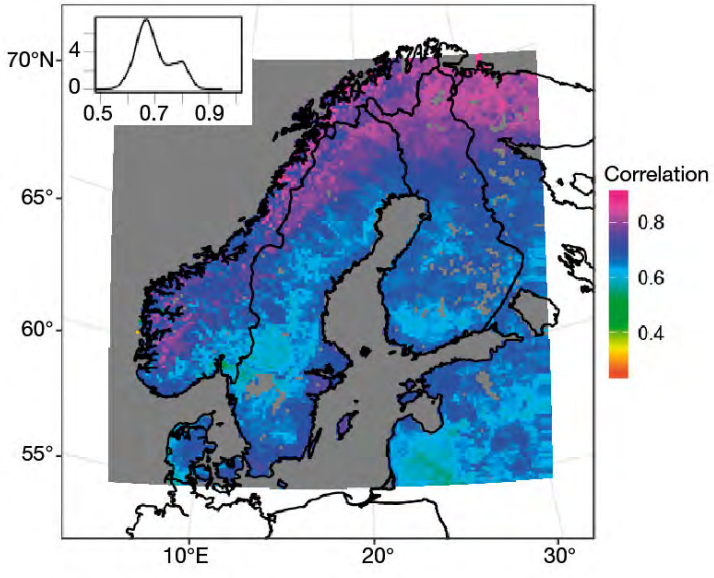

Fig. 5. Correlation coefficients between growing season length from HIRHAM5 and annual mean temperature from EC-Earth for Scandinavia for the RCP8.5 scenario from 2006 to 2100. Inset: density of correlation coefficients

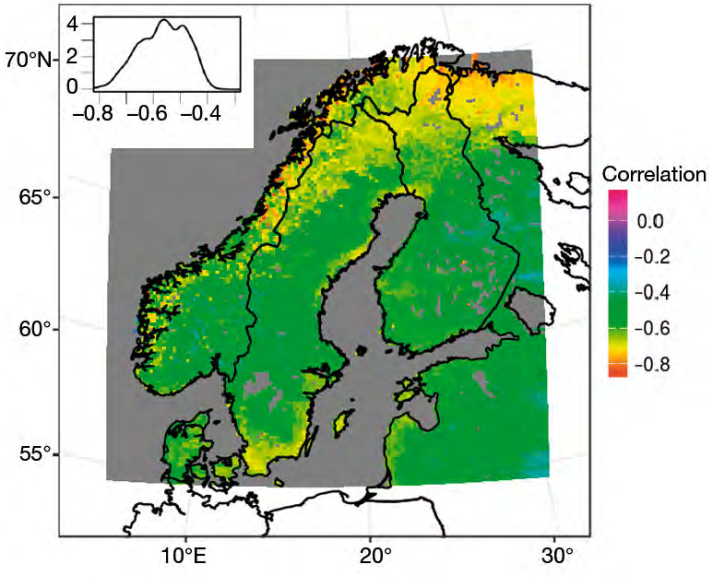

Fig. 6. Correlation between growing season onset from HIRHAM5 and annual mean temperature from EC-Earth for Scandinavia for the RCP8.5 scenario from 2006 to 2100. Inset: density of correlation coefficients

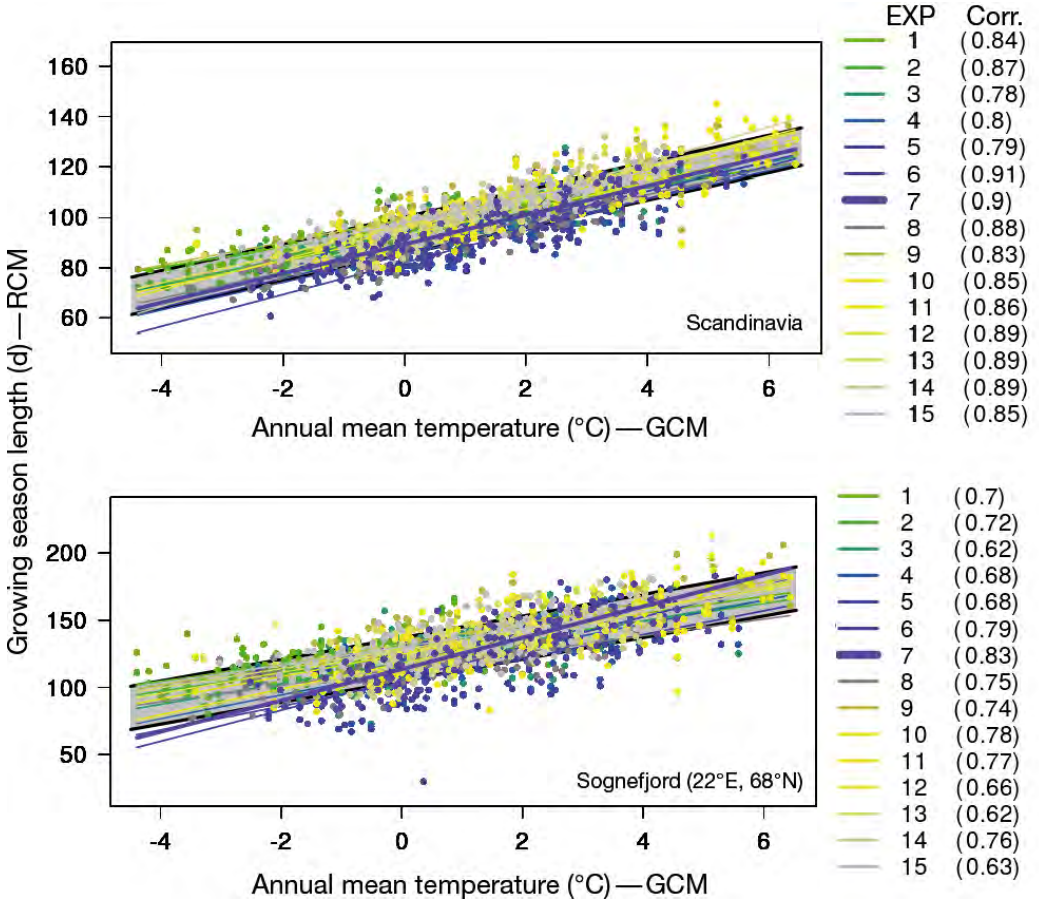

Fig. 7. Growing season length calculated from 15 EURO-CORDEX simulations for Scandinavia (top) and for Sognefjord (bottom) correlated with annual mean temperature from the respective forcing global climate models for the RCP8.5 scenario experiments from 2006 to 2100. The grey shaded area represents the likely prediction interval of the entire index–temperature population. EXP numbers (right) refer to downscaling experiments listed in Table 1. Parentheses: correlation coefficient

4. DISCUSSION

4.1. Assumption I

In Fig. 3 (growing season length), we find a correlation coefficient (r = 0.78) on the local scale enabling uncertainty to be quantified at this high resolution. For Sognefjord, we meet the high correlation requirement anticipated in Assumption I. For growing season onset in Fig. 4, the correlation with annual mean temperature is lower, but still provides valid and useful information for assessing the uncertainties associated with the projected climate index. For the 2 indices shown here, the uncertainty is assessable using the established relationship and the converted CMIP5 temperature changes indicated as vertical shaded areas in Figs. 3 & 4.

Not all indices show the same convincingly high temperature dependence as for growing season length and onset, but lower correlation merely results in wider confidence ranges and prediction intervals on the index–temperature correlation graph. This means that the uncertainty for a given index depends on the correlation coefficient, where a strong correlation narrows the index uncertainty and a weak correlation expands it. We suggest interpreting this as a realistic feature describing the actual index uncertainty for a future climate projection.

This should be distinguished from the climate index sensitivity of annual mean temperature change, which is indicated by the slope of the regression lines in Figs. 3 & 4. Strong dependency (steep slope) increases the likely index uncertainty range, whereas weak temperature dependency (shallow slope) decreases the index uncertainty for a constant correlation coefficient.

From Fig. 2, it is clear that EC-Earth shows a significantly larger temperature increase than other CMIP5 members. Almost all annual mean temperatures from EC-Earth 2081–2100 (based on RCP4.5 and RCP8.5, in total 40 points on the plot) exceed the general CMIP5 spread. An important factor here is

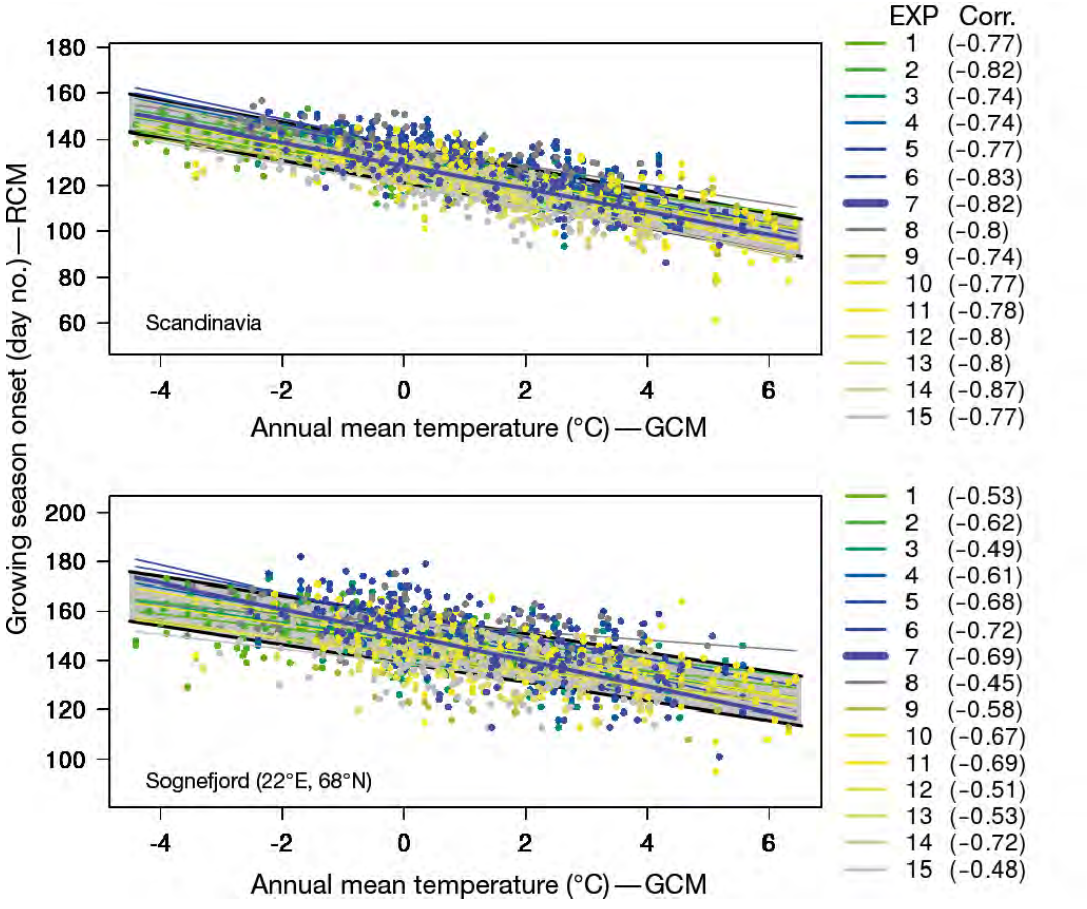

Fig. 8. As Fig. 7 but for growing season onset

that EC-Earth simulates the 21st century about 2°C colder in the Arctic, related to an excessive Arctic sea ice cover, and therefore also a larger temperature increase in the Arctic area when sea ice starts to disappear (Koenigk et al. 2013).

However, this will not affect the correlation and shape of the regression line because the index is derived from HIRHAM5 in matching warmer conditions. On the other hand, this method actually avoids overestimating the expected change in length of the growing season. So this adds to the benefits of using the proposed uncertainty quantification method.

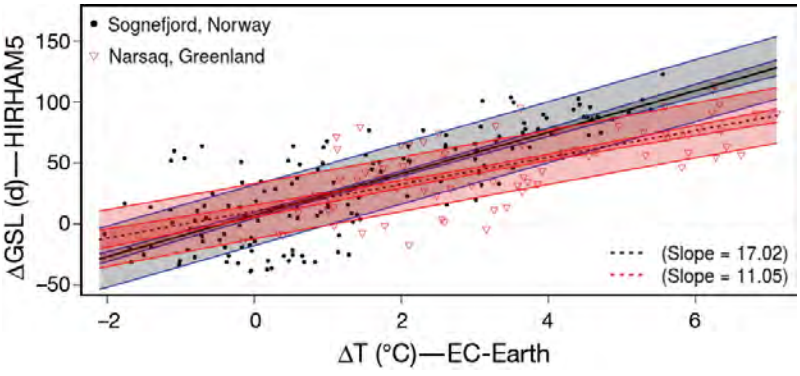

Fig. 9. Growing season length (GSL) from HIRHAM5 as a function of annual mean temperature (T) from EC-Earth for Sognefjord (black) and Narsaq (red). The black lines represent the best fit regression lines for each data set. Light and dark shaded areas are the likely prediction and confidence intervals, respectively

4.2. Assumption II

RCM-conducted climate indices exhibit statistically significant and good correlations with their forcing GCMs for the entire CORDEX ensemble. The correlation for each CORDEX member is evidently larger when considering all of Scandinavia than for a selected location.

In Figs. 7 & 8, all regression models show the same tendency. By merging all data points for the 15 RCMs, the majority of the individual regression lines fall within the 66% prediction range (the grey shaded areas in Figs. 7

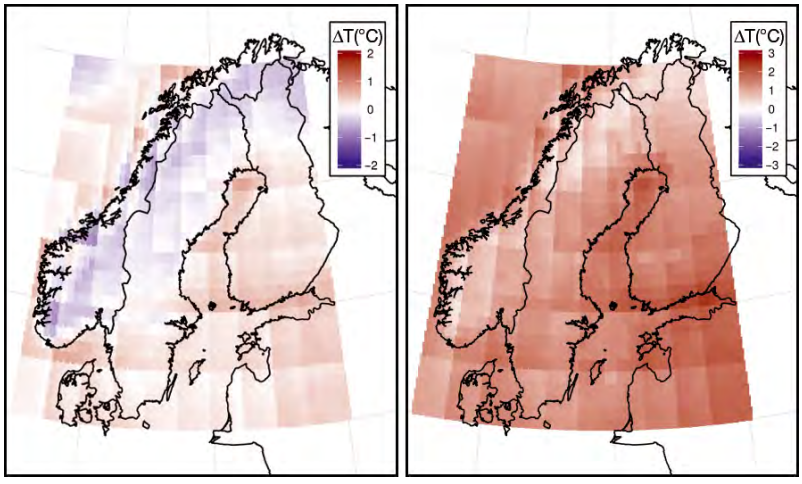

Fig. 10. Differences in low-end projections (17th percentiles, left) and high-end projections (83rd percentiles, right) between CMIP5 and CORDEX projected annual mean temperature (T) changes for the RCP8.5 scenario from 1986–2005 to 2081–2100

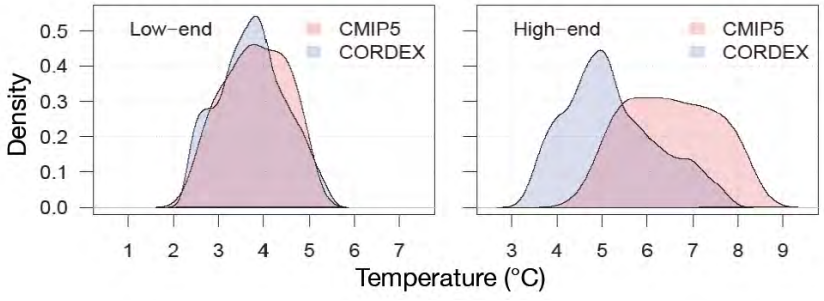

Fig. 11. Density plot of CMIP5 and CORDEX temperature changes from 1986–2005 to 2081–2100 for all Scandinavian grid points. Left shows low end of likely range (17th percentile) and right shows high end of likely range (83rd percentile)

& 8) for Scandinavia in general but also for the specific Sognefjord grid point. However, some of the regressions escape the prediction interval for low- and high-end GCM temperatures, especially for temperatures outside the projected range for the given GCM.

The analysis and quantification of climate index uncertainties should be done for limited areas or even at grid point level to benefit optimally from the high-resolution climate change simulation. By considering areas that are too large, the added information value from the GCM downscaling will be lost (Rockel 2015).

HIRHAM5 is indistinguishable from the CORDEX ensemble, where according to Jacob et al. (2014), projected temperature changes within CORDEX are significant according to a *t*-test or Mann-Whitney-Wilcoxon test, and also robust, with >66% of the models agreeing on the direction of projected temperature changes.

4.3. Assumption III

Fig. 9 together with Figs. 5 & 6 illustrate that the climate index temperature relation calculated from HIRHAM5 and EC-Earth is statistically significant for Narsaq in Greenland and Sognefjord in Norway and for the entire Scandinavian domain. Figs. 7 & 8 show that the latter holds for the entire CORDEX ensemble, and this gives us confidence in assuming the same relationship holds for Greenland.

Fig. 9 shows that the correlation is kept for the 2 locations; however, the different slopes indicate different temperature sensitivities for Narsaq and Sognefjord. This emphasises the importance of analysing every grid point of interest separately, to ensure reliable estimates of climate index changes and associated uncertainty estimates.

4.4. Assumption IV

The likely range of CORDEX temperature changes is to a large extent captured by CMIP5 projected temperature changes. In Figs. 10 & 11, the 83rd percentile temperature projections from CMIP5 are clearly larger than those from CORDEX, which is required to ensure that CMIP5 embraces the high end of the CORDEX likely range. Likewise, the difference between the CMIP5 and CORDEX low-end projections should be negative or close to zero to ensure that CMIP5 also captures the low end from CORDEX. This is only true for approximately half the land points in Scandinavia; however, positive areas in Fig. 10 do not exceed 0.5°C and are confined to areas with little topography (Greenland in general has a complex topography similar to the Norwegian west coast). The relatively small difference is also illustrated in the density plots in Fig. 11. The fact that CMIP5 consists of 39 GCMs whereas only 5 GCMs are downscaled within CORDEX is probably the main reason why CMIP5 to a large extent embraces the variance of CORDEX. By selecting 5 of 39 GCMs, the 83rd percentile will probably decrease and the 17th percentile increase because of the model selec-

tion itself. Applying the CMIP5 ensemble mean and likely range for projected temperature changes as an estimate of expected temperature changes will almost cover the expected likely range of CORDEX temperature changes. The role of boundary conditions from the GCM is generally greater than the role of the RCM, in particular for temperature (Déqué et al. 2007).

This argument is supported by the box and whisker plots in Fig. 12 that show the upper and lower quantiles and upper and lower bounds of RCM projected annual mean temperatures divided between 5 different GCMs for Scandinavia and Sognefjord. The GCMs introduce the first levels of uncertainty propagation from large- to small-scale temperature projections. In Fig. 12, the individual GCMs show different characteristics in terms of median values and 50% likely ranges. The differences or uncertainties are mainly caused by the GCM global energy budget and the climate sensitivity, which again is influenced by factors such as atmospheric stability and cloud feedback mechanisms (Lenderink et al. 2007, Kjellström et al. 2013). The next level of uncertainty is introduced by the RCMs in terms of small-scale physical processes such as small-scale convection and fine-scale interactions involving orography and land–sea transitions. The RCMs in Fig. 12 also tend to show only limited divergence from their driving GCM, indicating that the GCMs to a large extent control the temperature changes. This was in fact a main motivation for the design of the method proposed in the present study.

4.5. Uncertainty assessment technique in general

In addition to temperature-dependent climate indices, we also looked into precipitation-derived climate indices (not shown). Correlations were tested against GCM temperature and GCM precipitation. This demonstrated some limitations of this approach as an uncertainty quantification method. The precipitation-derived indices do not show statistically significant correlation with temperature projections. However, some precipitation-dependent indices do correlate with annual mean precipitation, but the inter-model likely range of CMIP5 precipitation projections is relatively large. Hence, in practice, converting that into index uncertainty appears unusable or at best serves to underline the relatively large uncertainty that always appears to be associated with regional precipitation projections. On regional and very local scales, we do not necessarily expect the precipitation to scale with the increasing global annual mean temperature predicted by the GCMs. Precipitation sensitivity to global warming can even be smaller in an emission scenario with larger greenhouse gas concentrations and aerosol emissions (Shiogama et al. 2010). Hence, the amount of precipitation is dependent on parameters other than temperature.

That being said, when changes in a given climate index are not correlated with the general temperature changes, the changes may not be significant at all, and may be mostly an artefact of natural variability. So, one might argue that with our method, all

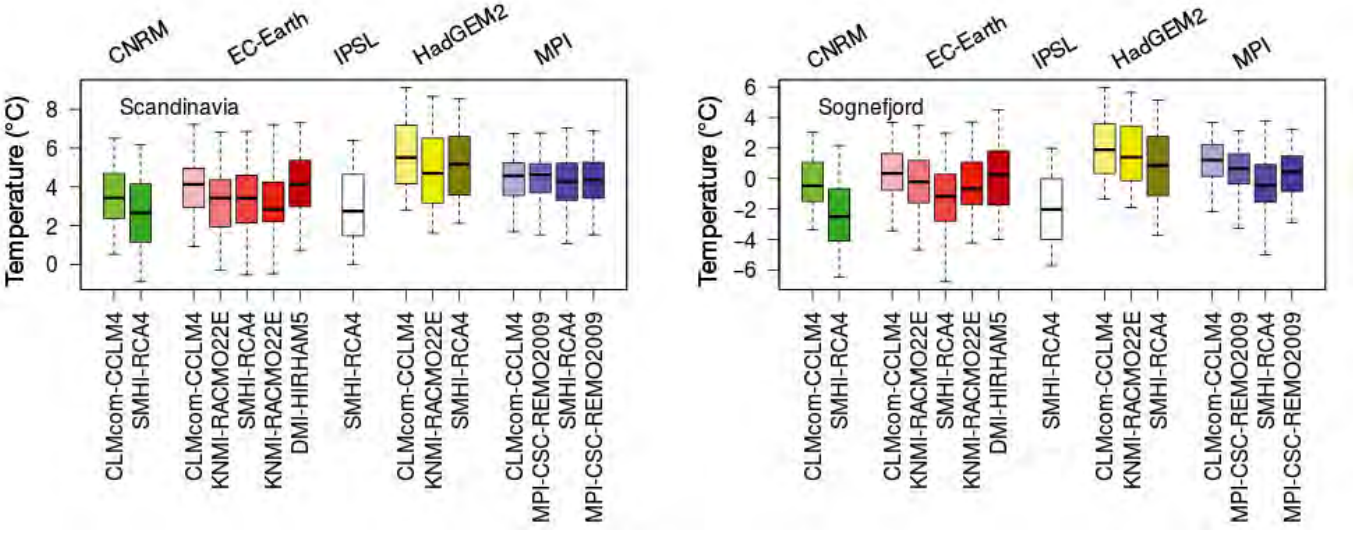

Fig. 12. Annual mean temperature for 2006–2100 for the RCP8.5 scenario simulated with the RCMs in CORDEX (see Table 1), for Scandinavia (left) and Sognefjord (right). The driving models are grouped by colour (green: CNRM-CERFACS-CNRM-CM5; red: ICHEC-EC-EARTH; white: IPSL-ENERIS; yellow: MOHC-HadGEM2-ES; blue: MPI-M- MPI-ESM-LR). Boxplots — midline: median; box: interquartile range; whiskers: lower and upper extreme values

changes in relevant climate indices are assessable, but the resulting change may be seen as being not statistically significant, and exhibiting a large year-to-year variation. The change in consecutive dry days (see Fig. 14) is an example of that.

The reports mentioned in the 'Introduction' (Christensen et al. 2015) present changes in more than 60 different indices for 2031–2050 and 2081–2100 for RCP4.5 and RCP8.5 relative to the historical period 1991–2010 based on dynamical downscaling with HIRHAM5 to 5.5 km. Corresponding uncertainties have been quantified applying a variant of the method presented here. However, the indices are derived from daily temperature, precipitation, humidity and wind projections, and do not all correlate well (if at all) with annual mean temperature changes in the driving GCM. Practically all climate indices which are not derived from temperature do not show the statistically significant correlation to annual mean temperature required to take advantage of this uncertainty assessment method.

In the attempt to develop and optimise the uncertainty assessment method, we had to choose between HIRHAM5-derived climate indices and 1 of 3 possible index–temperature correlations: (1) HIRHAM5 simulated annual mean temperature changes, (2) CMIP5 annual mean temperature changes, or (3) the forcing GCM, EC-Earth simulated annual mean temperature.

The first solution clearly results in the highest correlation coefficients, but the link to CMIP5 mean values and uncertainty information disappears. For the indices shown in Fig. 13, it would be unknown if the relatively high increase in annual mean temperature compared to CMIP5 originated from the GCM or from the RCM.

The second suggestion results in correlation coefficients that are too low, caused by the altered year-to-year variability as well as differences in topography and land–sea masks due to the jump in resolution between the driving model and the regional model.

The third option offering the highest possible correlation coefficient keeping the link to CMIP5

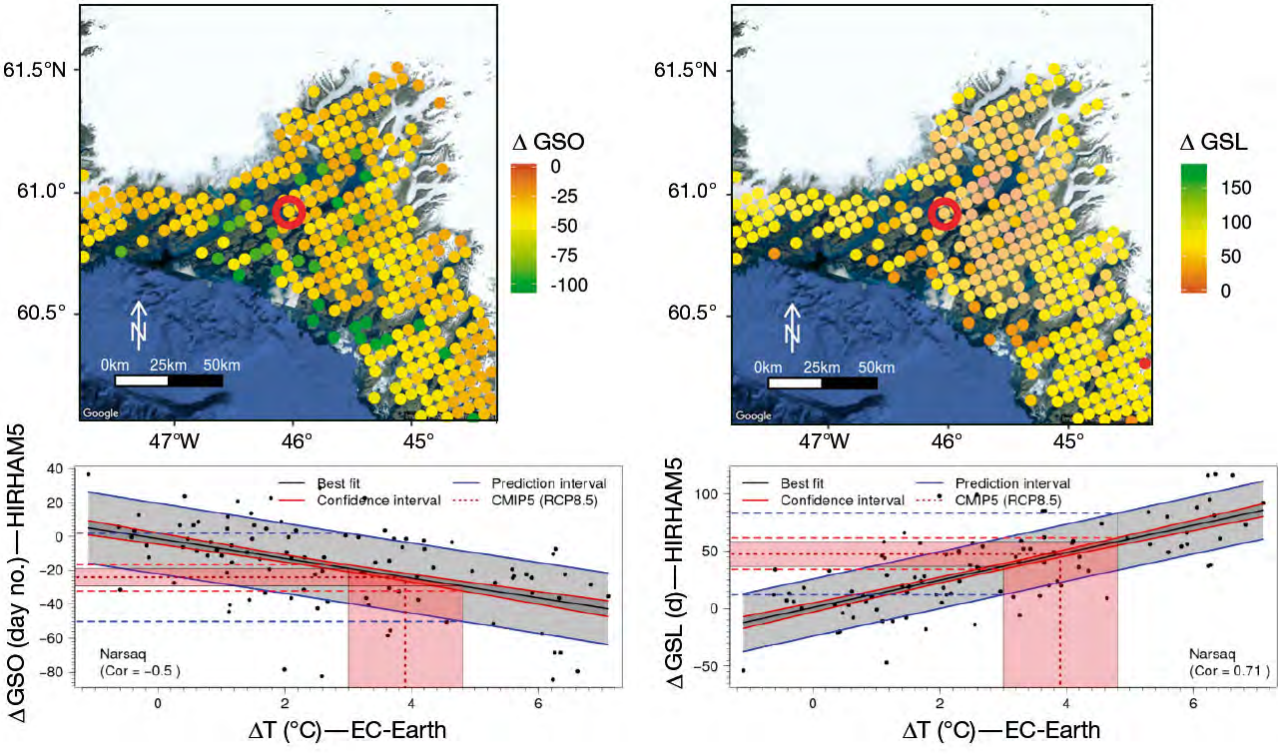

Fig. 13. Projected changes in growing season onset (GSO, left) and growing season length (GSL, right). The maps show changes for 2081–2100 relative to 1991–2010 for RCP8.5 for the area around Narsaq (red circle on the maps) in southern Greenland. The graphs show changes in annual indices from HIRHAM5 as a function of annual mean temperature (T) changes from EC-Earth. Each point represents one year within 2031–2050 and 2081–2100 relative to 1991–2010 for RCP4.5 and RCP8.5. CMIP5 ensemble mean (and likely ranges) temperature changes from 1991–2010 to 2081–2100 are displayed as vertical red dashed lines and red shaded areas. The black, red and blue lines are the best fitted linear regression model, its confidence interval and its prediction interval, respectively. The blue dashed lines represent projected prediction intervals. Cor: correlation coefficient

through the forcing GCM was therefore preferred. GCM–RCM comparison analysis (not shown) shows significant differences between HIRHAM5 and EC-Earth for Scandinavia both for absolute and for delta change values. Therefore, the link to the global models is required to ensure the full likely range for projected climate index changes.

Another way to improve the uncertainty assessment technique could be by correlating growing season onset from HIRHAM5 with mean spring temperature from the driving model EC-Earth, and using the available spring temperature variances from CMIP5. This will, through higher correlation coefficients, provide projections that are less uncertain. Likewise, growing season length could be correlated with relevant months from the GCM. However, this is beyond the scope of the present study. The main reason for scaling with global annual mean temperature is that it scales better with global annual mean temperature than does the seasonal mean, which also allows for better scale results between models (e.g. see Lynch et al. 2017, Osborn et al. 2018).

5. APPLICATION TO GREENLAND

The uncertainty assessment method is here applied for agriculture-relevant climate indices in southern Greenland around Narsaq (see inset map in Fig. 1). Here we present projected changes in the climate indices growing season length and onset, frost days and consecutive dry days, and quantify the corresponding uncertainties using the propounded technique.

If we follow the RPC8.5 scenario, an extension of growing season in Narsaq of 48 d towards the end of this century compared to 1991–2010 is expected. The corresponding uncertainty displayed in Fig. 13 is assessed to be ±15 d (see Table 2). The uncertainty estimate takes into account the likely range of projected CMIP5 simulations (horizontal red dashed lines in Fig. 13). The year-to-year variability from HIRHAM5 combined with the CMIP5 likely range is shown with the horizontal blue dashed lines. The likely range of the projected change in growing season length in Narsaq, including the year-to-year variability, is with this method projected to be 52 ± 36 d. This implies that even for years with a short growing season, by the end of this century, they will be longer than today's average length.

Table 2. Projected changes in climate indices relevant for agriculture in Narsaq and the surrounding area

Index (d)	Index change	CMIP5-related uncertainty	Total uncertainty (CMIP5 + year to year)
Length of growing season	52	15	36
Onset of growing season	−25	7	15
Frost days	−32	9	19
Consecutive dry days	−1	2	10

The growing season is with HIRHAM5 expected to start almost 1 mo earlier by the end of the 21st century compared to 1990–2010 (−25 ± 7 d), including the likely spread of CMIP5, and −25 ± 15 d also including the year-to-year variability (see Fig. 13). Equivalently, the amount of frost days displayed in Fig. 14 is expected to decrease by 32 ± 9 d including the likely CMIP5 spread and 32 ± 19 d also including the year-to-year variability. For consecutive dry days, the HIRHAM5 simulation identifies no statistically significant changes towards year 2100 (−1 ± 2 d and ±10 d) compared to 1991–2010 (see Fig. 14). This index does not correlate with annual mean temperature ($r = -0.04$); therefore, the uncertainty of ±10 d exclusively represents the year-to-year variability, which is not expected to change during this century.

As described in Section 1, the method prepares the ground for different index uncertainty interpretations. One useful application here is the estimated change in the length of the growing season, including the likely range based on the CMIP5 estimates of the projected index. The year-to-year variability can be compared to present-day local conditions in order to acertain if the result is consistent with observations. Projected changes for the 4 mentioned indices are listed in Table 2.

The projected index change and uncertainty can also be assessed for a given temperature increase. A 2°C warming for the area around Narsaq will expand the growing season by approximately 26 ± 24 d (Fig. 13, bottom right) including the likely prediction range. In the same way, changes in onset of growing season and number of frost nights are projected and evaluated.

Projected changes in growing season length and frost days towards the end of the 21st century in southern Greenland will make it possible to grow new crops with a short growing season, such as barley. The climate change also provides a longer growing season for potatoes and vegetables; however, the dominant crop in Greenland will probably still be pasture by the end of this century (Lehmann et al. 2017).

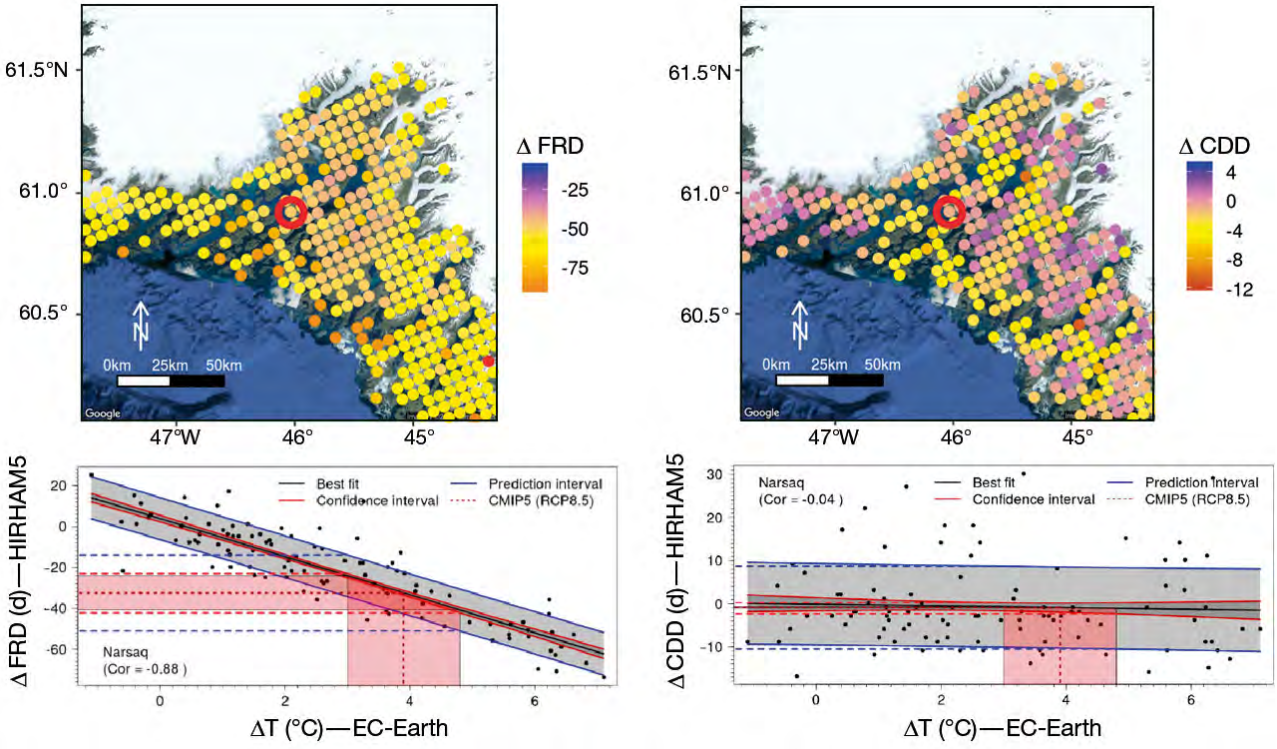

Fig. 14. Projected changes in number of annual frost days (FRD; left) and longest period with consecutive dry days (CDD; right) for 2081–2100 relative to 1991–2010 for the RCP8.5 scenario in Narsaq (red circle on the maps) and the surroundings. The graphs (bottom) show the relationship between the climate index from HIRHAM5 and annual mean temperature from EC-Earth for the ice free land point nearest Nasaq. Each point represents one year within the time slices 1991–2010, 2031–2050 and 2081–2100 for the scenarios RCP4.5 and RCP8.5. Black, red and blue lines: best fitted regression line, its confidence interval and prediction intervals, respectively. The CMIP5 projected temperature change for the RCP8.5 scenario in 2081–2100, including its likely spread, is indicated with vertical short dashed red lines and the red shaded area. Horizontal dashed lines: changes in projected climate index and corresponding likely ranges. The likely spread of CMIP5 mean temperature converted into likely spread of projected index values (red dashed lines) and to likely spread of year-to-year variability (horizontal blue dashed lines)

6. CONCLUSIONS

We have analysed a series of GCMs and RCMs and shown that temperature-dependent climate indices correlate well with temperature. In particular, correlations between HIRHAM5-based climate indices and EC-Earth annual mean temperatures can be seen as representative of the full information deducible from the EURO-CORDEX ensemble. We also find that the likely range of projected CMIP5 temperatures is larger than that of projected CORDEX temperatures for the upper end of the likely range, and comparable to CORDEX temperatures for the low end. The spread of projected temperature changes from the CMIP5 ensemble will therefore most likely cover the individual RCM projections for a given location.

Precipitation-related indices at the regional level like consecutive dry days are in general not statistically significantly correlated with annual mean temperatures, but do correlate with annual mean precipitation. Accordingly, the likely range of CMIP5 projected annual mean precipitation is very large compared to projected annual mean temperature. Hence, the uncertainty range will exceed the climate change signal. But this may well depict the state of the art, as model variability in precipitation projection is often very large at the grid point level (IPCC 2013). For the index consecutive dry days, which does not correlate with annual mean temperature, only the likely year-to-year variability can be quantified by use of this uncertainty assessment method.

On the other hand, we find that the spread of CMIP5 annual mean temperature change to a large degree is convertible to the HIRHAM5 projected climate index uncertainty for changes in growing season length and onset and for frost days. The uncertainty assessment method thus utilises uncertainty quantification of projected changes in climate indices from a single RCM for a geographical domain like Greenland, where only one or a few RCMs are available.

Acknowledgements. We acknowledge the World Climate Research Programme's Working Group on Regional Climate and the Working Group on Coupled Modelling, former coordinating body of CORDEX and responsible panel for CMIP5. We also thank the climate modelling groups (listed in Table 1 of this paper) for producing and making available their model output. The research leading to these results has received funding from the European Research Council under the European Union's Seventh Framework Programme (FP7/2007-2013)/ERC Grant Agreement no. 610055 as part of the ice2ice project and from the Danish Cooperation for Environment in the Arctic (DANCEA) under the Danish Energy Agency.

LITERATURE CITED

Akperov M, Rinke A, Mokhov II, Matthes H and others (2018) Cyclone activity in the Arctic from an ensemble of regional climate models (Arctic CORDEX). J Geophys Res Atmos 123:2537–2554

AMAP (Arctic Monitoring and Assessment Programme) (2017) Snow, water, ice and permafrost in the Arctic (SWIPA). AMAP, Oslo

Boberg F, Langen PL, Mottram RH, Christensen JH, Olesen M (2017) 21st-century climate change around Kangerlussuaq, west Greenland: from the ice sheet to the shores of Davis Strait. Arct Antarct Alp Res 50:S100006

Christensen JH, Christensen OB (2003) Severe summertime flooding in Europe. Nature 421:805–806

Christensen JH, Hewitson B, Busuioc A, Chen A and others (2007) Regional climate projections, Chap. 11. In: Solomon S, Qin D, Manning M, Chen Z and others (eds) Climate change 2007: the physical science basis. Contribution of Working Group I to the Fourth Assessment Report of the Intergovernmental Panel on Climate Change. Cambridge University Press, Cambridge, p 847–940

Christensen JH, Boberg F, Christensen OB, Lucas-Picher P (2008) On the need for bias correction of regional climate change projections of temperature and precipitation. Geophys Res Lett 35:L20709

Christensen JH, Olesen M, Boberg F, Stendel M, Koldtoft I (2015) Fremtidige klimaforandringer I Grønland: Qeqqata kommune. Tech Rep 15-04, Danish Meteorological Institute, Copenhagen

Christensen OB, Christensen JH, Machenhauer B, Botzet M (1998) Very high-resolution regional climate simulations over Scandinavia — present climate. J Clim 11:3204–3229

Christensen OB, Drews M, Christensen JH, Dethloff K, Ketelsen K, Hebestadt I, Rinke A (2006) The HIRHAM regional climate model. Version 5 (beta). Tech Rep 06-17, Danish Meteorological Institute, Copenhagen

Collins WJ, Bellouin N, Doutriaux-Boucher M, Gedney N and others (2011) Development and evaluation of an Earth-system model — HadGEM2. Geosci Model Dev 4: 1051–1075

Dee DP, Uppala SM, Simmons AJ, Berrisford P and others (2011) The ERA-Interim reanalysis: configuration and performance of the data assimilation system. QJR Meteorol Soc 137:553–597

Déqué M (2007) Frequency of precipitation and temperature extremes over France in an anthropogenic scenario: model results and statistical correction according to observed values. Global Planet Change 57:16–26

Déqué M, Rowell DP, Lüthi D, Giorgi F and others (2007) An intercomparison of regional climate simulations for Europe: assessing uncertainties in model projections. Clim Change 81:53–70

DFFL (Departementet for Fiskeri, Fangst og Landbrug) (2007) Visioner for det Grønlandske landbrug. Departementet for Fiskeri, Fangst og Landbrug, Nuuk

Di Luca A, de Elía R, Laprise R (2015) Challenges in the quest for added value of regional climate dynamical downscaling. Curr Clim Change Rep 1:10–21

Dufresne JL, Foujols MA, Denvil S, Caubel A and others (2013) Climate change projections using the IPSL-CM5 Earth system model: from CMIP3 to CMIP5. Clim Dyn 40:2123–2165

Feser F, Rockel B, von Storch H, Winterfeldt J, Zahn M (2011) Regional climate models add value to global model data: a review and selected examples. Bull Am Meteorol Soc 92:1181–1192

Giorgetta MA, Jungclaus J, Reick CH, Legutke S and others (2013) Climate and carbon cycle changes from 1850 to 2100 in MPI-ESM simulations for the Coupled Model Intercomparison Project Phase 5. J Adv Model Earth Syst 5:572–597

Giorgi F, Mearns LO (2003) Probability of regional climate change based on the reliability ensemble averaging (REA) method. Geophys Res Lett 30:1629

Giorgi F, Jones C, Asrar GR (2009) Addressing climate information needs at the regional level: the CORDEX framework. WMO Bull 58:175–183

Giorgi F, Torma C, Coppola E, Ban N, Schär C, Somot S (2016) Enhanced summer convective rainfall at alpine high elevations in response to climate warming. Nat Geosci 9:584–589

Giot O, Termonia P, Degrauwe D, De Troch R and others (2016) Validation of the ALARO-0 model within the EURO-CORDEX framework. Geosci Model Dev 9: 1143–1152

Hazeleger W, Wang X, Severijns C, Ştefănescu S and others (2012) EC-Earth V2.2: description and validation of a new seamless earth system prediction model. Clim Dyn 39:2611–2629

IPCC (2013) Stocker TF, Qin D, Plattner GK, Tignor M and others (eds) Climate change 2013: the physical science basis. Working Group I Contribution to the Fifth Assessment Report of the Intergovernmental Panel on Climate Change. Cambridge University Press, Cambridge

Jacob D, Elizalde A, Haensler A, Hagemann S and others (2012) Assessing the transferability of the regional climate model REMO to different COordinated Regional Climate Downscaling EXperiment (CORDEX) regions. Atmosphere 3:181–199

Jacob D, Petersen J, Eggert B, Alias A and others (2014) EURO-CORDEX: new high-resolution climate change projections for European impact research. Reg Environ Change 14:563–578

Kjellström E, Thejll P, Rummukainen M, Christensen JH, Boberg F, Christensen OB, Maule CF (2013) Emerging regional climate change signals for Europe under varying large-scale circulation conditions. Clim Res 56:103–119

Koenigk T, Brodeau L, Graversen RG, Karlsson J and others (2013) Arctic climate change in 21st century CMIP5 simulations with EC-Earth. Clim Dyn 40:2719–2743

Kupiainen M, Samuelsson P, Jones C, Jansson C and others (2011) Rossby Centre regional atmospheric model, RCA4. Rossby Centre Newsletter, Swedish Meteorological and Hydrological Institute, Norrköping. www.smhi.se/en/

research/research-departments/climate-research-rossby-centre2-552/rossby-centre-regional-atmospheric-model-rca4-1.16562

Langen PL, Mottram RH, Christensen JH, Boberg F and others (2015) Quantifying energy and mass fluxes controlling Godthåbsfjord freshwater input in a 5-km simulation (1991–2012). J Clim 28:3694–3713

Lehmann JO, Sharif B, Kjeldsen C (2017) Mulighed for klimatilpasning i landbrugserhvervet — status og handlemuligheder. http://naalakkersuisut.gl/~/media/Nanoq/Files/Attached%20Files/Klima/Klimatilpasning%20Landbrug/Klimatilpasningsredeg%C3%B8relse%20-%20dansk%20-%2020170519.pdf

Lenderink G, van Ulden A, van den Hurk B, Keller F (2007) A study on combining global and regional climate model results for generating climate scenarios of temperature and precipitation for the Netherlands. Clim Dyn 29: 157–176

Lucas-Picher P, Wulff-Nielsen M, Christensen JH, Aðalgeirsdóttir G, Mottram R, Simonsen SB (2012) Very high resolution regional climate model simulations over Greenland: identifying added value. J Geophys Res 117: D02108

Lynch C, Hartin C, Bond-Lamberty B, Kravitz B (2017) An open-access CMIP5 pattern library for temperature and precipitation: description and methodology. Earth Syst Sci Data 9:281–292

Maraun D (2016) Bias correcting climate change simulations — a critical review. Curr Clim Change Rep 2:211–220

Mastrandrea MD, Mach KJ, Plattner GK, Edenhofer O and others (2011) The IPCC AR5 guidance note on consistent treatment of uncertainties: a common approach across the working groups. Clim Change 108:675–691

Mayer S, Maule CF, Sobolowski S, Christensen OB and others (2015) Identifying added value in high-resolution climate simulations over Scandinavia. Tellus A Dyn Meteorol Oceanogr 67:24941

McSweeney CF, Jones RG, Lee RW, Rowell DP (2015) Selecting CMIP5 GCMs for downscaling over multiple regions. Clim Dyn 44:3237–3260

Mitchell JFB, Johns TC, Eagles M, Ingram WJ, Davis RA (1999) Towards the construction of climate change scenarios. Clim Change 41:547–581

Osborn TJ, Wallace CJ, Lowe JA, Bernie D (2018) Performance of pattern-scaled climate projections under high-end warming. I. Surface air temperature over land. J Clim 31:5667–5680

Pan Z, Christensen JH, Arritt RW, Gutowski WJ, Takle ES, Otieno F (2001) Evaluation of uncertainties in regional climate change simulations. J Geophys Res Atmos 106: 17735–17751

Persson G, Bärring L, Kjellström E, Strandberg G, Rummukainen M (2007) Climate indices for vulnerability assessments (No. 111). Swedish Meteorological and Hydrological Institute, Norrköping

Pithan F, Mauritsen T (2014) Arctic amplification dominated by temperature feedbacks in contemporary climate models. Nat Geosci 7:181–184

Rockel B (2015) The regional downscaling approach: a brief history and recent advances. Curr Clim Change Rep 1: 22–29

Rockel B, Will A, Hense A (2008) The regional climate model COSMO-CLM (CCLM). Meteorol Z (Berl) 347–348

Rosen J (2016) Cold truths at the top of the world. Nature 532:296–299

Rummukainen M (2016) Added value in regional climate modeling. Wiley Interdiscip Rev Clim Change 7:145–159

Samuelsson P, Jones CG, Will'En U, Ullerstig A and others (2011) The Rossby Centre regional climate model RCA3: model description and performance. Tellus A Dyn Meteorol Oceanogr 63:4–23

Shiogama H, Emori S, Takahashi K, Nagashima T, Ogura T, Nozawa T, Takemura T (2010) Emission scenario dependency of precipitation on global warming in the MIROC3.2 Model. J Clim 23:2404–2417

Sloth Madsen M, Maule CF, MacKellar N, Olesen JE, Christensen JH (2012) Selection of climate change scenario data for impact modelling. Food Addit Contam Part A 29: 1502–1513

Taylor KE, Stouffer RJ, Meehl GA (2012) An overview of CMIP5 and the experiment design. Bull Am Meteorol Soc 93:485–498

Tebaldi C, Arblaster JM (2014) Pattern scaling: its strengths and limitations, and an update on the latest model simulations. Clim Change 122:459–471

van Meijgaard E, van Ulft LH, Lenderink G, De Roode SR, Wipfler EL, Boers R, van Timmermans RMA (2012) Refinement and application of a regional atmospheric model for climate scenario calculations of western Europe. Rep No. KvR 054/12, Programme Office, Climate changes Spatial Planning, Nieuwegein

Vautard R, Gobiet A, Sobolowski S, Kjellström E and others (2014) The European climate under a 2°C global warming. Environ Res Lett 9:034006

Voldoire A, Sanchez-Gomez E, Mélia DS, Decharme B and others (2013) The CNRM-CM5.1 global climate model: description and basic evaluation. Clim Dyn 40: 2091–2121

Editorial responsibility: Filippo Giorgi, Trieste, Italy

Submitted: March 19, 2018; Accepted: September 3 ,2018
Proofs received from author(s): November 5, 2018

Paper II Olesen, M., Kaas, E., Christensen, J.H., Holme, C., 2019c Time evolution of Greenland surface mass balance by combining high-resolution climate modelling, in situ observations and ice cores. The Cryosphere [in review, 2019]

Time evolution of Greenland surface mass balance by combining high resolution climate modelling, in situ observations and ice cores

Martin Olesen[1], Jens Hesselbjerg Christensen[2,3], Eigil Kaas[2], Christian Holme[2]

[1]Danish Meteorological Institute, Lyngbyvej 100, DK-2100 Copenhagen Ø, Denmark
[2]Niels Bohr Institute, University of Copenhagen, Juliane Maries Vej 30, DK-2100 Copenhagen Ø, Denmark
[3]NORCE Norwegian Research Centre, Bjerknes Centre for Climate Research, Jahnebakken 5, 5007 Bergen, Norway

Correspondence to: Martin Olesen (mol@dmi.dk)

Abstract. Improved climate information is achieved by combining long weather records from the Greenlandic coastal stations and proxy measurements of temperature and solid accumulation from deep ice cores on the Greenland ice sheet and high-resolution simulations with the HIRHAM5 regional climate model. HIRHAM5 provides physically consistent information of temperature, precipitation, snow fall, melt and evaporation at a horizontal resolution of approximately 5.5 km for the period 1980-2014. This simulation is compared with the observed records and proxy data. By relating large scale correlations of various climate variables deduced from HIRHAM5, observed temperature and precipitation in situ records are prolonged 500 years back in time based on proxy data from deep ice cores. Surface mass balance (SMB) for selected drainage basins on the Greenland ice sheet and for the Renland ice cap are reconstructed and show decreasing trend lines towards present. The SMB for the drainage basin nearest Tasiilaq, decreases from + 0.5mm weq/yr for 1898-2014 to -5.4 mm weq/yr in 1980-2014. Correspondingly the SMB for the drainage basin nearest Danmarkshavn decreases from -0.3mm weq/yr for 1950-2014 to -1.1mm weq/yr in 1980-2014 and the SMB of the Renland ice cap decreases from +2.4mm weq/yr for 1950-2007 to -4.7mm weq/yr in 1980-2007. Finally the correlation patterns of temperature and precipitation illustrate the coverage of correlated weather stations and ice core drill site locations across Greenland.

Introduction

Weather and climate information across in situ climate stations, ice cores and a high-resolution Regional Climate Model (RCM) simulation make it possible to close gaps in observational time series and to extend regional climate model simulations beyond the simulation period (Langen et al., 2015; Vinther et al., 2006). Greenland temperature records, and precipitation records in particular, suffer under gaps and various error types (Boas and Wang, 2016) in otherwise valuable observation records. Surface mass balance (SMB) simulated with the regional climate model, HIRHAM5, based on the re-

analysis, ERA-Interim, reaches back to year 1980, where ERA-Interim begins. For outlined areas on the Greenland ice sheet, the HIRHAM5-simulated SMB is extendable, in cases of sufficient knowledge about correlated temperature and precipitation records (Langen et al., 2015). Spatial correlation patterns of e.g. temperature and precipitation for Greenland will in this context link the outlined area to relevant weather records. In this study extension and gap filling are implemented with a technique using temperature and precipitation correlation patterns across Greenland. Maps with spatial correlation patterns are prepared from a high resolution HIRHAM5 simulation (Langen et al., 2017) based on observations through the re-analysis ERA-Interim (Dee et al., 2011). With longer extended SMB time series based on observations long term trends can be compared with more recent trends.

Temperature and precipitation observations in Greenland

Long continuous temperature and precipitation time series are of utmost importance for identifying and understanding past climate variability, and for detecting more recent changes linked to global warming. Information on past and present climate in Greenland is essential for understanding and adapting to present and projected future climate changes in Greenland. But this information is also valuable for aligning ice core proxy time series and for comparisons at longer time scales (Jones and Mann, 2004; Masson-Delmotte et al., 2015; Vinther et al., 2010).

Weather and climate in Greenland have been systematically observed and recorded for more than a century from in situ stations near the towns of Nuuk, Tasiilaq, Upernavik and Ilulissat (Cappelen, 2018). These weather records are displayed together with a selection of the highest quality time series for temperature and precipitation in Figure 2 and Figure 3. On longer time scales, proxy records of temperature and solid accumulation are reconstructed from deep ice cores from the Greenland ice sheet. The proxy data has a temporally resolution at annual to seasonal centuries and millennia back in time (Andersen et al., 2006; Vinther et al., 2010). In addition to observations and proxy records, the weather and climate in Greenland from 1980-2014 is simulated with the RCM, HIRHAM5 (Christensen et al., 2006) based on a re-analysis product of gridded weather records as an evaluation simulation (Lucas-Picher et al., 2012).

Unfortunately gaps and errors do occur in observed temperature and precipitation time series (Figure 2 and Figure 3). This is due to the remote and poorly accessible location of the stations that are exposed to tough weather conditions. Attempts to extend and repair observation time series have among others been made by (Vinther et al., 2006). They used the neighbouring observation stations to close time series gaps to reconstruct intact observation records. In the current research, observation time series are reconstructed from correlation patterns together with observation time series and ice core proxy data, by identifying linked areas with highly correlated characteristics.

Surface mass balance of the Greenland ice sheet

Over the last decades many contributions to understanding and quantifying the surface mass balance (SMB) of the Greenland ice sheet have been published (Calanca et al., 2000; Box et al., 2012; Box, 2013; Mottram et al., 2017; Hanna et al., 2005; Cogley, 2009). Most of them with focus on state of the art maps of SMB, melt and solid accumulation distributions on the ice sheet. Correlation and alignment of individual pointwise ice core proxy time series have been published by e.g. (Vinther et al., 2010).

In this study a further step is taken to prepare spatial correlation maps for melt, summer temperature and solid accumulation for the entire Greenland ice sheet, based on the HIRHAM5 evaluation experiment mentioned above. The maps disclose connected characteristics all across Greenland. Thus, when weather records are available within the area of linked characteristics, it allows for extending simulated SMB time series back in time, if the weather records and simulated SMB are correlated in a statistically significant manner (referred to as "significantly correlated" throughout this paper). The reconstruction procedures assume that temperature and melt time series, as well as precipitation and solid accumulation time series, are statistically correlated, which is invariant over time.

Spatial correlation

Spatial correlation patterns determine valuable weather patterns across Greenland and guides in selecting linked time series at different locations, both for information comparison and data exchange. Correlated time series for selected grid points have already been calculated for a number of weather and climate parameters to link the Greenland ice sheet to large scale weather conditions like e.g. NAO or Greenland blocking index (Ballinger et al., 2017; Box et al., 2012; Hutterli et al., 2005; Ortega et al., 2014).

In addition to repairing and extending time series, spatial correlation patterns can provide an overview of the current climate information coverage from already existing weather stations and ice core drill site locations. If the correlation patterns reflect real in situ observations, they may provide a valuable basis for identifying sparsely covered areas when preparing new drill sites and new weather stations.

The correlation patterns over Greenland are deduced from the dynamical downscaling model, HIRHAM5, and are therefore physically consistent throughout the domain. Correlation patterns give an idea of the dominating scale of weather systems for a given location. Here we prepare and validate high resolution spatial correlation maps for summer temperature and solid accumulation, as well as fill the gaps in observation time series and extend HIRHAM5-simulated SMB time series. Uncertainties associated with time series reconstruction will be assessed by incorporating results from (Olesen et al., 2018).

While previous work (Boberg et al., 2018; Langen et al., 2015) has focused on model performance on the western part of Greenland, our main foci are locations on the east coast: Renland, Danmarkshavn and Tasiilaq, where Renland is a focus catchment in the ice2ice project mentioned in Acknowledgements, and hence of special interest in this work.

Method

Model and data description

The regional climate model HIRHAM5 is described in Christensen et al. (2006) and combines dynamics from the numerical weather prediction model HIRLAM7 (Eerola, K, 2006) and physics from the global climate model ECHAM5 (Roeckner et al., 2003). The subsurface scheme in HIRHAM5 has been extended with an off line component that handles liquid water flow and retention on the Greenland ice sheet (Langen et al., 2017). On the lateral boundaries and over open ocean HIRHAM5 is forced with the European re-analysis dataset ERA-Interim from ECMWF (Dee et al., 2011). The HIRHAM5 experiment used in this study has a horizontal resolution at 0.05 × 0.05 degree horizontal resolution (approximately 5.5 km) and covers 35 years (1980-2014).

Weather observations used in this study consist of monthly temperature and precipitation observation records collected and quality checked by the Danish Meteorological Institute (DMI) (Cappelen, 2018). Only years with full 12-month coverage are included in the correlation calculations. Ice core proxy data for temperature ($\delta^{18}O$) and accumulation rates are deduced from GRIP, NGRIP, DYE-3, NEEM, Camp Century and Renland documented by (Andersen et al., 2006; Vinther et al., 2010). The deep ice core drill site locations are displayed in Figure 1. The temporal resolution of $\delta^{18}O$ provides two annual seasons, identified as winter from November to April and summer from May to October, whereas accumulation rates are on an annual scale.

Preparation and validation of spatial correlation patterns

Spatial correlation are prepared by calculating Pearson's correlation coefficient, *r,* between time series for one selected grid point, *X,* and all land grid points, $Y_{i,j}$, in the domain of 402 × 602 grid points (corresponding to 0.05 × 0.05 degrees).

$$r(X, Y_{i,j}) = \frac{n\sum_{t=1}^{n} x_t y_{i,j,t} - \sum_{t=1}^{n} x_t \sum_{t=1}^{n} x_t y_{i,j,t}}{\sqrt{n\sum_{t=1}^{n} x_t^2 - \left(\sum_{t=1}^{n} x_{,t}\right)^2}\sqrt{n\sum_{t=1}^{n} y_{i,j,t}^2 - \left(\sum_{t=1}^{n} y_{i,j,t}\right)^2}} \qquad (1)$$

Where n is the number of years, x_t is the time series on the selected location and $y_{i,j,t}$ refers to the time series at the grid point *(i, j)*.

For all correlation patterns presented in this study, the distribution of significant correlation coefficients within a 95 % confidence level is colour-indicated from yellow to black on the maps. The critical 95% confidence value is calculated by bootstrapping the 35 time steps (the HIHRAM5 simulation period) with replacement to $r_{crit} = 0.33$.
HIRHAM5 based correlation maps presented in this study are:

- Summer temperatures (mean values of June, July and August) for all DMI-stations and ice core drill site locations
- Solid accumulation for ice core drill site locations
- Annual precipitation for all DMI-stations.

Validation of the correlation maps is primarily based on observations from coastal weather stations, where strong and weak correlation station combinations predicted from the correlation maps (from HIRHAM5 data) are tested between available observed temperature and precipitation time series. In this context, matrices with correlation coefficients for all weather station combinations give a good indication of the HIRHAM5-observation consistency. In addition to that, a corresponding matrix containing degrees of freedom (*df*) associated with each correlation test is presented to help explaining differences between HIRHAM5 and observations. For Pearson's correlation test *df* equals the number of overlapping time steps minus 2. $df = n_{overlap} - 2$ (von Storch and Zwiwes, 1998). Studies on ice core proxy data alignments are also used in this evaluation process (Andersen et al., 2006; Holme et al., 2019; Vinther et al., 2010). Finally, the correlation patterns are evaluated by comparing correlation patterns with dominating weather patterns and topography dependent weather events. For this evaluation the topography field within HIRHAM5 (used as part of the stationary climate input files) is compared with the correlation patterns based on individual weather stations.

SMB reconstruction

Reconstruction of HIRHAM5-simulated SMB time series is based on the general relation between SMB, precipitation (PR), evaporation (E) and runoff (R):

$$SMB = PR - E - R \qquad (2)$$

Precipitation equals the sum of solid accumulation (snowfall) and rain, and runoff is equal to liquid water from melt (M) on the ice sheet plus rain minus refreezing (RF) (Langen et al., 2015). Therefore,

$$SMB = Solid\ acc - E - M + RF \qquad (3)$$

High correlation between refreezing and melt plus rain justifies regression of simulated SMB from solid accumulation minus evaporation and melt. Simulated SMB time series can then be reconstructed from a fitted partial regression function of observed annual precipitation and summer temperature. This assumes that annual solid accumulation is closely linked to annual precipitation over the ice sheet, and that annual melt is linked to summer (JJA) temperature.

$$SMB_{recon} = \alpha PR_{OBS} - \left(\beta_1 T_{OBS} + \beta_2 T_{OBS}^2 + \beta_0\right) \qquad (4)$$

This idea was introduced by Langen et al. (2015) with focus on Nuuk and Nuuk fjord. The assumed link between melt and summer temperatures as well as solid accumulation and annual precipitation will be shown for time series for the drill site locations for solid accumulation-evaporation and annual precipitation and for drainage basins defined by Zwally et al. (2012) for simulated melt and JJA-temperature.

In this study, three reconstruction examples are presented. Here the relationships between melt and temperature, and solid accumulation and precipitation will be calculated as field averaged melt and solid accumulation values. The areas will be the most representative drainage basins defined by Zwally et al. (2012).

OBS reconstruction

Reconstruction of observed temperature and precipitation time series through correlation patterns and correlated time series are carried out directly from the best correlated observation time series and best correlated ice core. All time series are standardized to zero mean and standard deviation of one before reconstruction.

Ice cores consist of stable water isotopes (δ18O) stratified in well preserved annual layers. This feature offers two valuable properties. First, the isotopic composition correlates with the temperature in the cloud at the time of condensation (Dansgaard, 1964, 1954). Thus, ice core δ18O measurements can be used to reconstruct past temperature at the drill site. Second, the temperature correlated δ18O oscillations provide a measure of past annual accumulation rate if a depth-age chronology is available.

This study utilizes ice core measurements from Renland (past 214 years) and DYE-3 (past 500 years) to extend the weather records from the DMI-station in Tasiilaq. Previously, (Vinther et al., 2010) demonstrated that δ18O from DYE-3 correlated with the regional temperature back in time. For Renland, we use a stack of three local ice cores (presented in Holme et al. (2019)). If available, it is beneficial to use a δ18O stack as it amplifies the signal part of the data and thus its correlation with the local atmospheric conditions. While Holme et al. (2019) found that this δ18O stack's is not significantly correlated with Icelandic temperature in the period AD 1830-1910, we here assume that it still reflects the Greenlandic climate conditions back in time (acknowledging that it still remains uncertain to what extent the linear relationship between Renland δ18O and regional temperatures have varied back in time).

Precipitation can be reconstructed through an ice core's depth-age relationship. As each annual layer has a specific thickness depending on the amount of precipitation, past accumulation rate can be estimated if an annual layer's age is known together with the amount of thinning the layer has experienced.

Uncertainties

Uncertainties associated with the reconstructed time series are calculated by fitting a regression function to periods with an overlap between the simulated and reconstructed time series. From the regression function both prediction and confidence intervals are calculated. The confidence interval is used as a measure for the reconstructed regression line uncertainty, while the prediction interval is applied as a measure of the mean difference between the two time series for a given value. The prediction interval is calculated to contain 95% of the difference, and corresponds to the confidence interval for the response variable to the predictor (von Storch and Zwiwes, 1998). The prediction bounds follow the general expression: *sample estimate ± (t-multiplier × standard error).*

The formula notation is:

$$\hat{y}_h \pm t_{\left(\frac{\alpha}{2},n-2\right)} \times \sqrt{MSE \times \left(1+\frac{1}{n}+\frac{(x_h-\overline{x})^2}{\sum(x_i-\overline{x})^2}\right)} \qquad (5)$$

$\hat{y}_h$, is the predicted value, where the predictor is x_h

$t_{\left(\frac{\alpha}{2},n-2\right)}$, is the t-multiplier with n-2 degrees of freedom, where α is the confidence level

$\sqrt{MSE \times \left(1+\frac{1}{n}+\frac{(x_h-\overline{x})^2}{\sum(x_i-\overline{x})^2}\right)}$, is the standard error of the prediction, where MSE, is mean square error.

The predictions and confidence intervals appear as shallow hyperbolas (Olesen et al., 2018). The confidence intervals for the regression line is

$$\hat{y}_h \pm t_{\left(\frac{\alpha}{2}, n-2\right)} \times \sqrt{MSE \times \left(\frac{1}{n} + \frac{(x_h - \overline{x})^2}{\sum (x_i - \overline{x})^2}\right)} \quad (6)$$

The equation for prediction intervals differs from the corresponding equation for the confidence intervals associated with the regression line by having an extra MSE term, which is caused by the unknown variance of the prediction. By using this approach, each reconstructed value is given a specific uncertainty interval. Relatively small and high precipitation values are associated with large uncertainties. This idea was also presented in (Olesen et al., 2018). Uncertainties are calculated for both simulated SMB-reconstructions and for reconstructions of observation time series.

Reconstructed SMB time series including uncertainty intervals are compared with solid accumulation from upstream ice core measurements at locations that, according to the correlation maps, are expected to be significantly correlated with the relevant drainage basin.

Observation coverage across Greenland

Temperature and precipitation nearby an observation station or ice core drill site are generally strongly correlated with the observation point, but areas over longer distances may also be strongly correlated. In this context, spatial correlation patterns provide a useful tool to evaluate the extent to which a given parameter is spatially covered by observation stations and ice core drill sites across Greenland. Some areas are covered by more than one weather station or ice core drill site location for a given parameter, whereas other areas are not covered at all.

The parameter coverage of observation locations all across Greenland is investigated by combining all the correlation maps for a given parameter. This analysis is done by generating maps where each land grid point represents the highest correlation coefficient extracted from all the correlation maps based on individual observation and ice core locations.

Results

Weather records

Precipitation and temperature records from DMI-weather stations in Greenland used in this study consist of 13 weather stations for precipitation and 19 stations for temperature. Annual precipitation and annual mean temperature records are

shown in Figure 2 and Figure 3. Years with one or more missing monthly values are discarded to make sure that the annual values are raw observed records. The time period starts from the first full 12-month observation year and ends with the last year of the HIRHAM5 simulation (2014).

Spatial correlation patterns

Correlation maps presented here are calculated from equation 1 for annual precipitation and summer temperature for the DMI-weather stations, and solid accumulation minus evaporation and summer temperatures for 6 deep ice core drill site locations on the Greenland ice sheet. In the following three examples are presented. Correlation patterns for annual precipitation (1980-2014) correlated with the HIRHAM5 simulated time series for the land grid points closest to Nuuk, Tasiilaq and Danmarkshavn are shown in Figure 4. Similar maps are presented in Figure 5 for summer temperature (JJA). The critical correlation coefficient for statistically significant correlation within a 95% confidence level is $r = 0.33$. The critical value is fixed to yellow on the correlation maps. While dark colours represent a high correlation, everything towards red colours is not significantly correlated with the selected grid point.

The correlation patterns in Figure 4 are dominated by well-defined areas, where precipitation is significantly correlated to the weather station of interest. For the weather station in Nuuk the precipitation is strongly correlated in the area west of the ice sheet ridge in south Greenland, while some areas east of the ridge (the darkest red areas) are close to or just significantly anti-correlated to precipitation observed in Nuuk. The ice ridge represents an almost instantaneous shift from positive to negative correlation coefficients. Corresponding correlation patterns emerges on the correlation maps for Danmarkshavn and Tasiilaq.

Spatial correlation patterns for temperature in Figure 5 show more smooth correlation patterns compared to the precipitation correlation patterns. There are no areas, where temperature is close to anti-correlated with the temperature time series at the weather station grid point. The correlation pattern appears to be altitude dependent, and in a band along the ice sheet edge, temperatures are slightly stronger correlated with the temperature at the grid point nearest the weather station. This tendency appears most distinct for correlation coefficients w.r.t. Nuuk. The correlation for precipitation seems to depend on the topography slope direction rather than on altitude, in contrast to the temperature correlation patterns.

Validation of correlation patterns

Correlation maps prepared from the HIRHAM5 simulation are compared with observations to verify if the correlation patterns appearing on the maps in Figure 4 and Figure 5 also appear in an analogous combination of observation records.

Correlation matrices for precipitation

For each possible combination of weather stations the correlation coefficients are calculated and presented as correlation matrices for observed precipitation records in Figure 6 (top right). The corresponding relationships for HIRHAM5 time series in land grid points closest to the weather station locations are displayed after the same procedure (top left). Yellow is constrained at r = 0.33, which for HIRHAM5 corresponds to the critical value of statistically significant correlation within a 95% confidence level. For the observations the critical value for significant correlation is varying among the possible combinations of weather station records because of unequal record overlaps. As the critical value depends on the length of the overlapping records, the colour key for observation combinations only represents the correlation coefficient and not whether or not a combination is significantly correlated. Therefore the p-values, considering varying degrees of freedom, are displayed separately in the two lower plots.

Pearson's correlation coefficients for the HIRHAM5 simulation are calculated for 35 year time series (with degrees of freedom, $df = 33$) whereas for observations the number of overlapping years is varying from 4 to 107 years. The degrees of freedom corresponding to the correlation test for observations in Figure 6 (upper right matrix) is presented in Figure 7. Red colours indicates $df_{obs} > df_{HIR}$ and conversely blue colours indicate $df_{obs} < df_{HIR}$.

Correlation matrices for temperature

As for precipitation, correlation matrices are calculated for summer temperature. HIRHAM5 simulated time series and observation records are combined for 19 weather station locations and compared in Figure 8. The corresponding degrees of freedom matrix for observation records is shown in Figure 9. In contrast to precipitation, the number of statistically significant correlated combinations for temperature is remarkably higher for observation records than for HIRHAM5 simulated time series.

Slope direction of the Greenland topography

HIRHAM5 is simulated on the basis of a number of fixed climatology input files among which the topography is described via the geopotential height. Supplementary Figure S1 shows the slope direction of the topography. The gradient of each point is calculated from its four neighbour points, but only the direction (not the steepness) is displayed in the figure. Accordingly, ridges that appear sharp and well-defined may be relatively flat and smooth surfaces.

Reconstruction of precipitation and temperature records

Reconstruction from correlated observation stations

Precipitation is with a few gaps observed in Ilulissat from 1890 to 1984 (Cappelen, 2018) and will here be an example of an observation record reconstruction. Observed precipitation in Aasiaat and Sisimiut are significantly correlated with precipitation in Ilulissat with correlation coefficients $r = 0.65$ and $r = 0.66$ respectively, see correlation matrices in Figure 6. Extension and gap filling is calculated by fitting a linear regression function for the time series overlap between Ilulissat and the two correlated stations. The coefficients, a and b, are then used to reconstruct the precipitation time series in Ilulissat:

$$PR_{Ilul} = a_{ilul,assi} PR_{asi} + b_{ilul,assi} \text{ , and } PR_{Ilul} = a_{ilul,sisi} PR_{sisi} + b_{ilul,sisi}.$$

A combination of reconstructed precipitation values and originally observed time series from Ilulissat is illustrated in Figure 10. Uncertainties associated with the reconstruction are shown as grey shaded areas calculated 95% prediction intervals from the linear regression function (equation 5), so that reconstructed values are given with a specific uncertainty range.

Reconstruction of temperature records using ice core data

The DMI-weather station in Tasiilaq is here the case proving the benefit of extending weather records from ice core data. According to the correlation patterns in Figure 5 temperature is significantly correlated with the Tasiilaq both at DYE-3 and at Renland, whereas only DYE-3 is correlated with Tasiilaq for precipitation. Ice core locations are shown in Figure 1.

Annual mean temperature observed at Tasiilaq is significantly correlated with the temperature proxy record from the Renland ice core with a correlation coefficient, $r = 0.49$. In Figure 11 the observed time series is via a regression function between the two time series reconstructed to cover a 214 year period (upper plot). The reconstructed temperature is damped due to the regression function, but 66% of the damped signal is restored as the prediction interval (equation 5), indicated as light grey shaded area.

Annual mean temperature observed at Tasiilaq is significantly correlated with the temperature proxy record from the DYE-3 ice core with a correlation coefficient, $r = 0.40$, $r = 4.7$ and $r = 0.38$ for annual, summer and winter time series respectively. The observed time series is via a regression function between the two time series reconstructed in Figure 12 to cover a 500 year period, but here for annual, summer and winter (top, mid and bottom plot). Again 66% of the damped signal is restored by adding the prediction interval, indicated as light grey shaded area.

Reconstruction of precipitation records using ice core data

As for annual mean temperature observed at Tasiilaq, the precipitation is significantly correlated with the accumulation rate from the DYE-3 ice core with a correlation coefficient, $r = 0.32$ and a p-value, $p = 0.0048$. As for temperature, precipitation observed in Tasiilaq is reconstructed (see Figure 13).

Reconstruction of simulated SMB

Reconstruction of simulated SMB is calculated from observed precipitation and temperature (equation 4), and relies on the assumption that these parameters correspond to solid accumulation minus evaporation and melt respectively (see equation 2 and 3). The first step is to test the relationship between precipitation and solid accumulation as well as summer temperature and melt. Annual solid accumulation is linearly related with annual precipitation as shown in Figure 14 where the solid accumulation fraction of precipitation is reduced for areas with more precipitation like DYE-3, which is also the southernmost ice core drill site location. In comparison, NGRIP is far from the coast at high altitude, and precipitation falls only as snow. The correlation is statistically significant for the entire ice sheet, which is shown in Supplementary Figure S2 (left).

Melt is related to summer temperature through a second order regression function. In Figure 15 the best fitted regression lines are plotted for each drainage basin (Zwally et al., 2012). This is tested similarly for an exponential regression function and a simple linear function for comparison. The correlation is calculated as a measure of regression accuracy and is shown for all drainage basins (Zwally et al., 2012) in Figure 15 (bottom) for each of the three test functions. The highest correlation is found along the periphery of the ice sheet, see Supplementary Figure S2 (right).

SMB reconstruction for Tasiilaq

HIRHAM5-simulated SMB is extended back in time with a reconstruction based on observed summer temperatures and annual precipitation measured in Tasiilaq from 1980-2014, using the regression function (equation 4). Melt and solid accumulation as well as modelled SMB are spatially averaged over the drainage basin 4.2 (Zwally et al., 2012). Basin 4.2 reaches from the north-south orientated ice sheet ridge to the west coast, and is chosen from the correlation maps with reference point at Tasiilaq in Figure 1. Simulated SMB in this drainage basin increases from close to zero near the ice sheet ridge to almost 6 m liquid water equivalents per year for a few grid points on step slops near the coast, see Figure 16.

Observed summer temperature and annual precipitation are significantly correlated with modelled melt and solid accumulation within a 95% confidence level with $r = 0.41$ and $r = 0.64$ (See Supplementary Figure S3). This is consistent with the correlation patterns in Figure 4 and Figure 5. From 1980 to 2014 all time-series are standardized to zero mean and a

standard-deviation of one. Precipitation represents the main contribution to the SMB for this area as standardised precipitation shows a steeper slope of the regression line with SMB than standardised temperature.

From the best fitted regression line, uncertainties in terms of confidence interval (equation 6) associated with the regression line and the prediction interval (equation 5) is illustrated in Supplementary Figure S4. The intervals are added to the reconstructed SMB values in Figure 17. In Supplementary Figure S4 the standardised value of reconstructed SMB equal to one standard deviation for simulated SMB (illustrated with the green dashed line) furthermore illustrates the damping effect of the regression procedure. Surface mass balance is reconstructed from observed temperature, T and precipitation, PR for drainage basin 4.2 from: $SMB_{RECON} = 0.49PR_{OBS} - (0.12T_{OBS} + 0.05T_{OBS}^2)$. The correlation coefficient between modelled SMB and reconstructed SMB for 1980-2014 is r = 0.66, which is stronger than the correlation of simulated melt and observed summer temperature and correlation of simulated solid accumulation and observed precipitation, and hence significantly correlated within a 95% confidence interval.

Three trend lines are added to the SMB reconstruction in Figure 17. The black solid line is considering the full reconstructed period from 1898 to 2014 with an slightly increasing slope, *a1 = 0.5 mm weq/yr per year*, whereas the dashed lines cover the 35-years up to 2014 for reconstructed (black) and HIRHAM5-simulated SMB (red) with decreasing slopes, *a2 = -5.4 mm weq/yr per year* and *a3 = -7.8 mm weq/yr per year* respectively. The trend lines clearly indicate that a reduction in SMB occurs towards 2014. The gap in the beginning of the 20th century is due to missing values in the precipitation records. The 35 year trend line limit is chosen to enable direct comparison of time series.

SMB Reconstruction for Danmarkshavn

Reconstruction of SMB follows the same procedure as for Tasiilaq. The drainage basin 2.1 is the most temperature- and precipitation representative area, upstream from Danmarkshavn. Reconstruction of SMB for the drainage basin leading to Danmarkshavn differs from the Tasiilaq, because the dominating contributor here is temperature and not precipitation. The correlation coefficient between observed summer temperatures and modelled melt is *r = 0.73*. Between observed annual precipitation and modelled solid accumulation the correlation coefficient is *r = 0.51*. The reconstructed SMB time series upstream from Danmarkshavn is highly correlated with modelled SMB with a correlation coefficient, *r = 0.67* (see Figure 18), and hence significantly correlated within a 95% confidence interval.

Three trend lines are added in Figure 18. The black solid line is considering the full reconstructed period from 1998 to 2014 with a negative slope, *a1 = -0.2 mm weq/yr per year*, whereas the dashed lines cover the 35 years up to 2014 for the reconstructed and HIRHAM5-simulated SMB with slopes, *a2 = -1.1 mm weq/yr per year* and *a3 = -1.1 mm weq/yr per year* respectively. Also for Danmarkshavn, the trend lines clearly indicate that the decrease in SMB occurs or speeds up towards 2014.

SMB Reconstruction for Renland

Renland is as mentioned of special interest in this work. The nearest (and highest correlated) weather station to Renland is Ittoqqortoormiit. Observed JJA-temperature and annual mean precipitation measured at Ittoqqortoormiit weather station correlated with modelled annual melt and annual solid accumulation from HIRHAM5 *(r = 0.48 and r = 0.47)* is shown in Supplementary Figure S7. Melt and solid accumulation time series are averaged over all grid points on the Renland ice sheet area displayed in Figure 19 as the annual mean SMB from 1980-2014. Each dot in the map corresponds to a grid point in the HIRHAM5 high-resolution climate model.

SMB reconstructed for Renland is based on observations from Ittoqqortoormiit and is correlated with the simulated SMB with a correlation coefficient, $r = 0.54$. The degree of freedom is 24 due to observation gaps, but the correlation is still statistically significant within a 95% confidence level. The gaps the reconstructed SMB time series remain open, as neither of the surrounding in situ records are significantly correlated with the precipitation record for Ittoqqortoormiit.

Three trend lines are added in Figure 20. The black solid line is considering the full reconstructed period from 1950 to 2014 with a slope, *a1 = 2.4 mm weq/yr per year*, whereas the dashed lines cover 35 years up to 2014 for reconstructed (black) and HIRHAM5-simulated SMB (red) with slopes, *a2 = -4.7 mm weq/yr per year* and *a3 = -6.9 mm weq/yr per year* respectively. As for Tasiilaq and Danmarkshavn, the trend lines for Renland SMB development clearly indicate that the decrease is most pronounced towards 2014. Results from the three SMB reconstructions: Tasiilaq, Danmarkshavn and Renland are shown in Table 1.

Merged correlation coverage

Correlation maps for 6 and 12 ice core locations are merged by selecting the highest coefficients among the correlation coefficients calculated for each ice core locations separately. The left map in Supplementary Figure S8 show the coverage of six deep ice cores (Vinther et al., 2010) together, whereas the right map also includes six shallow transverse cores (Kjær, personal comm.)

Discussion

Validation of correlation patterns

Precipitation

The correlation matrices based on HIRHAM5 simulated and observed precipitation are used to evaluate the correlation patterns and appear to have similar structures (see the two upper plots in Figure 6). From the two lower plots it is clear that HIRHAM5 predicts more significantly correlated location combinations than observed. The difference is mainly due to gaps in observation records that reduce the amount of overlapping time steps and hence reduces the degrees of freedom, which again increases the critical value for significant correlation. When only 15 years of the observed precipitation is overlapping with the HIRHAM5 simulation period, the degrees of freedom is $df = 13$, and the critical value for significant correlation within a 95% confidence interval increases to $r_{crit} = 0.51$. Therefore, higher correlation coefficients are required to meet the criteria for statistically significant correlation.

More than half of the significant correlation combinations that appear in HIRHAM5 simulated precipitation and not found in the observed precipitation are involving the weather stations in Upernavik and Ilulissat, where observation of precipitation stopped in the 80's. Correlation combinations with short overlapping time periods are thus subject to low degrees of freedom, as shown in Figure 7. One exception here is the absent correlation between observed precipitation in Ilulissat and Nuuk and the difference here cannot be explained with an increased critical value for significant correlation.

HIRHAM5 and observation records show consistently that Ittoqqortoormiit and Danmarkshavn do not correlate with any other observation station. Also, Pituffik appears relatively isolated from other stations, except for a weak but statistically significant correlation with Aasiaat ($r = 0.37$) and Kangerlussuaq ($r = 0.45$), which is only depicted from observations.
Five significantly correlated combinations in the observation records should not correlate according to HIRHAM5. Two out of the five can be explained by relatively high degrees of freedom for the long observed time series in Tasiilaq, Nuuk and Ittoqqortoormiit. In total, that confines it to 3 out of 78 record combinations that are found within the observations but not captured by HIRHAM5. These, together with the opposite mismatch mentioned above for Nuuk and Ilulissat, may be caused by imprecise topography descriptions within HIRHAM5. In summary, an overall agreement in the location specific cross correlations of observed and simulated precipitation is identified with only a few exceptions.

Temperature

In Figure 8 we see that the number of significant correlated combinations is notable larger for observed than for simulated temperature. The observed temperature records are relatively long and with fewer missing values compared to the precipitation records, and therefore the critical value for statistical significance is correspondingly low. Nevertheless, some unexpected differences do occur: Temperature observed at Station Nord does correlate significantly with five other station records, which is not found for Station Nord in the simulation, even though the degrees of freedom are comparable. Similarly, temperature observed at Summit is significantly correlated with six other weather stations, which is not depicted by HIRHAM5, even though the degrees of freedom of time series for Summit does not exceed $df = 12$.

The disagreement between observed and simulated significantly correlated station combinations can in the majority of cases be explained with low degrees of freedom caused by gaps and not overlapping precipitation records, and the opposite for the longer temperature records. The gaps and time series overlap are shown in Figure 2 and Figure 3, where the 13 observed precipitation records and 19 temperature records are shown. From Figure 7 and Figure 9 it is clear that the number of significantly correlated combinations is expected to be smaller for observed precipitation compared to simulated precipitation and vice versa for temperature.

Slope direction and weather systems

The correlation patterns for precipitation can to large extent be explained by large scale weather systems and topography. Precipitation is in general regulated by water vapour content, atmospheric stability and circulation, and topography, whereas the major precipitation contribution over Greenland is produced by frontal cyclone weather systems (Chen et al., 1997). The geographical distribution of precipitation on climatological scale is mainly caused by the interaction between topography and geostrophic wind patterns. The Greenland ice sheet topography is characterised by possessing influencing physical barriers described by Ohmura and Reeh (1991) as roughly one north-south orientated ridge with three east-west ridges on the western side and two on the eastern site.

Rogers et al. (2004) showed the importance of distinguishing lee cyclones from Icelandic cyclones, as they produce opposite precipitation effects across the ice sheet, which is consistent with the general relationship between precipitation in Greenland, cyclone activity and large scale circulation. This is also consistent with the fact that large scale circulation is the dominating driver of accumulation variations in the central and southern part of Greenland, whereas cyclone activity is higher correlated with accumulation in north eastern Greenland (Hutterli et al., 2005). In a warmer world precipitation will in general increase in Greenland, where the drivers of accumulation changes are the large-scale circulation combined with the local topography (Merz et al., 2013).

By matching precipitation correlation patterns for e.g. Nuuk and Tasiilaq with slope directions in Supplementary Figure S1, the north south oriented ice sheet ridge clearly separates eastern and western correlation regimes caused by westerly and easterly winds and front systems. Smaller ice ridges appearing on the slope direction map are also pronounced in the correlation patterns of the solid accumulation correlated with Renland (See Supplementary Figure S6). To summarise, the correlation patterns evaluated in the light of dominating precipitation events in Greenland together with the slope direction map, supports the idea that the HIRHAM5 deduced correlation maps do represent a real world temperature and precipitation patterns.

Reconstruction of observations

Temperature and precipitation time series can be reconstructed from correlated weather records for gap filling, and from ice core time series for extending the observation records back in time. Correlation maps and correlation matrices in particular are practical tools to select the best correlated observation records. In the reconstruction procedure the variance of the reconstructed time series is reduced compared for the observed records. Reconstruction is calculated through a linear regression function, which at first does not include the variance of the original observation record. To solve this problem, the 66% prediction interval of the response variable is added as a prediction interval. Extension of observed temperature time series back in time show that the warming primarily has occurred within the last three decades. The trends in temperature is increasing gradually towards present consistent with significant temperature increases shown by Abermann et al. (2017) to be between 0.05 and .015 ˚C $year^{-1}$ for 1996-2014.

Reconstruction of SMB

HIRHAM5-simulated precipitation and temperature is strongly correlated with simulated solid accumulation minus evaporation and melt, which is also evident for observed precipitation and temperature. Based on the convincing linear relationship to solid accumulation, shown in Figure 14, precipitation is demonstrated to be a usable estimate for changes in solid accumulation in the reconstruction of simulated SMB. Summer temperature is likewise a good estimate for melt from the drainage basin, close to the location where the temperature is observed. A simulated SMB reconstruction from a partial regression function based on observed precipitation and temperature is therefore expected to produce realistic SMB estimates.

SMB-reconstructions for the three areas based on observations are all significantly correlated with the simulated SMB. Weather stations at Tasiilaq and Danmarkshavn are closer linked to simulated SMB at their respective drainage basins, than

Ittoqqortoormiit is to the Renland ice cap. The distance between Renland and Ittoqqortoormiit is about 200 km, but the correlation is higher in observations, than predicted from the correlation map.

As for observation reconstructions the procedure for SMB reconstruction introduces a damping effect through the regression approximation, resulting in reduced variance compared to original simulated time series. Again, the uncertainties in the form of a prediction interval restores 66% of the damped variance signal, as this prediction interval captures 66% of the simulated SMB variability relative to the regression line. By increasing the prediction interval to 95% confidence level, almost all damping will be restored, but this has the disadvantage of blowing up the uncertainty. Here the IPCC definition of likely range is followed (Mastrandrea et al., 2011). The surface mass balance in drainage basin 4.2 reconstructed from Tasiilaq weather records is decreasing towards present, where the last 35 years are decreasing with *6.1 mm weq/yr* annually, whereas the SMB is slightly increasing with *0.2 mm weq/yr* per year, considering the full reconstruction period from 1898 to 2014.

The reconstruction of SMB in Danmarkshavn in Figure 18 shows a convincing correlation with simulated SMB with a correlation coefficient $r = 0.67$. Contrary to basin 4.2, the SMB in drainage basin 2.1 is predominantly temperature controlled, where reconstruction from Tasiilaq is dominated by precipitation. The reconstructed SMB time series for basin 2.1 show a less negative trend towards 2014 compared SMB in basin 4.2.

The Renland SMB reconstruction is challenging, because even though the significantly correlated area to Renland is relatively large for precipitation, the three nearest good quality weather records are located in areas at the limit of significant correlation as displayed in Supplementary Figure S6. Tasiilaq is just south of the high correlated area and Danmarkshavn just the north of it and relatively low-lying (11m above sea level) compared to Renland. Considering both precipitation and temperature, Ittoqqortoormiit proves to match the Renland ice core data best, with correlation coefficients, $r = 47$ and 48 for temperature and precipitation, see Supplementary Figure S7. SMB at Renland is more temperature than precipitation dependent and the SMB reconstruction turns out to be strongly correlated with simulated SMB, with $r = 0.54$. This is stronger than correlations between observed temperature and precipitation and simulated melt and solid accumulation individually. Gaps in the reconstructed SMB time series will occur in all cases, where errors cannot be replaced with other significantly correlated observation records, which can be read directly from Figure 6.Figure 8

The reconstructed and simulated SMB have comparable regression lines for the last 35 years for Tasiilaq, Danmarkshavn and Renland, which to some extent verifies the accuracy of the reconstructed time series. Difference in slopes for the reconstructed and simulated time series, a2 and a3, for Renland can be ascribed to the missing values from 2007 and onwards for observations. The accelerating SMB decrease towards present for both Tasiilaq, Danmarkshavn and Renland is consistent with (Box, 2013; Fettweis et al., 2017; Hanna et al., 2011).

Correlation coverage

The maps in Supplementary Figure S8 indicate to what degree selected ice cores represent surface dynamics on the entire ice sheet represented by HIRHAM5. In this example maps are prepared for solid accumulation. The statistically significant correlation with six deep ice cores, shown in Supplementary Figure S8 (left) covers most of the ice sheet except for the north east part of Greenland National park. The remaining part is embraced by adding six transverse shallow cores Supplementary Figure S8 (right). The area with the lowest correlation coefficients is then the south-eastern part of the ice sheet. The six ice cores do cover most of the ice sheet for significantly correlated grid cells. However, by defining a higher critical value necessary for varies types of investigations, the coverage logically reduces and the deserted areas become more distinct, which may be useful information for future ice core planning.

Conclusions and perspectives

The spatial correlation maps are consistent with observations with relatively few exceptions. And the correlation patterns for precipitation and temperature appearing on the correlation maps do to large extent correspond to the effect of Greenland large scale weather systems and topography across the country. Only one combination of precipitation records showed unexpected absence of correlation in observations despite a relatively long time series. For temperature only one weather station does correlate significantly with six other stations in observations, but not for HIRHAM5.

Reconstruction of SMB from observation records are significantly correlated with HIRHAM5-simulated SMB for both the Tasiilaq and Danmarkshavn drainage basins and for the Renland ice cap. All three cases show decreasing trend lines for the period 1980 to 2014. Furthermore the trend line slopes are remarkably lower for the last decades compared to the full reconstruction periods, which indicates a decreasing or maybe decelerating SMB for these areas. The SMB for the drainage basin nearest Tasiilaq, decreases from + 0.5mm weq/yr for 1898-2014 to -5.4 mm weq/yr in 1980-2014. Correspondingly the SMB for the drainage basin nearest Danmarkshavn decreases from -0.3mm weq/yr for 1950-2014 to -1.1mm weq/yr in 1980-2014 and the SMB of the Renland ice cap decreases from +2.4mm weq/yr for 1950-2007 to -4.7mm weq/yr in 1980-2007. Additionally, the reconstructed SMB time series are confirmed by their trend line slopes comparable with the simulated trend line slopes in Table 1.

The distribution of ice cores do to large extent cover the solid accumulation characteristics across the Greenland ice sheet, meaning that nearly all locations on the ice sheet are correlated with at least one ice core location. The six deep ice cores do cover most of the ice, and by adding the six shallow cores, the Greenland ice sheet is close to full covered by ice cores in terms of solid accumulation correlations deduced from HIRHAM5.

Reconstructing surface mass balance time series back in time, based on in situ temperature and precipitation observations for Greenland is obviously a challenge, when only few long high quality observation records exist. For precipitation only four records reaches beyond 1950. In this study we even discarded all years, where one or more monthly values were missing, so a next step would be to repeat the exercise on at higher temporal resolution for observations (monthly or daily) and reconstruct the SMB from higher quality observation records. Furthermore this approach can be expanded to the entire Greenland ice sheet divided into the above-mentioned drainage basins, resulting in SMB time evolution reconstructions for different time periods, depending on the observations records. This will altogether provide an improved estimate of the time evolution of the total Greenland surface mass balance, based on high resolution modelling and in situ observations.

Acknowledgements

The research leading to these results has received funding from the European Research Council under the European Union's Seventh Framework Programme (FP7/2007-2013) / ERC Grant Agreement n.610055 as part of the ice2ice project and from the Danish Cooperation for Environment in the Arctic (DANCEA) under the Danish Energy Agency. We also thank Peter Thejll for his assistance with spatial statistics and Helle Astrid Kjær for making available and share unpublished data from six additional shallow ice core locations.

References

Abermann, J., Hansen, B., Lund, M., Wacker, S., Karami, M., Cappelen, J., 2017. Hotspots and key periods of Greenland climate change during the past six decades. Ambio 46, 3–11. https://doi.org/10.1007/s13280-016-0861-y

Andersen, K.K., Ditlevsen, P.D., Rasmussen, S.O., Clausen, H.B., Vinther, B.M., Johnsen, S.J., Steffensen, J.P., 2006. Retrieving a common accumulation record from Greenland ice cores for the past 1800 years. J. Geophys. Res. Atmospheres 111. https://doi.org/10.1029/2005JD006765

Ballinger, T.J., Hanna, E., Hall, R.J., Miller, J., Ribergaard, M.H., Høyer, J.L., 2017. Greenland coastal air temperatures linked to Baffin Bay and Greenland Sea ice conditions during autumn through regional blocking patterns. Clim. Dyn. 1–18. https://doi.org/10.1007/s00382-017-3583-3

Boas, L., Wang, P.., 2016. Quality con ntrol of Gre eenlandic weather and climate data a series 1958-2010 (No. 11-16), DMI Report. Danish Meteorological Institute.

Boberg, F., Langen, P.L., Mottram, R.H., Christensen, J.H., Olesen, M., 2018. 21st-century climate change around Kangerlussuaq, west Greenland: From the ice sheet to the shores of Davis Strait. Arct. Antarct. Alp. Res. 50, S100006. https://doi.org/10.1080/15230430.2017.1420862

Box, J.E., 2013. Greenland Ice Sheet Mass Balance Reconstruction. Part II: Surface Mass Balance (1840–2010). J. Clim. 26, 6974–6989. https://doi.org/10.1175/JCLI-D-12-00518.1

Box, J.E., Cressie, N., Bromwich, D.H., Jung, J.-H., van den Broeke, M., van Angelen, J.H., Forster, R.R., Miège, C., Mosley-Thompson, E., Vinther, B.M., McConnell, J.R., 2012. Greenland Ice Sheet Mass Balance Reconstruction. Part I: Net Snow Accumulation (1600–2009). J. Clim. 26, 3919–3934. https://doi.org/10.1175/JCLI-D-12-00373.1

Calanca, P., Gilgen, H., Ekholm, S., Ohmura, A., 2000. Gridded temperature and accumulation distributions for Greenland for use in cryospheric models. Ann. Glaciol. 31, 118–120. https://doi.org/10.3189/172756400781820345

Cappelen, J., 2018. Greenland - DMI Historical Climate Data Collection 1784-2017 (No. 18-04), DMI Report. Danish Meteorological Institute.

Chen, Q., Bromwich, D.H., Bai, L., 1997. Precipitation over Greenland Retrieved by a Dynamic Method and Its Relation to Cyclonic Activity. J. Clim. 10, 839–870. https://doi.org/10.1175/1520-0442(1997)010<0839:POGRBA>2.0.CO;2

Christensen, O.B., Drews, M., Christensen, J.H., Dethloff, K., Ketelsen, K., Hebestadt, I., Rinke, A., 2006. The HIRHAM regional climate model version 5. (DMI Technical Report No. 06-17). DMI, Copenhagen, Denmark.

Cogley, J.G., 2009. Geodetic and direct mass-balance measurements: comparison and joint analysis. Ann. Glaciol. 50, 96–100. https://doi.org/10.3189/172756409787769744

Dansgaard, W., 1964. Stable isotopes in precipitation. Tellus 16, 436–468. https://doi.org/10.1111/j.2153-3490.1964.tb00181.x

Dansgaard, W., 1954. The O18-abundance in fresh water. Geochim. Cosmochim. Acta 6, 241–260. https://doi.org/10.1016/0016-7037(54)90003-4

Dee, D.P., Uppala, S.M., Simmons, A.J., Berrisford, P., Poli, P., Kobayashi, S., Andrae, U., Balmaseda, M.A., Balsamo, G., Bauer, P., Bechtold, P., Beljaars, A.C.M., van de Berg, L., Bidlot, J., Bormann, N., Delsol, C., Dragani, R., Fuentes, M., Geer, A.J., Haimberger, L., Healy, S.B., Hersbach, H., Hólm, E.V., Isaksen, L., Kållberg, P., Köhler, M., Matricardi, M., McNally, A.P., Monge-Sanz, B.M., Morcrette, J.-J., Park, B.-K., Peubey, C., de Rosnay, P., Tavolato, C., Thépaut, J.-N., Vitart, F., 2011. The ERA-Interim reanalysis: configuration and performance of the data assimilation system. Q. J. R. Meteorol. Soc. 137, 553–597. https://doi.org/10.1002/qj.828

Eerola, K, 2006. About the performance of HIRLAM version 7.0. HIRLAM Newsl. 51, 93–102.

Fettweis, X., Box, J.E., Agosta, C., Amory, C., Kittel, C., Lang, C., van As, D., Machguth, H., Gallée, H., 2017. Reconstructions of the 1900–2015 Greenland ice sheet surface mass balance using the regional climate MAR model. The Cryosphere 11, 1015–1033. https://doi.org/10.5194/tc-11-1015-2017

Hanna, E., Huybrechts, P., Cappelen, J., Steffen, K., Bales, R.C., Burgess, E., McConnell, J.R., Steffensen, J.P., Van Den Broeke, M., Wake, L., Bigg, G., Griffiths, M., Savas, D., 2011. Greenland Ice Sheet surface mass balance 1870 to 2010 based on Twentieth Century Reanalysis, and links with global climate forcing. J. Geophys. Res. Atmospheres 116.

Hanna, E., Huybrechts, P., Janssens, I., Cappelen, J., Steffen, K., Stephens, A., 2005. Runoff and mass balance of the Greenland ice sheet: 1958-2003. J. Geophys. Res.-Atmospheres 110, D13108. https://doi.org/10.1029/2004JD005641

Holme, C., Gkinis, V., Lanzky, M., Morris, V., Olesen, M., Thayer, A., Vaughn, B.H., Vinther, B.M., 2019. Varying regional δ^{18}O–temperature relationship in high resolution stable water isotopes from East Greenland. Clim. Past Discuss. 1–26. https://doi.org/https://doi.org/10.5194/cp-2018-169

Hutterli, M.A., Raible, C.C., Stocker, T.F., 2005. Reconstructing climate variability from Greenland ice sheet accumulation: An ERA40 study. Geophys. Res. Lett. 32. https://doi.org/10.1029/2005GL024745

Jones, P.D., Mann, M.E., 2004. Climate over past millennia. Rev. Geophys. 42. https://doi.org/10.1029/2003RG000143

Langen, P.L., Fausto, R.S., Vandecrux, B., Mottram, R.H., Box, J.E., 2017. Liquid Water Flow and Retention on the Greenland Ice Sheet in the Regional Climate Model HIRHAM5: Local and Large-Scale Impacts. Front. Earth Sci. 4. https://doi.org/10.3389/feart.2016.00110

Langen, P.L., Mottram, R.H., Christensen, J.H., Boberg, F., Rodehacke, C.B., Stendel, M., van As, D., Ahlstrøm, A.P., Mortensen, J., Rysgaard, S., Petersen, D., Svendsen, K.H., Aðalgeirsdóttir, G., Cappelen, J., 2015. Quantifying energy and mass fluxes controlling Godthåbsfjord freshwater input in a 5 km simulation (1991-2012). J. Clim. https://doi.org/10.1175/JCLI-D-14-00271.1

Lucas-Picher, P., Wulff-Nielsen, M., Christensen, J.H., Aðalgeirsdóttir, G., Mottram, R., Simonsen, S.B., 2012. Very high resolution regional climate model simulations over Greenland: Identifying added value. J. Geophys. Res. Atmospheres 117, n/a–n/a. https://doi.org/10.1029/2011JD016267

Masson-Delmotte, V., Steen-Larsen, H.C., Ortega, P., Swingedouw, D., Popp, T., Vinther, B.M., Oerter, H., Sveinbjornsdottir, A.E., Gudlaugsdottir, H., Box, J.E., Falourd, S., Fettweis, X., Gallée, H., Garnier, E., Gkinis, V., Jouzel, J., Landais, A., Minster, B., Paradis, N., Orsi, A., Risi, C., Werner, M., White, J.W.C., 2015. Recent changes in north-west Greenland climate documented by NEEM shallow ice core data and simulations, and implications for past-temperature reconstructions. The Cryosphere 9, 1481–1504. https://doi.org/10.5194/tc-9-1481-2015

Mastrandrea, M.D., Mach, K.J., Plattner, G.-K., Edenhofer, O., Stocker, T.F., Field, C.B., Ebi, K.L., Matschoss, P.R., 2011. The IPCC AR5 guidance note on consistent treatment of uncertainties: a common approach across the working groups. Clim. Change 108, 675–691. https://doi.org/10.1007/s10584-011-0178-6

Merz, N., Raible, C.C., Fischer, H., Varma, V., Prange, M., Stocker, T.F., 2013. Greenland accumulation and its connection to the large-scale atmospheric circulation in ERA-Interim and paleoclimate simulations. Clim Past 9, 2433–2450. https://doi.org/10.5194/cp-9-2433-2013

Mottram, R., Boberg, F., Langen, P., Yang, S., Rodehacke, C., Christensen, J.H., Madsen, M.S., 2017. Surface mass balance of the Greenland ice sheet in the regional climate model HIRHAM5: Present state and future prospects 105–115.

Ohmura, A., Reeh, N., 1991. New precipitation and accumulation maps for Greenland. J. Glaciol. 37, 140–148. https://doi.org/10.3189/S0022143000042891

Olesen, M., Christensen, J.H., Kaas, E., Boberg, F., 2018. Robustness of high-resolution regional climate projections for Greenland: a method for uncertainty distillation. Clim. Res. 76, 253–268. https://doi.org/10.3354/cr01536

Ortega, P., Swingedouw, D., Masson-Delmotte, V., Risi, C., Vinther, B.M., Yiou, P., Vautard, R., Yoshimura, K., 2014. Characterizing atmospheric circulation signals in Greenland ice cores: insights from a weather regime approach. Clim. Dyn. 43, 2585–2605. https://doi.org/10.1007/s00382-014-2074-z

Roeckner, E., Bäuml, G., Bonaventura, L., Brokopf, R., Esch, M., Giorgetta, M., Hagemann, S., Kirchner, I., Kornblueh, L., Manzini, E., 2003. The atmospheric general circulation model ECHAM 5. PART I: Model description.

Rogers, J.C., Bathke, D.J., Mosley-Thompson, E., Wang, S.-H., 2004. Atmospheric circulation and cyclone frequency variations linked to the primary modes of Greenland snow accumulation. Geophys. Res. Lett. 31. https://doi.org/10.1029/2004GL021048

Vinther, B.M., Andersen, K.K., Jones, P.D., Briffa, K.R., Cappelen, J., 2006. Extending Greenland temperature records into the late eighteenth century. J. Geophys. Res. Atmospheres 111. https://doi.org/10.1029/2005JD006810

Vinther, B.M., Jones, P.D., Briffa, K.R., Clausen, H.B., Andersen, K.K., Dahl-Jensen, D., Johnsen, S.J., 2010. Climatic signals in multiple highly resolved stable isotope records from Greenland. Quat. Sci. Rev. 29, 522–538. https://doi.org/10.1016/j.quascirev.2009.11.002

von Storch, H., Zwiwes, F.W., 1998. Statistical analysis climate research | Climatology and climate change. Cambridge University Press.

Zwally, H.J., Mario, B.G., Matthew, A.B., Jack, L.S., 2012. Antarctic and Greenland Drainage Systems, GSFC Cryospheric Sciences Laboratory [WWW Document]. URL http://icesat4.gsfc.nasa.gov/cryo_data/ant_grn_drainage_systems.php (accessed 2.6.18).

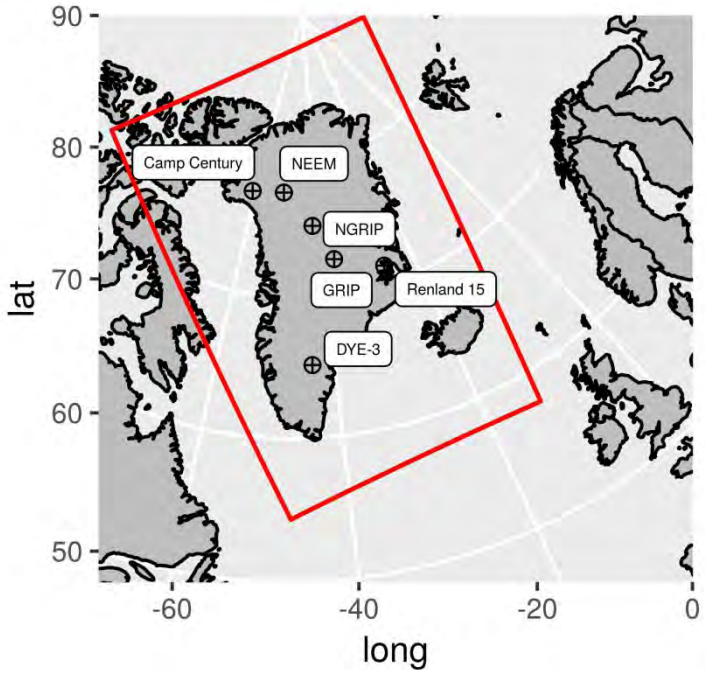

Figure 1: Location of the six deep ice cores used in this research. The red square encloses the HIRHAM5 domain on a rotated grid of 5.5 km resolution.

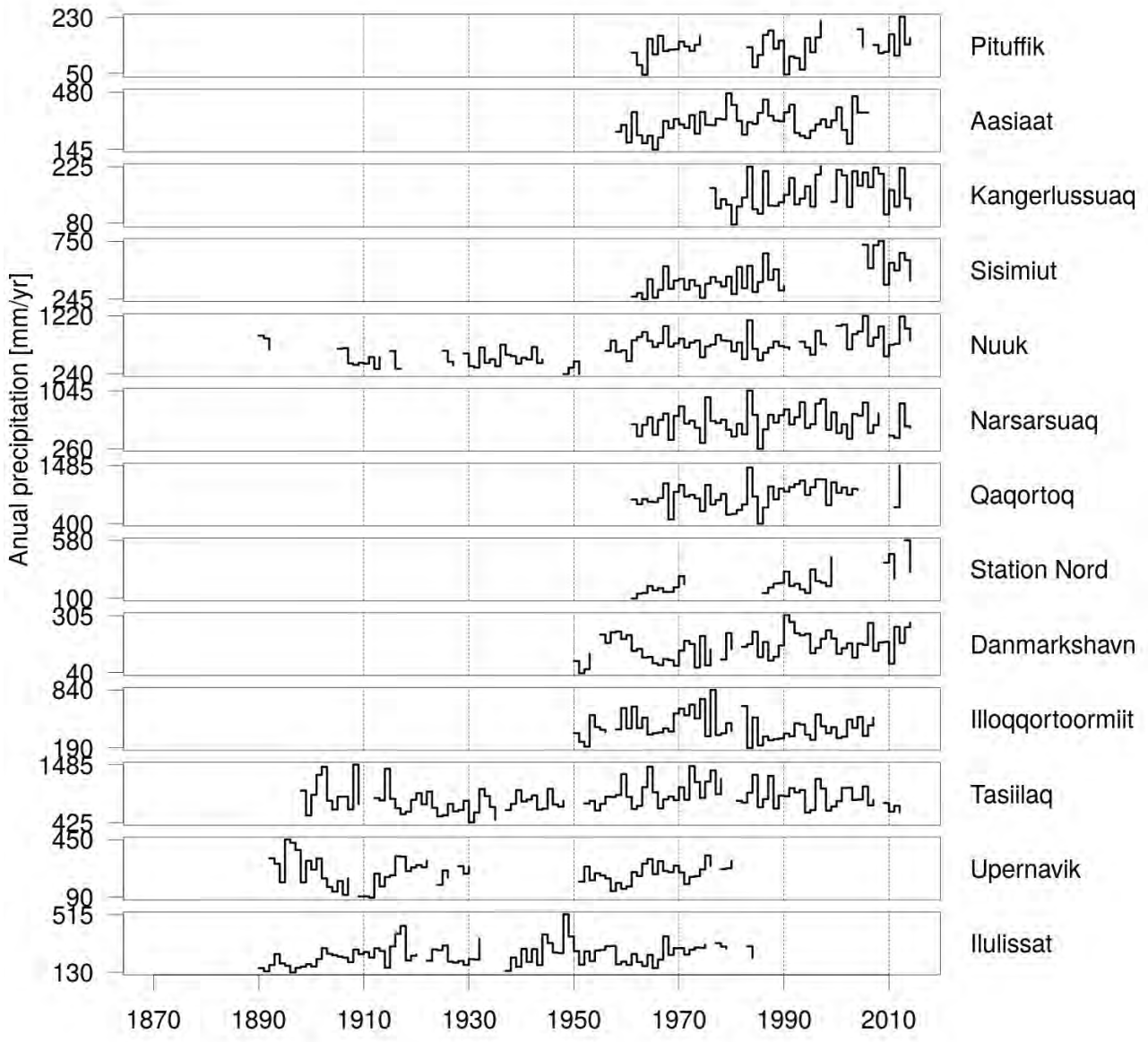

Figure 2: Annual precipitation observations from DMI-weather stations along the coast in Greenland. Only annual values with full monthly coverage are represented.

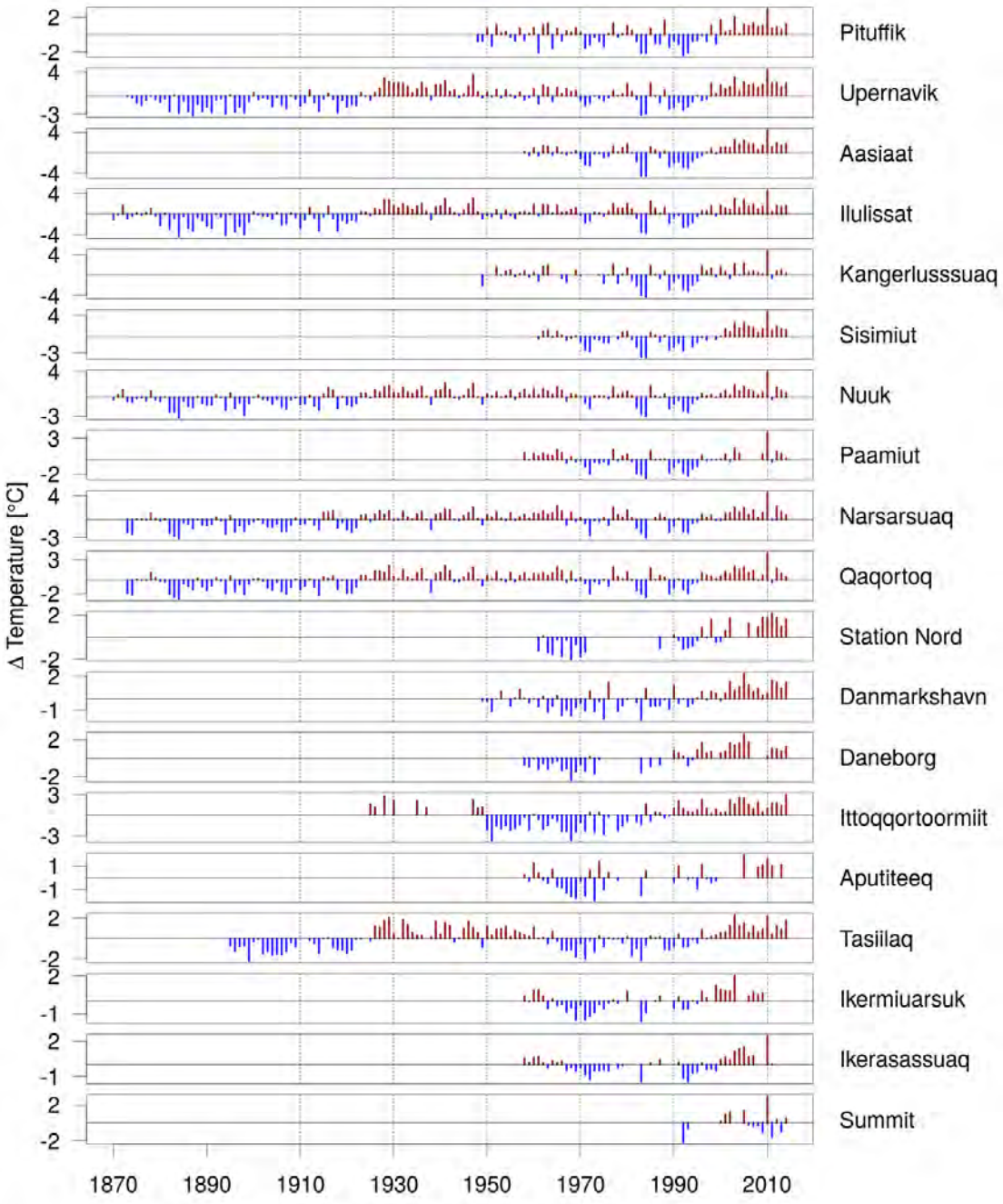

Figure 3: Annual mean temperature observed from DMI-weather stations along the coast in Greenland. Temperatures are normalized to the mean of the time series, where blue and red bars indicate smaller and greater than the mean. Only annual values with full monthly coverage are presented

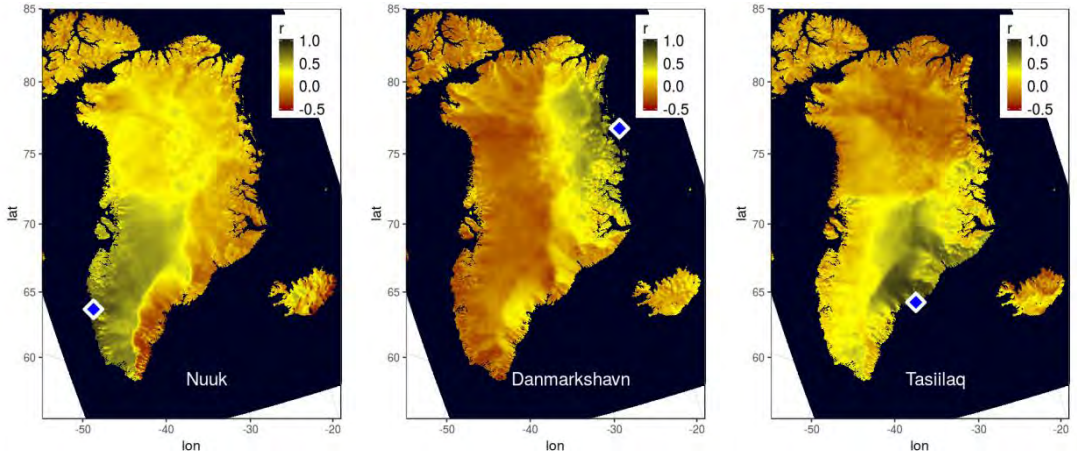

Figure 4: Correlation patterns for HIRHAM5 simulated annual precipitation time series 1980-2014. The maps represent correlation coefficients between each land grid point and the grid point closest to the weather stations in Nuuk, Danmarkshavn and Tasiilaq (from left to right). Critical correlation coefficient for significance at a 95% confidence level is r = 0.33 (set as yellow).

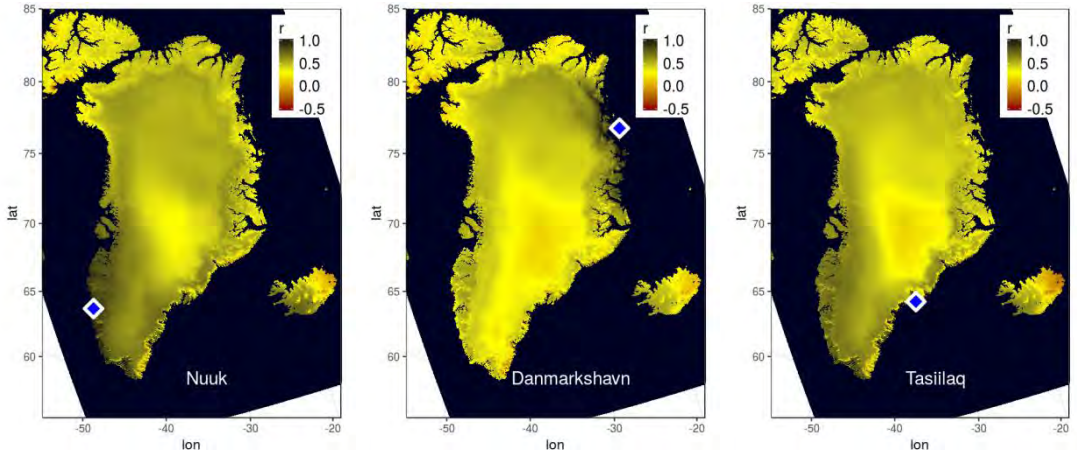

Figure 5: Correlation patterns for HIRHAM5 simulated summer (JJA) mean temperature time series 1980-2014. The maps represent correlation coefficients between each land grid point and the grid point closest to the weather stations in Nuuk, Danmarkshavn and Tasiilaq (from left to right). Critical correlation coefficient for significance at a 95% confidence level is r = 0.33 (set as yellow).

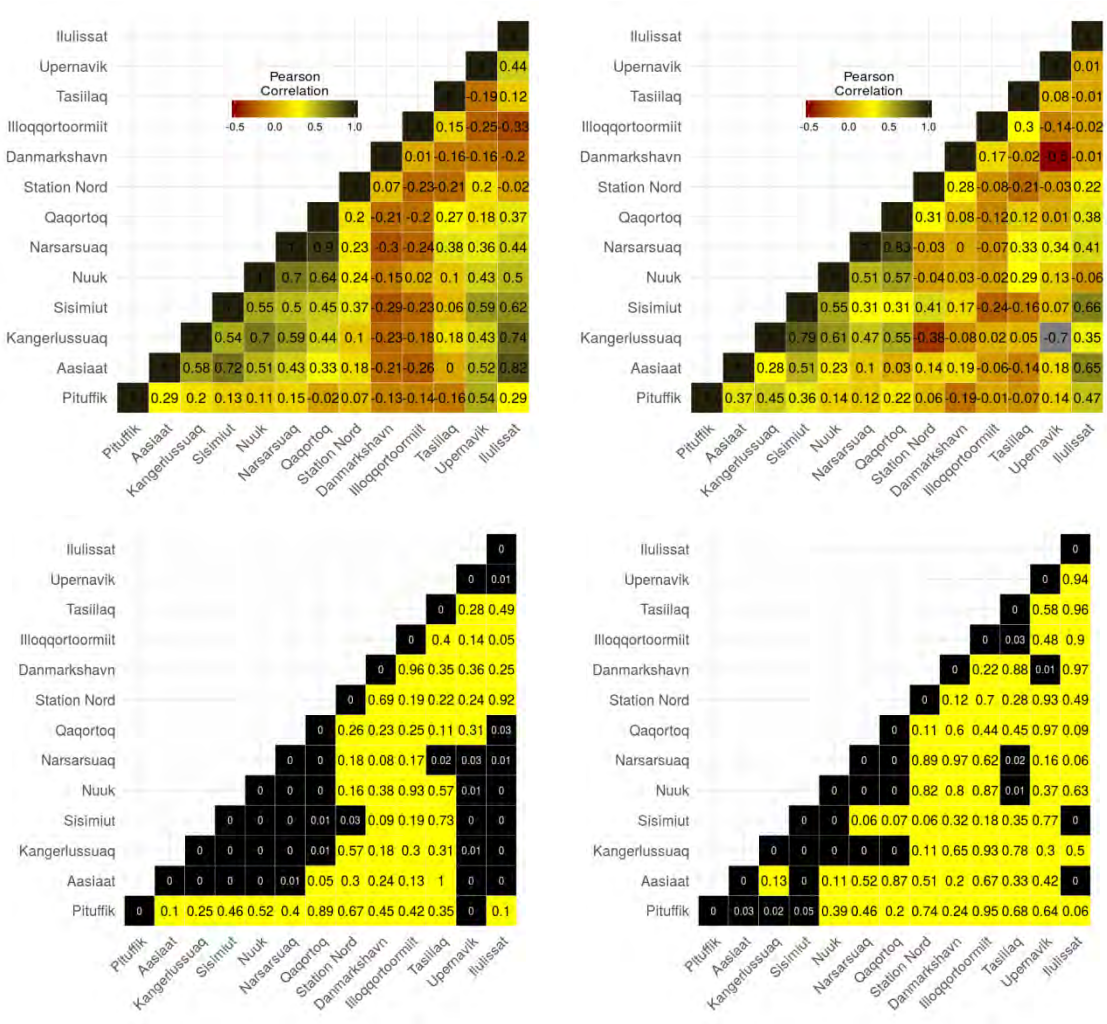

Figure 6: Correlation matrices for simulated (upper left) and observed (upper right) precipitation at 13 weather stations. Statistically significant (at a 95% confidence level) correlated weather station combinations are marked with black for simulations and observations (lower left and right). P-values are shown for the not significantly correlated station combinations (yellow squares).

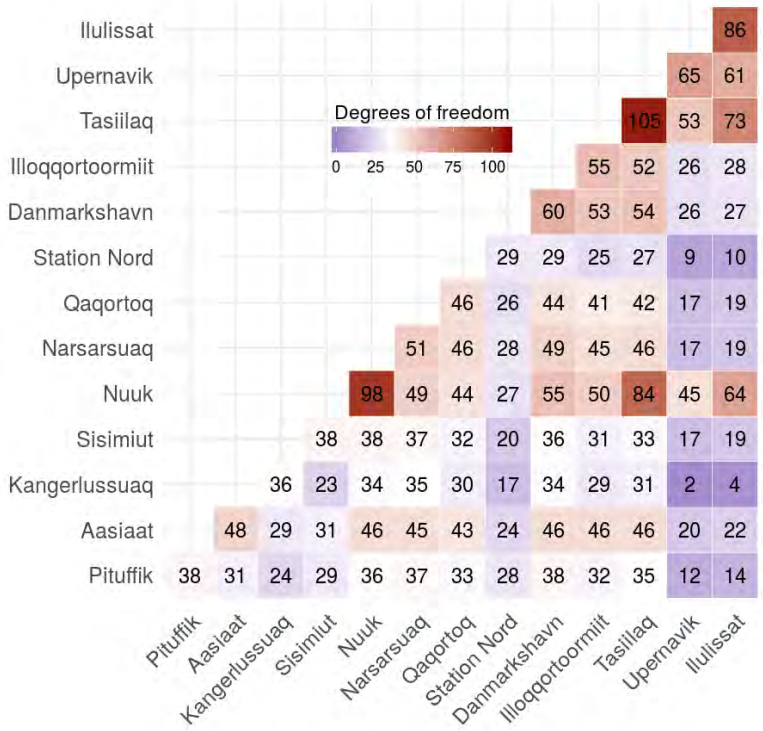

Figure 7: Degrees of freedom for observed precipitation for combinations of DMI-weather stations in Greenland. Red colours indicate higher degrees of freedom than in the HIRHAM5 35-year simulation (df > 33) and blue lower degrees of freedom.

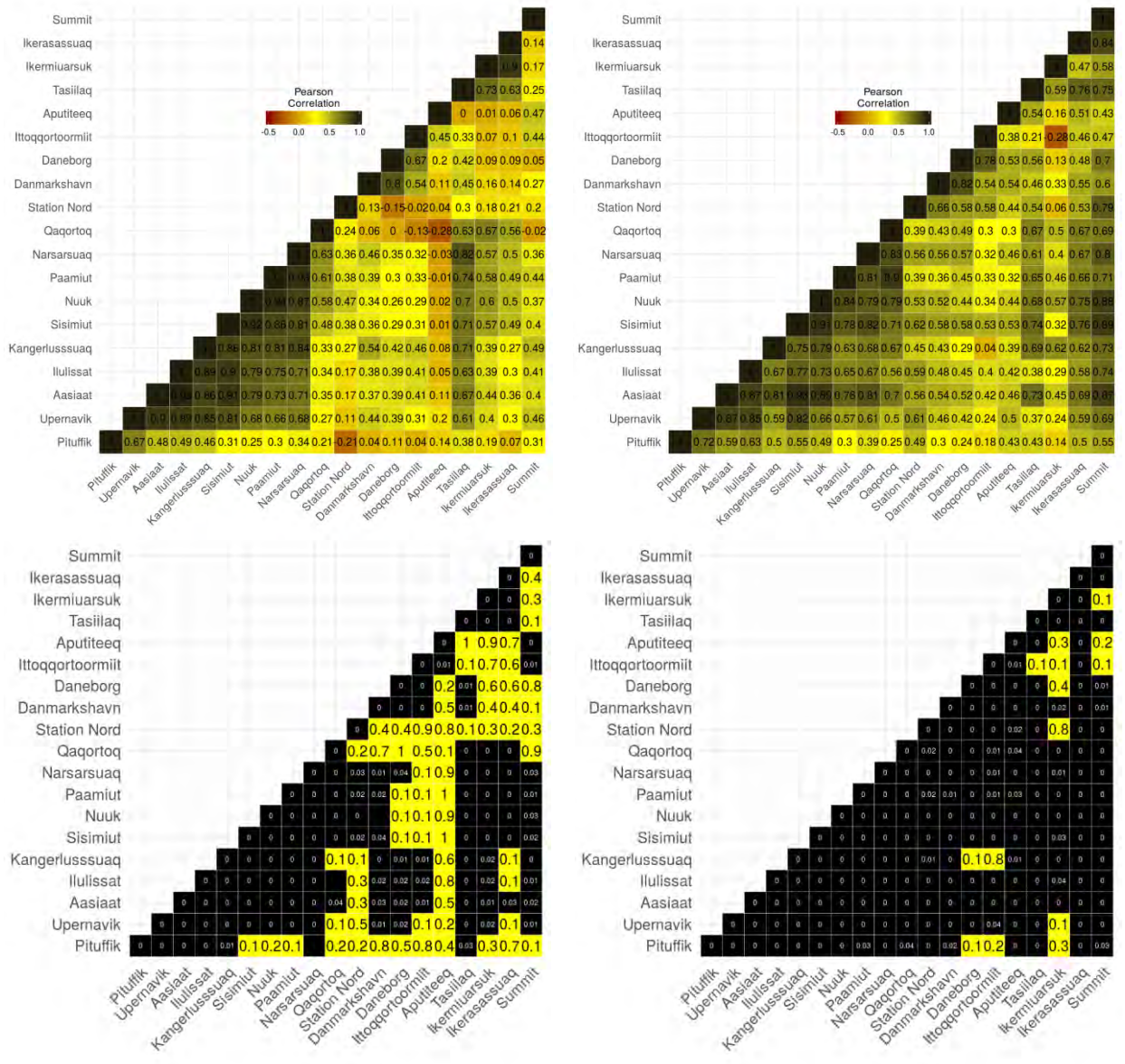

Figure 8: Correlation matrices for simulated (upper left) and observed (upper right) summer temperature at 19 weather stations. Statistically significant (at a 95% confidence level) correlated weather station combinations are marked with black for simulations and observations (lower left and right). P-values are shown for not significantly correlated station combinations (yellow squares).

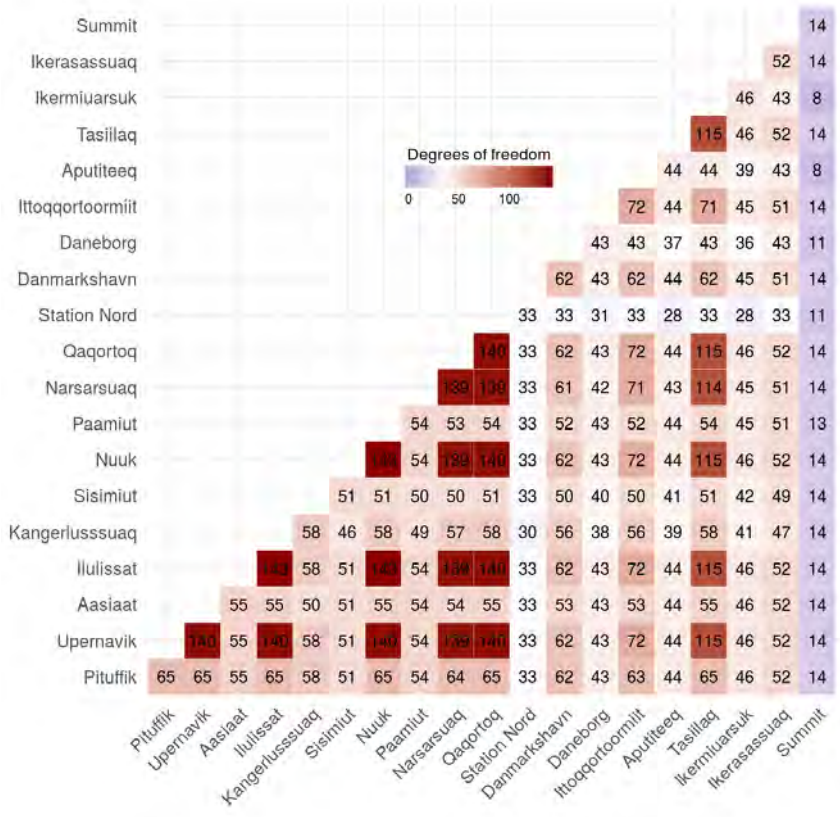

Figure 9: Degrees of freedom for observed summer temperature (JJA) for combinations of DMI-weather stations in Greenland. Red colours indicate higher degrees of freedom than in the HIRHAM5 35-year simulation (df > 33) and blue lower degrees of freedom.

5

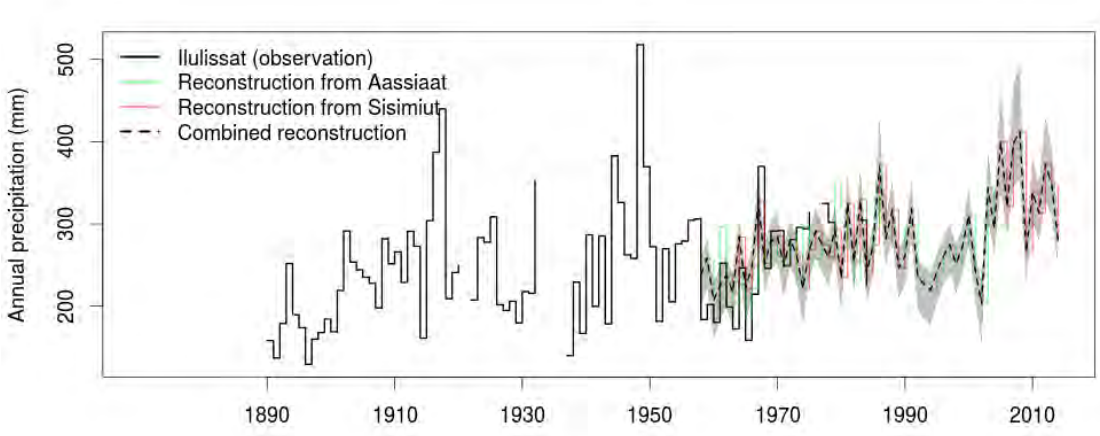

Figure 10: Reconstruction of observed precipitation in Ilulissat with observations from Aasiaat (green) and Sisimiut (red) and Aasiaat and Sisimiut combined (black dashed line). The prediction interval for the combined reconstruction is indicated with the grey shaded area.

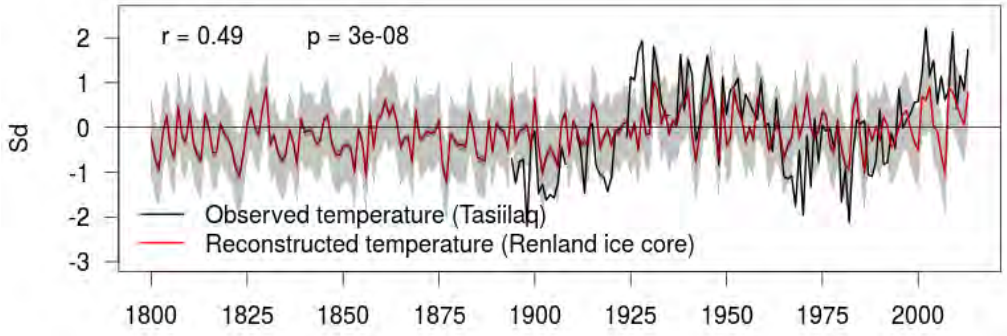

5

Figure 11: Reconstructed annual mean temperature (1800-2014) from Tasiilaq based on δ18O records from the Renland ice core (upper plot). The reconstructed time series (red) is significantly correlated with the observed time series (black) with r = 0.49 and p-value < 0.05. Grey shaded areas correspond to the 66% prediction interval for each reconstructed value and the dark shaded area close to the reconstructed curve is the confidence interval of the regression line.

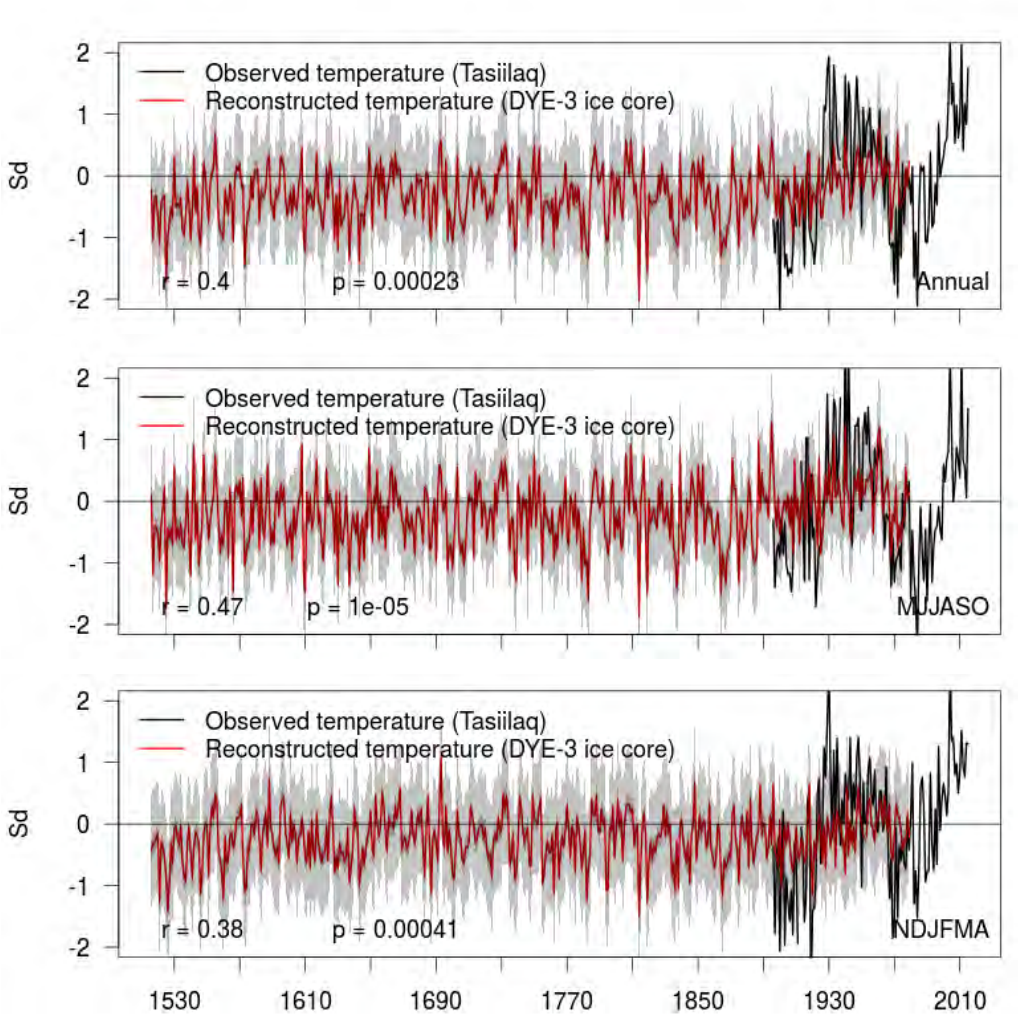

Figure 12: 500-year reconstructed temperature from Tasiilaq based on δ18O records from the DYE-3 ice core for annual mean (top), summer (mid) and winter (bottom). The reconstructed time series (red) is significantly correlated with the observed time series (black) with r = 0.40, r = 0.47 and r = 0.38 and p-value < 0.05 for annual, summer and winter. Grey shaded area corresponds to the 66% prediction interval for each reconstructed value.

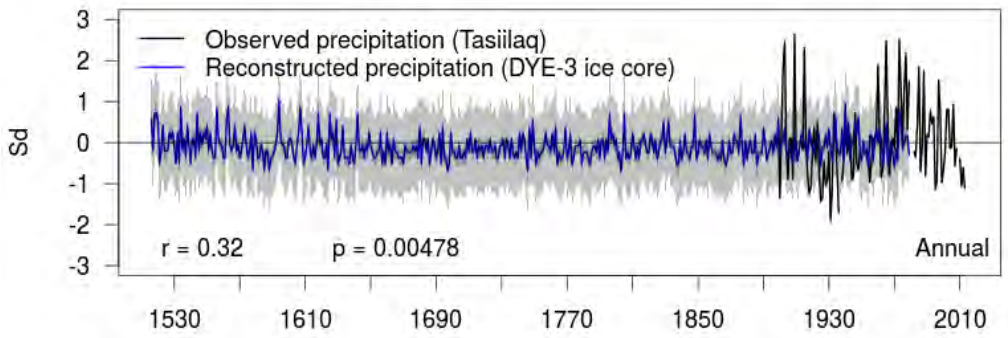

Figure 13: Reconstructed annual accumulated precipitation time series from Tasiilaq based on δ18O data from DYE-3 ice core for 1514-2014. The reconstructed time series (red) is significantly correlated with the observed time series (black) with r = 0.32 and p-value < 0.05. Grey shaded areas correspond to the 66% prediction interval for each reconstructed value.

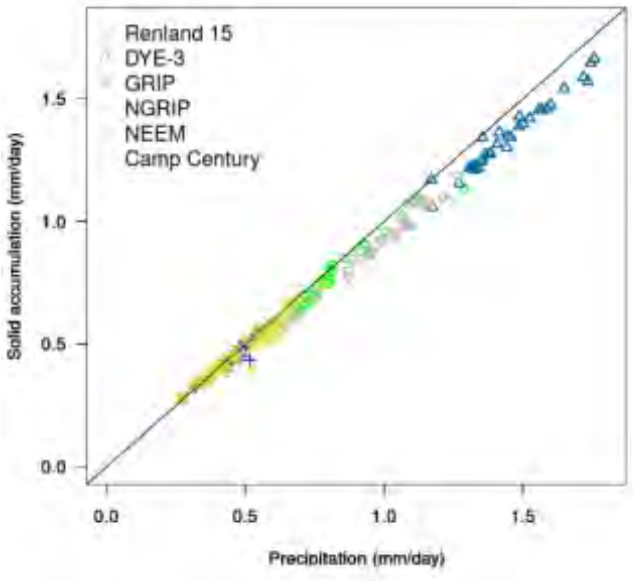

Figure 14: Relationship between HIRHAM5 modelled solid accumulation minus evaporation and annual precipitation for the 35-year time period (1980-2014) for the nearest grid point to the six deep ice core drill site locations.

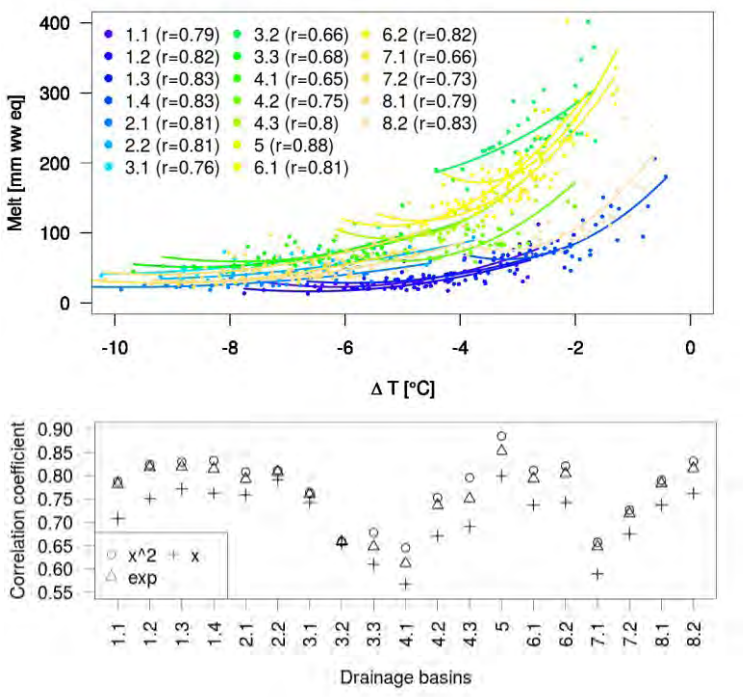

Figure 15: Relationships between HIRHAM5 modelled melt and summer temperatures (1980-2014) for each drainage basin are shown separately with second order regression functions (top right). Correlation coefficients for the linear, second order polynomial and exponential regression functions are compared for each drainage basin (Zwally et al., 2012), (bottom right).

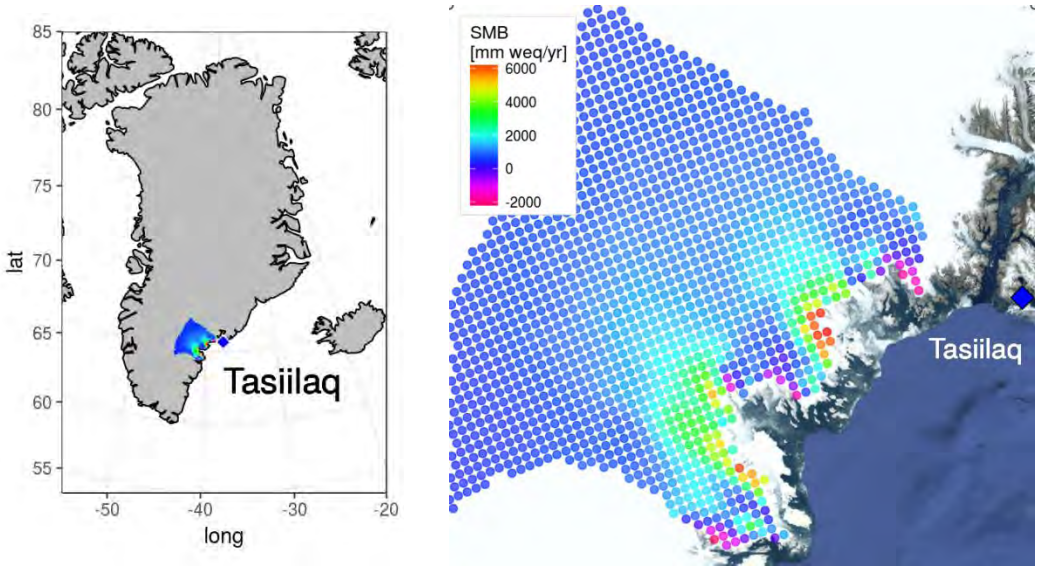

Figure 16: Drainage basin 4.2 (Zwally et al., 2012) showing annual mean SMB (1980-2014) simulated with HIRHAM5. The Tasiilaq weather station is indicated with a blue diamond.

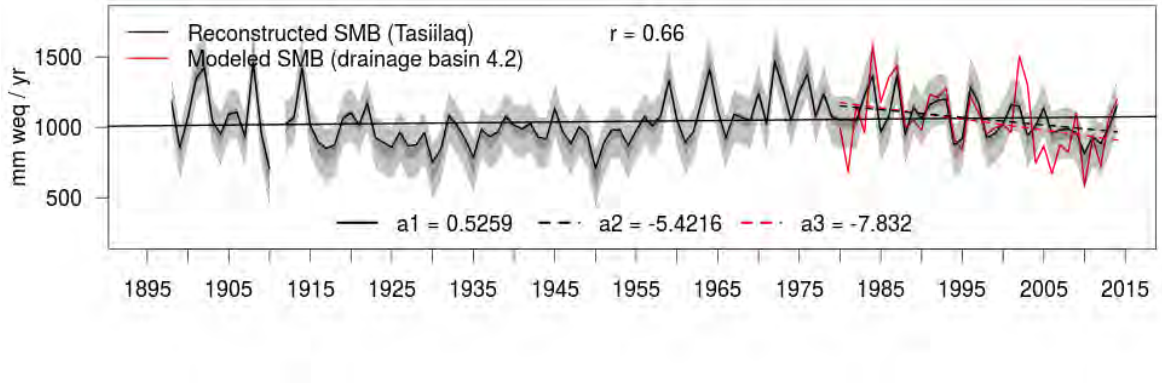

Figure 17: Reconstructed SMB for Tasiilaq (basin 4.2) for 1898-2014 (black line), HIRHAM5-simulated SMB for the drainage basin 4.2 from 1980-2014 (red). Confidence interval (dark grey) and prediction interval (light grey) are added the reconstructed SMB curve. The values a1, a2 and a3 are slopes of the regression lines.

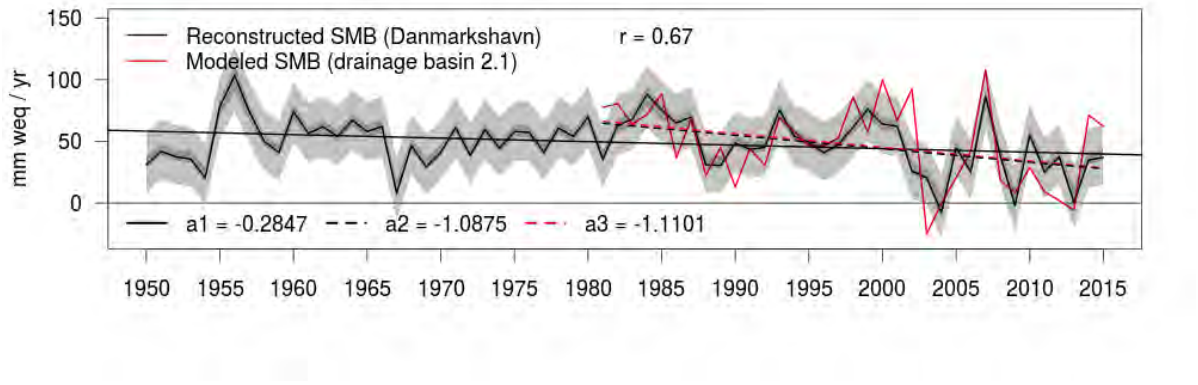

Figure 18: Reconstruction of simulated SMB for Danmarkshavn (drainage basin 2.1). The confidence interval for the regression line is shown as dark shaded area, and the prediction interval is light shaded area. The correlation coefficient between the reconstructed time series (black curve) and the simulated time series (red curve) is r = 0.67 for the overlapping period 1980-2014. The values a1, a2 and a3 are slopes of the regression lines.

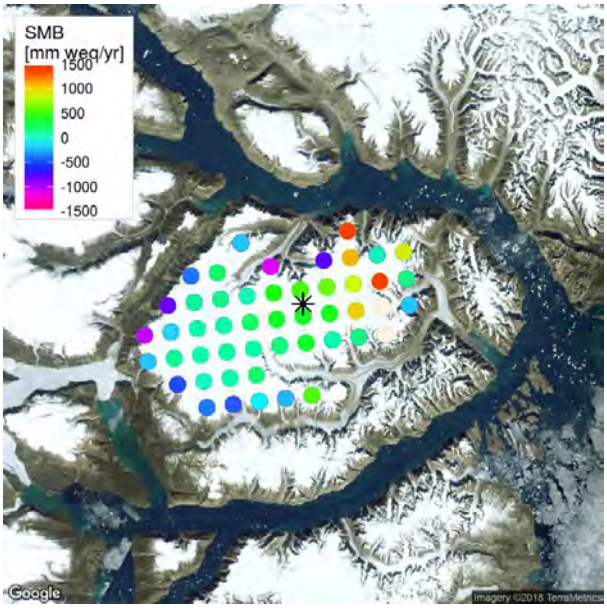

Figure 19: Annual mean SMB (1980-2014) simulated with HIRHAM5 on the Renland ice sheet in mm weq/yr. The black star indicates the ice core drill site location.

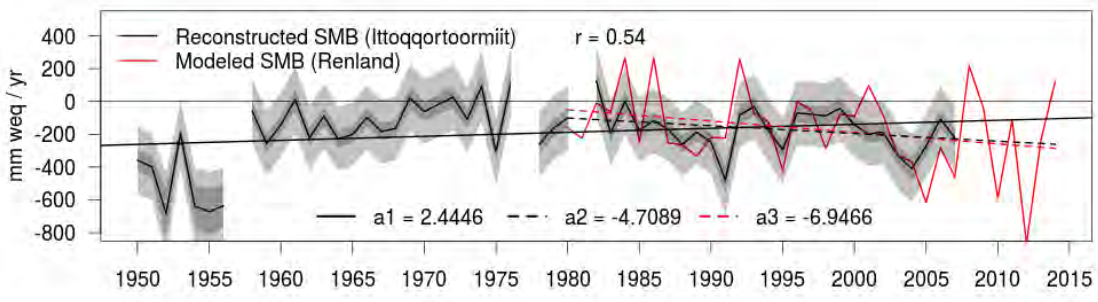

Figure 20: Reconstruction of SMB for the Renland ice cap for 1950-2007 (black line), modelled SMB from 1980-2014 (red). Confidence interval (dark grey) and prediction interval (light grey) are added to the SMB reconstruction. The values a1, a2 and a3 are slopes of the regression lines.

5

	Pearson's r	Slope a1	Slope a2	Slope a3
Tasiilaq	0.66	0.53	-5.42	-7.83
Danmarkshavn	0.67	-0.28	-1.09	-1-11
Renland	0.54	2.44	-4.71	-6.95

Table 1: Correlation coefficients between reconstructed and HIRHAM5-simulated SMB and regression line slopes for the full reconstructed SMB period (a1) and for 1980-2014 for the reconstructed SMB (a2) and simulated SMB (a3).

10

Supplementary figures

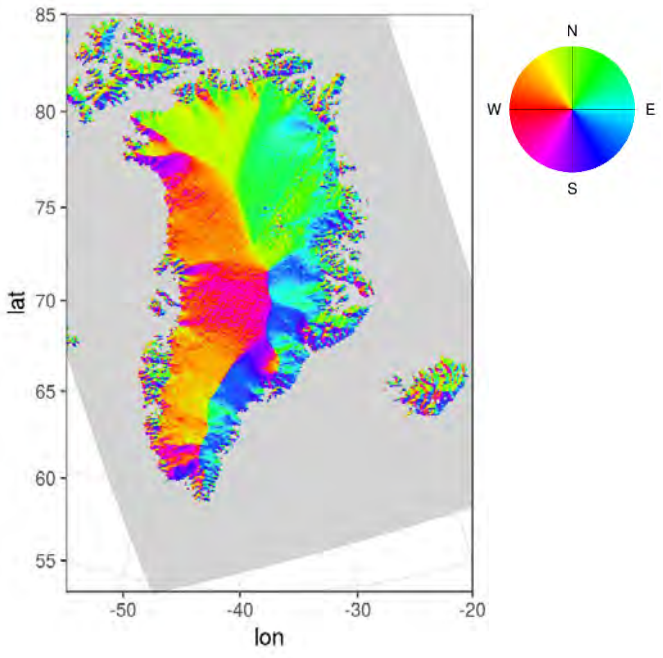

Supplementary Figure S1: Slope direction of the Greenland topography from the HIRHAM5 climatology files. The grey area is the sea-points within the HIRHAM5 simulation domain.

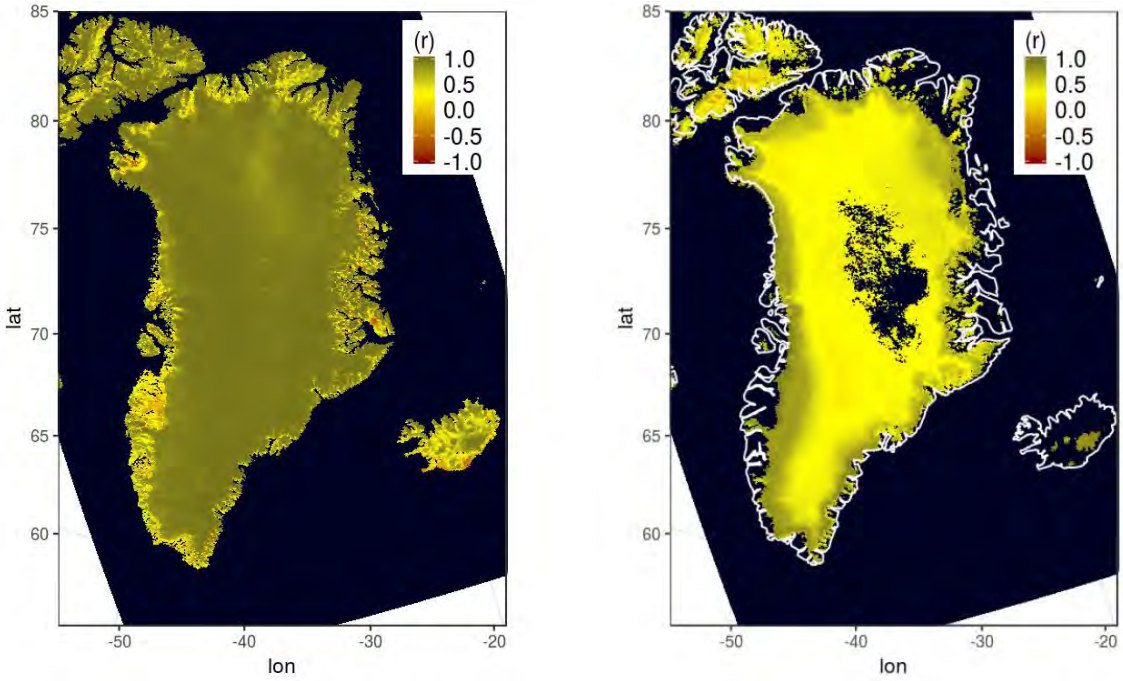

Supplementary Figure S2: Relationship between HIRHAM5 modelled solid accumulation minus evaporation and annual precipitation for 1980-2014 for each grid point in the HIRHAM5 domain (left) and for melt and summer mean temperature (JJA) for each ice covered grid point (right).

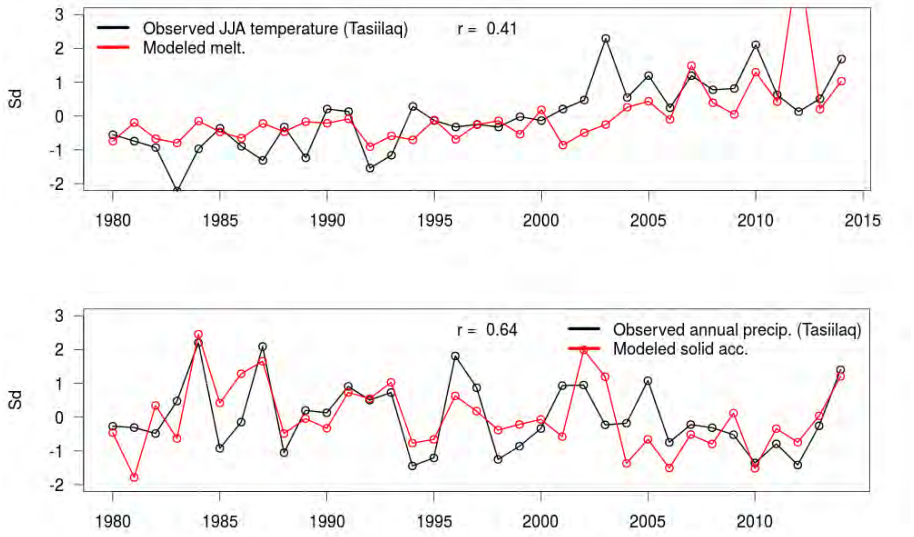

Supplementary Figure S3: Observed summer temperature (JJA) and modelled melt (upper plot) and observed precipitation and modelled solid accumulation (lower plot) for Tasiilaq. All values are standardized to zero mean and one standard deviation.

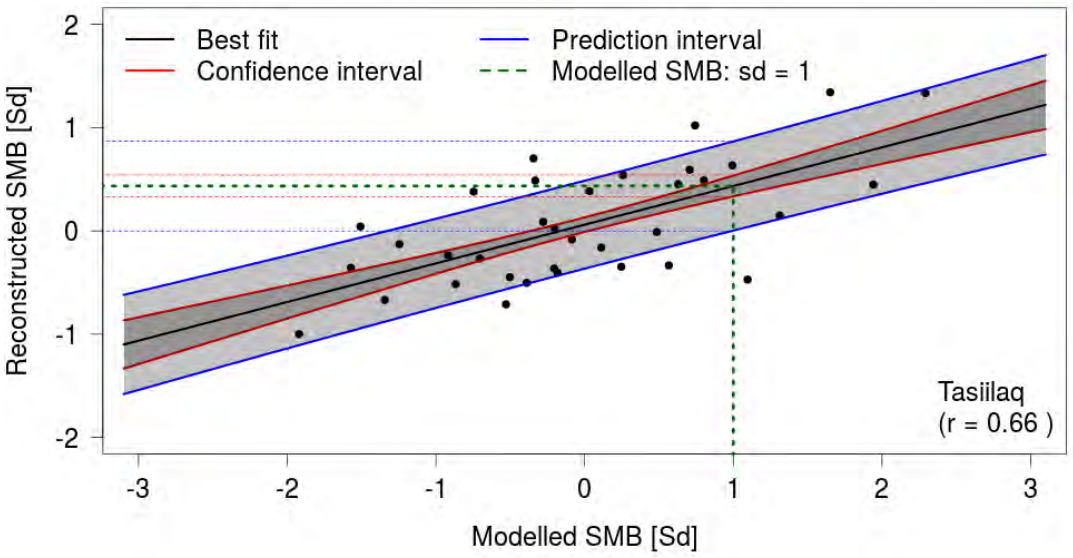

Supplementary Figure S4: Uncertainty estimates of reconstructed SMB. The black line is the best fitted regression line to the reconstructed and modelled SMB. The dark grey shaded area between red lines is the confidence interval for the regression line, and the prediction interval is the light shaded area between the blue lines. Green dashed lines indicate the translation of modelled SMB to reconstructed SMB, including confidence and prediction intervals (red and blue dashed lines).

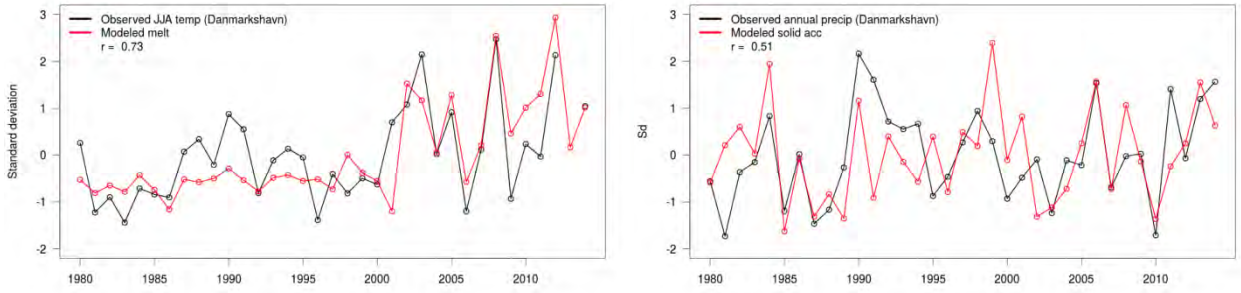

Supplementary Figure S5: Observed summer temperature (JJA) and modelled melt (top) and observed precipitation and modelled solid accumulation (bottom) for Danmarkshavn. All values are standardized with one standard deviation.

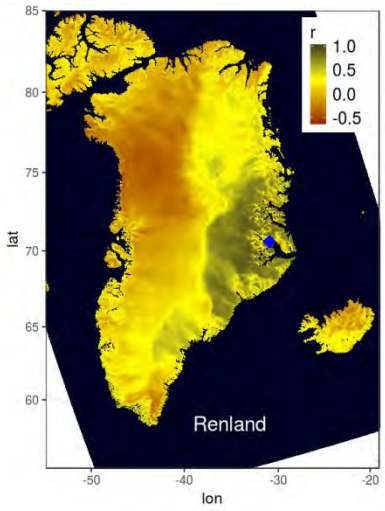

Supplementary Figure S6: Correlation map for HIRHAM5 simulated annual precipitation time series 1980-2014. The map represents correlation coefficients between each land grid point and the grid point closest to the drill site at Renland. Critical correlation coefficient for significance at a 95% confidence level is r = 0.33 (yellow).

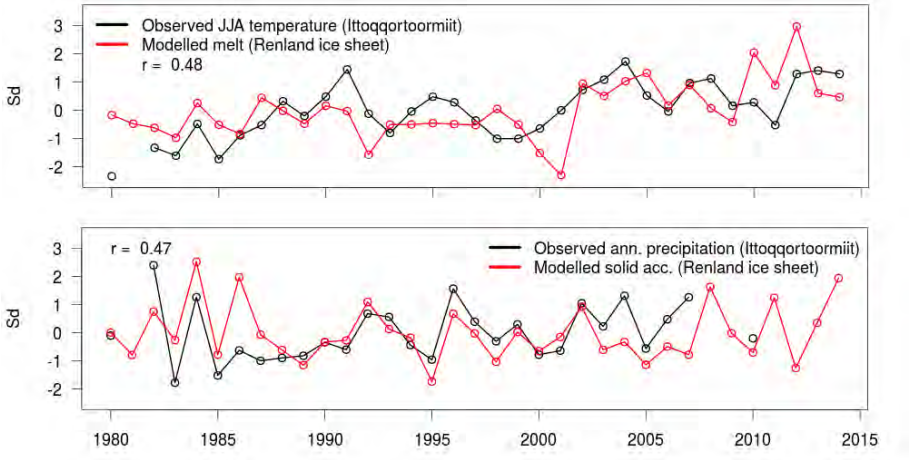

Supplementary Figure S7: Observed summer temperature (JJA) and modelled melt (top) and observed precipitation and modelled solid accumulation (bottom). Observation records come from Ittoqqortoormiit, and model data is from Renland. All values are standardized with one standard deviation.

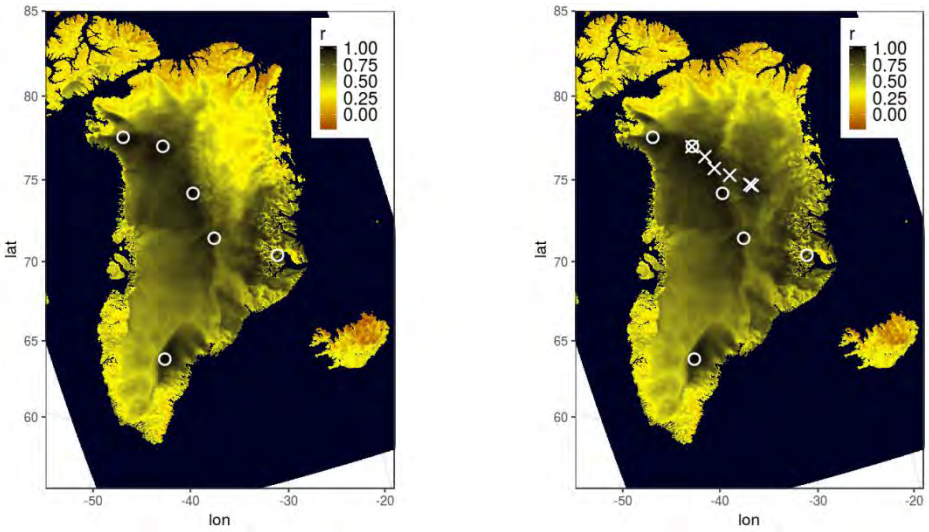

Supplementary Figure S8: Merged solid accumulation correlation maps for the six deep ice core locations (red circles, left) combined with the transverse shallow cores (crosses, right).

Paper III Boberg, F., Langen, P.L., Mottram, R.H., Christensen, J.H., Olesen, M., 2018. 21st-century climate change around Kangerlussuaq, west Greenland: From the ice sheet to the shores of Davis Strait. Arct. Antarct. Alp. Res. 50, S100006. [Published Apr 2018]

Arctic, Antarctic, and Alpine Research

An Interdisciplinary Journal

ISSN: 1523-0430 (Print) 1938-4246 (Online) Journal homepage: http://www.tandfonline.com/loi/uaar20

21st-century climate change around Kangerlussuaq, west Greenland: From the ice sheet to the shores of Davis Strait

F. Boberg, P. L. Langen, R. H. Mottram, J. H. Christensen & M. Olesen

To cite this article: F. Boberg, P. L. Langen, R. H. Mottram, J. H. Christensen & M. Olesen (2018) 21st-century climate change around Kangerlussuaq, west Greenland: From the ice sheet to the shores of Davis Strait, Arctic, Antarctic, and Alpine Research, 50:1, S100006

To link to this article: https://doi.org/10.1080/15230430.2017.1420862

ARCTIC, ANTARCTIC, AND ALPINE RESEARCH
2018, VOL. 50, NO. 1, e1420862 (13 pages)
https://doi.org/10.1080/15230430.2017.1420862

21st-century climate change around Kangerlussuaq, west Greenland: From the ice sheet to the shores of Davis Strait

F. Boberg[a], P. L. Langen[a], R. H. Mottram[a], J. H. Christensen[a,b], and M. Olesen[a]

[a]Danish Meteorological Institute, Copenhagen, Denmark; [b]Niels Bohr Institute, University of Copenhagen, Denmark

ABSTRACT

Using regional climate-model runs with a horizontal resolution of 5.5 km for two future scenarios and two time slices (representative concentration pathway [RCP] 4.5 and 8.5; 2031–2050 and 2081–2100) relative to a historical period (1991–2010), we study the climate change for the Qeqqata municipality in general and for Kangerlussuaq in particular. The climate-model runs are validated against observations of temperature and surface mass balance and a reanalysis simulation with the same model setup as the scenario runs, providing high confidence in the results. Clear increases in temperature and precipitation for the end of the 21st century are shown, both on and off the ice sheet, with an off–ice sheet mean annual temperature increase of 2.5–3°C for the RCP4.5 scenario and 4.8–6.0°C for the RCP8.5 scenario, and for precipitation an increase of 20–30% for the RCP4.5 scenario and 30–80% for the RCP8.5 scenario. Climate analogs for Kangerlussuaq for temperature and precipitation are provided, indicating that end-of-the-century Kangerlussuaq mean annual temperature is comparable with temperatures for the south of Greenland today. The extent of glacial retreat is also estimated for the Qeqqata municipality, suggesting that most of the ice caps south of the Kangerlussuaq fjord will be gone before the end of this century. Furthermore, the high-resolution runs are compared with an ensemble of six models run at a 50 km resolution, showing the need for high-resolution model simulations over Greenland.

ARTICLE HISTORY
Received 6 March 2017
Accepted 2 August 2017

KEYWORDS
Climate change; regional climate modeling; surface mass balance; Kangerlussuaq

Introduction

The climate of the Arctic is in rapid transition, with Greenland and its ice sheet already seeing the impacts of rising regional temperatures, including ice loss of approximately 234 ± 20 Gt yr^{-1} since 2003, contributing about 0.7 mm yr^{-1} to the sea level (Barletta, Sørensen, and Forsberg 2013; Shepherd et al. 2012). Future climate change is likely to continue to have a significant impact on both the ice sheet and adjacent areas, with a consequent effect on global and regional sea levels. The Greenland Ice Sheet contains about 10 percent of global freshwater reserves, sufficient to raise sea level by an average of about 7 m should it melt completely, meaning that the future change of the ice mass is of global concern. Locally, impacts from increasing amounts of ice-sheet mass loss, as well as regional climate change with increased extreme weather events and changes in long-term climate, have implications for infrastructure, industry, and agriculture. Recent work by Christensen et al. (2016) used a combination of global climate models from CMIP5 and high-resolution regional downscaling to determine what the future climate of Greenland will be like and how local inhabitants can best prepare for and adapt to, for example, permafrost degradation, enhanced flooding related to extreme weather events, and high melt rates (Mikkelsen et al. 2016), as well as the implications for fisheries, hunting, and agriculture. Climate change can have unpredictable consequences as, for example, in Greenland, where the length of the growing season is expected to increase during the 21st century, but there are also indications that periods of drought will increase. Both of these processes will affect agricultural productivity, and therefore proper technical solutions will be required to expand current crop production and livestock management, especially in regions further north in Greenland than are currently farmed. The habitable parts of Greenland, with the exception of the most southern locations, are also subject to changes in permafrost conditions. This is particularly an issue around Kangerlussuaq and more generally in the

CONTACT F. Boberg fbo@dmi.dk

Qeqqata municipality located in the discontinuous to continuous permafrost region of west Greenland (Christiansen and Humlum 2000). Here, the permafrost thaw potential has been classified as high (Daanen et al. 2011), which is confirmed by the results presented in Christensen et al. (2016). For these reasons, assessing the future climate of Greenland on both a regional and local scale is important both for infrastructure planning and future development as well as to more widely to identify processes and feedbacks that may affect ice-sheet mass loss.

In this study we focus on a well-populated region (by Greenland standards), with a number of infrastructural challenges on land and a significant area of ice sheet. The region around Kangerlussuaq and Sisimiut, Qeqqata municipality, is home to approximately 10,000 people, about one-fifth of the population of Greenland. The region also has a number of long-running observational datasets both on and off the ice sheet (Oerlemans and Vugts 1993; van den Broeke, Smeets, and van de Wal 2011; van de Wal et al. 2012; van de Wal and Russell 1994). These are useful to assess the performance of models and to allow the development of process-based estimates of expected change. Global climate models (GCMs) are run at institutes worldwide to assess the large-scale effects of global warming and make future projections. With the relatively coarse resolution (100–200 km) of the state-of-the-art GCMs currently in use, Greenland is often modeled as an island covered by ice without accounting for the significant processes occurring at the ice-sheet surface (e.g., Cullather et al. 2014). To resolve the finer details that are more useful for prescribed regions or for complex process studies, regional climate models (RCMs) are useful for dynamically down-scaling these climate projections. In Greenland, the RCMs RACMO (e.g., Ettema et al. 2009; Noël et al. 2016), MAR (e.g., Fettweis et al. 2017, 2013), and PolarMM5 (Burgess et al. 2010) as well as HIRHAM5 (Lucas-Picher et al. 2012) have previously been used for climate research. A comparison of the performance of early versions of these RCMs in Rae et al. (2012) showed some differences in performance. However, analysis by Mottram et al. (2017) and Vernon et al. (2013) shows that these RCMs produce similar values for surface mass balance over the ice sheet as a whole, although with some significant differences in the components of mass balance and in the spatial distribution of these components (e.g., Langen et al. 2015; Van As et al. 2014), partly attributable to different model resolution as well as different ice masks and potentially different parameterization schemes. Here, we focus on validating the HIRHAM5 simulations against observations, excluding a comparison with previous high-resolution downscalings.

More recently, Langen et al. (2015) used a detailed and updated version of RCM HIRHAM5 (Christensen et al. 2006) with high resolution (5.5 km), driven by reanalysis data (ERA-Interim; Dee et al. 2011) covering the whole of Greenland, to estimate the changes in ice-sheet surface mass balance for the drainage basin linked to the Godthåbsfjord. The HIRHAM5 model has been further refined with a number of additions that include a more sophisticated snow scheme suited to accurately capturing albedo feedbacks and processes within the snowpack (see Langen et al. 2017 for details). Also note that the HIRHAM5 model, as with most RCMs, has a fixed topography and does not account for feedback caused by surface elevation changes.

In this study we use the same model setup as in Langen et al. (2017), and force the model with the EC-Earth GCM (Hazeleger et al. 2012) at the lateral boundaries for two different future scenarios (representative concentration pathway [RCP] 4.5 and RCP8.5) and with the historical emissions forcing (Mottram et al. 2017). We run the model transiently for three time periods (1991–2010, 2031–2050, 2081–2100). Comparing the two later time periods with the former, a control period that overlaps with the ERA-Interim reanalysis experiments, we can thus project climate change in the Qeqqata region, both off and on the glacier.

The performance of the HIRHAM5 RCM, driven by the ERA-Interim reanalysis, has been fully evaluated by Langen et al. (2015, 2017) and by Mottram et al. (2017), showing that the ice sheet is well represented during present-day conditions with a surface mass balance in the ablation area close to observations but with an underestimation of the interannual variability of the number of melt days. We here use weather station observations to also evaluate the performance of the HIRHAM5 when forced with the EC-Earth historical scenario in order to validate the use of the EC-Earth GCM as forcing at the lateral boundaries. This gives us valuable insight to interpret the output of the model when forced with future simulations from EC-Earth.

Data

Observations

Monthly means of observed temperature are collected for five locations within the region of study. Cappelen (2016) provided station measurements for Sisimiut and Kangerlussuaq (see Figure 1). Data for the other three locations are as described by van den Broeke et al. (2011), using automatic weather stations (AWS) on the ice sheet

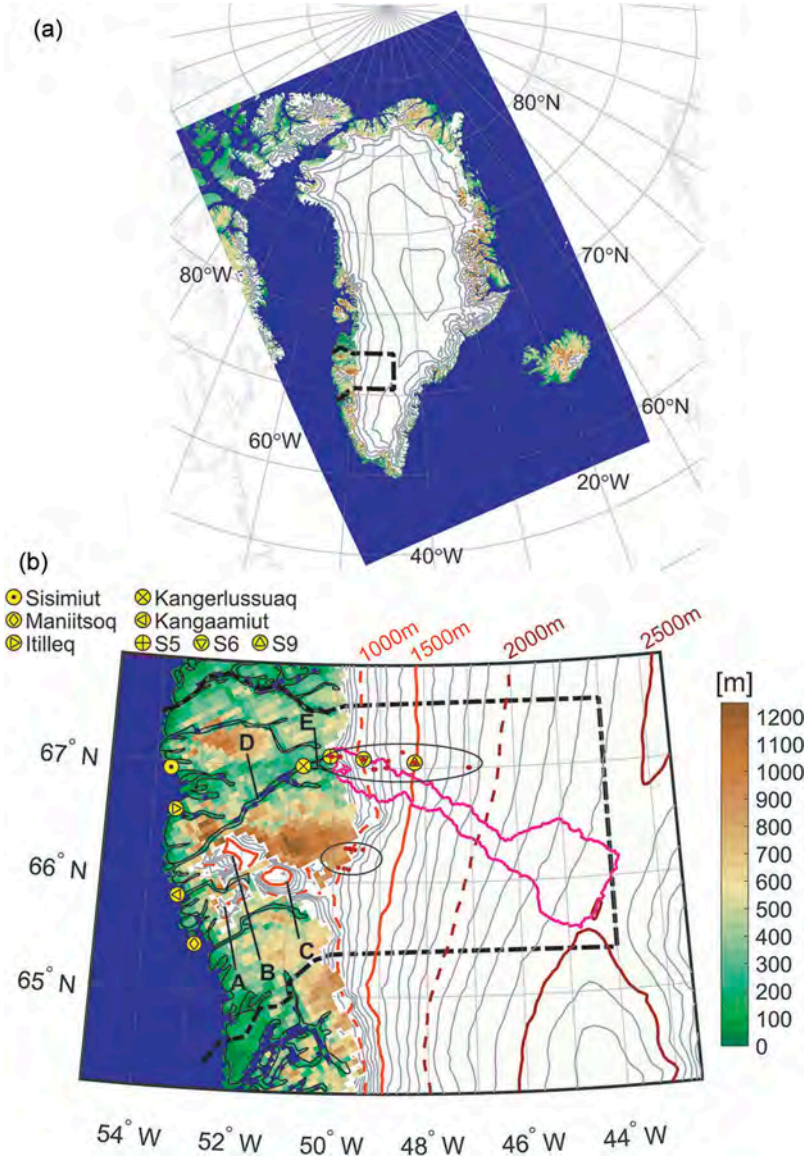

Figure 1. Model orography for the full model domain (a, top) and for the Qeqqata municipality (b, bottom). Sea points are given in blue, glacier-free land points in green/brown, and glacier points in white with added surface elevation contour lines. Also shown are the location of five villages and the S5, S6, and S9 weather stations (van de Wal et al. 2005). Three ice caps are given by letters A, B, and C and are named Qapiarfiup Sermia, Sukkertoppen Ice Cap, and Tasersiap Sermia, respectively. The fjord Kangerlussuaq is given by the letter D, and Watson River by the letter E. The Kangerlussuaq drainage basin is shown in magenta. The location of surface mass balance stations are given as red dots within two black ellipses.

(see Figure 1). These AWS are at surface elevations of 490 (S5), 1,020 (S6), and 1,520 m a.s.l. (S9) at distances of 6, 38, and 88 km from the ice-sheet margin, respectively.

Because the runoff of from the ice sheet is important for the local infrastructure (Mikkelsen et al. 2016), we estimate the amount of glacial freshwater input to the Watson River. For this calculation we use the drainage basin definition (see Figure 1) from Lindbäck et al. (2014, 2015), who used a single-direction flow algorithm and surface analysis in order to derive a drainage catchment on the hydraulic potential surface.

Models

HIRHAM5 (Christensen et al. 2006) is an RCM consisting of the dynamic core of the numerical weather forecast model HIRLAM together with the physics scheme from the GCM ECHAM. Compared with the HIRHAM5 version described in Christensen et al. (2006), a dynamic snow/ice scheme together with an updated snow/ice albedo scheme have been included in the model runs used in this study (see Langen et al. 2015, 2017 for details).

Table 1. List of all available CORDEX ARC-44 GCM-driven simulations used for comparison with the high-resolution run for Greenland.

	GCMs				
RCMs	CCCma-CanESM2	ICHEC-EC-EARTH	NCC-NorESM1-M	MPI-M-MPI-ESM-LR	Reference
DMI-HIRHAM5		x			Christensen et al. (2006)
SMHI-RCA4	x	x	x	x	Samuelsson et al. (2011)
MGO-RRCM				x	Shkolnik et al. (2007)

In this study, the HIRHAM5 RCM is forced at the boundaries by EC-Earth (Hazeleger et al. 2012). The Earth system model (ESM) EC-Earth is based on the operational seasonal forecast system of the European Centre for Medium-Range Weather Forecasts (ECMWF), but with an interactive atmosphere-ocean-sea ice coupling applied across the entire globe. When compared to other coupled models with similar complexity, the model performs well in simulating tropospheric fields and dynamic variables (Hazeleger et al. 2012). However, EC-Earth has a 2°C cold bias over the Arctic with an overestimation of sea-ice extent and thickness (Koenigk et al. 2013).

Five twenty-one-year time slices, dynamically downscaling the EC-Earth output over Greenland, have been performed. In these downscalings, HIRHAM5 is forced by EC-Earth only at the boundaries every six hours and with sea-ice cover and sea-surface temperatures once per day within the domain. The periods include a historical period (1990–2010), two periods for the RCP4.5 scenario (2030–2050 and 2080–2100), and two periods for the RCP8.5 scenario (2030–2050 and 2080–2100). The first year of each time slice was used as a spin-up and therefore not used, resulting in five twenty-year time slices used in this study. In addition to the online one-year spin-up of atmospheric conditions, we included an offline spin-up of about 100 years, looping over the first decade of each individual time-slice experiment, with focus on the subsurface conditions (Langen et al. 2017). We compare the EC-Earth forced regional downscalings for the historical period 1991–2010, with a simulation forced by ERA-Interim (ERA-I; Dee et al. 2011) but otherwise identical in setup (see Langen et al. 2017).

The HIRHAM5 simulations are validated using the observations given earlier. We also compare our high-resolution runs with a model ensemble consisting of all available CORDEX (Jones, Giorgi, and Asrar 2011) runs for the Artic domain (ARC-44), with a horizontal resolution of 50 km (see Table 1). The CORDEX database includes simulations from four GCMs downscaled with three regional climate models, including the simulations discussed in this article. With a horizontal resolution of 50 km, the CORDEX runs for the Arctic domain are not able to give a reasonable view of the nonglacier areas of Greenland having a clear influence from the ice sheet. We therefore only use the CORDEX data in validating the 5.5 km runs on the ice sheet.

Results

Model validation

Since EC-Earth is a dynamically self-consistent climate model, with variability being out of phase with reality, the regional downscaling over Greenland has to be compared against observations in a statistical sense and not compared month by month. A simple but efficient method is quantile-quantile plots, where model data and observations are ranked individually so that their quantiles are plotted against each other. Figure 2 gives quantile-quantile plots of monthly mean temperatures for the historical EC-Earth run as a function of observed monthly mean temperatures. Note that

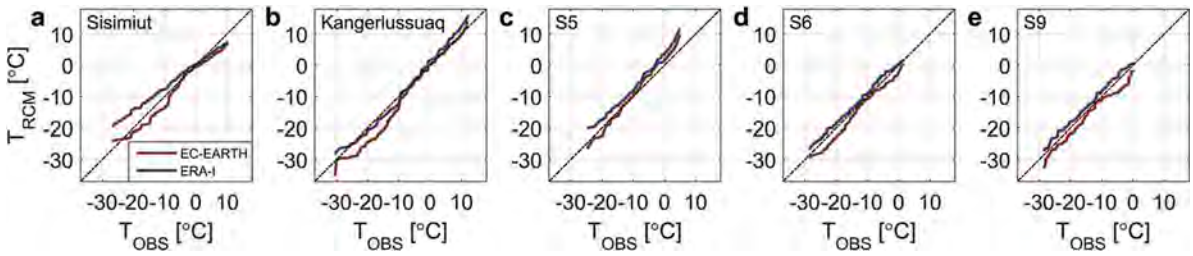

Figure 2. Quantile-quantile plots of monthly mean temperatures (model vs. observations). The global climate model (GCM)-driven historical simulation is shown in red while the ERA-I-driven simulation is shown in blue. Each panel represents a specific location and time period. (a) Sisimiut 1991–2010, (b) Kangerlussuaq 1991–2010, (c) weather station S5 1993–2010, (d) weather station S6 1995–2010, and (e) weather station S9 2000–2010.

the weather station data do not cover the full 1991–2010 period. Also shown are monthly mean temperatures taken from the ERA-I run used in Langen et al. (2017) and Mottram et al. (2017), and we see that the EC-Earth historical downscaling has a close match to observations for monthly mean temperatures, both off (panels A and B) and on (panels C, D, and E) the ice sheet, and it performs at the same level as the ERA-I downscaling.

Machguth et al. (2016) compiled an extensive set of surface mass balance (SMB) observations, with a total of 180 observational records within the Qeqqata municipality, overlapping in time with our experiment (cf. the red dots in the right panel of Figure 1). The individual observations have a very limited time span (from two months to two years), making the observations difficult to compare with the dynamically self-consistent GCM-driven simulations. Figure 3 therefore compares the observed SMBs with the ERA-I-driven simulation SMB only. Although the model shows a clear overestimation (26 percent on average based on the slope of an orthogonal least squares fit) of the rate of ice loss, the linear correlation between the 180 data points is relatively high and the RMSE value for the fitted line is relatively low.

Over the ice sheet, we make area-weighted sums of snowmelt and total runoff for grid points located within the Kangerlussuaq drainage basin (Lindbäck et al. 2014, 2015). As shown in Figure 4, we see a clear difference between the historical EC-Earth-driven run (black) and the ERA-I-driven run (green). For snowmelt, the ERA-I run has an average of 7.3 Gt yr^{-1} for 1991–2010, while the EC-Earth run has an average of 4.8 Gt yr^{-1}. This underestimation of melt is a consequence of a continental and North Atlantic summer cold bias in the driving EC-Earth present-day simulation (Hazeleger et al. 2012). This cold bias leads to downward fluxes of energy (particularly in downwelling longwave radiation) that are smaller than those in the ERA-I-driven run during the melting season (not shown). Nevertheless, the near-surface summer air temperatures in the EC-Earth-driven run at the on-ice stations (Figure 2C–E) are similar to or only slightly lower than those in the ERA-I-driven run because the near-surface air temperatures are kept close to the temperature of the melting surface. Why no cold bias is seen for the warm period in Figure 2B is unclear at this moment.

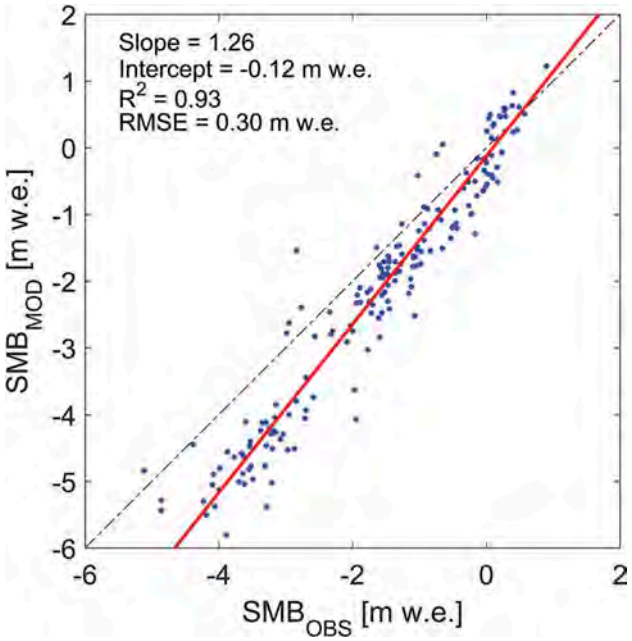

Figure 3. Scatter plot of observed and modeled surface mass balance (SMB) at 180 locations in Qeqqata municipality. An orthogonal linear fit to all data is shown in red together with statistics for the fit in the top left. Note that observations (and model data) cover uneven time periods, ranging from two months to as much as two years.

Climate change off the ice sheet

Figure 5 shows change in temperature (panels A–D) and change in precipitation (panels E–H) for the west part of Qeqqata municipality relative to the 1991–2010 historical period. The change in temperature is relatively uniform for all four individual scenario periods. This we mostly attribute to the similarity of the ice-free surfaces and the vicinity of large-scale homogeneous sources of heat (the ocean) and the ice sheet (cold buffer). At the annual time scale, this large-scale driver of change dominates. Certain topographically induced features show up somewhat more clearly at seasonal or shorter time scales (not shown). As shown in Table 2, we project an increase in annual temperature at the end of the 21st century of about 3°C for the RCP4.5 scenario and an increase of about 5.5°C for the RCP8.5 scenario for west Greenland (global mean values of annual temperature changes for EC-Earth are 2°C and 4°C for RCP4.5 and RCP8.5, respectively; i.e., the regional values using HIRHAM5 are 50% and 40% above the global means for RCP4.5 and RCP8.5, respectively). This increase in temperature will intensify the local/regional water cycle, and in line with the general expected increase in precipitation in the polar regions, Qeqqata will also likely experience an overall increase in precipitation. This change in precipitation is less uniform, as seen in Figure 5E–H, with an intensification of the present-day pattern of rainfall. This pattern largely reflects

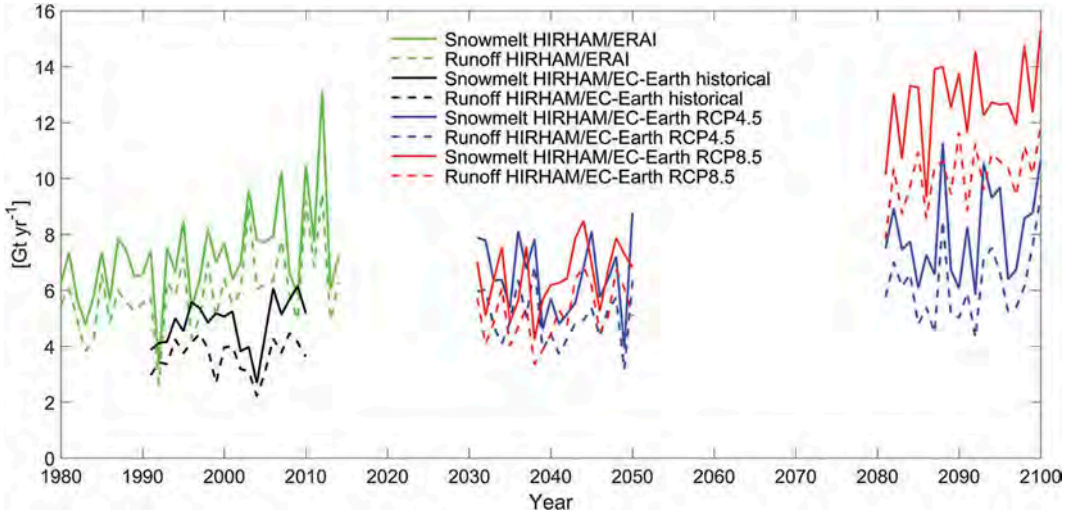

Figure 4. Change in snowmelt (solid lines) and total surface runoff (dashed lines) for the Kangerlussuaq drainage basin for the historical period (black), representative concentration pathway [RCP] 4.5 (blue), and RCP8.5 (red). Also shown, in green, is snowmelt and runoff for the ERA-I-driven run for 1980–2014.

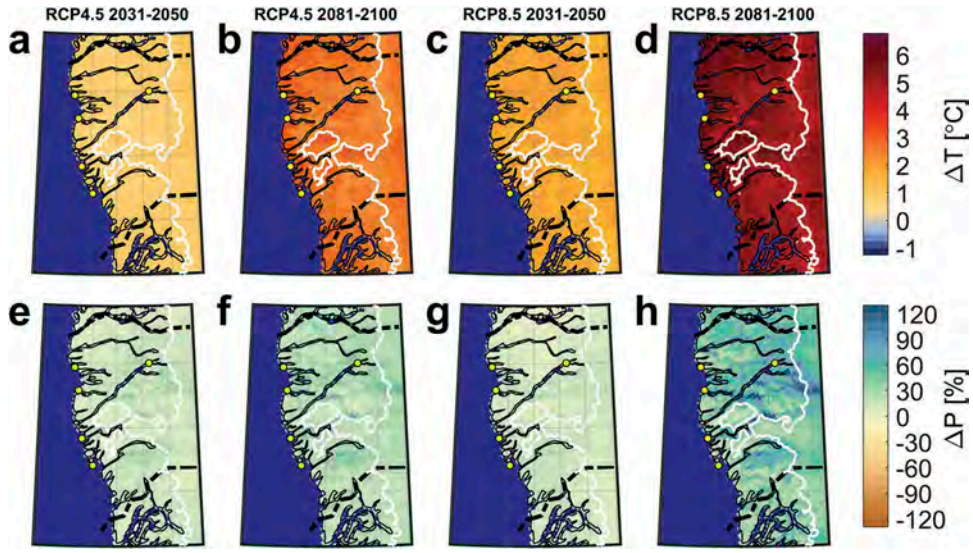

Figure 5. Change in annual temperature and precipitation for western Qeqqata. (a, e) representative concentration pathway [RCP] 4.5 2031–2050 change relative to 1991–2010; (b, f) RCP4.5 2081–2100 change relative to 1991–2010; (c, g) RCP8.5 2031–2050 change relative to 1991–2010; and (d, h) RCP8.5 2081–2100 change relative to 1991–2010. See the Figure 1 caption for an explanation of the yellow markers. The white line outlines the ice sheet.

Table 2. Changes in annual mean temperature and precipitation relative to the 1991–2010 historical period for five locations in Qeqqata.

	RCP4.5 2031–2050		RCP4.5 2081–2100		RCP8.5 2031–2050		RCP8.5 2081–2100	
Location	ΔT (°C)	ΔP (%)	ΔT (°C)	ΔP (%)	ΔT (°C)	ΔP (%)	ΔT (°C)	ΔP (%)
Sisimiut	0.9	11	3.0	28	1.9	15	6.0	40
Kangerlussuaq	0.9	17	2.4	34	2.0	8	4.8	81
Maniitsoq	0.8	12	2.9	23	1.8	16	5.3	34
Kangaamiut	0.8	16	2.9	27	1.8	21	5.5	34
Itilleq	0.9	15	2.8	34	1.9	17	5.6	58

the rugged topography of the region, with the Sukkertoppen Ice Cap and Tasersiap Sermia catching much of the precipitation and Kangerlussuaq lying in its rain shadow. For Kangerlussuaq, at the end of the century we project an increase in precipitation of up to about 300 mm yr^{-1}, with the largest contribution the result of an increase in rainfall. A general shift in the rain/snowfall ratio is seen over most of the land areas of Greenland (not shown, Christensen et al. 2016).

Another way to study the change in temperature and precipitation is to use future climate analogs for these variables. Climate analogs in this part of Greenland can be seen as an attempt to identify what the future climatic setting of the region will look like. Taking the area around Kangerlussuaq as representative for the landscape in this continental climate setting, we can search for locations in present-day climate that already look like the projected future for Kangerlussuaq. Figure 6 shows the annual mean climate analog for Kangerlussuaq for the RCP8.5 scenario. For temperature (panel A), the mid-century analog (orange) is identified with locations close to the Nuuk region, while the end of the century analog (red) is closer to the present-day climate of the Qaqortoq region. Thus, the analog first moves toward the ocean outward from Kangerlussuaq fjord and then southward as the temperature continues to increase. For precipitation (Figure 6B), however, the analog is moving northward and closer to the sea where the annual precipitation amount is about 300 mm higher than the current value for Kangerlussuaq. This is seen as a change from the very dry, Arctic desert-like conditions around Kangerlussuaq to wetter locations, which today can be found north of Kangerlussuaq, where a moist gradient is found seaward of Kangerlussuaq and in particular toward Disko Bay.

While agriculture may extend into these northern regions as a result of warming, the complexity of the climate analogs being quite different for temperature and precipitation suggests that the future conditions in the region will be far different than those currently experienced in the south of Greenland, where agriculture is currently largely confined.

Climate change on the ice sheet

As seen in Figure 4, melt and runoff rates intensify in both scenarios for the Kangerlussuaq drainage basin. The increases are rather modest (~35% for melt and ~38% for runoff in RCP4.5, with similar values for RCP8.5, 36% and 42%, respectively) in the 2031–2050 period, but become much larger toward the end of the century (~67% and ~165% for melt and 70% and 178% for runoff in the RCP4.5 and RCP8.5 runs, respectively). Comparing the end-of-century changes in temperature from the previous section with end-of-century melt rates, we get 22 percent $°C^{-1}$ (67%, 3.0°C) for RCP4.5 and 30 percent $°C^{-1}$ (165%, 5.5°C) for RCP8.5. These small-area totals agree well with the

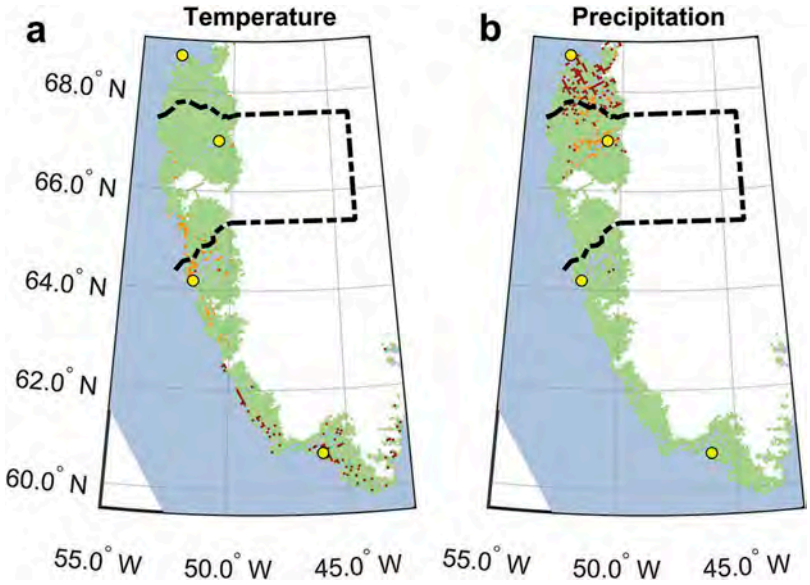

Figure 6. Climate analogs for temperature (a) and precipitation (b) for grid points having an elevation within 200 m compared to the grid point representing Kangerlussuaq using the representative concentration pathway [RCP] 8.5 scenario only. For temperature, the orange color represents areas that for the 1991–2010 historical period have annual mean temperatures close to (±0.25°C) the annual mean temperature of Kangerlussuaq for the RCP8.5 scenario 2031–2050. Similarly, red color is for the RCP8.5 2081–2100 period. For precipitation, the interval is ±25 mm yr^{-1}. The yellow symbols (from north to south) mark the location of Aasiaat, Kangerlussuaq, Nuuk, and Qaqortoq.

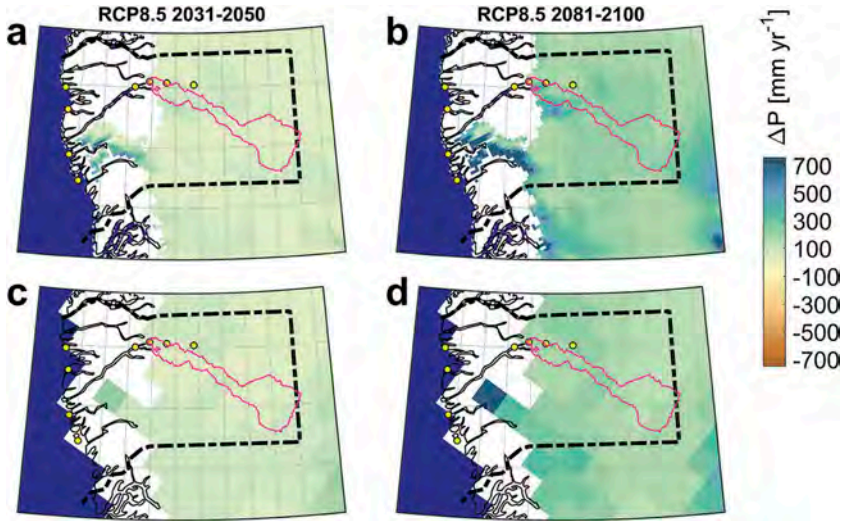

Figure 7. Change in precipitation for model glacier grid points in Qeqqata using the 5.5 km simulation (a, b) compared with the ensemble median for the 50 km CORDEX Arctic runs (c, d). (a, c) representative concentration pathway [RCP] 8.5 2031–2050 change relative to 1991–2010; (b, d) RCP8.5 2081–2100 change relative to 1991–2010. The Kangerlussuaq drainage basin is shown in magenta. See the Figure 1 caption for an explanation of the yellow markers.

Greenland-wide total of 30 percent $°C^{-1}$ found by Fettweis et al. (2008). With average melt and runoff rates doubled or tripled in the RCP8.5 scenario, massive melt and flooding events such as those affecting the Watson River in 2012 (Mikkelsen et al. 2016) will become quite common. Even in the RCP4.5 scenario, several spikes comparable to the ERA-I-driven 2012 value occur when taking into account the 2.4 Gt yr^{-1} offset between the two present-day references.

In Figure 7, we compare our RCP8.5 scenario experiments (minus the historical period) with a 5.5 km horizontal resolution with an ensemble median of the currently available 50 km resolution CORDEX Arctic runs for the Qeqqata region. The change in annual precipitation is of the same magnitude for the 5.5 km simulations as for the 50 km ensemble median, but the details given by the 5.5 km simulations far exceed the 50 km median. We note in particular the clear north-south gradient in the precipitation signal for Sukkertoppen Ice Cap and neighboring east-west-oriented glaciers, seen both in the near term as well as in the end-of-century time slice. Similarly, a topographically induced local enhancement at the southern end of the Watson River drainage basin is a unique feature because of the higher resolution (compare also with Figure 1). Similar plots as in Figure 7 were also made using temperature data (not shown) showing a close resemblance between the 5.5 km simulation and the 50 km ensemble median.

Figure 8 shows the change in SMB for RCP4.5 (panels A and B) and for RCP8.5 (panels C and D) relative to the historical run. For the mid-century time slice (panels A and C) the change is comparable for both scenarios, with values close to −0.5 m yr^{-1} west of 48°W. East of 48°W the SMB change is positive but close to zero. For the end-of-century time slice (panels B and D), the difference in temperature change (cf. Figure 5) and increased runoff rates (Figure 4) are clearly reflected in the SMB change. For the RCP8.5 scenario, the area with a negative change in SMB (the ablation area) is clearly expanding higher up on the ice sheet, and the low-elevation value changes by as much as −2 m yr^{-1}.

The effect of this drastic change in SMB on the ice sheet is estimated as shown in Figure 9. By fitting a second-degree polynomial to annual SMB values for the two time slices for the RCP8.5 scenario relative to the historical period, we estimate the cumulative change in SMB for the 2011–2100 period. Here, we interpret this cumulative change in SMB as a change in ice-sheet thickness (in a manner similar to what was done in the final sensitivity experiments in Fettweis et al. 2013). If the resulting surface lowering exceeds the ice-sheet thickness (Morlighem et al. 2014) for a specific grid cell, that grid cell is then shown as a nonglacial grid cell in Figure 9. The most clear effect of ice-sheet retreat in this region is seen for the three ice caps located south of the Kangerlussuaq fjord (Sukkertoppen Ice Cap, Tasersiap Sermia, and Qapiarfiup Sermia). Here we assume, for the sake of simplicity and illustration, that (1) changes in ice flow are negligible, such that increased outward flow is unable to counter the SMB-driven surface lowering, and (2) the area was

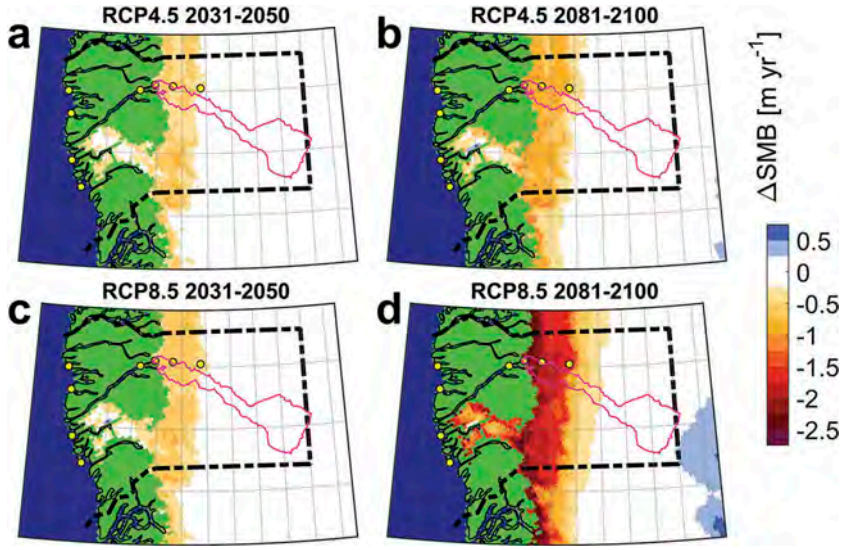

Figure 8. Change in surface mass balance for model glacier grid points in Qeqqata. (a) Representative concentration pathway [RCP] 4.5 2031–2050 change relative to 1991–2010; (b) RCP4.5 2081–2100 change relative to 1991–2010; (c) RCP8.5 2031–2050 change relative to 1991–2010; and (d) RCP8.5 2081–2100 change relative to 1991–2010. The Kangerlussuaq drainage basin is shown in magenta. See the Figure 1 caption for an explanation of the yellow markers.

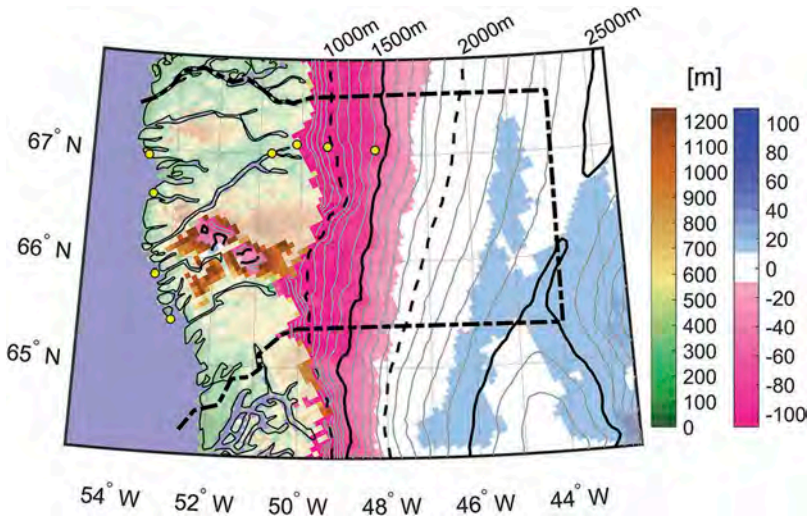

Figure 9. Glacial retreat in Qeqqata for the representative concentration pathway [RCP] 8.5 2081–2100 scenario relative to the 1991–2010 historical period, assuming that changes in ice flow are negligible and that the area was in equilibrium during the 1991–2010 reference period. Nonglacier grid cells during the historical period are shown in transparent green/brown colors. Glacier grid cells during the historical period that become nonglacier during the RCP8.5 scenario are shown in nontransparent green/brown colors. For grid cells that are glacier during all of the scenario period, the magenta/blue color map represents the change in elevation, while the contour lines give the elevation at the end of the 21st century. See the Figure 1 caption for an explanation of the yellow markers.

in equilibrium during the 1991–2010 reference period. Changes in ice flow, if included, would likely decrease our estimates of surface lowering by increasing the amount of mass moved from the ice-sheet interior toward the margin. Alternatively, the 1991–2010 period was most likely not in equilibrium (Colgan, Thomsen, and Citterio 2015a) and the addition of this reference-period imbalance would further increase our surface-lowering estimates. On the Sukkertoppen Ice Cap in particular, there is little potential for increased flow to counter the SMB-driven retreat.

Discussion

In Figure 2B (Kangerlussuaq), when comparing simulated and observed monthly mean temperatures, we note an offset for the cold period where the EC-Earth

simulation is about 4°C lower than observations, but when the monthly mean temperature is above −10°C the model values show a very close match to observations. We also note that for Sisimiut (Figure 2A), located close to the sea, the slope of the ERA-I curve is relatively far from unity, suggesting a damping effect from the sea. Overall, the EC-Earth-driven run is colder than the ERA-I-driven run. This suggests that the reason for the better agreement in the EC-Earth-driven run may be for the wrong reasons; HIRHAM is unable to get very cold at a coastal grid point, unless the sea is fully ice covered.

The offset between the two present-day runs (EC-Earth historical and ERA-I driven) in Figure 4 illustrates the importance of referencing downscaled future scenarios with corresponding present-day runs. In this case we compare the EC-Earth-driven scenarios relative to the corresponding EC-Earth-driven present-day run; although, when doing so, one implicitly ignores potential nonlinearities whereby the magnitude of climate change can depend on the reference state (e.g., Boberg and Christensen 2012; Fettweis et al. 2013).

In this study we have analyzed high-resolution climate projections in detail to determine the likely future effects of climate change on the Qeqqata region of west Greenland. The detail provided by the high-resolution simulations is complemented by the consistency in the climate output by the available regional climate models for this region. This combination of CORDEX data and HIRHAM5 downscaling is particularly powerful for picking up local effects not otherwise captured. Of the higher-resolution models previously run for Greenland, the results are certainly comparable.

Given the very large area covered by glacier ice in this region it is unsurprising that many of the effects are seen initially in the glaciers of the region. In particular, the retreat and near disappearance of the small local ice caps in this region by the end of the century under the high-emissions scenario will have a substantial effect on the geography of the region. The increase in melt and runoff across the ice sheet is also likely to have a significant effect in river catchments such as the Watson River, which flows through Kangerlussuaq. This work suggests, therefore, that careful planning is necessary to ensure that infrastructure can withstand future extreme events that will likely become more common. Similarly, higher meltwater discharge into the fjords in this region may also have an effect on fisheries (e.g., Swalethorp et al. 2016) and needs to be taken into account.

There are few realistic analogs at the present day in Greenland for the warmer and relatively wetter climate around Kangerlussuaq, which suggests that narratives around the extension of agricultural productivity or naive approximations of ecosystem changes may be flawed. Much more work must be done by agronomists and ecologists to determine the likely impact of these projected changes on the ecosystem, wildlife, and the potential for agricultural development in this region. Alternatively, the retreat of the ice caps does provide much greater possibilities for the development of mineral resources, such as the Isua iron-ore mining prospect (Colgan et al. 2015b). The sustained increase in melt also provides an opportunity for the development of hydropower resources in this region that could provide significant power for both industrial and domestic applications (Ahlstrøm et al. 2008).

At the same time, it is notable that for the high-resolution simulations presented here, the changes in surface mass balance and both snow and ice melt scale linearly according to emissions. This suggests that, for surface mass loss processes at least, the impact of climate change on the ice sheet can still be mitigated by reductions in greenhouse gas emissions and/or content in the atmosphere. Finally, we should note that although we have focused on Qeqqata municipality in west Greenland, much of this study is relevant for many other areas, particularly in western Greenland. The retreat of the ice caps south of the fjord Kangerlussuaq is consistent with modeling by several groups focused on small glaciers and ice caps globally (e.g., Radić et al. 2014; Huss and Hock 2015; Marzeion, Jarosch, and Hofer 2012), suggesting that many of the small local glaciers will disappear from Greenland before the end of the 21st century, particularly under the high emissions RCP8.5 scenario.

The disappearance of these glaciers and the substantial retreat of the ablation zone in this area also pose a challenge to climate and ice-sheet models. The orography of the region will change substantially, potentially changing the local surface mass budget. In large-scale regional climate models such as HIRHAM5, the ice mask and topography are kept constant, and estimates of full Greenland surface mass balance may also therefore mislead. There are a number of conflicting errors. First, areas that become ice free are still counted within the surface mass budget. Second, lower elevation because of melting can enhance further melt as a feedback. Third, the ice-sheet surface slope may steepen because of the increased melt and precipitation, leading to enhanced orographic uplift and precipitation. Outside of uncoupled climate/ice-sheet models, these processes are not accounted for and there may therefore be significant uncertainties in SMB as a result.

The fact that the overall level of change in precipitation (see Figure 7) is a good match between the

HIRHAM5 5.5 km simulations and the CORDEX 50 km median change indicates that the detailed changes in the very high-resolution simulation may offer clear added value compared to coarser-resolution simulations, particularly in the complex outline of terminating glacier outlets such as for the Watson River drainage basin. However, the low density of observations in Greenland makes it difficult to statistically assess if there is an improvement in precipitation gained from higher-resolution modeling, as suggested by, for example, Lucas-Picher et al. (2012), but assessment of high-resolution models of Europe unambiguously demonstrate a significant improvement in precipitation (e.g., Prein et al. 2015). The improvement shown by Prein et al. (2015) is attributed to improved representation of orography, an improvement that is also shown in the 5.5 km simulations for Greenland when compared with the CORDEX 50 km simulations.

Conclusion

Using observations of temperature both off and on the ice sheet together with SMB observations for validation, the 5.5 km resolution historical simulation has shown high confidence in the results. The historical simulation has been compared with four scenario runs: two mid-century runs for RCP4.5 and RCP8.5 and two end-of-century runs for RCP4.5 and RCP8.5. Changes in annual mean temperature (precipitation) for five locations are close to 1°C (10–20%) for the mid-century RCP4.5 time period and in the range 2.5–3°C (20–30%) for the end-of-century RCP4.5 scenario. For the RCP8.5 time slices, the changes in temperature (precipitation) are in the range 1.8–2°C (8–20%) and 4.8–6.0°C (30–80%) for mid-century and end-of-century, respectively.

We also searched for locations with a present-day climate comparable with the projected future for Kangerlussuaq using the RCP8.5 scenario. For temperature, the mean climate analog is found close to the Nuuk region for the mid-century period while the end-of-century analog is found in the Qaqortoq region. For precipitation, however, the analog is moving northward and closer to the sea, where the annual precipitation is about 300 mm higher than the present-day value for Kangerlussuaq. When studying climate change on the ice sheet, melt and runoff rates are found to significantly increase for the Kangerlussuaq drainage basin for both scenarios. The increase in melt is 67 percent for the end-of-century RCP4.5 scenario and 165 percent for the end-of-century RCP8.5 scenario. Corresponding values for end-of-century runoff are 70 percent and 178 percent for the RCP4.5 and RCP8.5, respectively, indicating more frequent massive melt and flooding events. Furthermore, when comparing the 5.5 km simulations with available 50 km CORDEX scenario simulations for precipitation on the ice sheet, similar levels of change were found on large scales, but the details given by the 5.5 km simulation suggest added value compared to coarser-resolution simulations.

The future change in SMB was also studied showing an upward expanding ablation zone toward the end of the 21st century for both RCP4.5 and RCP8.5. The cumulative change in SMB is furthermore used in an attempt to estimate ice-sheet retreat in Qeqqata municipality, suggesting that the majority of the ice caps south of the fjord Kangerlussuaq will be gone by the end of this century.

Acknowledgments

The authors thank the two anonymous reviewers whose comments and suggestions helped improve and clarify this manuscript. The authors would also like to thank Katrin Lindbäck for providing the subglacial catchment area and Paul Smeets and the Institute for Marine and Atmospheric Research, Utrecht University (UU/IMAU), for providing the AWS data. We acknowledge the World Climate Research Programme's Working Group on Regional Climate, and the Working Group on Coupled Modelling, former coordinating body of CORDEX and responsible panel for CMIP5. We also thank the climate modeling groups (listed in Table 1) for producing and making available their model output.

Funding

The research leading to these results has received funding from the European Research under the European Community's Seventh Framework Programme (FP7/ 2007-2013)/ERC grant agreement 610055 as part of the ice2ice project, from the Danish Cooperation for Environment in the Arctic (DANCEA) under the Danish Energy Agency as part of the project "Datagrundlag for klimatilpasningsindsatsen I Grønland," and by Nordic Centers of Excellence eSTICC (eScience Tool for Investigating Climate Change in northern high latitudes) funded by Nordforsk grant 57001.

References

Ahlstrøm, A. P., R. Mottram, C. Nielsen, N. Reeh, and S. B. Andersen. 2008. Evaluation of the future hydropower potential at Paakitsoq, Ilulissat, West Greenland. *Danmarks Og Grønlands Geologiske Undersøgelse Rapport* 31:16.

Barletta, V. R., L. S. Sørensen, and R. Forsberg. 2013. Scatter of mass changes estimates at basin scale for Greenland and Antarctica. *The Cryosphere* 7:1411–32. doi:10.5194/tc-7-1411-2013.

Boberg, F., and J. H. Christensen. 2012. Overestimation of Mediterranean summer temperature projections due to model deficiencies. *Nature Climate Change* 2:433–36. doi:10.1038/nclimate1454.

Burgess, E. W., R. R. Forster, J. E. Box, E. Mosley-Thompson, D. H. Bromwich, R. C. Bales, and L. C. Smith. 2010. A spatially calibrated model of annual accumulation rate on the Greenland Ice Sheet (1958–2007). *Journal of Geophysical Research* 115:1–14. doi:10.1029/2009JF001293.

Cappelen, J. 2016. *Weather observations in Greenland 1958–2015*. Danish Meteorological Institute Technical Report 16-08, Danish Meteorological Institute, Copenhagen.

Christensen, J. H., M. Olesen, F. Boberg, M. Stendel, and I. Koldtoft. 2016. *Fremtidige klimaforandringer I Grønland: Qeqqata Kommune*. Danish Meteorological Institute Technical Report 15-04, Danish Meteorological Institute, Copenhagen.

Christensen, O. B., M. Drews, J. H. Christensen, K. Dethloff, K. Ketelsen, I. Hebestadt, and A. Rinke. 2006. *The HIRHAM regional climate model, version 5*. Danish Meteorological Institute Technical Report 06-17, Danish Meteorological Institute, Copenhagen.

Christiansen, H. H., and O. Humlum. 2000. Permafrost, *Topografisk Atlas Grønland*, ed. B. H. Jakobsen, J. Böcher, N. Nielsen, R. Guttesen, O. Humlum, and E. Jensen, 32–35. Copenhagen: C. A. Reitzets Forlag.

Colgan, W., J. Box, M. Andersen, X. Fettweis, B. Csatho, R. Fausto, D. van As, and J. Wahr. 2015b. Greenland high-elevation mass balance: Inference and implication of reference period (1961–90) imbalance. *Annals of Glaciology* 56:105–17 doi:10.3189/2015AoG70A967.

Colgan, W., H. Thomsen, and M. Citterio. 2015a. Unique applied glaciology challenges of proglacial mining. *Geological Survey of Denmark and Greenland Bulletin* 33:61–64.

Cullather, R. I., S. M. J. Nowicki, B. Zhao, and M. J. Suarez. 2014. Evaluation of the surface representation of the Greenland Ice Sheet in a general circulation model. *Journal of Climate* 27:4835–56. doi:10.1175/JCLI-D-13-00635.1.

Daanen, R., P. Ingeman-Nielsen, S. S. Marchenko, V. E. Romanovsky, N. Foged, M. Stendel, J. H. Christensen, and K. Hornbech Svensen. 2011. Permafrost degradation risk zone assessment using simulation models. *The Cryosphere* 5:1043–56. doi:10.5194/tc-5-1043-2011.

Dee D. P., S. M. Uppala, A. J. Simmons, P. Berrisford, P. Poli, S. Kobayashi, U. Andrae, M. A. Balmaseda, G. Balsamo, P. Bauer, et al. 2011. The ERA-Interim reanalysis: Configuration and performance of the data assimilation system. *Quarterly Journal of the Royal Meteorological Society* 137:553–97. doi:10.1002/qj.v137.656.

Ettema, J., M. R. van den Broeke, E. van Meijgaard, W. J. van de Berg, J. L. Bamber, J. E. Box, and R. C. Bales. 2009. Higher surface mass balance of the Greenland ice sheet revealed by high-resolution climate modeling. *Geophysical Reserach Letters* 36:L12501. doi:10.1029/2009GL038110.

Fettweis, X., J. E. Box, C. Agosta, C. Amory, C. Kittel, C. Lang, D. van As, H. Machguth, and H. Gallée. 2017. Reconstructions of the 1900–2015 Greenland ice sheet surface mass balance using the regional climate MAR model. *The Cryosphere* 11:1015–33. doi:10.5194/tc-11-1015-2017.

Fettweis, X., B. Franco, M. Tedesco, J. H. van Angelen, J. T. M. Lenaerts, M. R. van den Broeke, and H. Gallée. 2013. Estimating the Greenland ice sheet surface mass balance contribution to future sea level rise using the regional atmospheric climate model MAR. *The Cryosphere* 7:469–89. doi:10.5194/tc-7-469-2013.

Fettweis, X., E. Hanna, H. Gallée, P. Huybrechts, and M. Erpicum. 2008. Estimation of the Greenland ice sheet surface mass balance for the 20th and 21st centuries. *The Cryosphere* 2:117–29. doi:10.5194/tc-2-117-2008.

Hazeleger, W., X. Wang, C. Severijns, S. Ştefănescu, R. Bintanja, A. Sterl, K. Wyser, T. Semmler, S. Yang, B. van den Hurk, et al. 2012. EC-Earth V2.2: Description and validation of a new seamless earth system prediction model. *Climate Dynamics* 39:2611–29. doi:10.1007/s00382-011-1228-5.

Huss, M., and R. Hock. 2015. A new model for global glacier change and sea-level rise. *Frontiers of Earth Science* 3:54. doi:10.3389/feart.2015.00054.

Jones, C., F. Giorgi, and G. Asrar. 2011. The Coordinated Regional Downscaling Experiment: CORDEX, an international downscaling link to CMIP5. *CLIVAR Exchanges* 16:34–40.

Koenigk, T., L. Brodeau, R. G. Graversen, J. Karlsson, G. Svensson, M. Tjernström, U. Willen, and K. Wyser. 2013. Arctic climate change in 21st century CMIP5 simulations with EC-Earth. *Climate Dynamics* 40:2720–42. doi:10.1007/s00382-012-1505-y.

Langen, P. L., R. S. Fausto, B. Vandecrux, R. H. Mottram, and J. E. Box. 2017. Liquid water flow and retention on the Greenland ice sheet in the Regional Climate Model HIRHAM5: Local and large-scale impacts. *Frontiers of Earth Science* 4:110. doi:10.3389/feart.2016.00110.

Langen, P. L., R. H. Mottram, J. H. Christensen, F. Boberg, C. B. Rodehacke, M. Stendel, D. van As, A. P. Ahlstrøm, J. Mortensen, S. Rysgaard, et al. 2015. Quantifying energy and mass flux controlling Godthåbsfjord freshwater input in a 5-km simulation (1991–2012). *Journal of Climate* 28:3694–713. doi:10.1175/JCLI-D-14-00271.1.

Lindbäck, K., R. Pettersson, S. H. Doyle, C. Helanow, P. Jansson, S. S. Kristensen, L. Stenseng, R. Forsberg, and A. L. Hubbard. 2014. High-resolution ice thickness and bed topography of a land-terminating section of the Greenland Ice Sheet. *Earth System Science Data* 6:331–38. doi:10.5194/essd-6-331-2014.

Lindbäck, K., R. Pettersson, A. L. Hubbard, S. H. Doyle, D. van As, A. B. Mikkelsen, and A. A. Fitzpatrick. 2015. Subglacial water drainage, storage, and piracy beneath the Greenland ice sheet. *Geophysical Research Letters* 42:7606–14. doi:10.1002/2015GL065393.

Lucas-Picher, P., M. Wulff-Nielsen, J. H. Christensen, G. Aðalgeirsdóttir, R. Mottram, and S. Simonsen. 2012. Very high resolution in regional climate model simulations for Greenland: Identifying added value. *Journal of Geophysical Research* 117:D02108. doi:10.1029/2011JD016267.

Machguth, H., H. H. Thomsen, A. Weidick, A. P. Ahlstrøm, J. Abermann, M. L. Andersen, S. B. Andersen, A. A. Bjørk, J. E. Box, R. J. Braithwaite, et al. 2016. Greenland surface mass-balance observations from the ice-sheet ablation area and local glaciers. *Journal of Glaciology* 62:861–87. doi:10.1017/jog.2016.75.

Marzeion, B., A. H. Jarosch, and M. Hofer. 2012. Past and future sea-level change from the surface mass balance of glaciers. *The Cryosphere* 6:1295–322. doi:10.5194/tc-6-1295-2012.

Mikkelsen, A. B., A. Hubbard, M. MacFerrin, J. E. Box, S. H. Doyle, A. Fitzpatrick, B. Hasholt, H. L. Bailey, K. Lindbäck, and R. Pettersson. 2016. Extraordinary runoff from the Greenland ice sheet in 2012 amplified by hypsometry and depleted firn retention. *The Cryosphere* 10:1147–59. doi:10.5194/tc-10-1147-2016.

Morlighem, M., E. Rignot, J. Mouginot, H. Seroussi, and E. Larour. 2014. Deeply incised submarine glacial valleys beneath the Greenland Ice Sheet. *Nature Geoscience* 7:418–22. doi:10.1038/ngeo2167.

Mottram, R. H., F. Boberg, P. Langen, S. Yang, C. Rodehacke, J. H. Christensen, and M. S. Madsen. 2017. Surface mass balance of the Greenland ice sheet in the Regional Climate Model HIRHAM5: Present state and future prospects. *Low Temperature Science* 75:1–11.

Noël, B., W. J. van de Berg, H. Machguth, S. Lhermitte, I. Howat, X. Fettweis, and M. R. van den Broeke. 2016. A daily, 1 km resolution data set of downscaled Greenland ice sheet surface mass balance (1958–2015). *The Cryosphere* 10:2361–77. doi:10.5194/tc-10-2361-2016.

Oerlemans, J., and H. F. Vugts. 1993. A meteorological experiment in the melting zone of the Greenland Ice Sheet. *Bulletin of the American Meteorological Society* 74:355–66. doi:10.1175/1520-0477(1993)074<0355:AMEITM>2.0.CO;2.

Prein, A. F., A. Gobiet, H. Truhetz, K. Keuler, K. Goergen, C. Teichmann, C. F. Maule, E. van Meijgaard, M. Déqué, G. Nikulin, et al. 2015. Precipitation in the EURO-CORDEX 0.11 and 0.44 simulations: High resolution, high benefits? *Climate Dynamics* 46:383–412. doi:10.1007/s00382-015-2589-y.

Radić, V., A. Bliss, A. C. Beedlow, R. Hock, E. Miles, and J. G. Cogley. 2014. Regional and global projections of twenty-first century glacier mass changes in response to climate scenarios from global climate models. *Climate Dynamics* 42 (1–2):37–58. doi:10.1007/s00382-013-1719-7.

Rae, J. G. L., G. Aðalgeirsdóttir, T. L. Edwards, X. Fettweis, J. M. Gregory, H. T. Hewitt, J. A. Lowe, P. Lucas-Picher, R. H. Mottram, A. J. Payne, et al. 2012. Greenland ice sheet surface mass balance: Evaluating simulations and making projections with regional climate models. *The Cryosphere* 6:1275–94. doi:10.5194/tc-6-1275-2012.

Samuelsson, P., C. G. Jones, U. Willén, A. Ullerstig, S. Gollvik, U. Hansson, C. Jansson, E. Kjellström, G. Nikulin, and K. Wyser. 2011. The Rossby Centre Regional Climate model RCA3: Model description and performance. *Tellus A* 63:4–23. doi:10.1111/j.1600-0870.2010.00478.x.

Shepherd A., E. R. Ivins, A. Geruo, V. R. Barletta, M. J. Bentley, S. Bettadpur, K. H. Briggs, D. H. Bromwich, R. Forsberg, N. Galin, et al. 2012. A reconciled estimate of ice-sheet mass balance. *Science* 338:1183–1189.

Shkolnik, I. M., V. P. Meleshko, and V. M. Kattsov. 2007. The MGO climate model for Siberia. *Russian Meteorology and Hydrology* 32:351–59.

Swalethorp, R., T. Nielsen, A. Thompson, M. Møhl, and P. Munk. 2016. Early life of an inshore population of West Greenlandic cod *Gadus morhua*: Spatial and temporal aspects of growth and survival. *Marine Ecology Progress Series* 555:185–202. doi:10.3354/meps11816.

van As, D., M. Langer Andersen, D. Petersen, X. Fettweis, J. H. van Angelen, J. T. M. Lenaerts, M. R. M. van den Broeke, J. Lea, C. E. Bøggild, A. P. Ahlstrøm, et al. 2014. Increasing meltwater discharge from the Nuuk region of the Greenland ice sheet and implications for mass balance (1960–2012). *Journal of Glaciology* 60:314–22. doi:10.3189/2014JoG13J065.

van de Wal, R. S. W., W. Boot, C. J. P. P. Smeets, H. Snellen, M. R. van den Broeke, and J. Oerlemans. 2012. Twenty-one years of mass balance observations along the K-transect, West Greenland. *Earth System Science Data* 4:31–35. doi:10.5194/essd-4-31-2012.

van de Wal, R. S. W., W. Greuell, M. R. van den Broeke, C. H. Reijmer, and J. Oerlemans. 2005. Surface mass-balance observations and automatic weather station data along a transect near Kangerlussuaq, West Greenland. *Annals of Glaciology* 42:311–16. doi:10.3189/172756405781812529.

van de Wal, R. S. W., and A. Russell. 1994. A comparison of energy balance calculations, measured ablation and melt-water runoff near Søndre Strømfjord, West Greenland. *Global Planetary Change* 9:29–38. doi:10.1016/0921-8181(94)90005-1.

van den Broeke, M. R., C. J. P. P. Smeets, and R. S. W. van de Wal. 2011. The seasonal cycle and interannual variability of surface energy balance and melt in the ablation zone of the west Greenland ice sheet. *The Cryosphere* 5:377–90. doi:10.5194/tc-5-377-2011.

Vernon, C. L., J. L. Bamber, J. E. Box, M. R. van den Broeke, X. Fettweis, E. Hanna, and P. Huybrechts. 2013. Surface mass balance model intercomparison for the Greenland ice sheet. *The Cryosphere* 7:599–614. doi:10.5194/tc-7-599-2013.

Paper IV Holme, C., Gkinis, V., Lanzky, M., Morris, V., Olesen, M., Thayer, A., Vaughn, B.H., Vinther, B.M., 2018. Varying regional δ18O–temperature relationship in high resolution stable water isotopes from East Greenland. Clim. Past Discuss. 1–26. [in review, 2019]

Clim. Past Discuss., https://doi.org/10.5194/cp-2018-169
Manuscript under review for journal Clim. Past
Discussion started: 13 December 2018

Climate of the Past Discussions
Open Access
EGU

Varying regional δ^{18}O–temperature relationship in high resolution stable water isotopes from East Greenland

Christian Holme[a], Vasileios Gkinis[a], Mika Lanzky[a,b], Valerie Morris[c], Martin Olesen[d], Abigail Thayer[c], Bruce H. Vaughn[c], and Bo M. Vinther[a]

[a]Centre for Ice and Climate, The Niels Bohr Institute, University of Copenhagen, Denmark
[b]Department of Geosciences, University of Oslo, Norway
[c]Institute of Arctic and Alpine Research, University of Colorado Boulder, Boulder, Colorado, USA
[d]Danish Climate Centre, Danish Meteorological Institute, Copenhagen, Denmark

Correspondence: Christian Holme (christian.holme@nbi.ku.dk)

Abstract. This study examines the stable water isotope signal (δ^{18}O) of three ice cores drilled on the Renland peninsula (East Greenland coast). While ice core δ^{18}O measurements qualitatively are a measure of the local temperature history, the δ^{18}O variability actually reflects the integrated hydrological activity that the deposited ice experienced from the evaporation source to the condensation site. Thus, as Renland is located next to a fluctuating sea ice cover, the transfer function used to infer past temperatures from the δ^{18}O variability is potentially influenced by variations in the local moisture conditions. The objective of this study is therefore to evaluate the δ^{18}O variability of ice cores drilled on Renland and examine what amount that can be attributed to regional temperature variations. In the analysis, three ice cores are utilized to create stacked summer, winter and annually averaged δ^{18}O signals (AD 1801-2014). The imprint of temperature on δ^{18}O is first examined by correlating the δ^{18}O stacks with instrumental temperature records from East Greenland (AD 1895-2014) and Iceland (AD 1830-2014) and with the regional climate model HIRHAM5 (AD 1980-2014). The results show that the δ^{18}O variability correlates with regional temperatures on both a seasonal and an annual scale between 1910-2014 while δ^{18}O is uncorrelated with Iceland temperatures between 1830-1909. Our analysis indicates that the unstable regional δ^{18}O-temperature correlation does not result from changes in weather patterns through respectively strengthening and weakening of the North Atlantic Oscillation. Instead, the results imply that the varying δ^{18}O-temperature relation is connected with the volume flux of sea ice exported through Fram Strait (and south along the coast of East Greenland). Notably, the δ^{18}O variability only reflects the variations in regional temperature when the temperature anomaly is positive and the sea ice export anomaly is negative. It is hypothesized that this could be caused by a larger sea ice volume flux during cold years which suppresses the Iceland temperature signature in the Renland δ^{18}O signal. However, more isotope-enabled modeling studies with emphasis on coastal ice caps are needed in order to quantify the mechanisms behind this observation. As the amount of Renland δ^{18}O variability that reflects regional temperature varies with time, the results have implications for studies performing regression-based δ^{18}O-temperature reconstructions based on ice cores drilled in the vicinity of a fluctuating sea ice cover.

Clim. Past Discuss., https://doi.org/10.5194/cp-2018-169
Manuscript under review for journal Clim. Past
Discussion started: 13 December 2018

Climate of the Past Discussions
Open Access
EGU

1 Introduction

Polar ice caps store deposited precipitation as stratified ice layers thousands of years back in time. This precipitation consists of stable water isotopes (δ^{18}O, δD) that work as a direct proxy of the relative depletion of a water vapor mass in its transport from the evaporation source to the site where condensation takes place (Epstein et al., 1951; Mook, 2000). This traceability manifests as a correlation between δ^{18}O and the temperature in the cloud at the time of condensation (Dansgaard, 1954, 1964). Thus, a relationship between δ^{18}O and temperature is preserved in annual layers of precipitation on an ice cap. Hence, by drilling ice cores at polar sites such as Antarctica and Greenland, it is possible to access past temperatures imprinted in the δ^{18}O signal. Several studies have examined the relation between temperature and ice core δ^{18}O, and its linear or quadratic relationship has regularly been used as a transfer function to infer past temperature (Jouzel and Merlivat, 1984; Johnsen et al., 1989; Jouzel et al., 1997; Johnsen et al., 2001; Ekaykin et al., 2017). While it is evident that δ^{18}O and temperature covary, the δ^{18}O signal is also affected by changes in sea ice and atmospheric circulation (Noone and Simmonds, 2004; Steig et al., 2013). Changes in the atmospheric circulation can be triggered by climatic oscillation modes (e.g. the North Atlantic Oscillation, Southern Annual Mode, Pacific Decadal Oscillation etc.) which affect the δ^{18}O variability as they influence precipitation patterns (Vinther et al., 2010; Ekaykin et al., 2017). Additionally, changes in sea ice extent affect the local moisture conditions which particularly influence the coastal precipitated δ^{18}O variability (Bromwich and Weaver, 1983; Noone and Simmonds, 2004). Such variations have implications for a simple regression-based reconstruction of temperature from δ^{18}O as the variability patterns between the ice core isotope signal and the oscillation modes and sea ice extent can have varied in strength back in time. Furthermore, in studies that analyze the relationship between polar precipitated δ^{18}O and temperature, the temperature record is often substantially shorter than the δ^{18}O series. While this is inevitable when performing temperature reconstructions, utilizing a short temperature record complicates the possibility of verifying if the estimated δ^{18}O-temperature relation is stable with time.

The aim of this study is to examine how much of the δ^{18}O variability (AD 1801-2014) from a stack of ice cores drilled on the Renland peninsula, Eastern Greenland, can be attributed to temperature variations (map in Fig. 1). In the analysis, seasonally averaged δ^{18}O time series have been compared with regional temperatures through instrumental temperature records located on the coasts of East Greenland (AD 1895-2014) and Iceland (AD 1821-2014) and the regional atmospheric climate model HIRHAM5 $2\,\mathrm{m}$ temperature output (AD 1980-2014). The δ^{18}O signal is divided into its seasonal components as it potentially improves the reconstruction of variability in weather regimes and past temperatures (Vinther et al., 2003b, 2010; Zheng et al., 2018). As Renland is located at the coast, its hydrological conditions are connected with the sea ice that annually is transported south along the coast of East Greenland. Relatively small loss in regional sea ice extent ($\approx 10\%$ or less) has previously been found to influence local Greenland moisture source water vapor which is traceable in the corresponding ice core deuterium excess values (Klein and Welker, 2016). The deuterium excess signal ($\mathrm{d_{xs}} = \delta\mathrm{D} - 8 \cdot \delta^{18}\mathrm{O}$, (Dansgaard, 1964)) contains information about the kinetic fractionation occurring when moisture evaporates from the ocean surface and ice core $\mathrm{d_{xs}}$ has been found to correlate with relative humidity and sea surface temperature at the source region (Jouzel and Merlivat, 1984; Johnsen et al., 1989). Thus, besides investigating the regional δ^{18}O–temperature relationship, this study examines if changes in the Arctic sea ice extent can be detected in the Renland stable water isotopes.

Clim. Past Discuss., https://doi.org/10.5194/cp-2018-169
Manuscript under review for journal Clim. Past
Discussion started: 13 December 2018

2 The ice cores

The Renland ice cap has an area of $1200\,\mathrm{km}^2$ with an average ice thickness of a few hundred meters. It is separated from the main Greenlandic ice sheet as a small peninsula on the east coast of Greenland (map in Fig. 1). The ice cap experiences a high annual accumulation rate of around $0.47\,\mathrm{m\,ice/year}$ with an annual surface temperature of $-18^{\circ}\mathrm{C}$. Renland has probably never been overridden by the Inland ice as it is surrounded by deep branches of the Scoresbysund Fjord which effectively drains the Inland ice (Johnsen et al., 1992). Additionally, the small width of the ice cap which is constrained by the surrounding mountains prohibits the ice elevation from significant increases from present day height. As a result, the ice cap has not experienced any ice sheet elevation changes for the past 8000 years (except for slight uplift due to isostatic rebound) (Vinther et al., 2009). This implies that lapse-rate controlled temperature variations resulting from a varying ice sheet thickness will be negligible.

This study utilizes three ice cores drilled on Renland in the analyses (Table 1). Two cores were drilled next to each other in the year 1988 (main (M) and shallow (S) cores) while the third was drilled approximately $2\,\mathrm{km}$ away in 2015 as part of the REnland ice CAP project (RECAP). The 1988 M and RECAP cores extend over the past 120 ka while the 1988 S core only covers the time back to the year 1801. Despite two cores covering the past interglacial and glacial period, the study focuses on the period AD 1801-2014 as we here have three overlapping ice core records and instrumental temperature recordings. Moreover, the separation of the summer and winter signals is better facilitated when the annual layers not are obliterated due to diffusion and ice thinning.

The records from 1988 were measured on a Isotope Ratio Mass Spectroscopy (IRMS) with a discrete resolution of $5.0\,\mathrm{cm}$ while the RECAP core was measured using cavity ringdown spectroscopy (Picarro L2130) on a Continuous Flow Analysis (CFA) system with a nominal resolution of $0.5\,\mathrm{cm}$. For the RECAP core, the years 2011-2014 are covered by the snow pit core A6 drilled next to the drill site. The A6 core was measured discretely with a sample size of $5.0\,\mathrm{cm}$ on a Picarro L2130. This was done as the porous snow in the upper firn column easily inhibits a stable measurement flow in the CFA analysis which complicates precise water isotope measurements.

Table 1. The subset of the three ice cores used in this study: processing information, analysis and coordinates.

Cores	Coordinates	Time span	Depth span	Meas.	Resolution	Analysis
RECAP	$71^{\circ}\,18'\,18''\,\mathrm{N}; 26^{\circ}\,43'\,24''\,\mathrm{W}; 2315\,\mathrm{m.a.s.l.}$	$1801-2014$	$111.7\,\mathrm{m}$	$\delta^{18}\mathrm{O}$, $\delta\mathrm{D}$	$0.5\,\mathrm{cm}$	CFA-L2130
1988 M	$71^{\circ}\,18'\,17''\,\mathrm{N}; 26^{\circ}\,43'\,24''\,\mathrm{W}; 2340\,\mathrm{m.a.s.l.}$	$1801-1987$	$92.5\,\mathrm{m}$	$\delta^{18}\mathrm{O}$	$5.0\,\mathrm{cm}$	IRMS
1988 S	$71^{\circ}\,18'\,17''\,\mathrm{N}; 26^{\circ}\,43'\,24''\,\mathrm{W}; 2340\,\mathrm{m.a.s.l.}$	$1801-1987$	$91.6\,\mathrm{m}$	$\delta^{18}\mathrm{O}$	$5.0\,\mathrm{cm}$	IRMS

3 Diffusion correction

Firn diffusion dampens the annual oscillations in the $\delta^{18}\mathrm{O}$ data. This takes place while firn (snow that survived a season) is transformed into ice in the top 60-80 meters of the ice sheet. During this densification process, air in the open porous firn

Clim. Past Discuss., https://doi.org/10.5194/cp-2018-169
Manuscript under review for journal Clim. Past
Discussion started: 13 December 2018

Climate of the Past Discussions
Open Access
EGU

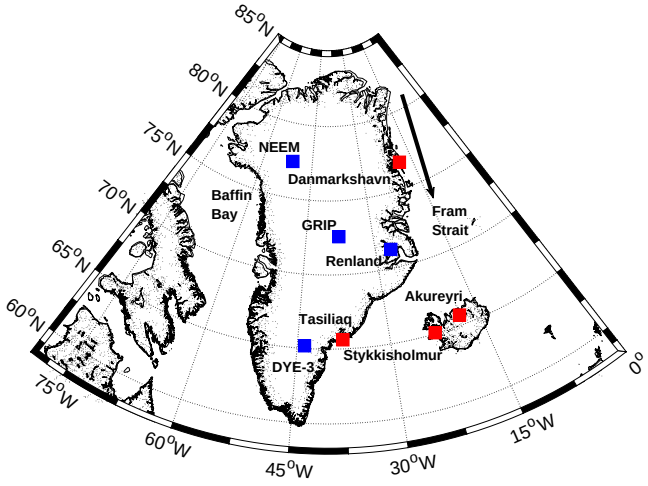

Figure 1. Locations of ice core drill sites (blue squares) and the instrumental temperature records (red squares). Sea ice exported from Fram Strait is represented by the black arrow.

is interconnnected which enables the stable water isotopes in the firn air to mix with the snow grains (Johnsen, 1977). This molecular diffusion process makes the δ^{18}O signal become increasingly more smooth with depth until pore close-off. The firn diffusion of stable water isotopes imposes two challenges on the analysis presented in this study. First, the diffusion of the annual oscillations creates artificial trends in summer and winter season time series of δ^{18}O (Vinther et al., 2010). Secondly, it introduces a bias when comparing the ice cores drilled in 1988 with the ice core drilled in 2015. For instance, the δ^{18}O signal representing the year 1987 has only experienced 1 year of firn diffusion in the 1988 ice cores while it has experienced 28 years of firn diffusion in the 2015 core. The δ^{18}O signal for overlapping years will therefore be more attenuated in the 2015 core.

As this study compares the seasonally averaged δ^{18}O signals of three ice cores drilled in different years, it is necessary to ensure that each δ^{18}O record has the same firn diffusive properties with depth. This is typically achieved by correcting each δ^{18}O record such that the effect of increasing smoothing with depth is removed by deconvolving the measured δ^{18}O signal to restore the originally deposited signal. However, Renland frequently experiences summer melting which causes steep isotopic gradients in the firn. Such high frequency gradients complicate a deconvolution of the measured δ^{18}O signal (Cuffey and Steig, 1998; Vinther et al., 2010). Instead, this study forward diffuses the three δ^{18}O records with depth such that each δ^{18}O series has been influenced by the same amount of firn diffusion. Diffusion of stable water isotopes is typically described by the diffusion length (σ) which is the average vertical displacement of a water molecule (units in meters). Thus, the δ^{18}O series are forward diffused ($\delta^{18}O_{fd}$) such that each record has the same σ with depth. Despite that such a smoothing procedure slightly mixes the summer and winter signals, a distinction of the seasonal components is still possible due to Renland's thick annual layers greatly exceeding the diffusion length.

Clim. Past Discuss., https://doi.org/10.5194/cp-2018-169
Manuscript under review for journal Clim. Past
Discussion started: 13 December 2018

Climate of the Past Discussions

The procedure below outlines in three steps how this was done separately for the 2015, 1988 M and 1988 S cores.

Step 1: First, the amount of diffusion that the measured $\delta^{18}\mathrm{O}$ signal already has experienced with depth is computed through the diffusion length's density dependence (for origin see Gkinis et al. (2014); Holme et al. (2018)):

$$\sigma^2(\rho) = \frac{1}{\rho^2} \int_{\rho_o}^{\rho} 2\rho^2 \left(\frac{\mathrm{d}\rho}{\mathrm{d}t}\right)^{-1} D(\rho)\, \mathrm{d}\rho \tag{1}$$

where $D(\rho)$ is the firn diffusivity and $\mathrm{d}\rho/\mathrm{d}t$ is the densification rate. This study uses the firn diffusivity parameterization of Johnsen et al. (2000) (described in Appendix A) that employs the site–dependent parameters of temperature ($-18^{\circ}\mathrm{C}$), accumulation rate (0.47 m ice/year), surface pressure (0.75 atm) and density. Density is here modeled with depth by fitting a Herron and Langway (1980) densification model to density measurements from the drill sites. From Eq. 1, it is possible to calculate the diffusion length that each layer has experienced ($\sigma^2(\rho)$) (left subplot in Fig. C1).

Step 2: Equation 1 can be used to calculate the auxiliary diffusion needed to transform a $\delta^{18}\mathrm{O}$ record into having a uniform diffusion length independent of depth. An auxiliary diffusion ($\sigma^2(\rho)_{aux}$) is calculated as the difference between the final diffusion length at the pore close–off density ($\sigma^2(\rho_{pc} = 804.3\,\mathrm{kg/m^3})$) and the diffusion length at a given layer in meters of ice–equivalent depth:

$$\sigma^2(\rho)_{aux} = \left(\left(\frac{\rho_{pc}}{\rho_i}\right)^2 \sigma^2(\rho_{pc}) - \left(\frac{\rho(z)}{\rho_i}\right)^2 \sigma^2(\rho) \right) \cdot \left(\frac{\rho_i}{\rho(z)}\right)^2 \tag{2}$$

where the fraction $\rho_i/\rho(z)$ ultimately is multiplied in order to transform the $\sigma^2(\rho)_{aux}$ from representing ice–equivalent depth to density–equivalent depth (as the annual oscillations are squeezed during firn compaction). Using Eq. 2, an auxiliary diffusion profile with respect to density (and thus depth) is calculated for an ice core (left subplot in Fig. C1).

Step 3: Forward diffusion is then simulated through a convolution of the measured data ($\delta^{18}\mathrm{O}_{meas}$) with a Gaussian filter ($\mathcal{G}$) with a standard deviation equal the auxiliary diffusion length as this is mathematically equivalent to firn diffusion (Johnsen, 1977):

$$\delta^{18}\mathrm{O}_{fd}(z) = \delta^{18}\mathrm{O}_{meas} * \mathcal{G} \tag{3}$$

where

$$\mathcal{G}(z) = \frac{1}{\sigma_{aux}\sqrt{2\pi}}\, e^{-z^2/\left(2\sigma^2_{aux}\right)} \tag{4}$$

As the auxiliary diffusion length decreases with depth, the width of the Gaussian filter changes accordingly. Thus, the convolution (using the σ_{aux} for the corresponding depth) is applied on a moving $2\,\mathrm{m}$ section which is shifted in small steps equal to the sampling interval. For each convolved data section, only the midpoint of the sliding window is retained as the new forward diffused $\delta^{18}\mathrm{O}_{fd}$ value. In order to avoid tail-problems when diffusing the top 2 meter measurements, the $\delta^{18}\mathrm{O}_{meas}$ data were extended by using its prediction filter coefficients estimated from a maximum entropy method algorithm by Andersen (1974). This assumes that the extended series has the same spectral properties as the original series. After applying this smoothing routine on the entire record, a $\delta^{18}\mathrm{O}_{fd}$ series with constant σ is obtained. A comparison between $\delta^{18}\mathrm{O}_{fd}$ and $\delta^{18}\mathrm{O}_{meas}$ is shown in Fig. C1.

Clim. Past Discuss., https://doi.org/10.5194/cp-2018-169
Manuscript under review for journal Clim. Past
Discussion started: 13 December 2018

4 Chronology

It is important to ensure that the chronologies of the three ice cores are synchronous before comparing the δ^{18}O variability. The two cores drilled in 1988 were manually dated by counting the summer maxima and winter minima in the δ^{18}O series and verified by identifying signals of volcanic eruptions in the electrical conductivity measurements (Vinther et al., 2003b, 2010). For the 2015 RECAP core, the period 1801-2007 was dated with the annual layer algorithm (StratiCounter) presented in Winstrup et al. (2012) and the years 2007-2014 were manually counted similar to the 1988 cores (the RECAP chronology is presented in Simonsen et al. (2018, in review)). The annual layer algorithm uses signals in the ice core that all have annual oscillations or peaks such as the chemical impurities (Na^+, Ca, SO_4^{2-} and NH_4^+), electrical conductivity and stable water isotopes. Even though the model automatically count years, the chronology is still restricted by the same volcanic eruptions as in the 1988 cores. The model marks a year when Na^+ has a peak which indicates winter. Na^+ is a result of the transport of salt from the ocean and it peaks during winter due the strong winds during the fall. As the timing of this winter peak might not be similar to the timing of the δ^{18}O series' winter minima (used for the 1988 cores), this study has tuned the RECAP dating presented Simonsen et al. (2018, in review) slightly. For each year, this is done by tuning the timing of the summer and winter in the dated RECAP record to match with the maximum and minimum of the δ^{18}O series. The chronology is only shifted a maximum of a few months and it is only changed within a given year. This ensures that the modified dating profile remains consistent with the original chronology while it facilitates an optimal comparison between the manually dated and the automatically dated stable water isotopes profiles.

In order to analyze the seasonal signals of the δ^{18}O series we need to distinguish between snow deposited during summer and winter. Under the assumption that δ^{18}O and temperature extremes in the Greenland region occur simultaneously, Vinther et al. (2010) found best to define the summer and winter seasons such that they each contain 50% of the annual accumulation. Besides maximizing the amount of utilized data, this definition ensures that the winter and summer signals contain no overlapping data. This study has therefore defined the summer and winter seasons similar to Vinther et al. (2010). The summer, winter and annually averaged δ^{18}O data used in this study are thus seasonal/annual averages of the forward diffused δ^{18}O series.

5 δ^{18}O variability on Renland

The three ice cores' δ^{18}O data as a representative of the isotope hydrology on Renland is first evaluated by calculating Pearson correlation coefficients and signal to noise variance ratios (SNR) on the forward diffused δ^{18}O records in the overlapping period 1801-1987. The correlation coefficient is a metric that describes the linear relation between two signals and it has been calculated for different combinations of the presented ice cores (Table 2). For all correlation coefficient calculations throughout this study, the level of significance is estimated based on a Monte Carlo routine described in Appendix B. From the results displayed in Table 2, it is evident that the lowest correlation coefficients are found for the winter averaged data with values ranging from $0.60 - 0.78$ while the summer and annually averaged signals have higher values ranging from approximately $0.64 - 0.84$. The high correlation coefficients indicate that there is a strong linear relationship between the δ^{18}O records. This is further illustrated by the visual covariation of the annually averaged δ^{18}O records in Fig. 2. In all instances, the highest

Clim. Past Discuss., https://doi.org/10.5194/cp-2018-169
Manuscript under review for journal Clim. Past
Discussion started: 13 December 2018

Climate of the Past Discussions
Open Access
EGU

correlations are found when correlating the two ice cores drilled in 1988. This might be attributed to the use of similar dating method and their close proximity. Nonetheless, all the presented ice cores correlated significantly during the 1801-1987 period.

Table 2. Correlation coefficients (r) calculated for different combinations of δ^{18}O records for the period 1801-1987 ($p < 0.05$).

Season	r (2015/1988 M)	r (2015/1988 S)	r (1988 M/1988 S)
Winter	0.63	0.60	0.78
Summer	0.66	0.65	0.82
Annual	0.64	0.66	0.84

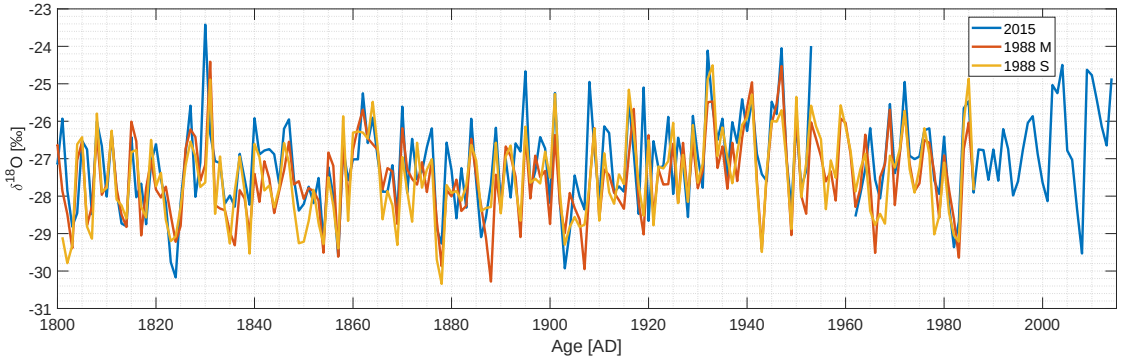

Figure 2. Annually averaged δ^{18}O for respectively the RECAP 2015 (blue), 1988 M (red) and 1988 S (yellow) cores with age.

The δ^{18}O variability can be further analyzed by examining the mean single series SNR which provides an insight into the amount of signal and noise in the δ^{18}O series. Noise can originate from depositional effects such as wind shuffling of snow, melt layers and from dating uncertainties ($\pm 1\,\mathrm{year}$) in between the three cores. By averaging n (3) overlapping ice core data records, the mean single series SNR is calculated by comparing the variance of an averaged record (VAR_s) with the mean of the variances ($\overline{\mathrm{VAR}}$) for the n individual records (Johnsen et al., 1997; Vinther et al., 2006):

$$\mathrm{SNR} = \frac{\mathrm{VAR}_s - \frac{\overline{\mathrm{VAR}}}{n}}{\overline{\mathrm{VAR}} - \mathrm{VAR}_s} \tag{5}$$

The SNR results are shown in Table 3. Similar to the high correlation, it is evident that merging the two 1988 records results in the highest SNR values. Moreover, the summer averaged signal has a higher SNR compared to the winter averaged signal which probably is a consequence of winters having more windy conditions that generates redeposition of snow. A similar pattern have previously been found for the seasonal isotopes of GRIP ($n = 5$; SNR summer: 0.70, winter: 0.51), Dye-3 ($n = 2$; SNR summer: 1.73, winter: 1.56) and NEEM ($n = 4$; SNR summer: 1.28, winter: 0.64) (map in Fig. 1) (Vinther, 2003a; Zheng et al., 2018). This comparison also shows that the SNR values of the three Renland ice cores are high compared to GRIP, Dye-3

Clim. Past Discuss., https://doi.org/10.5194/cp-2018-169
Manuscript under review for journal Clim. Past
Discussion started: 13 December 2018

Climate of the Past Discussions

Table 3. Mean signal to noise variance ratios calculated for the summer, winter and annually averaged data using respectively two and three cores in the period 1801-1987.

Merged cores	SNR winter	SNR summer	SNR annual
1988 M, 2015	1.65	1.73	1.73
1988 M, 1988 S	3.53	4.46	5.05
1988 M, 1988 S, 2015	2.01	2.36	2.43

and NEEM which likely can be attributed to a combination of a high accumulation rate and a good cross-dating between the compared cores.

From this analysis, the study can comment on two things. First, the two 1988 cores have the most robust common signal of all the tested combinations. As this was for two adjacently drilled ice cores, utilizing all three records still result in a larger spatial atmospheric representativeness of the region. Secondly, the high SNR and correlation coefficients imply that the chronologies from the annual layer detection algorithm and the manual counting are consistent. This has implications for future ice core science as manual layer counting can be a slow and inefficient procedure. Thus, manual counting can effectively be replaced with the StratiCounter software by Winstrup et al. (2012) for ice cores where several datasets that contain observable annual peaks or oscillations are available.

The high combined SNR values and correlation coefficients indicate that it is beneficial to combine the time series into a stacked δ^{18}O record. We choose to employ all three ice cores as that increases the spatial representativeness of δ^{18}O while it provides water isotopic variability for the years 1988-2014. A stacked record is typically created by averaging the time series but the time span 1801-2014 consists of an inhomogeneous amount of data records as only the RECAP core contains data in the 1988-2014 period while it also has a gap between 1954-1961 due to missing ice samples. Thus, it is important to implement a variance correction in order to avoid bias issues when averaging time series with nonuniform length (Osborn et al., 1997; Jones et al., 2001). This variance correction (c) can be expressed directly through the SNR values in Table 3 and the number of records (m) used in the averaging for the given year (derivation can be found in Vinther et al. (2006)):

$$c = \sqrt{\frac{\mathrm{SNR}}{\mathrm{SNR} + \frac{1}{m}}} \tag{6}$$

Before stacking, the three time series are standardized based on the period of overlap (1801-1987) ($\delta^{18}\mathrm{O}_{\mathrm{std}}$ has mean = 0 and standard deviation = 1). An average $\delta^{18}\mathrm{O}_{\mathrm{avr}}$ value is then calculated by multiplying c onto the mean $\delta^{18}\mathrm{O}_{\mathrm{std}}$ for each year:

$$\delta^{18}\mathrm{O}_{\mathrm{avr}} = c \cdot \frac{1}{m} \sum_{i=1}^{m} \delta^{18}\mathrm{O}_{\mathrm{std}_i} \tag{7}$$

The amplitude and variability of the original δ^{18}O series are then restored by using the average variance ($\overline{\mathrm{VAR}}$) and the average ($\overline{\delta^{18}\mathrm{O}}$) of the three time series (from the period where the time series were standardized):

$$\delta^{18}\mathrm{O}_{\mathrm{stack}} = \delta^{18}\mathrm{O}_{\mathrm{avr}} \cdot \sqrt{\overline{\mathrm{VAR}}} + \overline{\delta^{18}\mathrm{O}} \tag{8}$$

Clim. Past Discuss., https://doi.org/10.5194/cp-2018-169
Manuscript under review for journal Clim. Past
Discussion started: 13 December 2018

Climate of the Past Discussions
Open Access
EGU

Figure 3 shows the summer, winter and annual $\delta^{18}O_{stack}$ series for the period 1801-2014. In the figure, a 5 year moving average has been applied on the stacked records in order filter out any remaining high frequency noise variability. From the figure, it is evident that the summer averaged signal is less depleted than the annual and winter averaged signals. Moreover, the summer signal has the largest trend in $\delta^{18}O$ with an increase of $0.54‰/century$ while the winter and annually averaged data show lower increases of respectively $0.24‰/century$ and $0.37‰/century$. The amount of variability that correlates with temperature will be examined in Sect. 6.

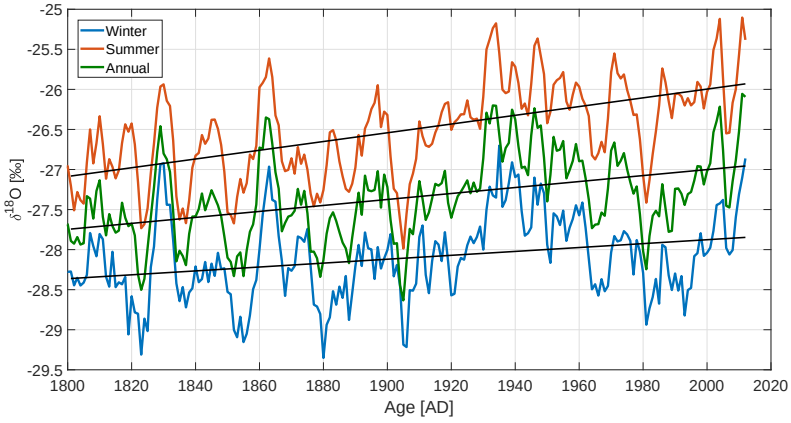

Figure 3. Summer (red), winter (blue) and annually averaged (green) $\delta^{18}O$ stacks together with their corresponding linear trends (black lines) for the period 1801–2014. A moving average of 5 years has been applied on all the time series. For the unfiltered series, the reader is referred to Figs. 4, C2 and C3.

6 The temperature signature in $\delta^{18}O$

6.1 Correlation with instrumental temperature records

The relationship between Renland $\delta^{18}O$ variability and temperature is first investigated by comparing the stacked $\delta^{18}O$ series with instrumental temperature records. This study uses the nearest and longest temperatures recordings from Greenland (Tasiilaq and Danmarkshavn) and Iceland (Akureyri and Stykkisholmur) - locations are shown in Fig. 1. The Greenland temperature records are available from the Danish Meteorological Institute (http://www.dmi.dk/laer-om/generelt/dmi-publikationer/tekniske-rapporter/) and the Iceland temperatures are available from the Icelandic Met Office (http://en.vedur.is/climatology/data/#a). For the temperature measurements, the seasons have been defined similar to Vinther et al. (2010) with summer extending from May-October and winter from November-April. Figure 4 shows the annually averaged $\delta^{18}O$ stack together with the annually averaged temperature measurements (winter and summer averages are shown in Fig. C2 and C3). Visually, the past 100 years of summer, winter and annually averaged $\delta^{18}O$ signals of Renland covary with the regional temperature. How-

Clim. Past Discuss., https://doi.org/10.5194/cp-2018-169
Manuscript under review for journal Clim. Past
Discussion started: 13 December 2018

ever, the years 1830-1910 show periods with both anticorrelation and correlation. Besides the visual covariation, correlation coefficients between the temperature recordings and the δ^{18}O stacks are calculated and shown in Table 4. The correlations with the winter averaged data are in general the lowest while annual and summer signals have similar high correlations at all the sites. The best correlation with the Renland δ^{18}O signal is found for the annual averages at Tasiilaq ($r = 0.50$). Additionally, applying a 5 year moving mean on the δ^{18}O and temperature series increases all the correlations (i.e. the Tasiilaq correlation coefficient increases to r = 0.72).

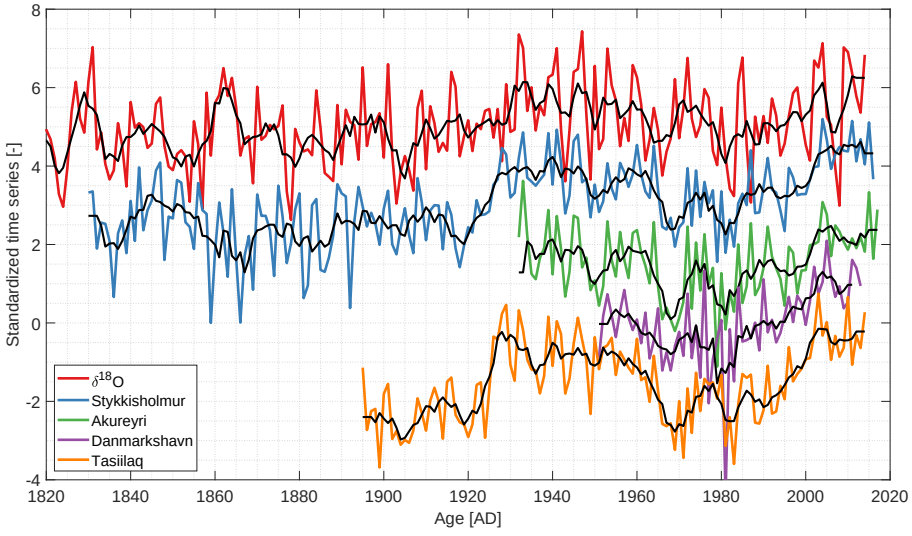

Figure 4. Annually averaged δ^{18}O and temperature series. For visualization, the time series have been standardized and shifted vertically. The black curves represent a moving average of 5 years.

Table 4. Correlation coefficients between the δ^{18}O stack and instrumental temperature records ($p < 0.05$) on both a 1 year resolution and with a 5 year moving mean applied (in bold).

Record	Stykkisholmur	Akureyri	Danmarkshavn	Tasiilaq
Period	$1830-2014$	$1931-2014$	$1951-2014$	$1895-2014$
r winter	0.29 / $\mathbf{0.51}$	0.30 / $\mathbf{0.56}$	0.21 / $\mathbf{0.51}$	0.41 / $\mathbf{0.64}$
r summer	0.40 / $\mathbf{0.58}$	0.45 / $\mathbf{0.69}$	0.30 / $\mathbf{0.62}$	0.37 / $\mathbf{0.61}$
r annual	0.48 / $\mathbf{0.62}$	0.40 / $\mathbf{0.58}$	0.35 / $\mathbf{0.63}$	0.50 / $\mathbf{0.72}$

The high correlation between δ^{18}O and temperature implies that the region's temperature variability is imprinted in the Renland δ^{18}O stack. Conventionally, a simple interpretation in terms of local temperature can then be achieved by using the linear relation between δ^{18}O and temperature. However, this requires that the linear relationship between temperature and δ^{18}O is stable throughout time. In order to examine this, correlation coefficients between Stykkisholmur temperature and

Clim. Past Discuss., https://doi.org/10.5194/cp-2018-169
Manuscript under review for journal Clim. Past
Discussion started: 13 December 2018

Climate of the Past Discussions
Open Access
EGU

δ^{18}O have been calculated on a 50 year running window and shown in Fig. 5. Here Stykkisholmur is chosen as it has the longest temperature record while we selected a window size of 50 years in order to include enough independent data as the time series have been smoothed with a 5 year moving mean. This analysis indicates that the Stykkisholmur temperature and the δ^{18}O stack only correlates in the period 1910-2014. For winter, summer and annual averages, the average correlation in the period 1910-2014 is 0.56, 0.65 and 0.66 while it severely reduces to -0.02, -0.02 and 0.004 in the 1830-1909 period. Thus, the high correlation coefficients presented in Table 4 is only a result of the high correlations in the 1910-2014 period. This could explain why the highest δ^{18}O-temperature correlation was found at Tasiilaq as it only extended back to 1895. Consequently, the regional δ^{18}O-temperature relationship between Renland isotopes and the Iceland temperature record is not constant through time. While it remains unknown if the temperature on Iceland and Renland was similar between 1830-1909, it is certain that the Renland δ^{18}O variability does not represent the temperature variability at Iceland in said period. Thus, even though the δ^{18}O variability probably reflects the local temperature on Renland, the results show that the decorrelation scale of this δ^{18}O-temperature relationship was different in the 1830-1909 period.

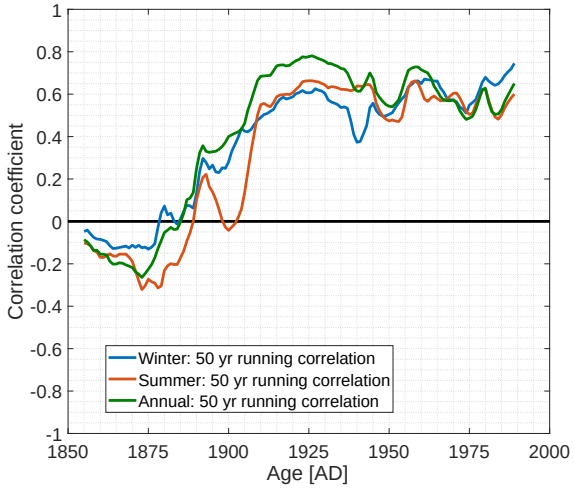

Figure 5. Running correlation of 50 years between the Stykkisholmur temperature and the δ^{18}O stack for respectively winter (blue), summer (red) and annual averages (green). Both the δ^{18}O and temperature data were first smoothed with a 5 year moving mean. Each year represents the midpoint of the running window.

6.2 Correlation with the HIRHAM5 2 m temperature output

The spatial extent of the correlation between the δ^{18}O signal and temperature is further investigated by using $2\,\mathrm{m}$ temperature output from the regional climate model, HIRHAM5 (Christensen et al., 2007). This particular HIRHAM5 simulation (Langen et al., 2017) covers the entire Greenlandic region including Iceland. At the lateral boundaries and over the ocean, the model is driven with the European Re-Analysis dataset, ERA-Interim (Dee et al., 2011). This study uses monthly averaged data (1980-2014) on a horizontal resolution of 0.05° ($\sim 5.5\,\mathrm{km}$) converted to summer and winter temperatures by averaging May-October

Clim. Past Discuss., https://doi.org/10.5194/cp-2018-169
Manuscript under review for journal Clim. Past
Discussion started: 13 December 2018

Climate of the Past Discussions

and November-April, respectively. The RECAP core is used instead of the stacked record as the analysis is on data from the satellite era, which is minimally available in the 1988 cores. The correlation maps are shown in Fig. 6. The results show significant positive correlations between the winter signals of HIRHAM5 $2\,\mathrm{m}$ temperature and the RECAP $\delta^{18}\mathrm{O}$. Moreover, the high correlations ($r > 0.5$) that extend over most of Greenland, irrespectively of the ice divide, indicate that the winter temperature variability over Greenland is imprinted in the Renland $\delta^{18}\mathrm{O}$ signal. Results furthermore show that there is no statistically significant correlation between $\delta^{18}\mathrm{O}$ and temperature east of Renland in areas regularly covered by sea ice. For the summer and annually averaged signals, the correlations are lower ($r \sim 0.4 - 0.5$) and they only cover the east coast region. This local spatial pattern is consistent with Vinther et al. (2010) who found that the summer averaged $\delta^{18}\mathrm{O}$ data from different Greenlandic ice cores were less internally coherent than the corresponding winter data. This could explain why the summer $\delta^{18}\mathrm{O}$ variability of the RECAP core only correlates with the local temperatures on the coast of East Greenland. Moreover, the variance in summer averaged temperatures over Greenland is very low as shown in Fig. 7. The low variance is due to the HIRHAM5 summer temperatures reaching a maxima just below $0^{\circ}\mathrm{C}$ at places with constant ice cover. For instance, Fig. 8 shows the monthly averaged HIRHAM5 temperature from a grid point on Renland where it is evident that the monthly averaged temperature fluctuations during summer are very small. Thus, the small temperature fluctuations can limit the possibility of interpreting the spatial extent of summer and annual temperature variability imprinted in the $\delta^{18}\mathrm{O}$ signal.

All in all, these results support the correlations from Sect. 6.1 that showed high correlations between $\delta^{18}\mathrm{O}$ and temperature in the 1910-2014 period.

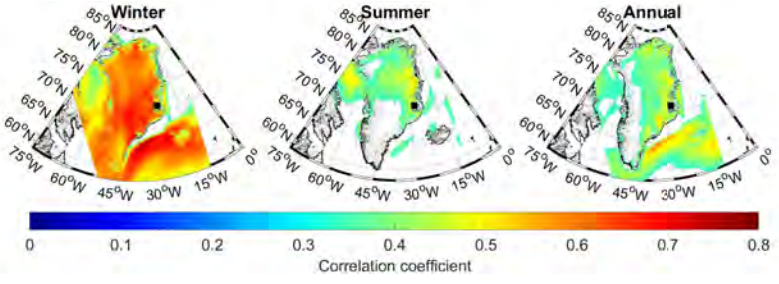

Figure 6. Figures showing the correlation between winter (left), summer (middle) and annually (right) averaged RECAP $\delta^{18}\mathrm{O}$ and HIRHAM5 temperatures. Only correlations with $p < 0.05$ are shown.

7 The North Atlantic Oscillation's imprint on $\delta^{18}\mathrm{O}$

The North Atlantic Oscillation (NAO) describes fluctuations in atmospheric pressure at sea level between Iceland and the Azores. A strengthening and weakening of respectively the low pressure system over Iceland and high pressure system over the Azores control both the direction and strength of westerly winds and storm tracks over the North Atlantic. Such changes

Clim. Past Discuss., https://doi.org/10.5194/cp-2018-169
Manuscript under review for journal Clim. Past
Discussion started: 13 December 2018

Climate of the Past Discussions
Open Access
EGU

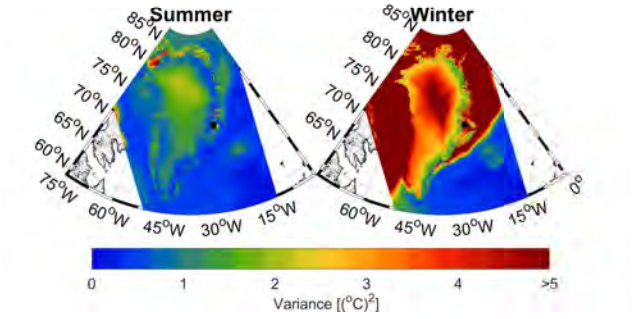

Figure 7. Variances of the summer (left) and winter averaged temperatures (right). A maximum variance of $5(^{\circ}\mathrm{C})^2$ is displayed in order to emphasize the small variance in the summer averaged signal.

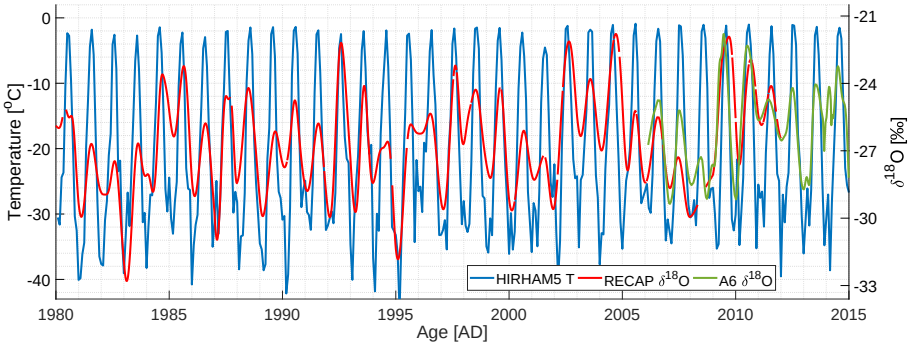

Figure 8. Monthly averaged $2\,\mathrm{m}$ temperature from a grid point on Renland (blue curve) plotted together with the forward diffused $\delta^{18}\mathrm{O}$ from the RECAP ice core (red curve) and A6 snow pit core (green curve).

in the NAO have previously been found to have an imprint on precipitation in western Greenland (Appenzeller et al., 1999). Correspondingly, the winter isotope signal of West and South Greenland ice cores have previously been found to anticorrelate with the atmospheric circulation changes from NAO (Vinther et al., 2003b, 2010). Despite that Vinther et al. (2010) showed that ice cores drilled on the Greenland east coast revealed no connection with the NAO, this study examines said correlation in order to determine if changes in the NAO can be linked to the varying $\delta^{18}\mathrm{O}$-temperature relationship.

While the NAO is best described through a principal component analysis of multiple sea level pressure records in the North Atlantic region, this study uses an approximation where the NAO index is based on pressure observations only near the two centers of action of the surface pressure field (the Azores/Iberian Peninsula and Iceland). Such an approximation was carried out by Jones et al. (1997) who reconstructed the NAO variation back to 1821 (and since extended up to present time). This

Clim. Past Discuss., https://doi.org/10.5194/cp-2018-169
Manuscript under review for journal Clim. Past
Discussion started: 13 December 2018

study uses a slightly modified version of this NAO index by Vinther et al. (2003c) who improved the NAO record in the period 1821-1856 by using extra pressure series.

The connection between the NAO index and seasonally (and annually) averaged δ^{18}O stacks is examined by estimating their correlation. Correlation coefficients have been calculated on 5 year moving averages of the NAO and δ^{18}O stacks and shown in Table 5 (the annual NAO record is plotted in Fig. 9). The level of significance is estimated based on a Monte Carlo routine described in Appendix B. In the complete 1821-2014 period, the summer, winter and annually averaged NAO and δ^{18}O data are uncorrelated with coefficients of 0.01, -0.05 and 0.02, respectively,. If we instead examine the time before and after the δ^{18}O-temperature correlation terminated (the year 1909), the summer and annually averaged data yield positive correlations of 0.29 and 0.30 between 1821-1909 while the winter and annually averaged data yield negative correlations -0.25 and -0.22 between 1910-2014. Thus, there is a varying relation between the NAO and the δ^{18}O data and the weak δ^{18}O-NAO anticorrelation coincides with a covarying δ^{18}O-temperature relation. However, the weak correlations during 1821-1919 imply that the NAO only can account for around $8-9\%$ of the corresponding δ^{18}O variability. It therefore seems unlikely that respectively strengthening and weakening of the NAO cause changes in the δ^{18}O-temperature relation.

Table 5. Correlation coefficients between the δ^{18}O stack and NAO index. Both time series have been smoothed with a 5 year moving mean. Only the numbers in bold are statistically significant ($p < 0.05$).

Period	$1821-1909$	$1910-2014$	$1821-2014$
r winter	0.15 ($p=0.16$)	**-0.25** ($p=0.01$)	-0.05 ($p=0.52$)
r summer	**0.29** ($p<0.01$)	-0.15 ($p=0.13$)	0.01 ($p=0.85$)
r annual	**0.30** ($p<0.01$)	**-0.22** ($p=0.02$)	0.02 ($p=0.82$)

8 The impact of sea ice fluctuations on the stable water isotopes

8.1 Fram Strait sea ice export

In this section, it is investigated if there is a connection between the Renland δ^{18}O variability and the sea ice export (SIE) through the Fram Strait (map in Fig. 1). Multi-year sea ice from the Arctic Ocean is exported southward through Fram Strait along the eastern coast of Greenland into the Greenland Sea. Fluctuations in this sea ice volume flux have a direct effect on the amount of open water located east and northeast of Renland. As δ^{18}O is an integrated signal of the hydrological activity along the moisture transport pathway from evaporation source to deposition, the open water which facilitates moist and mild climatic conditions will likely affect the isotopic composition of the precipitation deposited on Renland. Essentially, besides the temperature dependence of isotopic fractionation during local condensation, δ^{18}O contains information about the amount of water mass that is removed from the air during the poleward transport and the continuous contribution of local water mixing with the transported water mass (Noone and Simmonds, 2004).

Clim. Past Discuss., https://doi.org/10.5194/cp-2018-169
Manuscript under review for journal Clim. Past
Discussion started: 13 December 2018

Climate of the Past Discussions

This analysis uses a Fram Strait SIE record covering the period 1820-2000 reconstructed by Schmith and Hansen (2002). It is an ice volume flux record $\left[\mathrm{km}^3/\mathrm{yr}\right]$ based on historical observations of multi-year sea ice obtained from ship logbooks and ice charts. As the record represents the annual SIE, only the annually averaged $\delta^{18}\mathrm{O}$ stack is used in the analysis. Figure 9 shows the SIE together with the annually averaged $\delta^{18}\mathrm{O}$ stack and the RECAP $\mathrm{d_{xs}}$ record ($\mathrm{d_{xs}}$ is only available for the RECAP core). A correlation analysis is carried out in order to quantify any covariation of the records. For a moving average of 5 years applied on the time series, there is an anticorrelation of -0.54 ($p < 0.01$) between the annual SIE and $\delta^{18}\mathrm{O}$ while there is no significant correlation between $\mathrm{d_{xs}}$ and the SIE ($r = -0.08$). From the correlation analyses, it is clear that $\delta^{18}\mathrm{O}$ anticorrelates with SIE while it correlates with temperature (Sect. 6.1). In order to examine if these correlations apply simultaneously, correlation coefficients have been calculated on a 50 year running window. The level of significance is estimated based on a Monte Carlo routine described in Appendix B. The results are plotted in Fig. 10. In the past 100 years, the Stykkisholmur temperature record is found to correlate with Renland $\delta^{18}\mathrm{O}$ while it (as similar to $\delta^{18}\mathrm{O}$) anticorrelates with SIE through Fram Strait. This likely indicates that warm temperatures result in less sea ice that can be exported away from the Arctic Ocean. However, this pattern ceases to exist previous to the early 1900s such that neither the $\delta^{18}\mathrm{O}$ signal or temperature share any correlation with the SIE. This synchronous decrease in correlation indicates that the uncorrelated $\delta^{18}\mathrm{O}$–temperature relation cannot be explained by dating errors in the ice core chronologies. Furthermore, as discussed in Sect. 7 and shown as running correlations in Fig. 10, the varying $\delta^{18}\mathrm{O}$-temperature correlation cannot be a consequence of the NAO controlling the $\delta^{18}\mathrm{O}$ variability. Moreover, Fig. 10 also shows that changes in local moisture source regions are not traceable through the $\mathrm{d_{xs}}$-SIE correlation.

In order to examine this $\delta^{18}\mathrm{O}$-temperature correlation hiatus, the connection between the SIE anomaly and the $\delta^{18}\mathrm{O}$-temperature relation is plotted in Fig. 11 (SIE anomaly is here defined as the deviation from the mean flux). As a 5 year moving mean has been applied on the time series, only every 5 point is used in the analysis. From the figure, it is clear that on years when the normalized temperature is positive ($T_{\mathrm{norm}} = T - T_{mean}$), there is always a negative SIE anomaly and a high $\delta^{18}\mathrm{O}$-temperature correlation of 0.83. Whereas, for $T_{\mathrm{norm}} < 0$ there is no $\delta^{18}\mathrm{O}$-temperature correlation ($r = 0.02$) which coincides with a combination of both positive and negative SIE anomalies. Besides showing that higher temperatures coincide with less multi-year sea ice being transported south (likely due to an already lower extent of sea ice), it appears that lower temperatures coincide with more fluctuations in the SIE which possibly reduce the $\delta^{18}\mathrm{O}$-temperature correlation. These results imply that the $\delta^{18}\mathrm{O}$ variability can be dominated by other climatic conditions such as SIE, and does not only represent variations in regional temperature for an extended period of time.

8.2 Sea ice concentration and sea surface temperature

The Arctic sea ice concentration (SIC) data (fractional ice cover in percentage) from the ERA-Interim reanalysis (Dee et al., 2011) has been correlated with the RECAP $\delta^{18}\mathrm{O}$ and $\mathrm{d_{xs}}$ series and the results are shown in Figs. 12 and 13 (1980-2014). Similar to Sect. 6.2, summer refers to May-October and winter refers to November-April. In the case of $\mathrm{d_{xs}}$, only the annually averaged data is used as its seasonal components is smeared out after the $\delta^{18}\mathrm{O}$ and $\delta\mathrm{D}$ data have been forward diffused. The results show a large patch of anticorrelation between $\delta^{18}\mathrm{O}$ and SIC in the Baffin Bay area ($r \approx -0.4$) outside West Greenland for both winter and annually averaged data. Presumably, this indicates that the climate at Renland is similar to the

Clim. Past Discuss., https://doi.org/10.5194/cp-2018-169
Manuscript under review for journal Clim. Past
Discussion started: 13 December 2018

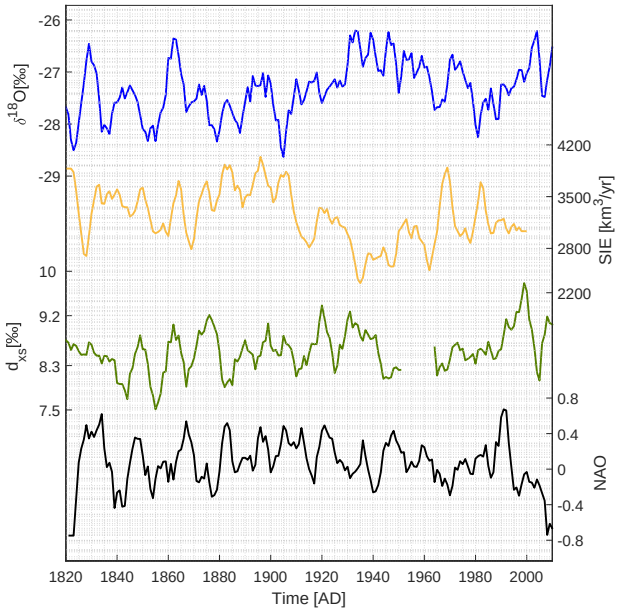

Figure 9. Annually averaged δ^{18}O stack (blue curve), Fram Strait SIE (yellow curve), d_{xs} (green curve) and NAO index (black curve). A 5 year moving average has been applied on all the data.

climate at Baffin Bay which controls the advance and retreat of the sea ice extent. A similar connection was found in Sect. 6.2 which showed that winter averaged δ^{18}O signal correlated with temperatures all over Greenland. Resembling anticorrelations between NEEM δ^{18}O and Baffin Bay SIC have previously been found (Steen-Larsen et al., 2011; Zheng et al., 2018). Moreover, the results are consistent with Faber et al. (2017) who found that changes in the Baffin Bay sea ice coverage can impact the δ^{18}O precipitation over Greenland (by using an atmospheric general circulation model coupled with water isotopologue tracing (isoCAM3)). Furthermore, the analysis shows only a small patch of correlation between the δ^{18}O series and the SIC south of Fram Strait. However, this is not necessarily inconsistent with the significant anticorrelation presented in Sect. 8.1. Possibly, this nuance can be explained by the SIE representing the annual discharge of multi-year sea ice (ice volume flux) while the SIC represents the fractional ice cover in percentage (area).

The connection between the Renland stable water isotopes and the local climate conditions is further investigated by correlating the RECAP d_{xs} signal with the Arctic SIC and sea surface temperature (SST). Figure 13 shows that there exists small patches of positive correlation patterns between the d_{xs} signal and the SIC in the Arctic Ocean and south of Baffin Bay. As these areas are very small, it is difficult to evaluate the connection between the extent of SIC and d_{xs} at Renland. The d_{xs} signal is further examined by checking if it reflects the local SST variability. This has been done by correlating the d_{xs} signal with the SST data in the Arctic region from ERA-Interim data (1980-2014). From Fig. 13, it is evident that there barely exists patches

Clim. Past Discuss., https://doi.org/10.5194/cp-2018-169
Manuscript under review for journal Clim. Past
Discussion started: 13 December 2018

Climate of the Past Discussions
Open Access
EGU

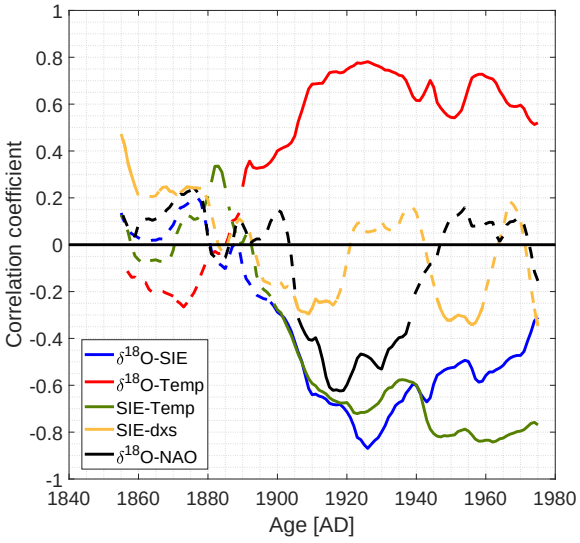

Figure 10. Running correlations of 50 years between Stykkisholmur temperature and the δ^{18}O stack (red), SIE and the δ^{18}O stack (blue), SIE and Stykkisholmur temperature (green), the δ^{18}O stack and the NAO index (black) and d_{xs} with SIE (yellow). The solid lines represent significant correlation ($p < 0.05$) while the dashed lines are insignificant $p > 0.05$. Each year represents the midpoint of the running window.

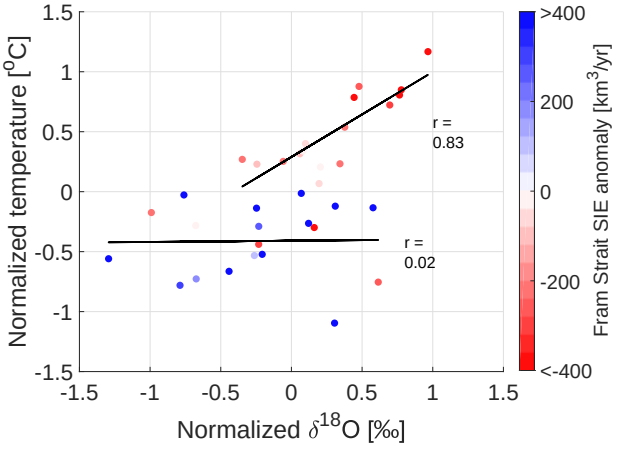

Figure 11. Normalized annual temperature plotted with respect to normalized annual δ^{18}O where colors indicate strength of the Fram Strait sea ice export anomaly. A 5 year moving average has been applied to all the time series but only every 5 point is displayed and used in the analysis. The solid black lines represent linear fits between δ^{18}O and temperature for positive and negative temperature anomalies.

with significant correlation. Thus, it is difficult to assess whether the RECAP d_{xs} record directly reflects the local SST or SIC variability during the 1980-2014 period. More analysis on what controls the Renland d_{xs} signal is needed in future research.

Clim. Past Discuss., https://doi.org/10.5194/cp-2018-169
Manuscript under review for journal Clim. Past
Discussion started: 13 December 2018

Climate of the Past Discussions
Open Access
EGU

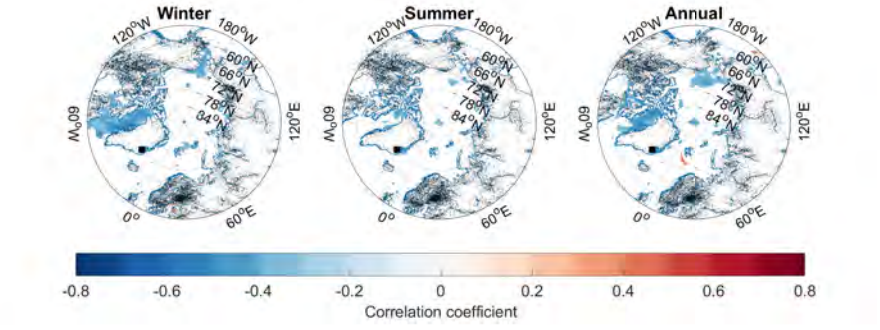

Figure 12. Maps showing the correlation coefficients between the ERA-Interim sea ice concentration and the RECAP δ^{18}O data for the 1980-2014 period ($p < 0.05$).

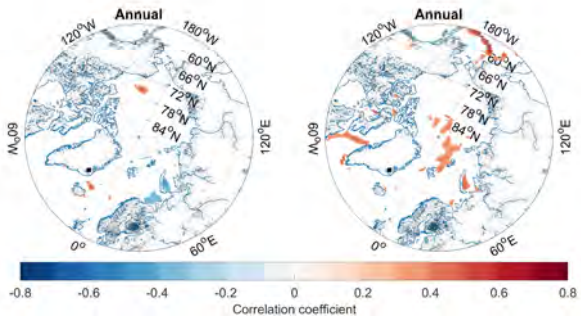

Figure 13. Maps showing the d_{xs}-SST (left) and d_{xs}-SIC correlation coefficients between annually averaged data from RECAP and ERA-Interim covering the 1980-2014 period ($p < 0.05$).

9 Discussion

The analysis showed that the strength of the SIE have varied in the past and that its fluctuations could be connected with the regional δ^{18}O-temperature relationship. Despite the apparent connection, this study has not proved any causality between the δ^{18}O-temperature relation and the Fram Strait SIE. Still, a proposed hypothesis for this connection is that the fluctuating SIE conditions during cold years impose changes in the location of the local moisture sources which suppress the imprint of Iceland temperature variability in Renland δ^{18}O. It is likely that this connection has its strongest impact on ice cores drilled at the coastal regions near sea ice as Vinther et al. (2010) found that the δ^{18}O records of Greenlandic ice cores drilled in South and Central Greenland correlated well with a Southwest Greenland instrumental temperature series in the period 1785-

Clim. Past Discuss., https://doi.org/10.5194/cp-2018-169
Manuscript under review for journal Clim. Past
Discussion started: 13 December 2018

1980 (Vinther et al., 2006). With reference to this temperature series, Fig. C4 shows that these temperatures do not have a stable linear covariation with the Renland δ^{18}O stack (winter averages are here chosen as that constitutes the longest and most homogeneous record). Besides that Renland obviously is located far away from the Southwest Greenland instrumental temperature stations, this contrariety might result from the isotope distillation process being more manifested as a temperature variability in the δ^{18}O signal when the precipitation has journeyed further and risen in altitude more than that of the coastal region, further depleting the δ^{18}O signal. In order to evaluate this hypothesis, more studies using isotope-enabled modeling are needed. The impact of changes in sea ice on the Arctic δ^{18}O precipitation has previously been investigated by Faber et al. (2017) who found that the δ^{18}O precipitation on Greenland only responded to perturbations of the Baffin Bay sea ice coverage. However, they used a horizontal resolution of $\sim 1.4^{\mathrm{o}}\,\mathrm{x}\,1.4^{\mathrm{o}}$ which barely resolved the Renland Ice Cap of $\sim 1200\,\mathrm{km}^2$. Thus, a further examination of how changes in sea ice extent is connected with the coastal Greenlandic precipitation on a higher spatial resolution grid is essential in order to evaluate this hypothesis.

Moreover, while this study found that the Renland δ^{18}O signal anticorrelated with variations in the sea ice extent outside West Greenland (Sect. 8.2), a similar pattern was found with the HIRHAM5 temperature correlations presented in Sect. 6.2. It is therefore likely that the connection represents a reduced sea ice coverage due to increasing temperatures rather than an actual interconnection between Renland δ^{18}O and Baffin Bay sea ice.

10 Conclusions

This study found that by quantifying the mean signal to noise variance ratios, a robust seasonal δ^{18}O signal (1801-2014) could be extracted by stacking three ice cores from Renland. This δ^{18}O stack was correlated with instrumental temperature records from East Greenland and Iceland and with the HIRHAM5 $2\,\mathrm{m}$ temperature output. Results showed that there were high correlations between δ^{18}O and regional temperatures on both a seasonal and annual scale between 1910-2014. A similar anticorrelation was found between the δ^{18}O stack and the amount of sea ice exported through Fram Strait. However, both correlations stopped in the 1830-1909 period. The results indicated that the varying regional temperature variability in the δ^{18}O signal could not be explained by the North Atlantic Oscillation. Instead, the linear δ^{18}O-temperature relation depended on whether the temperatures were warmer or colder than the temperature anomaly. Warm years were associated with a high correlation and accompanied by less sea ice transported south along the coast while cold years were associated with zero correlation that accompanied a fluctuating amount of sea ice along the coast. These results implied that changes in the extent of open water outside Renland might affect the local moisture conditions. Hence, greater sea ice flux along the coast of Greenland may suppress the Iceland temperature signature in the d18O signal; however, this was not confirmed by correlations between $\mathrm{d_{xs}}$ and sea surface temperature in the Arctic region. Thus, more high resolution isotope-enabled modeling focused on the effect of Arctic sea ice on coastal precipitation are needed in order to quantify this process.

These results have implications for ice core temperature reconstructions based on the linear relationship between δ^{18}O variability and local temperature records. For Renland, the linear δ^{18}O-temperature relationship was unstable with time which implied that the annual-to-decadal variability of δ^{18}O measured in an ice core could not be directly attributed to temperature

Clim. Past Discuss., https://doi.org/10.5194/cp-2018-169
Manuscript under review for journal Clim. Past
Discussion started: 13 December 2018

variability. Similar conditions might apply for other ice cores drilled in the vicinity of a fluctuating sea ice cover. This reinforces the interpretation that δ^{18}O is an integrated signal of all the hydrological activity that a vapor mass experiences from the evaporation at the source to its condensation at the drill site.

Appendix A: Firn diffusivity

This study uses the firn diffusivity parameterization of Johnsen et al. (2000):

$$D(\rho) = \frac{m p D_{\mathrm{a}i}}{R T \alpha_{\mathrm{i}} \tau} \left(\frac{1}{\rho} - \frac{1}{\rho_{\mathrm{ice}}} \right) \tag{A1}$$

which depends on the molar weight of water (m), the saturation vapor pressure (p), diffusivity of water vapor (D_{ai}), the molar gas constant (R), the site temperature (T), the ice–vapor fractionation factor (α_i) and the firn air tortuosity (τ). Similar to Johnsen et al. (2000) and subsequently used in Simonsen et al. (2011); Gkinis et al. (2014); Holme et al. (2018), we used the following definitions which can be parameterized through annual mean surface temperature, annual accumulation rate, surface pressure and density (ρ):

- Saturation vapor pressure over ice (Pa) (Murphy and Koop, 2006):

$$p = \exp\left(9.5504 - \frac{5723.265}{T} + 3.530 \ln(T) - 0.0073 T\right) \tag{A2}$$

- $D_{\mathrm{a}i}$: diffusivity of water vapor (for isotopologue i) in air ($\mathrm{m^2 s^{-1}}$). For the diffusivity of the abundant isotopologue water vapor D_{a} (Hall and Pruppacher, 1976):

$$D_{\mathrm{a}} = 2.1 \cdot 10^{-5} \left(\frac{T}{T_o}\right)^{1.94} \left(\frac{P_o}{P}\right) \tag{A3}$$

  with $P_{\mathrm{o}} = 1$ Atm, $T_{\mathrm{o}} = 273.15$ K and P, T the ambient pressure (Atm) and temperature (K). Additionally from Merlivat and Jouzel (1979) $D_{a^2\mathrm{H}} = 0.9755 D_{\mathrm{a}}$ and $D_{\mathrm{a}^{18}\mathrm{O}} = 0.9723 D_{\mathrm{a}}$

- R: molar gas constant $R = 8.3144\ \mathrm{m^3 Pa K^{-1} mol^{-1}}$

- α_{i}: Ice – Vapor fractionation factor. we use the formulations by Majoube (1970) and Merlivat and Nief (1967) for $\alpha^{\delta\mathrm{D}}_{\mathrm{s/v}}$ and $\alpha^{\delta^{18}\mathrm{O}}_{\mathrm{s/v}}$ respectively.

$$\alpha_{\mathrm{Ice/Vapor}}\left({}^2\mathrm{H}/{}^1\mathrm{H}\right) = 0.9098 \exp(16288/T^2) \tag{A4}$$

$$\alpha_{\mathrm{Ice/Vapor}}\left({}^{18}\mathrm{O}/{}^{16}\mathrm{O}\right) = 0.9722 \exp(11.839/T) \tag{A5}$$

(A6)

Clim. Past Discuss., https://doi.org/10.5194/cp-2018-169
Manuscript under review for journal Clim. Past
Discussion started: 13 December 2018

Climate of the Past Discussions

– τ: The firn tortuosity (Schwander et al., 1988):

$$\frac{1}{\tau} = 1 - b \cdot \left(\frac{\rho}{\rho_{\mathrm{ice}}}\right)^2 \quad \rho \leq \frac{\rho_{\mathrm{ice}}}{\sqrt{b}},\ b = 1.3 \tag{A7}$$

Based on Eq. (A7), $\tau \to \infty$ for $\rho > 804.3\,\mathrm{kg\,m^{-3}}$

Appendix B: Significance analysis

In this study, time series have often been smoothed with a 5 year moving mean before estimating their correlation. Potentially, this results in artificially improved correlation coefficients as a moving mean is a low-pass filter. It is therefore necessary to quantify the significance of the linear relationship ($p-$value) by running a Monte Carlo simulation. This study test said significance by examining what correlation coefficients we would estimate if we had random generated data instead of the δ^{18}O signal (following the procedure proposed by Macias-Fauria et al. (2011)). For simplicity, this section refers to the correlation between δ^{18}O and temperature while it applies equally for all types of time series.

Synthetic data are created by generating time series with the same power spectrum as the δ^{18}O signal. This study uses a method outlined in Ebisuzaki (1977) that is based on a random resampling of the δ^{18}O signal in the frequency domain. The synthetic time series is then found by taking the inverse fast Fourier transform of the shuffled signal. This procedure retains the same autocorrelation as the input time series hereby mimicking the influence of a 5 year moving mean applied on data.

This procedure is simulated 1000 times. For each iteration, the correlation coefficient between the synthetic δ^{18}O series and the temperature series is calculated. From this Monte Carlo routine, an empirical probability distribution function that describes the relation between synthetic generated data and the temperature series is obtained. From this distribution, it is possible to compute the $p-$value which describes how probable it is that the correlation between δ^{18}O and temperature is significantly different from that of the synthetic δ^{18}O and temperature. In this study, $p-$values below 0.05 are considered statistically significant.

Appendix C: Figures

Competing interests. The authors declare that they have no conflict of interest.

Acknowledgements. The RECAP ice coring effort was financed by the Danish Research Council through a Sapere Aude grant, the NSF through the Division of Polar Programs, the Alfred Wegener Institute, and the European Research Council under the European Community's Seventh Framework Programme (FP7/2007-2013)/ ERC grant agreement 610055 through the Ice2Ice project and the Early Human Impact project (267696). The authors acknowledge the support of the Danish National Research Foundation through the Centre for Ice and Climate at the Niels Bohr Institute (Copenhagen, Denmark).

Clim. Past Discuss., https://doi.org/10.5194/cp-2018-169
Manuscript under review for journal Clim. Past
Discussion started: 13 December 2018

Climate of the Past Discussions
Open Access
EGU

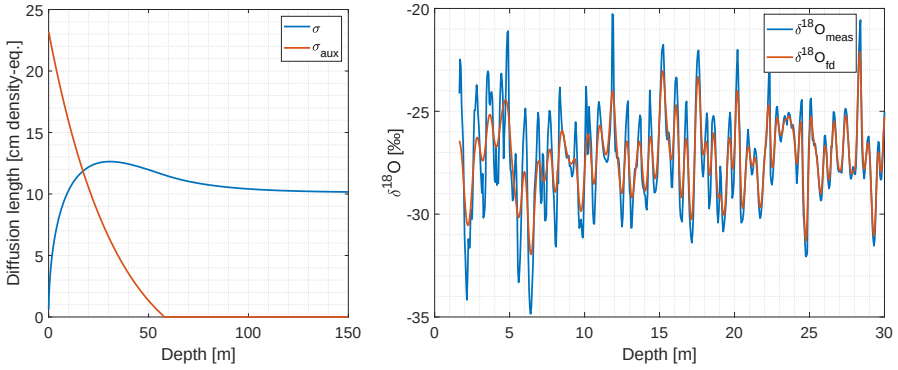

Figure C1. Left: Modeled firn diffusion with depth (σ; blue) and calculated auxiliary diffusion length that should be applied on the measured δ^{18}O data (σ_{aux}; red). After the pore close–off ($\rho_{pc} = 804.3\,\mathrm{kg\,m^{-3}}$), $\sigma_{aux} = 0$ as σ just changes due to the compaction of firn. Right: The measured δ^{18}O data (blue) and the forward-diffused δ^{18}O data (red) for the 1988 M core.

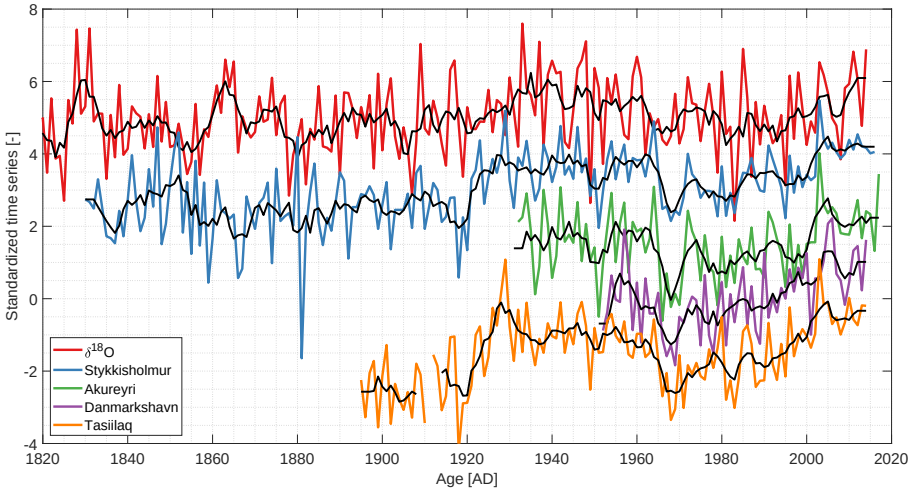

Figure C2. Winter averaged δ^{18}O and temperature series. For visualization, the time series have been standardized and shifted vertically. The black curves represent a moving average of 5 years.

References

Andersen, N.: On the calculation of filter coefficients for maximum entropy spectral analysis, Geophysics, 39, 69–72, 1974.

Appenzeller, C., Schwander, J., Sommer, S., and Stocker, T. F.: The North Atlantic Oscillation and its imprint on precipitation and ice accumulation in Greenland, Geophysical Research Letters, 25, 1939–1942, 1999.

Bromwich, D. H. and Weaver, C. J.: Latitudinal displacement from main moisture source controls δ^{18}O of snow in coastal Antarctica, Nature, 301, 145–147, 1983.

Clim. Past Discuss., https://doi.org/10.5194/cp-2018-169
Manuscript under review for journal Clim. Past
Discussion started: 13 December 2018

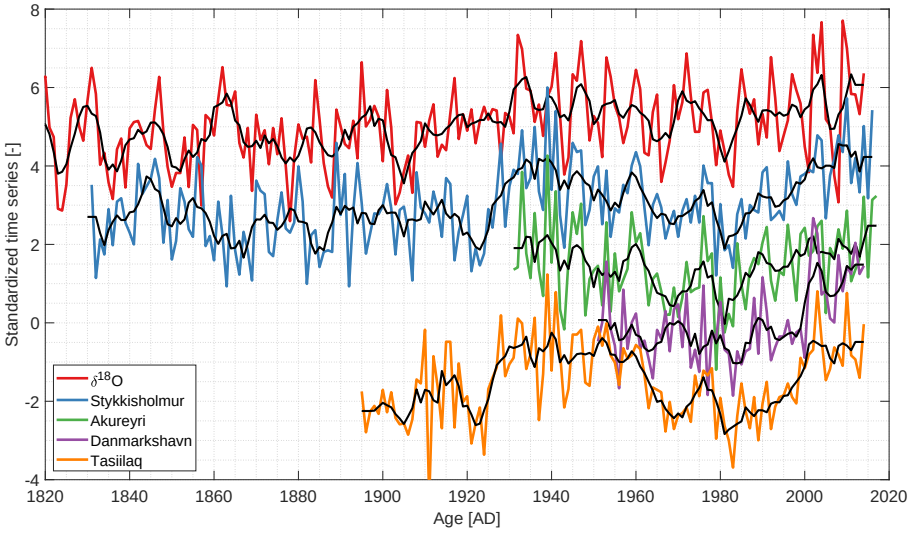

Figure C3. Summer averaged δ^{18}O and temperature series. For visualization, the time series have been standardized and shifted vertically. The black curves represent a moving average of 5 years.

Christensen, O. B., Drews, M., Christensen, J. H., Dethloff, K., Ketelsen, K., Hebestadt, I., and Rinke, A.: The HIRHAM Regional Climate Model Version 5, Technical report 06-17, Danish Climate Centre, DMI, 2007.

Cuffey, K. M. and Steig, E. J.: Isotopic diffusion in polar firn: implications for interpretation of seasonal climate parameters in ice-core records, with emphasis on central Greenland, Journal of Glaciology, 44, 273–284, 1998.

Dansgaard, W.: The ^{18}O-abundance in fresh water, Geochimica et Cosmochimica Acta, 6, 241–260, 1954.

Dansgaard, W.: Stable isotopes in precipitation, Tellus B, 16, 436–468, 1964.

Dee, D. P., Uppala, S. M., Simmons, A., Berrisford, P., Poli, P., Kobayashi, S., Andrae, U., Balmaseda, M., Balsamo, G., Bauer, d. P., et al.: The ERA-Interim reanalysis: Configuration and performance of the data assimilation system, Quarterly Journal of the royal meteorological society, 137, 553–597, 2011.

Ebisuzaki, W.: A method to estimate the statistical significance of a correlation when the data are serially correlated, Journal of Climate, 10, 2147–2153, 1977.

Ekaykin, A. A., Vladimirova, D. O., Lipenkov, V. Y., and Masson-Delmotte, V.: Climatic variability in Princess Elizabeth Land (East Antarctica) over the last 350 years, Climate of the Past, 13, 61–71, 2017.

Epstein, S., Buchsbaum, R., Lowenstam, H., and Urey, H.: Carbonate-water isotopic temperature scale, Geological Society of America Bulletin, 62, 417, 1951.

Faber, A.-K., Vinther, B. M., Sjolte, J., and Pedersen, R.: How does sea ice influence δ^{18}O of Arctic precipitation?, Atmospheric Chemistry and Physics, 17, 5865–5876, 2017.

Gkinis, V., Simonsen, S. B., Buchardt, S. L., White, J. W. C., and Vinther, B. M.: Water isotope diffusion rates from the NorthGRIP ice core for the last 16,000 years - glaciological and paleoclimatic implications, Earth and Planetary Science Letters, 405, 2014.

Clim. Past Discuss., https://doi.org/10.5194/cp-2018-169
Manuscript under review for journal Clim. Past
Discussion started: 13 December 2018

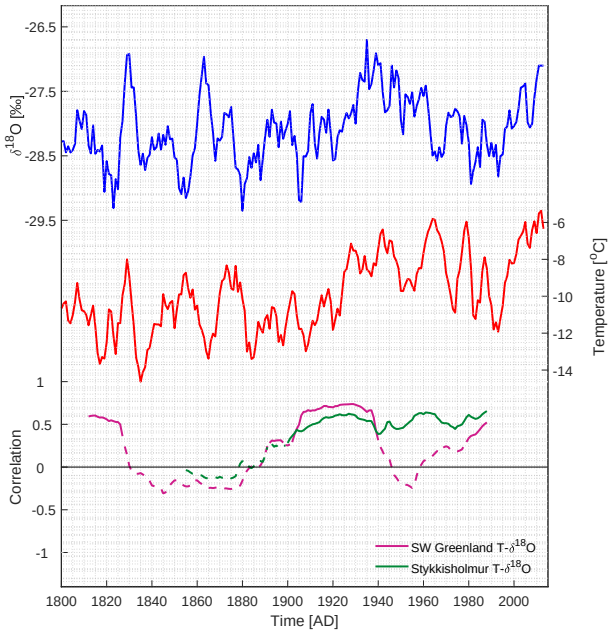

Figure C4. Top: 5 year moving average of the winter averaged δ^{18}O stack. Mid: 5 year moving average of the December-January-February averaged Southwest Greenland temperatures from Vinther et al. (2006). Bottom: 50 year running correlations between δ^{18}O and Southwest Greenland (magenta) and δ^{18}O and Stykkisholmur (green). Each year represents the midpoint of the running window. Solid lines are significant correlations and dashed lines are insignificant ($p > 0.05$).

Hall, W. D. and Pruppacher, H. R.: The Survival of Ice Particles Falling from Cirrus Clouds in Subsaturated Air, Journal of the Atmospheric Sciences, 33, 1995–2006, 1976.

Herron, M. M. and Langway, C. C.: Firn Densification: An Empiricial Model, Journal of Glaciology, 25, 1980.

Holme, C., Gkinis, V., and Vinther, B. M.: Molecular diffusion of stable water isotopes in polar firn as a proxy for past temperatures, Geochemica et Cosmochimica Acta, 225, 128–145, 2018.

Johnsen, S., Clausen, H. B., Cuffey, K. M., Hoffmann, G., Schwander, J., and Creyts, T.: Diffusion of stable isotopes in polar firn and ice: the isotope effect in firn diffusion, Physics of Ice Core Records, pp. 121–140, 2000.

Johnsen, S. J.: Stable Isotope Homogenization of Polar Firn and Ice, Isotopes and Impurities in Snow and Ice, pp. 210–219, 1977.

Johnsen, S. J., Dansgaard, W., and White, J.: The origin of Arctic precipitation under present and glacial conditions, Tellus, 41B, 452–468, 1989.

Johnsen, S. J., Clausen, H. B., Dansgaard, W., Gundestrup, N. S., Hansson, M., Jonsson, P., Steffensen, J. P., and Sveinbjornsdottir, A. E.: A "deep" ice core from East Greenland, Meddelelser om Groenland, Geoscience, 29, 3–22, 1992.

Johnsen, S. J., Clausen, H. B., Dansgaard, W., Gundestrup, N. S., Hammer, C. U., Andersen, U., Andersen, K. K., Hvidberg, C. S., Dahl-Jensen, D., Steffensen, J. P., Shoji, H., Sveinbjornsdottir, A. E., White, J., Jouzel, J., and Fisher, D.: The δ^{18}O record along the Greenland

Ice Core Project deep ice core and the problem of possible Eemian climatic instability, Journal of Geophysical Research, 102, 26 397—-26 410, https://doi.org/10.1029/97JC00167, 1997.

Johnsen, S. J., Dahl-Jensen, D., Gundestrup, N., Steffensen, J. P., Clausen, H. B., Miller, H., Masson-Delmotte, V., Sveinbjornsdottir, A. E., and White, J.: Oxygen isotope and palaeotemperature records from six Greenland ice-core stations: Camp Century, Dye-3, GRIP, GISP2, Renland and NorthGRIP, Journal of Quaternary Science, 16, 2001.

Jones, P. D., Jonsson, T., and Wheeler, D.: Extension to the North Atlantic oscillation using early instrumental pressure observations from Gibraltar and south-west Iceland, International Journal of Climatology, 17, 1433–1450, 1997.

Jones, P. D., Osborn, T. J., Briffa, K. R., Folland, C. K., Horton, E. B., Alexander, L. V., Parker, D. E., and Rayner, N. A.: Adjusting for sampling density in grid box land and ocean surface temperature time series, Journal of Geophysical Research, 106, 3371–3380, 2001.

Jouzel, J. and Merlivat, L.: Deuterium and oxygen 18 in precipitation: modeling of the isotopic effects during snow formation, Journal of Geophysical Research-Atmospheres, 89, 11 749 – 11 759, 1984.

Jouzel, J., Alley, R. B., Cuffey, K. M., Dansgaard, W., Grootes, P., Hoffmann, G., Johnsen, S. J., Koster, R. D., Peel, D., Shuman, C. A., Stievenard, M., Stuiver, M., and White, J.: Validity of the temperature reconstruction from water isotopes in ice cores, Journal Of Geophysical Research-Oceans, 102, 26 471–26 487, 1997.

Klein, E. S. and Welker, J. M.: Influence of sea ice on ocean water vapor isotopes and Greenland ice core records, Geophysical Research Letters, 43, 12,475–b12,483, 2016.

Langen, P. L., Fausto, R. S., Vandecrux, B., Mottram, R. H., and Box, J. E.: Liquid Water Flow and Retention on the Greenland Ice Sheet in the Regional Climate Model HIRHAM5: Local and Large-Scale Impacts, Front. Earth Sci., 2017.

Macias-Fauria, M., Grinsted, A., Helama, S., and Holopainen, J.: Persistence matters: Estimation of the statistical significance of paleoclimatic reconstruction statistics from autocorrelated time series, Dendrochronologia, 30, 179–187, 2011.

Majoube, M.: Fractionation factor of ^{18}O between water vapour and ice, Nature, 226, 1970.

Merlivat, L. and Jouzel, J.: Global Climatic Interpretation of the Deuterium-Oxygen 18 Relationship for Precipitation, Journal of Geophysical Research, 84, 1979.

Merlivat, L. and Nief, G.: Fractionnement Isotopique Lors Des Changements Detat Solide-Vapeur Et Liquide-Vapeur De Leau A Des Temperatures Inferieures A 0 Degrees C, Tellus, 19, 122–127, 1967.

Mook, J.: Environmental Isotopes in the Hydrological Cycle Principles and Applications, International Atomic Energy Agency, 2000.

Murphy, D. M. and Koop, T.: Review of the vapour pressures of ice and supercooled water for atmospheric applications, Q.J.R. Meteorol. Soc., 131, 1539–1565, 2006.

Noone, D. and Simmonds, I.: Sea ice control of water isotope transport to Antarctica and implications for ice core interpretation, Journal of Geophysical Research, 109, 2004.

Osborn, T., Briffa, K. R., and Jones, P. D.: Adjusting Variance for sample-size in tree-ring chronologies and other regional mean time series, Dendrochronologies, 15, 1997.

Schmith, T. and Hansen, C.: Fram Strait Ice Export during the Nineteenth and Twentieth Centuries Reconstructed from a Multiyear Sea Ice Index from Southwestern Greenland, Journal of Climate, 16, 2782–2791, 2002.

Schwander, J., Stauffer, B., and Sigg, A.: Air mixing in firn and the age of the air at pore close-off, Annals of Glaciology, pp. 141 –145, 1988.

Simonsen, M. F., Baccolo, G., Borunda, A., Delmonte, B., Goldstein, S., Grindsted, A., Kjaer, H. A., Sowers, T., Svensson, A., Vinther, B. M., Winckler, G., Winstrup, M., and Vallelonga, P.: Ice core dust particle size reveals past glacier extent in East Greenland, In review in Nature Communication, ., 2018, in review.

Simonsen, S. B., Johnsen, S. J., Popp, T. J., Vinther, B. M., Gkinis, V., and Steen-Larsen, H. C.: Past surface temperatures at the NorthGRIP drill site from the difference in firn diffusion of water isotopes, Climate of the Past, 7, 2011.

Steen-Larsen, H. C., Masson-Delmotte, V., Sjolte, J., Johnsen, S. J., Vinther, B. M., Bréon, F., Clausen, H. B., Dahl-Jensen, D., Falourd, S., Fettweis, X., Gallée, H., Jouzel, J., Kageyama, M., Lerche, H., Minster, B., Picard, G., Punge, H. J., Risi, C., Salas, D., Schwander, J., Steffen, K., Sveinbjornsdottir, A. E., Svensson, A., and White, J.: Understanding the climatic signal in the water stable isotope records from the NEEM shallow firn/ice cores in northwest Greenland, Journal of Geophysical Research, 116, 2011.

Steig, E. J., Ding, Q., White, J. W. C., Kuttel, M., Rupper, S. B., Neumann, T. A., Neff, P. D., Gallant, A. J. E., Mayewski, P. A., Taylor, K. C., Hoffmann, G., Dixon, D. A., Schoenemann, S., M., M. B., Schneider, D. P., Fudge, T. J., Schauer, A. J., Teel, R. P., Vaughn, B., Burgener, L., Williams, J., and Korotkikh, E.: Recent climate and ice-sheet change in West Antarctica compared to the past 2000 years, Nature Geoscience, 6, 2013.

Vinther, B. M.: Seasonal δ^{18}O Signals in Greenland Ice Cores, Master's thesis, University of Copenhagen, Denmark, 2003a.

Vinther, B. M., Johnsen, S. J., Andersen, K. K., Clausen, H. B., and Hansen, A. W.: NAO signal recorded in the stable isotopes of Greenland ice cores, Geoph. Res. Lett., 30, 2003b.

Vinther, B. M., Andersen, K. K., Hansen, A. W., Schmidth, T., and Jones, P. D.: Improving the Gibraltar/Reykjavik NAO Index, Geoph. Res. Lett., 30, 2003c.

Vinther, B. M., Andersen, K. K., Jones, P. D., Briffa, K. R., and Cappelen, J.: Extending Greenland temperature records into the late eighteenth century, Journal of Geophysical Research, 111, 2006.

Vinther, B. M., Buchardt, S. L., Clausen, H. B., Dahl-Jensen, D., Johnsen, S. J., Fisher, D. A., Koerner, R. M., Raynaud, D., Lipenkov, V., Andersen, K. K., Blunier, T., Rasmussen, S. O., Steffensen, J. P., and Svensson, A. M.: Holocene thinning of the Greenland ice sheet, Nature, 461, 2009.

Vinther, B. M., Jones, P. D., Briffa, K. R. and. Clausen, H. B., Andersen, K. K., Dahl-Jensen, D., Johnsen, S. J., and Clausen, H. B.: Climatic signals in multiple highly resolved stable isotope records from Greenland, Quaternary Science Reviews, 29, 522–538, 2010.

Winstrup, M., Svensson, A. M., Rasmussen, S. O., Winther, O., Steig, E. J., and Axelrod, A. E.: An automated approach for annual layer counting in ice cores, Clim. of the Past, 8, 1881–1895, 2012.

Zheng, M., Sjolte, J., Alolphi, F., Vinther, B. M., Steen-Larsen, H. C., Popp, T. J., and Muscheler, R.: Climate information preserved in seasonal water isotope at NEEM: relations with temperature, circulation and sea ice, Clim. of the Past, 14, 1067–1078, 2018.

Report I Christensen, J.H., Olesen, M., Boberg, F., Stendel, M., Koldtoft, I., 2015a. Fremtidige klimaforandringer I Grønland: Kujalleq Kommune (Scientific report 15-04 (1/6)). Danish Meteorological Institute.

DMI
Energi-, Forsynings- og Klimaministeriet

Videnskabelig rapport 15-04 (1/6)

Fremtidige klimaforandringer i Grønland: Kujalleq Kommune

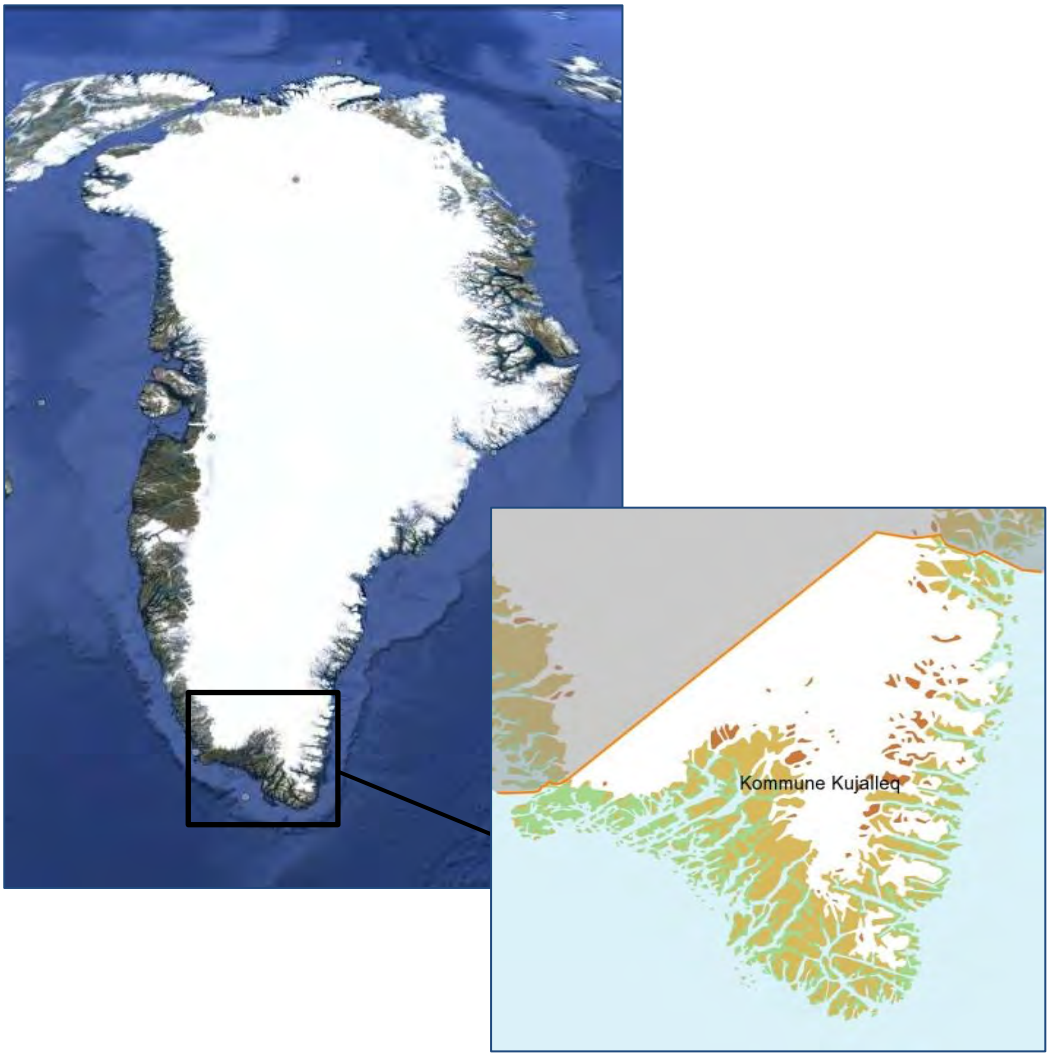

København 2016

DMI
Energi-, Forsynings- og Klimaministeriet

Kolofon

Serietitel:
Videnskabelig rapport 15-04 (1/6)

Titel:
Fremtidige klimaforandringer i Grønland: Kujalleq Kommune

Forfattere:
Jens Hesselbjerg Christensen, Martin Olesen, Fredrik Boberg, Martin Stendel, Iben Koldtoft

Forsidefoto:
Googlemap og Nunagis Kort

Ansvarlig institution:
Danmarks Meteorologiske Institut

Sprog:
Dansk

Emneord:
Grønland, temperatur, nedbør, havis og klima

Url:
http://www.dmi.dk/laer-om/generelt/dmi-publikationer/videnskabelige-rapporter/

Digital ISBN:
978-87-7478-662-7

Versions dato:
04.01.16

Link til hjemmeside:
www.dmi.dk/groenland/klimaforandringer

Finansiering:
Projektet vedr. ”Datagrundlag for klimatilpasningsindsatsen i Grønland” er finansieret med støtte fra Klimastøtten til Arktis under Energi-, Forsynings-, og Klimaministeriet.

Book Chapter Olesen, M., Arnbjerg-Nielsen, K., Hansen, A.S., 2015. “What is a climate model?”, chapter 3 in “Climate adaptation - why and how?”, Miljøbiblioteket. Aarhus University Press.

3 Forventninger til fremtidens klima

Klimaforskerne bruger modeller til at beregne, hvordan vejret vil udvikle sig hvis mængden af drivhusgasser i atmosfæren stiger. En vigtig forudsætning er, hvordan vi tror udviklingen vil være i verdens samlede udledning af drivhusgasser. Det afhænger bl.a. af den globale udvikling. Klimamodellerne kan give os tal for fx hvor meget temperaturen kan stige i Danmark i fremtiden.

Jorden set fra rummet.
Foto: Colourbox.

Foto: Colourbox.

Foto: PetraD, Colourbox.

Hvad er en klimamodel

Den globale opvarmning afhænger først og fremmest af indholdet og dermed udledningerne af drivhusgasser i atmosfæren. Til at beregne fremtidens klima anvender klimaforskerne klimamodeller, som bruges til at beregne, hvordan klimaet udvikler sig frem i tiden under en række forudsætninger og antagelser. Modellerne, som beregner den fysiske udvikling i klimasystemet, tager udgangspunkt i information om forskellige mulige udviklinger i atmosfærens koncentration af drivhusgasser samt andre faktorer, som kan virke enten opvarmende eller nedkølende. Det vil sige, at fremtidens klima beregnes ud fra forskellige fremtidsscenarier. Klimaudviklingen beregnes med udgangspunkt i koncentrationsscenarier – såkaldte RCP-scenarier (se tabel 1), som er mulige bud på udviklingen af fremtidens globale koncentrationer af drivhusgasser i atmosfæren.

Klimamodellerne opdeles i globale og regionale modeller, hvor en global model beregner klimaets udvikling for hele jorden, mens en regional model dækker et mindre område svarende til f.eks. Europa, men til gengæld i højere opløsning, dvs. med mere lokale data. En global model kan f.eks. anvendes til at undersøge vekselvirkninger mellem atmosfæren, oceanerne, jordens overflade og is, mens de regionale modeller har en højere geografisk detaljegrad. En kombineret global og regional model giver mulighed for at få mere detaljerede og lokale data. En regional model er i stand til at beregne klimaudviklingen på mindre skala og gengiver detaljer som f.eks. forekomsten af bjerge, søer, fjorde og beplantning langt bedre. Derfor anvendes regionale klimaberegninger som input til såkaldte effektmodeller til beregning af klimapåvirkninger af f.eks. grundvand og økosystemer og til at vurdere fremtidens muligheder inden for vindproduktion.

Tabel 3.1 De fire RCP-scenarier, der benyttes af FN's klimapanel IPCC. RCP står for Representative Concentration Pathways (Repræsentative koncentrationsveje). Ppm er en forkortelse for 'parts per million' dvs. milliontedele.

Betegnelse	Drivhusgaskoncentration	Ændring i global middeltemperatur i 2081-2100 [°C]	Udvikling i udledning af drivhusgasser
RCP8.5	Over 1370 ppm CO_2-ækvivalent i 2100	3,7 (± 1,1)	Stigende
RCP6.0	Ca. 850 ppm CO_2-ækvivalent ved stabilisering efter 2100	2,2 (± 0,8)	Stabilisering
RCP4.5	Ca. 650 ppm CO_2-ækvivalent ved stabilisering efter 2100	1,8 (± 0,7)	Stabilisering
RCP2.6	Topper ved ca. 490 ppm CO_2-ækvivalent før 2100 og aftager derefter	1,0 (± 0,7)	Topper og aftager derefter – forudsætter ambitiøs reduktion af udslippet

Fremtidens klima i Danmark

Beregninger med en koblet regional klimamodel for Danmark kan give et bud på, hvordan klimaet vil udvikle sig i Danmark i fremtiden. Danmarks klima er under forandring. Danmark får i fremtiden et generelt varmere og vådere vejr med flere ekstreme vejrhændelser. Vi kan forvente mere nedbør særligt om vinteren, mens sommeren forventes at byde på både længere tørkeperioder og kraftigere nedbørshændelser, når det faktisk regner. Den igangværende vandstandsstigning omkring Danmark forventes at fortsætte sin kurs frem mod år 2100. Og endelig bidrager et stigende havniveau til at fremtidens stormfloder vil virke hyppigere og kraftigere.

Temperatur

Den fremtidige opvarmning i Danmark vil være i tråd med den udvikling, som allerede er observeret, se figur 1. Desuden følger temperaturudviklingen i Danmark i store træk den globale udvikling. Temperaturen vil stige og dermed give os mildere vintre og varmere somre med flere og længere hede- og varmebølger. Den fremtidige opvarmning afhænger af atmosfærens koncentration af drivhusgasser. I figur 1 er temperaturudviklingen vist for det høje scenarie (RCP8.5) med høje koncentrationer af drivhusgasser og for det lave scenarie (RCP2.6) med relativt lavere koncentrationer af drivhusgasser. Se mere om scenarier i afsnittet om klimamodeller.

I slutningen af det 21. århundrede (2081-2100) forventes den årlige middeltemperatur i forhold til referenceperioden (1986-2005) at være steget med mellem 1,2 ± 0,5 °C og 3,7 ± 1,0 °C for henholdsvis det lave og høje scenarie af koncentrationer. Se tabel 2. Opdelt på årstider vil den største stigning forekomme om somme-

Figur 3.1 Temperatur: Ændring i årlig middeltemperatur i Danmark i forhold til referenceperioden 1986-2005. Sort kurve: Observationer fra 1874 til 2005. Blå og rød kurve: Modelsimuleringer for perioden 2005-2100 for henholdsvis RCP2.6-scenariet og RCP8.5-scenariet. De skraverede områder angiver vurderede usikkerheder på temperaturstigningerne. For de samme scenarier er med hhv. grøn og orange angivet resultater baseret på CRES' detaljerede koblede klimamodel for Danmark. Til højre ses middeltemperaturstigningerne for de sidste 20 år af simuleringen.

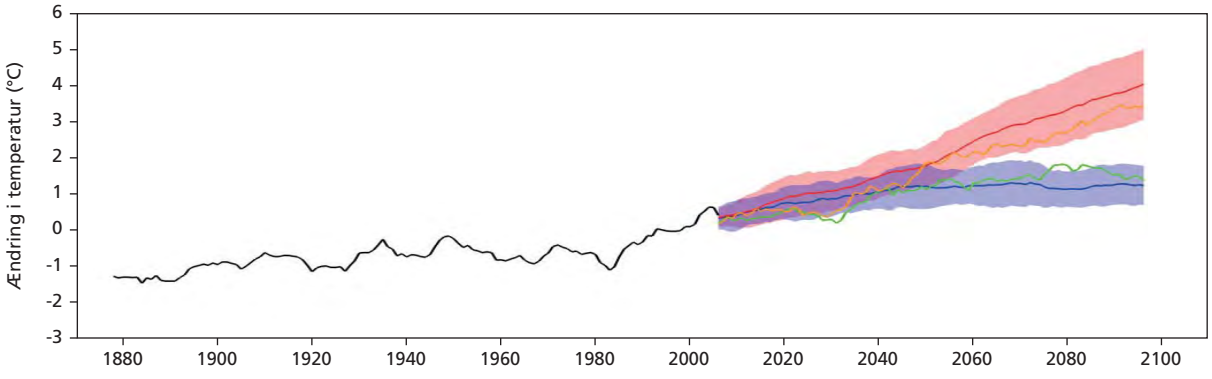

Tabel 3.2 Temperaturændringer for Danmark i grader Celsius i scenarieperioden 2081-2100 i forhold til referenceperioden 1986-2005. Tallene er angivet for hvert af de to scenarier RCP2.6 og RCP8.5. Tallene i parentes angiver usikkerheden (+/- standardafvigelsen) på middelværdien for 23 modelkørsler.

Temperatur [˚C]	RCP2.6	RCP8.5
Årlig	1,2 (± 0,5)	3,7 (± 1,0)
Vinter	1,2 (± 0,7)	3,7 (± 0,9)
Forår	1,2 (± 0,5)	3,2 (± 0,8)
Sommer	1,2 (± 0,8)	4,0 (± 1,5)
Efterår	1,3 (± 0,6)	4,0 (± 1,1)

Tabel 3.3 Nedbørsændringer for Danmark angivet som procentvise ændringer for scenarieperioden 2081-2100 i forhold til referenceperioden 1986-2005. Tallene er angivet for hvert af de to scenarier RCP2.6 og RCP8.5. Tallene i parentes angiver usikkerheden (+/- standardafvigelsen) på middelværdien for 23 modelkørsler.

Nedbør [%]	RCP2.6	RCP8.5
Årlig	1,6 (± 4,6)	6,9 (± 6,1)
Vinter	3,1 (± 7,9)	18,0 (± 12,0)
Forår	3,7 (± 11,1)	10,7 (± 12,6)
Sommer	-0,5 (± 9,6)	-16,6 (± 21,0)
Efterår	0,8 (± 7,2)	10,2 (± 10,9)

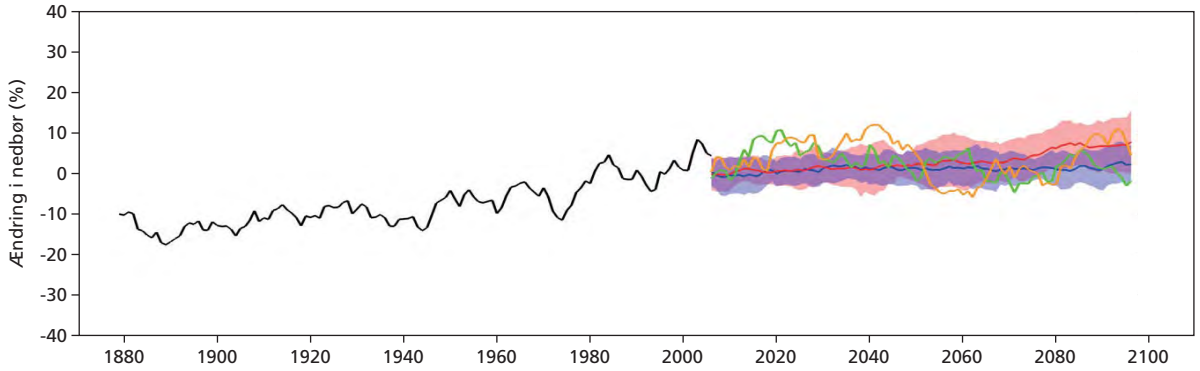

Figur 3.2 Nedbør: Årlig nedbørsændring i Danmark i procent i forhold til referenceperioden 1986-2005. Sort kurve: Observationer fra 1874 til 2005. Blå og rød kurve: Modelsimuleringer for perioden 2005-2100 for henholdsvis RCP2.6-scenariet og RCP8.5-scenariet. De skraverede områder angiver vurderede usikkerheder på nedbørsændringen. For de samme scenarier er med hhv. grøn og orange angivet resultater baseret på CRES' detaljerede koblede klimamodel for Danmark. Til højre ses den gennemsnitlige nedbørsændring for de sidste 20 år af simuleringen.

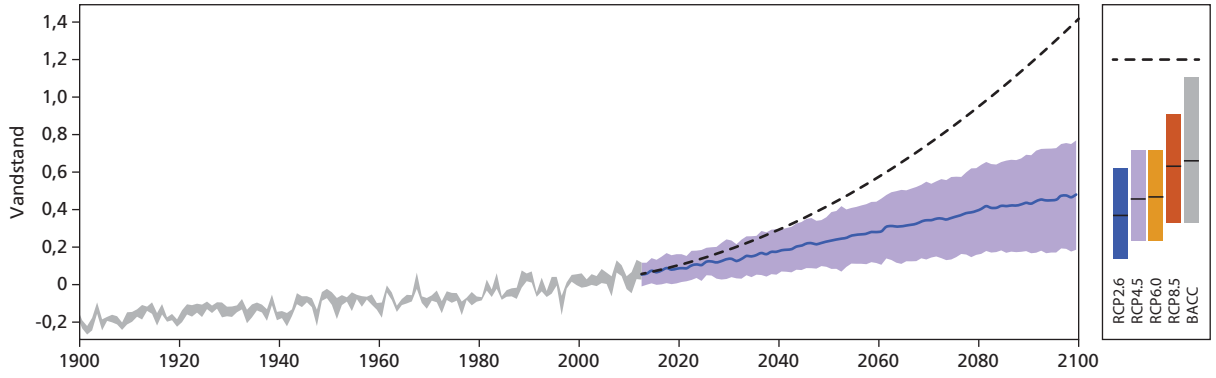

Figur 3.3 Vandstand. Den absolutte middelvandstand ved Danmark i meter for årene 1900-2100. Den grå skygge for år 1900-2012 viser den observerede årlige middelvandstand ved danske vandstandsmålere, korrigeret for landhævning. Den blå streg for år 2012-2100 viser middelvandstanden i Nordsøen for RCP4.5 scenariet, og skyggen angiver usikkerheden for dette scenarie. Den stiplede linje angiver DMI's estimat af en øvre grænse for vandstandsstigninger. I højre side af figuren vises middelværdi og usikkerheder for fire forskellige scenarier for perioden 2081-2100. Den stiplede linje viser DMI's øvre bud for denne periode.

ren, hvor middeltemperaturen i 2081-2100 forventes at være steget med 4,0 ± 1,5 °C i forhold til i dag for det høje scenarie. Tilsvarende vil temperaturen om vinteren være steget med 3,7 ± 0,9 °C for det høje scenarie.

Det fremgår af figur 1 og tabel 2, at selv for det meget ambitiøse scenarie RCP2.6, der indeholder store reduktioner i udledningerne, kan en temperaturstigning ikke undgås. Ikke desto mindre har det stor betydning for den fremtidige temperaturudvikling i Danmark (og globalt), hvilket scenarie for drivhusgasudslip man tager udgangspunkt i.

Nedbør

Vi får i fremtiden generelt mere nedbør i Danmark. Med den globale opvarmning kan atmosfæren indeholde mere vanddamp, og det fører til en stigning i nedbør i Danmark. Ifølge klimamodellerne skal vi forvente et ændret nedbørsmønster både med hensyn til den gennemsnitlige mængde, den årlige fordeling og intensiteten. Vinter, forår og efterår bliver vådere, mens sommersæsonen bliver tørrere.

Frem mod slutningen af det 21. århundrede viser modelstudier med en gruppe af mange klimamodeller en klar tendens til mere årlig nedbør i det nordlige Europa herunder også i Danmark.

Ændringerne fordeler sig ulige henover året. For det høje scenarie (RCP8.5) forventes vinternedbøren at stige med 18,0 % ± 12,0 % frem mod slutningen af dette århundrede. Omvendt forventes sommernedbøren at aftage med 16,6 % ± 21,0 % frem mod 2100.

Modellerne tegner et billede af, at Danmark ligger på grænsen mellem det nordlige Skandinavien mod nord, hvor sommernedbøren generelt stiger, og det centrale, østlige og sydlige Europa mod syd, hvor sommernedbøren aftager. Derfor er beregningen af sommernedbøren forbundet med større usikkerheder, end det er tilfældet for vinternedbøren.

Tabel 3.4 Absolut middelvandstandsstigning for Danmark fra 1986-2005 til 2081-2100 i meter.

Vandstand [m]	RCP2.6	RCP8.5
	0,34 (0,1 – 0,6)	0,61 (0,3 – 0,9)

Havniveauet

Havniveauet ved alle danske kyster – undtagen i Nordjylland – er stigende, og man kan forvente, at stigningerne bliver kraftigere i de næste 100–200 år på grund af klimaforandringerne. I 2081-2100 forventer man, at havniveauet omkring Danmark er steget 60 cm (± 30 cm) for det høje scenarie, men kan risikere at stige med 1,2 m i forhold til i dag. Hvor meget havniveauet stiger, er forbundet med en del usikkerhed, især fordi det er usikkert, hvordan smeltende gletsjere og iskapper vil påvirke verdenshavene. I Danmark bliver stigningen delvist kompenseret af landhævninger, særligt for nordlige områder, og der er også forskelle i havniveauændringerne mellem landsdelene. Ændringerne i havniveau vil sammen med ændrede vindmønstre føre til hyppigere og øgede stormflodshøjder, særligt i Vadehavet.

Ekstremvejr

Vi får flere og mere ekstreme vejrhændelser i Danmark. Beregninger med klimamodeller viser, at en øget drivhuseffekt fører til ændringer i hyppighed, intensitet og varighed af ekstreme vejrhændelser. Danmark vil få flere og længerevarende hedebølger. Vi får ændrede nedbørsmønstre med somre, som dels vil være præget af længere tørre perioder og dels rammes af flere kraftige nedbørshændelser. Vintrene vil generelt være præget af mere nedbør. Havniveauet vil fortsat stige og medføre både hyppigere og øgede stormflodshøjder, selv med uændrede vindforhold. I det følgende tegnes et billede af fremtiden under antagelsen om et business-as-usual-scenarie, dvs. et scenarie med fortsatte høje globale udledninger af drivhusgasser (se kapitel 4.1).

Temperatur

Den gennemsnitlige årlige temperatur stiger. Det betyder, at varmerekorder både sommer og vinter løbende bliver slået. Vi forventer derfor at se flere varmerekorder frem mod år 2100. Vi vil opleve flere og længere hedebølger. Ifølge klimamodellerne vil antallet af hedebølgedage i slutningen af dette århundrede være steget til mere end 3 gange det antal, vi har i dag.

Nedbør

Vi får flere kraftige nedbørshændelser i Danmark. Trods de forventede tørrere somre i Danmark kan vi forvente gradvist flere og kraftigere nedbørshændelser frem mod 2100. De største ændringer vil forekomme for de mest ekstreme hændelser – relativt set. Det vil sige, at jo kraftigere en hændelse, desto hyppigere vil den forekomme i slutningen af dette århundrede i forhold til i dag. En kraftig nedbørshændelse, hvor der fx falder mere end 20 mm nedbør på et døgn, vil forekomme 2 til 3 gange hyppigere i slutningen af dette århundrede end i dag.

Regnmålere fra Sønæs. Foto: Lotte Kunstmann.


25 ÅR
10 ÅR
100 ÅR

Storme og stormfloder

Modelsimuleringer viser en svag tendens til, at storme over farvandene omkring Danmark vil tage til frem mod år 2100. Vinden forøges i et bælte på Danmarks breddegrader – fra Storbritannien til Baltikum. Modellerne viser, at nuværende 10-års stormhændelser (storme så kraftige, at de i gennemsnit kun forekommer én gang hvert 10. år) sandsynligvis vil være et par procent kraftigere omkring Danmark i slutningen af dette århundrede.

De øgede stormflodshøjder i fremtiden skyldes dels den generelle ændring i havniveauet og dels effekten på kystlinjen af ændrede vindmønstre. Et stigende havniveau har stor betydning for, hvor ofte en given stormflodshøjde overskrides.

Ved København er en såkaldt 100-årshændelse i dag på 1,5 meter. Det vil sige en vandstand så høj, at den i gennemsnit kun opnås med 100 års mellemrum. Hvis middelvandstanden stiger 0,5 meter, vil denne stormflodshøjde blive nået hvert andet år. Det vil altså sige, at man i København må forberede sig på langt hyppigere oversvømmelser ved havnefronterne og en tilsvarende tendens gør sig gældende for alle Danmarks kystnære områder.

Tabel over ændringer i klimaekstremer for hele landet.

Klimaparametre for Danmark. En række klimaparametre er angivet for 1990, 2050 og 2100. Tallene i de tre kolonner repræsenterer midler over perioderne: 1961-1990, 2021-2050 og 2071-2100. Alle tal er fra modelkørsler med opløsning 25×25 km, og derfor vil de beregnede ekstremværdier generelt være mindre end observerede ekstremer, der normalt vil bygge på punktmålinger. Til fremskrivningerne er benyttet det tidligere brugte A1B-scenarie, der nogenlunde svarer til scenarie RCP6.0.

Parametre	1990	2050	2100
Kulde			
Frostdøgn [døgn/år]	85 (± 8)	61 (± 7)	29 (± 5,3)
Varme			
Varme sommernætter [døgn/år]	8 (± 4)	13 (± 4)	44 (± 13)
Hedebølgedage [døgn/år]	1,5 (± 0,6)	2,8 (± 1,0)	5,0 (± 2,6)
Længste hedebølge [døgn]	3,2 (± 0,7)	4,2 (± 0,9)	5,6 (± 1,9)
Varmebølgedage [døgn/år]	5,8 (± 1,4)	8,7 (± 2,2)	13,9 (± 4,7)
Længste varmebølge [døgn]	6,9 (± 1,1)	8,2 (± 1,4)	10,1 (± 3,3)
Nedbør			
Nedbørshændelser > 10 mm [døgn/år]	19 (± 2)	22 (± 2)	26 (± 3)
Nedbørshændelser > 20 mm [døgn/år]	2 (± 0,3)	3 (± 0,5)	5 (± 0,7)
Årets største døgnsum [mm]	70 (± 8)	75 (± 8)	81 (± 10)
Årets største 5-døgnssum [mm]	94 (± 6)	100 (± 5)	108 (± 7)
Middelintensitet af nedbør [mm/døgn]	5,0 (± 0,2)	5,2 (± 0,2)	5,6 (± 0,2)